Trimetallic N-heterocyclic carbene complexes

Ellul, Charles

Award date:
2011

Awarding institution:
University of Bath

TRIMETALLIC N-HETEROCYCLIC CARBENE COMPLEXES

Charles Edward Brian Ellul

A thesis submitted in partial fulfilment of the requirements for the degree of

Doctor of Philosophy

University of Bath

Department of Chemistry

April 2011

Acknowledgements

I would foremost like to thank Dr Mike Whittlesey for giving me the opportunity to work in a fantastic laboratory environment for the past three and a half years and for putting up with my standard answer that everything is going ‘fine’. In addition to this I would like to thank Mike for reading through my reports and this thesis correcting what can be only described as suspect English with an incessant use of commas.

I would also like to thank Dr Sofia Pascu for help with the tripodal NHC chemistry, Dr John Lowe for his help with all my NMR enquires, Dr Anneke Lubben for issues regarding mass spectrometry and especially Dr Mary Mahon for teaching me all about the wonderful world of X-ray crystallography and for putting up with my queries when things weren’t quite making sense.

I have been really fortunate to work with a great bunch of lab mates over the years, including Olly and Steve who provided me with so much help and quality banter at the start of my PhD. Mikey Page (the mandatory lab Australian) who has kindly helped with the grammar contained within this thesis and who has been a great source of information and advice. I would also like to thank him for putting up with my continual jokes regarding his mother country and his sense of direction. Of course I cannot forget Minty ‘Ledge’ Ledger, Tom Martin and Elena Mas-Marzá, and past MChems, including Matty ‘Ryan Sidebottom’ Crittall, Graham ‘G man’ Reed and Pete ‘Jockey’ Elson who have made my time in the lab so interesting and so much fun.

I would like to finally thank my parents for their continued support (both emotional and more importantly financial), encouragement and an unwavering belief in my abilities, which dates back to a time where I received my A grade for GSCE English Language, they were so impressed they didn’t quite believe it.

Abstract

This thesis describes the coordination chemistry of a range of mono- and tridentate N-heterocyclic carbenes (NHCs). It contains three distinct areas of chemistry; the synthesis and catalysis of NHC cluster compounds of ruthenium and osmium, the synthesis and reactivity of novel NHC palladium carbonyl clusters and use of the tripodal NHC ligand timteb^{R} (R = ^{t}Bu or dipp) for the preparation of catalytically active Pd and Cu complexes.

The reactions of $Ru_3(CO)_{12}$ and $Os_3(CO)_{12}$ have been carried out with the NHCs IMes, IPr, I^{t}Bu, 6^{i}Pr$_2$ and 6*o*-Tol, and have led to the formation of a number of compounds. The smaller IMes ligand leads to the formation of $Ru(IMes)(CO)_4$ (**2.5**) and $Ru(IMes)_2(CO)_3$ (**2.6**) which co-crystallised together. The bulkier IPr, I^{t}Bu and 6^{i}Pr$_2$ ligands generated cluster NHC complexes. For IPr and I^{t}Bu, evidence has been observed for abnormal binding of the ligand in the formation of Ru_3(ab-IPr)$(CO)_{11}$ (**2.7**) and Os_3(ab-I^{t}Bu)$(CO)_{11}$ (**2.8**), whereas 6^{i}Pr$_2$ gave the coordinatively unsaturated cluster complex $Ru_3(6^{i}Pr_2)(\mu\text{-}CO)_2(CO)_8$ (**2.10**). The catalytic activity of Ru_3(ab-NHC)$(CO)_{11}$, $Ru_3(\mu\text{-}H)$(dab-NHC)$(CO)_9$ (NHC = I^{t}Bu or IAd, **2.1**-**2.4**) as well as the unsaturated compound **2.10** have been investigated for the regioselective acylation of pyridine.

The first examples of a range of palladium NHC clusters $Pd_3(NHC)_3(\mu\text{-}CO)_3$ where NHC = IMes (**3.1**), I^{i}Pr$_2$ (**3.2**) or I^{n}Bu$_2$ (**3.3**) have been synthesised. The addition and ligand substitution reactions of **3.1** have also been investigated, forming $Pd_3(IMes)_3(\mu\text{-}SO_2)_3$ (**3.4**) upon reaction with SO_2.

A series of *bis*-NHC and mixed phosphine/NHC palladium(II) complexes (timteb^{tBu})$\{PdI_2(ICy)\}_3$ (**4.1**), (timteb^{tBu})$\{PdI_2(PPh_3)\}_3$ (**4.2**) and (timteb^{dipp})$\{PdI_2(PPh_3)\}_3$ (**4.3**) all bearing a tripodal NHC ligand, have been synthesised. The tripodal NHC ligands have also been coordinated to copper(I) centres to give complexes of the form $[(timteb^{R})Cu_3(\mu_3\text{-}O)]X$, where R/X = ^{t}Bu/$PF_6$ (**4.4**) and dipp/BF_4 (**4.5**). The Pd and Cu compounds have been studied in a range of catalytic coupling reactions including Suzuki-Miyaura and Sonogashira C-C coupling reactions as well as Ullmann type C-O and C-N reactions.

Compound labels and abbreviations

Compound Labels

The following table lists compound numbers used throughout this work for fully characterised new complexes; each number relates explicitly to a specific compound shown in the table below.

Compound number	Compound
2.1	Ru_3(ab-I^{t}Bu)$(CO)_{11}$
2.2	Ru_3(ab-IAd)$(CO)_{11}$
2.3	$Ru_3(\mu$-H)(dab-I^{t}Bu)$(CO)_9$
2.4	$Ru_3(\mu$-H)(dab-IAd)$(CO)_9$
2.5	Ru(IMes)$(CO)_4$
2.6	$Ru(IMes)_2(CO)_3$
2.7	Ru_3(ab-IPr)$(CO)_{11}$
2.8	Os_3(I^{t}Bu)$(CO)_{11}$
2.9	Os_3(IAd)$(CO)_{11}$
2.10	Ru_3(6^{i}Pr$_2$)$(\mu$-CO$)_2(CO)_8$
3.1	$Pd_3(IMes)_3(\mu$-CO$)_3$
3.2	Pd_3(I^{i}Pr$_2)_3(\mu$-CO$)_3$
3.3	Pd_3(I^{n}Bu$)_3(\mu$-CO$)_3$
3.4	$Pd_3(IMes)_3(\mu$-SO$_2)_3$
4.1	(timteb^{tBu})$\{PdI_2(ICy)\}_3$
4.2	(timteb^{tBu})$\{PdI_2(PPh_3)\}_3$
4.3	(timteb^{dipp})$\{PdI_2(PPh_3)\}_3$
4.4	[(timteb^{tBu})$Cu_3(\mu_3$-O)]PF_6
4.5	[(timteb^{dipp})$Cu_3(\mu_3$-O)]BF_4

Abbreviations – Spectroscopic

NMR	Nuclear magnetic resonance
δ	NMR chemical shift
J_{YZ}	Coupling constant of Y to Z
HMQC	Heteronuclear multiple quantum coherence
HMBC	Heteronuclear multiple bond correlation
COSY	Correlation spectroscopy

s	Singlet
d	Doublet
t	Triplet
q	Quartet
sept	Septet
m	Multiplet
br	Broad
IR	Infrared
ν(L)	IR shift of ligand L
GC	Gas chromatography
DFT	Density functional theory

Abbreviations – Unit

h	Hour
min	Minute
s	Second
K	Kelvin
°	Degree
ppm	Parts per million
Hz	Hertz
MHz	Megahertz
cm^{-1}	Wavenumber
Å	Angstrom
g	Gram
mg	Milligram
mL	Millilitre
µL	Microlitre
mol	Mole
mmol	Millimole

Abbreviations – Chemical

NHC	N-Heterocyclic carbene
ab-NHC	Abnormally bound N-heterocyclic carbene
dab-NHC	N-Heterocyclic carbene bound through both C4 and C5 positions

Mes	Mesityl (2,4,6-trimethylphenyl)
Ad	Adamantyl
Dipp	2,6-diisopropylphenyl
IMe_2	1,3-*bis*(methyl)imidazol-2-ylidene
IMe_4	1,3,4,5-tetramethyl-imidazol-2-ylidene
IEt_2Me_2	1,3-diethyl-4,5-dimethyl-imidazol-2-ylidene
I^iPr_2	1,3-*bis*(isopropyl)imidazol-2-ylidene
$I^iPr_2Me_2$	1,3-diisopropyl-4,5-dimethyl-imidazol-2-ylidene
ICy	1,3-*bis*(cyclohexyl)imidazol-2-ylidene
I^nBu	1,3-*bis*(*n*-butyl)imidazol-2-ylidene
IPh_2	1,3-*bis*(phenyl)imidazol-2-ylidene
IMes	1,3-*bis*(2,4,6-trimethylphenyl)imidazol-2-ylidene
IPr	1,3-*bis*(2,6-diisopropylphenyl)imidazol-2-ylidene
I^tBu	1,3-*bis*(*tert*-butyl)imidazol-2-ylidene
IAd	1,3-*bis*(1-adamantyl)imidazol-2-ylidene
$SIMe_2$	1,3-*bis*(methyl)imidazolin-2-ylidene
$SIEt_2$	1,3-*bis*(ethyl)imidazolin-2-ylidene
SIPr	1,3-*bis*(2,6-diisopropylphenyl)imidazolin-2-ylidene
$SIPr{\cdot}C_6F_5H$	1,3-*bis*(2,6-diisopropylphenyl)-2-(pentafluoro-phenyl)imidazolidene
SI^tBu	1,3-*bis*(*tert*-butyl)imidazolin-2-ylidene
6^iPr_2	1,3-*bis*(isopropyl)-3,4,5,6-tetrahydropyrimidin-2-ylidene
6*o*-Tol	1,3-*bis*(*o*-tolyl)-3,4,5,6-tetrahydropyrimidin-2-ylidene
6Mes	1,3-*bis*(2,4,6-trimethylphenyl)-3,4,5,6-tetrahydropyrimidin-2-ylidene
7Mes	1,3-*bis*(2,4,6-trimethylphenyl)-4,5,6,7-tetrahydro-3*H*-[1,3]diazepin-2-ylidene
$TIME^{tBu}$	1,1,1-{*tris*(3-*tert*-butyl-imidazol-2-ylidene)methyl}ethane
$TIME^{nBu}$	1,1,1-{*tris*(3-*n*-butyl-imidazol-2-ylidene)methyl}ethane
$TIMEN^{tBu}$	*tris*-{2-(3-*tert*-butylimidazol-2-ylidene)ethyl}amine
$TIMEN^{Xyl}$	*tris*-{2-(3-2,6-dimethylphenyl-imidazol-2-ylidene)ethyl}amine
$timtmb^{tBu}$	1,3,5-*tris*{(*tert*-butyl-imidazol-2-ylidene)methyl}-2,4,6-trimethylbenzene
$timteb^{tBu}$	1,3,5-*tris*{(*tert*-butyl-imidazol-2-ylidene)methyl}-2,4,6-triethylbenzene
$timteb^{dipp}$	1,3,5-*tris*{(2,6-diisopropylphenyl-imidazol-2-ylidene)methyl}-2,4,6-triethylbenzene

Contents

1.1 Introduction

1.1.1 N-Heterocyclic carbenes

N-Heterocyclic carbenes (NHCs) have been widely studied as a class of ligand for organometallic chemistry, especially for applications in homogenous catalysis[1] ever since the first stable NHC was isolated in 1991 by Arduengo.[2] Since then the field of NHC chemistry has expanded rapidly and extends to a significant range of areas and topics which are still increasing today.

NHCs are neutral ligands that contain a carbon atom bearing a lone pair of electrons which is incorporated into a heterocyclic ring with vicinal amino substituents. There are two main types of NHC consisting of either an unsaturated or saturated heterocyclic ring (**Figure 1.1.1**).

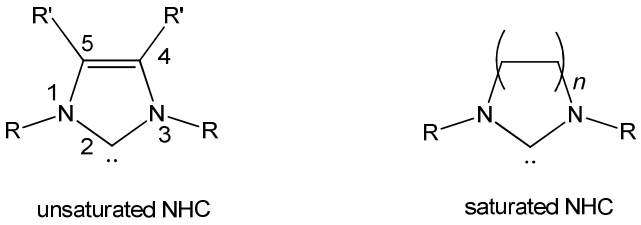

Figure 1.1.1: Pictorial representation of unsaturated and saturated NHCs.

The nitrogen atoms vicinal to the lone pair play an important role in reducing the reactivity of the carbenic carbon, as first demonstrated by Wanzlick and co-workers.[3] The nitrogen atoms in NHCs create a 'push-pull' system (**Figure 1.1.2**) helping to stabilise the lone pair of electrons in two ways. In the first instance, electronegativity of the nitrogen atoms withdraws σ-electron density away from the carbene. Secondly, the nitrogen atoms donate π-electron density into the empty p-orbital of the sp^2 hybridised carbon. These properties reduce the electrophilicity and the reactivity of the carbene. Additionally for unsaturated NHCs, further stability is gained from the aromaticity of the heterocyclic ring.

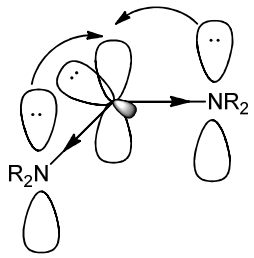

Figure 1.1.2: Sigma (σ) and π stabilisation of the carbene.

Five-membered carbenes were the first type of NHCs discovered by Wanzlick and Öfele in the late 1960s with publications detailing the syntheses of $[Hg(IPh_2)_2]^{2+}$ and $Cr(IMe_2)(CO)_5$ utilising *in situ* generated NHCs.[4,5] Since the isolation of the first free NHC in 1991, a number of reliable synthetic routes have been reported leading to the formation of various NHCs. These methods generally involve the elimination of a stable molecule such as a chloride salt,[6] K_2S,[7] or an organic species and provide a favourable energy path for the formation of the free carbene as shown in **Scheme 1.1.1**.[8]

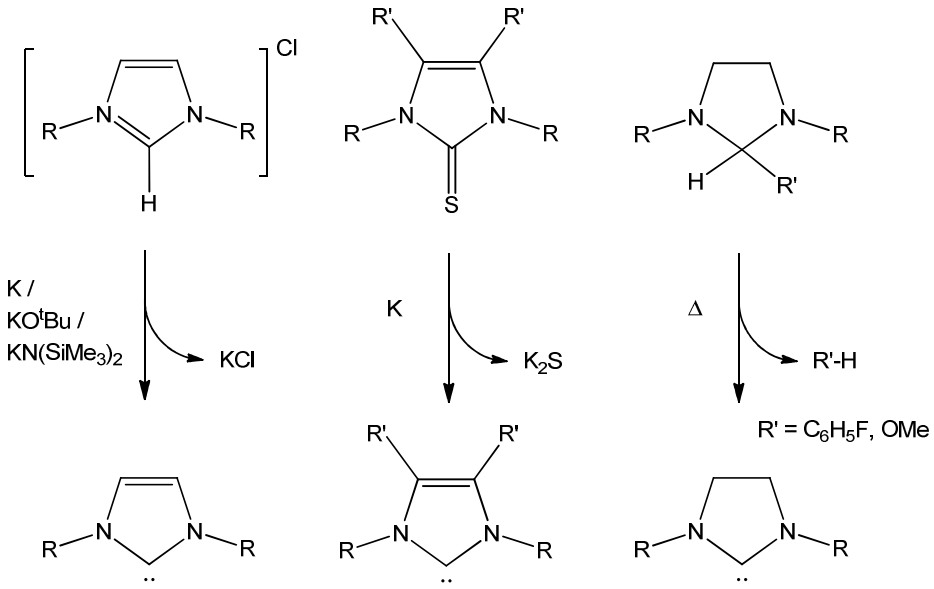

Scheme 1.1.1: A range of synthetic routes to free NHCs.

NHCs can be easily modified, enabling the tuning of the steric and electronic properties to suit each reaction. It is possible to functionalise the side arms (R) to incorporate a range of aryl and alkyl substituents of differing sizes enabling control over the sterics of the carbene.[1g, 9] The R groups can also contain donor atoms leading to the formation of multidentate NHCs.[10] The backbone position (R') can also be functionalised, using a plethora of moieties including

electronegative groups (e.g. chlorine),[11] alkyl and aryl groups,[1c, 1e, 12] or by benzannulation.[13] Another way to alter the properties of the NHC is by changing the size of the N-heterocycle, for example, increasing the ring size to 6 or 7 atoms resulting in ring expanded NHCs, which are more basic than their 5-membered analogues.[14] This has recently been demonstrated by O'Donoghue and co-workers who reported experimental pK_a values for a large series of NHCs and showed that $I^iPr_2Me_2$ and 6^iPr_2 exhibit significantly different pK_a values of 21.1 and 28.2 respectively.[15]

1.1.2 Electronic and steric properties of NHCs

The electronic properties of NHCs have been determined via a number of methods, including measurement of metal-ligand bond dissociation energies (BDEs),[16] pK_a values of the free ligands (as above)[17] and ν_{CO} stretching frequencies of NHC containing metal carbonyl complexes (**Table 1.1.1**).[18] The table shows that complexes with NHC ligands exhibit much lower carbonyl stretching frequencies than their phosphine counterparts. This is attributed to the stronger σ donating abilities of NHCs leading to a more electron rich metal centre, thereby increasing the back donation into the π* antibonding orbitals of the carbonyl ligands. These findings show that the least electron donating NHC is still a stronger σ-donor than the very electron rich PCy_3 ligand. Due to this increased σ-donor ability, there is an increase in metal-ligand bond strength that has resulted in fewer examples of the dissociation of NHCs from metal centres compared with phosphines.[19] This is especially beneficial for catalysis, as catalysts bearing NHC ligands are less inclined to decompose during a catalytic cycle or to require the presence of additional ligands to maintain their activity.

Ligand	ν_{CO} (CH_2Cl_2, cm^{-1})	Ligand	ν_{CO} (CH_2Cl_2, cm^{-1})
6Mes	1987, 2071	IMes	1970, 2051
7Mes	1987, 2069	IPr	1970, 2052
SIMes	1996, 2081	PCy_3	1971, 2056
IMes	1995, 2080	PPh_3	1990, 2069

Table 1.1.1: ν_{CO} for $RhCl(NHC)(CO)_2$ (left) and $Ni(L)(CO)_3$ (L = NHC or PR_3) (right).

The quantification of steric properties of ligands is hugely important to help rationalise not only reaction mechanisms but also catalytic performances of M-L complexes. This was achieved for tertiary phosphines in the 1970s by the widely used Tolman cone angle which allowed the measurement of the 3-dimensional size and shape of phosphine ligands.[20] The first attempts to measure the steric properties of NHCs were reported in 1999 and utilised Tolman's classification of

sterics.[21] The accuracy of the model was later improved by altering the definition of the ligand sterics. NHCs have an additional bond between the metal and the N-substituent which leads to a more 'fence like' geometry compared to the 'cone shape' of tertiary phosphines.[16]

This new model was coined 'percentage buried volume' ($\%V_{Bur}$), and is defined as the percent of the total volume of a sphere occupied by a ligand. The $\%V_{Bur}$ model describes a sphere of radius 3 Å designed to represent the coordination sphere of the metal centre, with the metal carbene bond length set at 2 Å which corresponds to the average metal carbene bond length (**Figure 1.1.3**).[22]

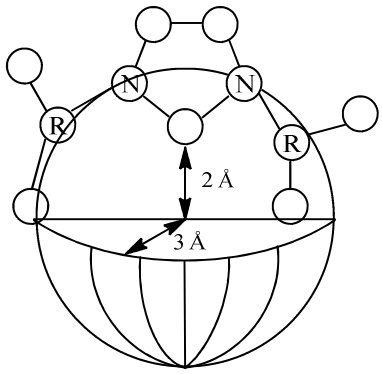

Figure 1.1.3: Pictorial representation of percent buried volume, $\%V_{Bur}$.

This model allows for the accurate quantification of the steric properties of an NHC bound to a metal centre. For example, an NHC with large bulky N-substituents will occupy a large volume of the sphere leading to a high value for $\%V_{Bur}$. It is also applicable to phosphines, enabling a direct comparison of NHCs with phosphines as shown in **Table 1.1.2**.

Ligand	$\%V_{bur}$	Ligand	$\%V_{bur}$
IMe_4	26.1	SIMes	36.9
PMe_3	27.3	IAd	39.8
ICy	27.4	P^tBu_3	43.9
PPh_3	34.8	IPr	44.5
IMes	36.5	SIPr	47.0

Table 1.1.2: $\%V_{bur}$ values calculated from crystallographic structures of AuCl(L) (L = PR_3 or NHC).[22]

Ring-expanded carbenes have higher $\%V_{Bur}$ values compared with their 5-membered analogues, for example, 6Mes has a value of 42.9 compared to 36.1 for IMes.[23] This is due to the increased N-C-N angle in the former (6Mes: 117.0(4)°, IMes: 107.29(12)°).[18c, 24] The increased angle forces the N-substituents to point more directly into the coordination sphere of the metal, increasing the steric influence. However, it is important to note that $\%V_{Bur}$ values are calculated from solid state structures and therefore conclusions made about complexes in solution should be considered with care and not over analysed. Despite this, the model still represents the best tool to analyse and understand the steric properties of NHCs.

1.1.3 N-Heterocyclic carbenes in catalysis

As previously mentioned, NHCs have been used as supporting ligands for a large array of catalytic reactions.[1] One such example is alkene metathesis where in terms of impact, they have, without doubt, revolutionised the field.[25] During the 1990s, the most active catalysts for metathesis reactions were based on molybdenum[12b, 26] and the Grubbs 1st generation *bis*-phosphine ruthenium complex.[27] However in 1999, the groups of Herrmann, Grubbs and Nolan independently reported the synthesis of a number of NHC containing analogues of the 1st generation catalyst that displayed superior activities. The most successful of these featured the substitution of one phosphine ligand for IMes or SIMes to afford what are known as Grubbs 2nd generation catalysts (**Figure 1.1.4**).[28,29]

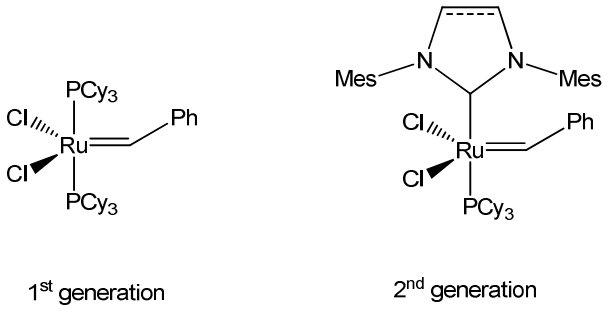

Figure 1.1.4: Grubbs 1st and 2nd generation metathesis catalysts.

The second generation catalysts were found to be stable to air and moisture and also exhibited extremely high activities for ring opening metathesis polymerisation (ROMP), ring closing metathesis (RCM) and cross metathesis (CM) reactions. The success of the ruthenium NHC based catalysts is due to two main reasons. The stability of the coordinated alkene intermediate is greatly increased by the strongly σ donating NHC, due to the increased back-bonding from the ruthenium metal centre to the alkene (**C**), even though the initial rate of PCy_3 dissociation to form the 14 electron intermediate (**B**) is reduced by the presence of the carbene. The increased electron

density on the metal centre is also thought to accelerate the oxidative addition step forming (**D**) shown in **Scheme 1.1.2**.

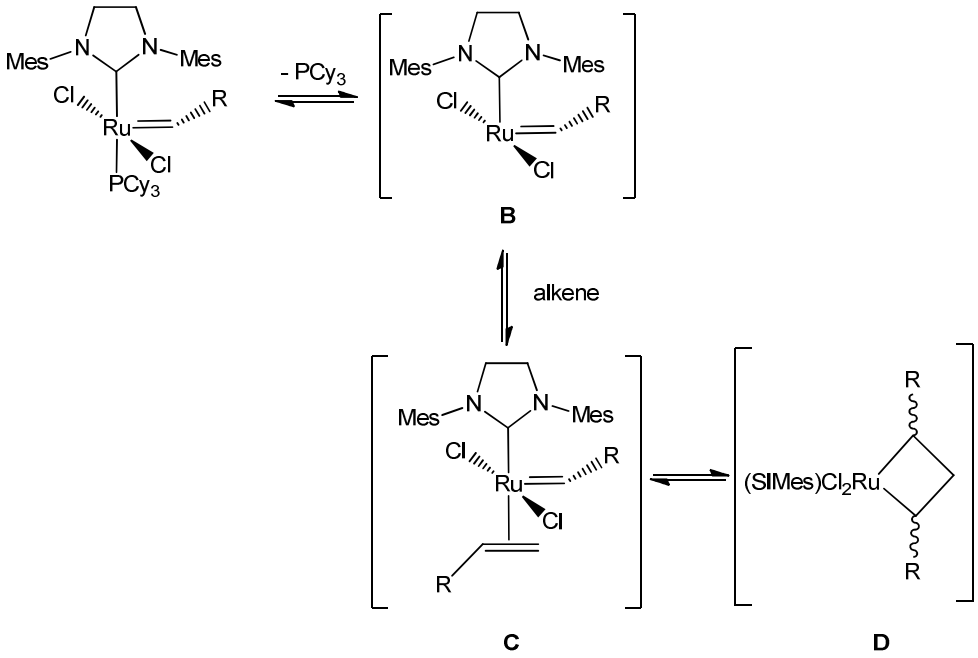

Scheme 1.1.2: A generalised reaction mechanism of ruthenium catalysed alkene metathesis.

In addition, the increased C_{NHC}-Ru bond strength allows catalysis to be run at much higher temperatures without degradation, allowing unreactive, highly substituted organic molecules to be accessed.[30] For example, Sinha *et. al.* used Grubbs' 2nd generation catalyst for the RCM of a heterocycle containing 16 atoms and recorded a yield of 89%, where in comparison, the 1st generation system was inactive.[31] Another example of the increased activity of the 2nd generation ruthenium SIMes catalyst is shown by the relative reaction rates for the RCM of 4,4-dicarboethoxy-2-methyl-1,6-heptadiene (**Scheme 1.1.3**) and ROMP of 1,5-cyclooctadiene (**Table 1.1.3**) for which the 2nd generation catalyst exhibits reaction rates which are 138 and 27 times faster than for the 1st generation catalyst.[32]

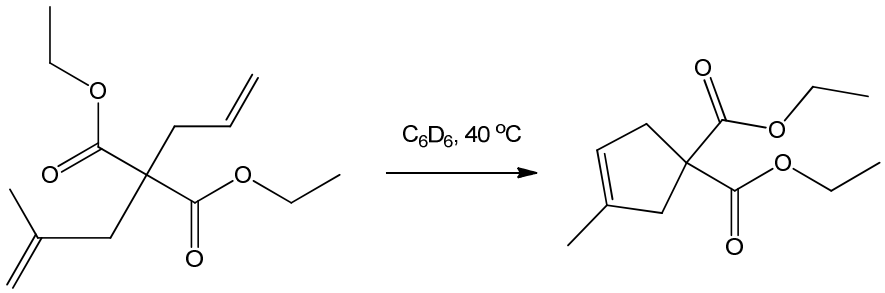

Scheme 1.1.3: Ring closing metathesis of 4,4-dicarboethoxy-2-methyl-1,6-heptadiene.

Catalyst	RCM (*k*)	ROMP (*k*)
$RuCl_2(PCy_3)_2$=CHPh	1	1
$RuCl_2(SIMes)(PCy_3)$=CHPh	138	27

Table 1.1.3: Relative rates for RCM/ROMP of 4,4-dicarboethoxy-2-methyl-1,6-heptadiene and 1,5-cyclooctadiene respectively between Grubbs 1st and 2nd generation catalyst.

1.1.4 Non-innocent behaviour of NHCs

Whilst in the majority of examples, NHCs are innocent spectator ligands which bond solely through the 2 free electrons in the C2 position, (**Figure 1.1.1**) this is not always the case. A large amount of work has shown that the N-substituents of the carbene can undergo C-H,[33] C-C[34] and C-N activation,[35] as well as forming agostic bonds to help to stabilise a reactive metal centre.[36]

An NHC can also coordinate to the metal via the C4/C5 backbone position rather than the expected C2 position, dubbed abnormal binding. This was first observed by Crabtree and co-workers in 2001 when they isolated an iridium phosphine hydride complex with an abnormally bound pyridine-tethered NHC (**Scheme 1.1.4**).[37]

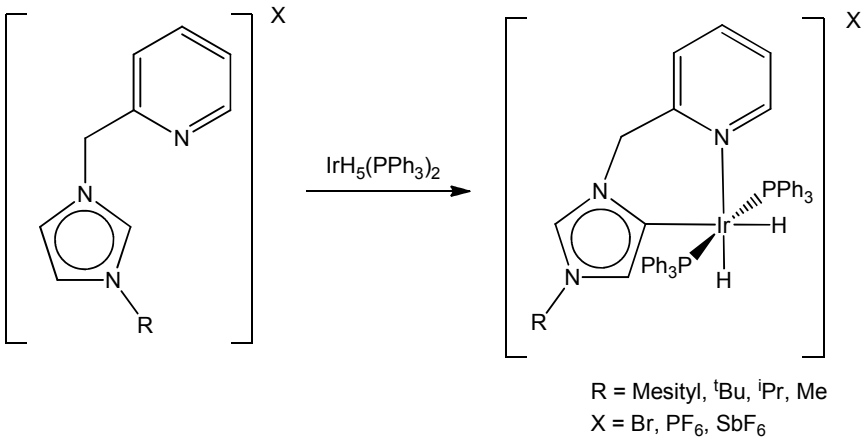

Scheme 1.1.4: The first abnormal NHC (ab-NHC) complex synthesised by Crabtree.

Since 2001 a range of abnormal complexes have been synthesised with many transition metals, including Fe, Ru, Os, Rh, Ir, Pd, Pt, Cu and Au.[38] The isolation of a free abnormal NHC was recently reported by Bertrand and co-workers, achieved by blocking the C2 position while stabilising the carbene with extremely bulky substituents (**Figure 1.1.5**).[39]

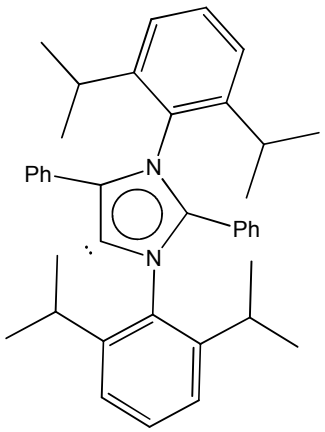

Figure 1.1.5: The isolable sterically stabilised 'free' abnormal NHC.

Abnormally bound NHCs exhibit different steric and electronic properties to their normal counterparts. The coordination via the C4/5 carbon means that only one of the N-substituents will be directed towards the coordination sphere of the metal centre, reducing the overall steric bulk of the NHC. They also display increased binding energies (increased σ-donation), a consequence of a more unstable carbenic carbon as it is now vicinal to only one nitrogen atom within the heterocycle.[40] The effect of the increased σ-donation is illustrated in the carbonyl stretching frequencies observed for $IrCl(NHC)(CO)_2$,[41] shown in **Figure 1.1.6**.

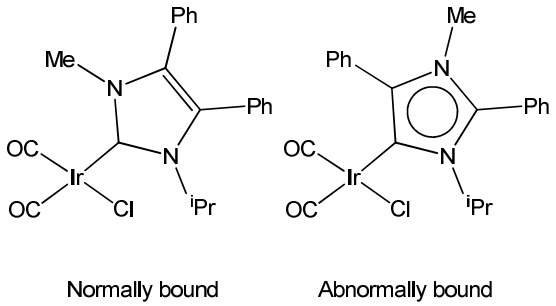

Compound	ν_{CO} (cm^{-1})
Normally bound	1974, 2059
Abnormally bound	1961, 2045

Figure 1.1.6: Comparison of the IR carbonyl stretches of $IrCl(NHC)(CO)_2$ and $IrCl(ab\text{-}NHC)(CO)_2$.

In general, complexes bearing abnormal ligands are often generated fortuitously, due to the prevalence of *in situ* deprotonation of imidazolium salts rather than the use of free NHCs. However, the targeted synthesis of abnormal complexes can be achieved by blocking the C2 position of the carbene. For example, palladium(II) complexes bearing both normal and abnormal *bis*-NHC ligands have been generated by Albrecht and co-workers by simply moving a methyl group from the C4 to C2 position (**Figure 1.1.7**). The synthesis of these compounds allows for the direct comparison of the properties exhibited by the different binding modes. One interesting example is the differing catalytic activity for the hydrogenation of cyclooctene to cyclooctane. The abnormal carbene complex shows good catalytic activity reaching a conversion of 57% after 1 h and ~100% after 8 h. In contrast, the normal complex was inactive and even after 20 h, no hydrogenation products were observed.[42]

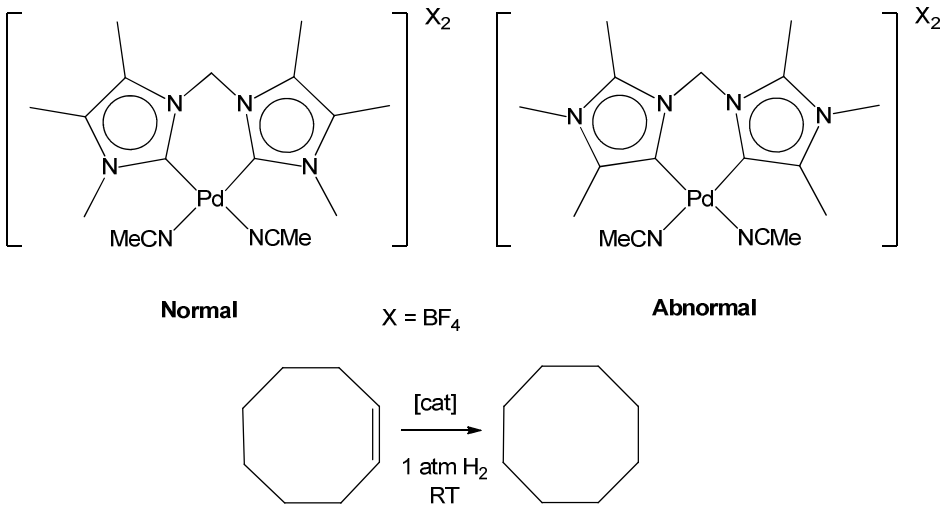

Figure 1.1.7: Normal and abnormal Pd(II) complexes for alkene hydrogenation.

1.1.5 Multidentate N-heterocyclic carbenes

Multidentate carbene ligands have led to the formation of a range of compounds whose stability is entropically improved by the chelate effect. The most popular class of these ligands are bidentate and *mer*-tridentate (*pincer*) *bis*-carbene ligands, the first of which were coordinated to Pd then later to other transition metals, including Rh, Ru and Ir.[43] Multidentate ligands are often prepared by the direct reaction between two or three equivalents of the corresponding N-alkylimidazole (or N-arylimidazole) and one equivalent of the desired alkyl/aryl dihalide (or trihalide) forming the linker holding the arms of the ligand.[44] For example, Peris and co-workers generated the bidentate NHC precursor (**Scheme 1.1.5**) by reaction of 2 equivalents of N-Me or N-^{t}Bu imidazole with diiodomethane.[45]

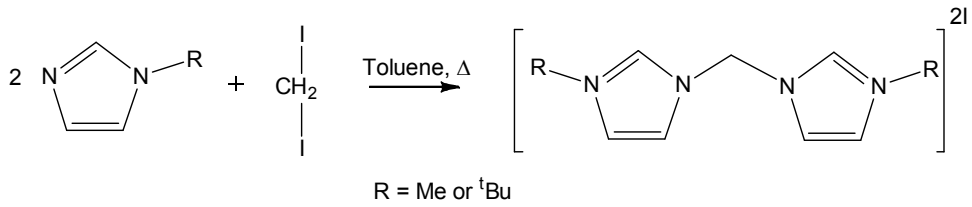

Scheme 1.1.5: Synthesis of a bidentate NHC precursor from an N-alkyl imidazole and diiodomethane.

As with monodentate NHC carbenes the topological and electronic properties can be modulated by varying the N-substituents, backbone and linker groups. In particular changing the linker group can have a dramatic effect on the products of a reaction. For example, it has been observed that the coordination of *bis*(imidazolylidene) ligands to $[RhCl(COD)]_2$ generates Rh(I) and Rh(III) species, depending on the linker lengths. Long linker groups have been shown to favour the formation of square planar Rh(I) complexes, whereas short linkers can afford pseudo-octahedral Rh(III) complexes (**Figure 1.1.8**).[46]

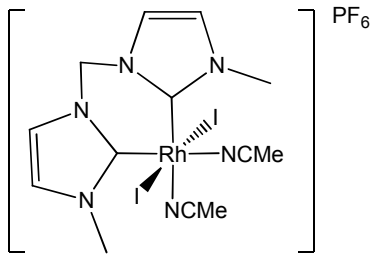

Figure 1.1.8: The pseudo-octahedral binding of a chelating NHC in $[RhI_2(bis\text{-NHC})(NCMe)_2]PF_6$.

In addition to this *bis*-NHC ligands with short linker groups do not always bind in a chelating manner. This has been shown by the reaction of a range of *in situ* formed *bis*-NHCs with $[RhCl(COD)]_2$ and KBr affording di-metallic complexes as shown **Scheme 1.1.6**. Even though the reaction mechanism is not well understood, the addition of KBr is significant as it encourages the preformed dibromide compound, which in turn favours the formation of the di-metallic complex. The mononuclear complex is generated in the absence of KBr.[46a, 47]

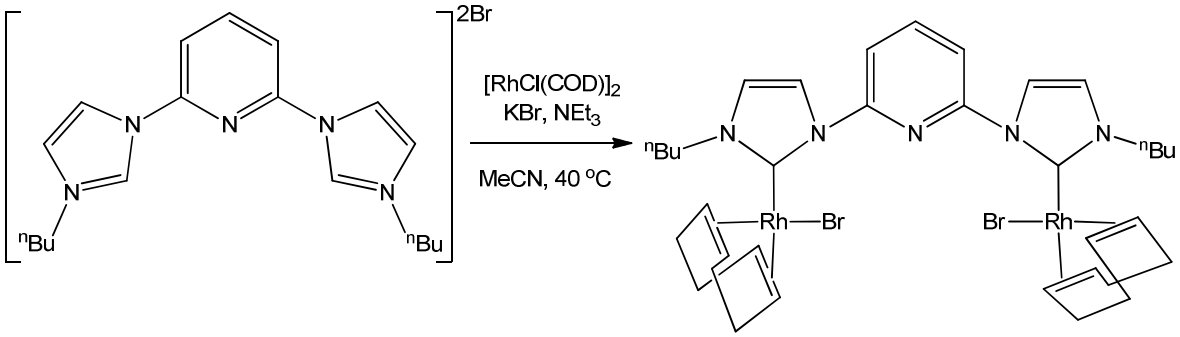

Scheme 1.1.6: Formation of an NHC di-rhodium complex.

Many studies describing the use of the multidentate *bis*-NHCs or tridentate (*pincer*) *bis*-carbenes have been carried out, whereas the use of *tris*-carbene ligands (tripodal NHCs) is scarce.[10d]

1.2 Thesis synopsis

This thesis describes the use of N-heterocyclic carbenes as supporting ligands for the formation of ruthenium, osmium, palladium and copper complexes. The results are separated into three chapters, each containing a different aspect of NHC chemistry. Each chapter contains a separate introduction described therein.

Chapter 2 illustrates the reaction of a selection of saturated and unsaturated NHCs with $M_3(CO)_{12}$ (M = Ru, Os), investigating the effects of NHC steric bulk on the nature of the products formed.

Chapter 3 describes the first examples of palladium clusters bearing a range of N-aryl and N-alkyl NHCs and the reactivity of the resulting compounds.

Chapter 4 reports the synthesis and coordination of tripodal NHCs to palladium and copper, and the use of isolated $(NHC)Pd_3$ and $(NHC)Cu_3$ complexes in catalytic C-C, C-N and C-O bond forming reactions.

Chapter 5 contains the experimental details of the compounds reported in the thesis.

1.3 References

1. (a) Kantchev, E. A. B.; O'Brien, C. J.; Organ, M. G., *Angew. Chem. Int. Ed.* **2007**, *46,* 2768-2813; (b) Scholl, M.; Ding, S.; Lee, C. W.; Grubbs, R. H., *Org. Lett.* **1999**, *1,* 953-956; (c) Herrmann, W. A., *Angew. Chem. Int. Ed.* **2002**, *41,* 1290-1309; (d) Herrmann, W. A.; Öfele, K.; Von Preysing, D.; Schneider, S. K., *J. Organomet. Chem.* **2003**, *687,* 229-248; (e) Hahn, F. E.; Jahnke, M. C., *Angew. Chem. Int. Ed.* **2008**, *47,* 3122-3172; (f) Glorius, F. A., *Top. Organomet. Chem.* **2007**, *21*; (g) Nolan, S. P., *N-Heterocyclic Carbenes in Synthesis*. Wiley-VCH: Weinheim, 2006.
2. Arduengo, A. J.; Harlow, R. L.; Kline, M., *J. Am. Chem. Soc.* **1991**, *113,* 361-363.
3. (a) Wanzlick, H. W.; Kleiner, H. J.; Noack, M., *Chem. Ber-Recl.* **1963**, *96,* 3024; (b) Wanzlick, H. W., *Angew. Chem. Int. Ed.* **1962**, *74,* 129; (c) Wanzlick, H. W.; Kleiner, H. J., *Angew. Chem. Int. Ed.* **1961**, *73,* 493; (d) Wanzlick, H. W.; Esser, F.; Kleiner, H. J., *Chem. Ber-Recl.* **1963**, *96,* 1208-1212.
4. Wanzlick, H. W.; Schonher, H., *Angew. Chem. Int. Ed.* **1968**, *7,* 141-142.
5. Öfele, K., *J. Organomet. Chem.* **1968**, *12,* 42-43.
6. Bonnet, L. G.; Douthwaite, R. E.; Kariuki, B. M., *Organometallics* **2003**, *22,* 4187-4189.
7. Kuhn, N.; Kratz, T., *Synthesis* **1993**, 561-562.
8. Nyce, G. W.; Csihony, S.; Waymouth, R. M.; Hedrick, J. L., *Chem.-Eur. J.* **2004**, *10,* 4073-4079.
9. Kuhl, O., *Chem. Soc. Rev.* **2007**, *36,* 592-607.
10. (a) McGuinness, D. S.; Cavell, K. J., *Organometallics* **2000**, *19,* 741-748; (b) Pugh, D.; Danopoulos, A. A., *Coord. Chem. Rev.* **2007**, *251,* 610-641; (c) Mata, J. A.; Poyatos, M.; Peris, E., *Coord. Chem. Rev.* **2007**, *251,* 841-859; (d) Meyer, K.; Bart, S. C., *Adv. Inorg. Chem.* **2008**, *60,* 1-30.
11. Arduengo, A. J.; Davidson, F.; Dias, H. V. R.; Goerlich, J. R.; Khasnis, D.; Marshall, W. J.; Prakasha, T. K., *J. Am. Chem. Soc.* **1997**, *119,* 12742-12749.
12. (a) Crudden, C. M.; Allen, D. P., *Coord. Chem. Rev.* **2004**, *248,* 2247-2273; (b) Bazan, G. C.; Khosravi, E.; Schrock, R. R.; Feast, W. J.; Gibson, V. C.; Oregan, M. B.; Thomas, J. K.; Davis, W. M., *J. Am. Chem. Soc.* **1990**, *112,* 8378-8387.
13. Hahn, F. E.; Wittenbecher, L.; Boese, R.; Blaser, D., *Chem.-Eur. J.* **1999**, *5,* 1931-1935.
14. (a) Iglesias, M.; Beetstra, D. J.; Knight, J. C.; Ooi, L. L.; Stasch, A.; Coles, S.; Male, L.; Hursthouse, M. B.; Cavell, K. J.; Dervisi, A.; Fallis, I. A., *Organometallics* **2008**, *27,* 3279-3289; (b) Newman, P. D.; Cavell, K. J.; Kariuki, B. M., *Organometallics* **2010**, *29,* 2724-2734.

15. Higgins, E. M.; Sherwood, J. A.; Lindsay, A. G.; Armstrong, J.; Massey, R. S.; Alder, R. W.; O'Donoghue, A. C., *Chem. Commun.* **2011**, *47,* 1559-1561.
16. Hillier, A. C.; Sommer, W. J.; Yong, B. S.; Petersen, J. L.; Cavallo, L.; Nolan, S. P., *Organometallics* **2003**, *22,* 4322-4326.
17. Magill, A. M.; Cavell, K. J.; Yates, B. F., *J. Am. Chem. Soc.* **2004**, *126,* 8717-8724.
18. (a) Dorta, R.; Stevens, E. D.; Scott, N. M.; Costabile, C.; Cavallo, L.; Hoff, C. D.; Nolan, S. P., *J. Am. Chem. Soc.* **2005**, *127,* 2485-2495; (b) Denk, K.; Sirsch, P.; Herrmann, W. A., *J. Organomet. Chem.* **2002**, *649,* 219-224; (c) Iglesias, M.; Beetstra, D. J.; Kariuki, B.; Cavell, K. J.; Dervisi, A.; Fallis, I. A., *Eur. J. Inorg. Chem.* **2009**, 1913-1919.
19. Herrmann, W. A.; Elison, M.; Fischer, J.; Kocher, C.; Artus, G. R. J., *Angew. Chem. Int. Ed.* **1995**, *34,* 2371-2374.
20. Tolman, C. A., *Chem. Rev.* **1977**, *77,* 313-348.
21. Huang, J. K.; Schanz, H. J.; Stevens, E. D.; Nolan, S. P., *Organometallics* **1999**, *18,* 2370-2375.
22. Clavier, H.; Nolan, S. P., *Chem. Commun.* **2010**, *46,* 841-861.
23. Calculated from AgCl(NHC).
24. Measured from RhCl(NHC)(COD).
25. (a) Trnka, T. M.; Grubbs, R. H., *Acc. Chem. Res.* **2001**, *34,* 18-29; (b) Grubbs, R. H.; Chang, S., *Tetrahedron* **1998**, *54,* 4413-4450.
26. Bazan, G. C.; Oskam, J. H.; Cho, H. N.; Park, L. Y.; Schrock, R. R., *J. Am. Chem. Soc.* **1991**, *113,* 6899-6907.
27. Schwab, P.; Grubbs, R. H.; Ziller, J. W., *J. Am. Chem. Soc.* **1996**, *118,* 100-110.
28. (a) Yet, L., *Chem. Rev.* **2000**, *100,* 2963-3007; (b) Heck, M. P.; Baylon, C.; Nolan, S. P.; Mioskowski, C., *Org. Lett.* **2001**, *3,* 1989-1991; (c) Hamilton, J. G.; Frenzel, U.; Kohl, F. J.; Weskamp, T.; Rooney, J. J.; Herrmann, W. A.; Nuyken, O., *J. Organomet. Chem.* **2000**, *606,* 8-12; (d) Bielawski, C. W.; Grubbs, R. H., *Angew. Chem. Int. Ed.* **2000**, *39,* 2903-2906; (e) Choi, T. L.; Chatterjee, A. K.; Grubbs, R. H., *Angew. Chem. Int. Ed.* **2001**, *40,* 1277-1279.
29. The NHC shown in **Figure 1.1.4** is drawn with a sp^2 hybridised carbon bonded to the metal centre, this is the same for all NHCs drawn within this thesis.
30. Sanford, M. S.; Love, J. A.; Grubbs, R. H., *J. Am. Chem. Soc.* **2001**, *123,* 6543-6554.
31. Sun, J.; Sinha, S. C., *Angew. Chem. Int. Ed.* **2002**, *41,* 1381-1383.
32. Trnka, T. M.; Morgan, J. P.; Sanford, M. S.; Wilhelm, T. E.; Scholl, M.; Choi, T. L.; Ding, S.; Day, M. W.; Grubbs, R. H., *J. Am. Chem. Soc.* **2003**, *125,* 2546-2558.
33. (a) Ledger, A. E. W.; Mahon, M. F.; Whittlesey, M. K.; Williams, J. M. J., *Dalton Trans.* **2009**, 6941-6947; (b) Burling, S.; Paine, B. M.; Nama, D.; Brown, V. S.; Mahon, M. F.; Prior, T. J.; Pregosin, P. S.; Whittlesey, M. K.; Williams, J. M. J., *J. Am. Chem. Soc.* **2007**,

129, 1987-1995; (c) Burling, S.; Mahon, M. F.; Paine, B. M.; Whittlesey, M. K.; Williams, J. M. J., *Organometallics* **2004**, *23,* 4537-4539; (d) Davies, C. J. E.; Page, M. J.; Ellul, C. E.; Mahon, M. F.; Whittlesey, M. K., *Chem. Commun.* **2010**, *46,* 5151-5153; (e) Hitchcock, P. B.; Lappert, M. F.; Pye, P. L., *J. Chem. Soc., Chem. Commun.* **1977**, 196-198; (f) Hong, S. H.; Chlenov, A.; Day, M. W.; Grubbs, R. H., *Angew. Chem. Int. Ed.* **2007**, *46,* 5148-5151; (g) Huang, J. K.; Stevens, E. D.; Nolan, S. P., *Organometallics* **2000**, *19,* 1194-1197.

34. (a) Jazzar, R. F. R.; Macgregor, S. A.; Mahon, M. F.; Richards, S. P.; Whittlesey, M. K., *J. Am. Chem. Soc.* **2002**, *124,* 4944-4945; (b) Viciano, M.; Sanaú, M.; Peris, E., *Organometallics* **2007**, *26,* 6050-6054; (c) Prades, A.; Viciano, M.; Sanaú, M.; Peris, E., *Organometallics* **2008**, *27,* 4254-4259; (d) Gnanamgari, D.; Sauer, E. L. O.; Schley, N. D.; Butler, C.; Incarvito, C. D.; Crabtree, R. H., *Organometallics* **2009**, *28,* 321-325.

35. Burling, S.; Mahon, M. F.; Powell, R. E.; Whittlesey, M. K.; Williams, J. M. J., *J. Am. Chem. Soc.* **2006**, *128,* 13702-13703.

36. (a) Burling, S.; Mas-Marzá, E.; Valpuesta, J. E. V.; Mahon, M. F.; Whittlesey, M. K., *Organometallics* **2009**, *28,* 6676-6686; (b) Häller, L. J. L.; Page, M. J.; Macgregor, S. A.; Mahon, M. F.; Whittlesey, M. K., *J. Am. Chem. Soc.* **2009**, *131,* 4604-4605.

37. Grundemann, S.; Kovacevic, A.; Albrecht, M.; Faller, J. W.; Crabtree, R. H., *Chem. Commun.* **2001**, 2274-2275.

38. (a) Arnold, P. L.; Pearson, S., *Coord. Chem. Rev.* **2007**, *251,* 596-609; (b) Schuster, O.; Yang, L. R.; Raubenheimer, H. G.; Albrecht, M., *Chem. Rev.* **2009**, *109,* 3445-3478; (c) Ellul, C. E.; Mahon, M. F.; Saker, O.; Whittlesey, M. K., *Angew. Chem. Int. Ed.* **2007**, *46,* 6343-6345.

39. Aldeco-Perez, E.; Rosenthal, A. J.; Donnadieu, B.; Parameswaran, P.; Frenking, G.; Bertrand, G., *Science* **2009**, *326,* 556-559.

40. (a) Lavallo, V.; Canac, Y.; DeHope, A.; Donnadieu, B.; Bertrand, G., *Angew. Chem. Int. Ed.* **2005**, *44,* 7236-7239; (b) Lavallo, V.; Canac, Y.; Prasang, C.; Donnadieu, B.; Bertrand, G., *Angew. Chem. Int. Ed.* **2005**, *44,* 5705-5709.

41. Chianese, A. R.; Kovacevic, A.; Zeglis, B. M.; Faller, J. W.; Crabtree, R. H., *Organometallics* **2004**, *23,* 2461-2468.

42. (a) Heckenroth, M.; Neels, A.; Garnier, M. G.; Aebi, P.; Ehlers, A. W.; Albrecht, M., *Chem.-Eur. J.* **2009**, *15,* 9375-9386; (b) Heckenroth, M.; Khlebnikov, V.; Neels, A.; Schurtenberger, P.; Albrecht, M., *Chem. Cat. Chem.* **2011**, *3,* 167-173.

43. Peris, E.; Crabtree, R. H., *Coord. Chem. Rev.* **2004**, *248,* 2239-2246.

44. (a) Kocher, C.; Herrmann, W. A., *J. Organomet. Chem.* **1997**, *532,* 261-265; (b) Albrecht, M.; Crabtree, R. H.; Mata, J.; Peris, E., *Chem. Commun.* **2002**, 32-33.

45. Albrecht, M.; Miecznikowski, J. R.; Samuel, A.; Faller, J. W.; Crabtree, R. H., *Organometallics* **2002**, *21,* 3596-3604.

46. (a) Poyatos, M.; Sanaú, M.; Peris, E., *Inorg. Chem.* **2003**, *42,* 2572-2576; (b) Mata, J. A.; Chianese, A. R.; Miecznikowski, J. R.; Poyatos, M.; Peris, E.; Faller, J. W.; Crabtree, R. H., *Organometallics* **2004**, *23,* 1253-1263.

47. (a) Poyatos, M.; Mata, J. A.; Falomir, E.; Crabtree, R. H.; Peris, E., *Organometallics* **2003**, *22,* 1110-1114; (b) Poyatos, M.; Marquez, F.; Peris, E.; Claver, C.; Fernandez, E., *New. J. Chem.* **2003**, *27,* 425-431.

2.1 Introduction

2.1.1 Ruthenium carbonyl cluster chemistry

The reactivity of the ruthenium carbonyl cluster $Ru_3(CO)_{12}$ has been previously explored with a number of two electron donor ligands including phosphines, arsines and acetonitrile,[1] but until recently there were very few examples with NHCs. Initial studies reported by Lappert and co-workers in 1977 involved the reaction between the enetetramine $(SIEt_2)_2$ and $Ru_3(CO)_{12}$ at an elevated temperature to generate the mono substituted triruthenium cluster complex $Ru_3(SIEt_2)(CO)_{11}$ shown in **Scheme 2.1.1**.[2]

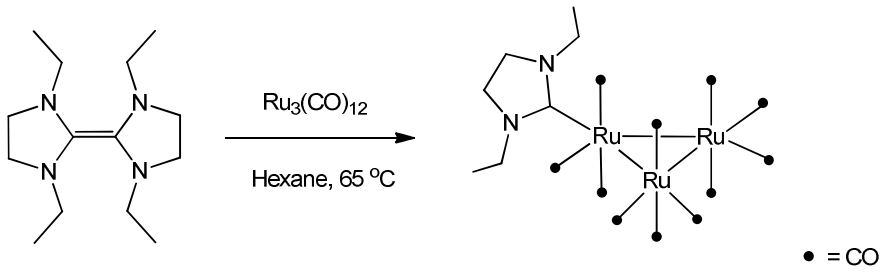

Scheme 2.1.1: Synthesis of $Ru_3(SIEt_2)(CO)_{11}$ from reaction of $(SIEt_2)_2$ and $Ru_3(CO)_{12}$.

This area of research was neglected until 2005 when Cabeza and co-workers reported that $Ru_3(CO)_{12}$ reacted with the *in situ* prepared IMe_2 carbene to give the analogous product, $Ru_3(IMe_2)(CO)_{11}$. In this case, however, double C-H activation of an N-Me group was observed upon mild heating. Remarkably this process could be reversed by simple addition of carbon monoxide at room temperature, as shown in **Scheme 2.1.2**.[3]

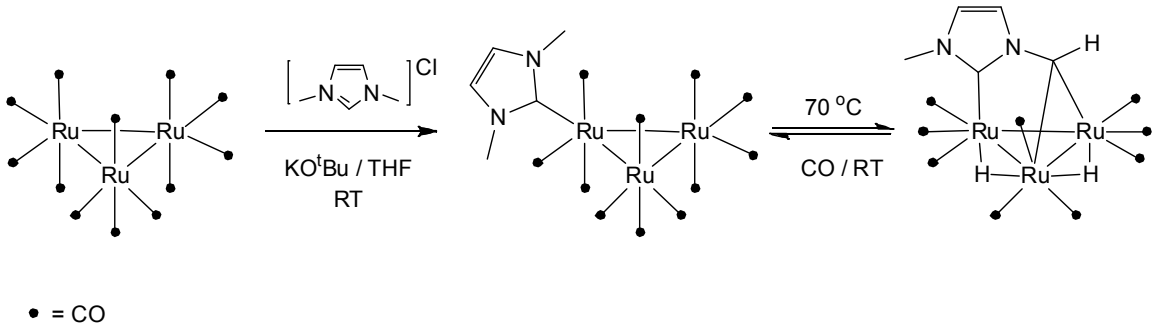

Scheme 2.1.2: The coordination and reversible C-H bond activation of IMe_2.

Cabeza *et. al.* also reported the treatment of $Ru_3(CO)_{12}$ with a single equivalent of IMes to afford $Ru_3(IMes)(CO)_{11}$, whereas the attempted coordination of the bulkier IPr failed even at elevated temperatures. This was rationalised by DFT calculations which suggested a high kinetic barrier to coordination for the larger IPr ligand.[4] In contrast, Bruce and co-workers reported reaction of $Ru_3(CO)_{12}$ with 3 equivalents of both IMes and IPr (Ru_3:NHC), although unlike the observations made by Cabeza, this resulted in the cleavage of the Ru_3 cluster to afford the mononuclear ruthenium tetracarbonyl compounds $Ru(NHC)(CO)_4$.[5] Cleavage of the ruthenium cluster has also been observed by the Whittlesey group with 6 equivalents the small alkyl substituted NHCs IEt_2Me_2, I^iPr_2 and $I^iPr_2Me_2$ although these reactions resulted in the formation of *bis*-NHC tricarbonyl complexes $Ru(NHC)_2(CO)_3$ (**Scheme 2.1.3**).[6]

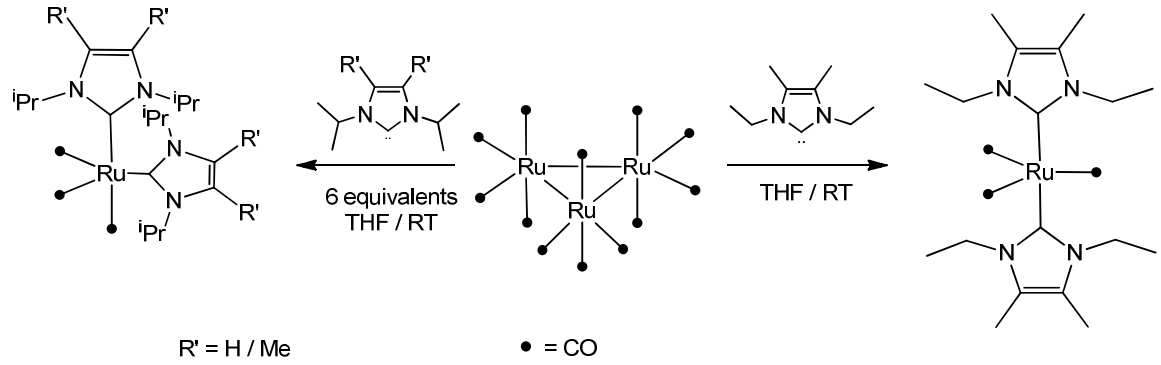

Scheme 2.1.3: The reaction of N-alkyl substituted NHCs with $Ru_3(CO)_{12}$.

Reaction of the more sterically encumbered N-alkyl substituted NHCs I^tBu and IAd with $Ru_3(CO)_{12}$ led to the retention of the Ru_3 core and formation of the abnormally bound NHC complexes $Ru_3(ab\text{-}NHC)(CO)_{11}$ (NHC = I^tBu (**2.1**), IAd (**2.2**)).[7] These compounds were shown to undergo C-H activation at the remaining backbone position upon mild heating as shown in **Scheme 2.1.4** affording complexes of the form $Ru_3(\mu\text{-}H)(dab\text{-}NHC)(CO)_9$ (NHC = I^tBu (**2.3**), IAd (**2.4**)). The observation of the abnormal binding mode can be rationalised by assuming that the approach of the C2 site of the carbene is blocked off by the steric bulk of the N-groups, leading to the NHC binding via the backbone to alleviate steric hindrance round the metal centre.

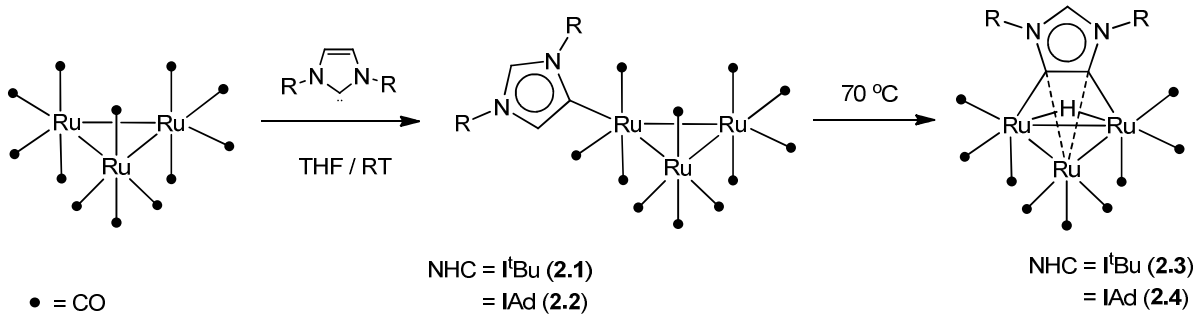

Scheme 2.1.4: Formation of abnormal complexes with bulky NHCs and their subsequent C-H activation.

The C-H activation seen in NHC cluster compounds has been investigated by Cabeza and co-workers by modelling the activation of $M_3(IMe_2)(CO)_{11}$ (M = Ru, Os) by DFT calculations. The activation of both Ru and Os clusters was shown to proceed via a similar mechanistic route. In the first step, the NHC ligand moves from an equatorial to an axial position, increasing the proximity of the N-substituents to the metal centre. After this, thermal decarbonylation, the slowest step, can occur (with a higher barrier for Os), followed by C-H activation to remove the unsaturation of the compound. Although the reactions are generally endothermic, loss of CO makes the reactions essentially irreversible, driving them to completion.[8]

2.1.2 Osmium carbonyl cluster chemistry

Osmium forms complexes which are often analogous to those of ruthenium, but generally require more forcing reaction conditions due to the increased Os-Os and Os-L bond strengths. This is exemplified by the reaction of $Os_3(CO)_{12}$ with IMe_2 which forms $Os_3(IMe_2)(CO)_{11}$ to display the same subsequent double C-H activation as $Ru_3(IMe_2)(CO)_{11}$, but requires heating in toluene at 110 °C.[9]

Another example of Os NHC chemistry has been reported by Cabeza *et. al.* who reacted the coordinatively unsaturated 46-electron cluster $Os_3(\mu\text{-}H)_2(CO)_{10}$ with a variety of NHCs (IMe_2, IPh_2 and IMes). In all three cases the CO substitution product $Os_3(\mu\text{-}H)_2(NHC)(CO)_9$ was generated. However for IMes it was also possible to isolate an addition product $Os_3H(\mu\text{-}H)(IMes)(CO)_{10}$ (**Scheme 2.1.5**). This was rationalised by DFT calculations, which pointed to the formation of the addition product as an intermediate prior to CO loss and the generation of $Os_3(\mu\text{-}H)_2(NHC)(CO)_9$. In the case of IMes, a significantly higher energy barrier was revealed, allowing for the isolation of the addition product alongside $Os_3(\mu\text{-}H)_2(IMes)(CO)_9$.[10]

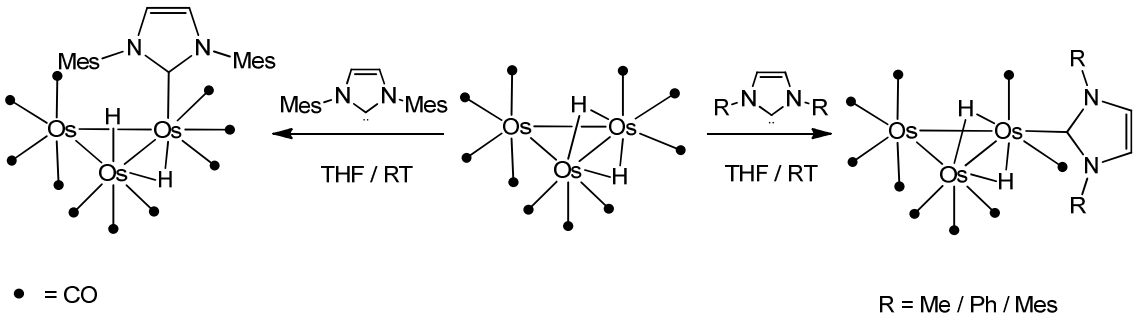

Scheme 2.1.5: The addition and substitution reactions of $Os_3(\mu\text{-}H)_2(CO)_{10}$ with NHCs.

A further example has been published by Clyburne *et. al.* who reported the formation of $Os_4(\mu\text{-}H)_4(IMes)(CO)_{11}$ via transmetalliation of $Os_4(\mu\text{-}H)_4(CO)_{12}$ with IMesAgCl.[11] Subsequent thermolysis of $Os_4(\mu\text{-}H)_4(IMes)(CO)_{11}$ in benzene at 200 °C for 24 h in a high pressure tube afforded two unexpected products. The first was the abnormal isomer $Os_4(\mu\text{-}H)_4(ab\text{-}IMes)(CO)_{11}$, while the second contained an IMes ligand which had undergone the triple C-H activation of a mesityl methyl group along with coupling to a partially dehydrogenated benzene molecule, as shown in **Scheme 2.1.6**.

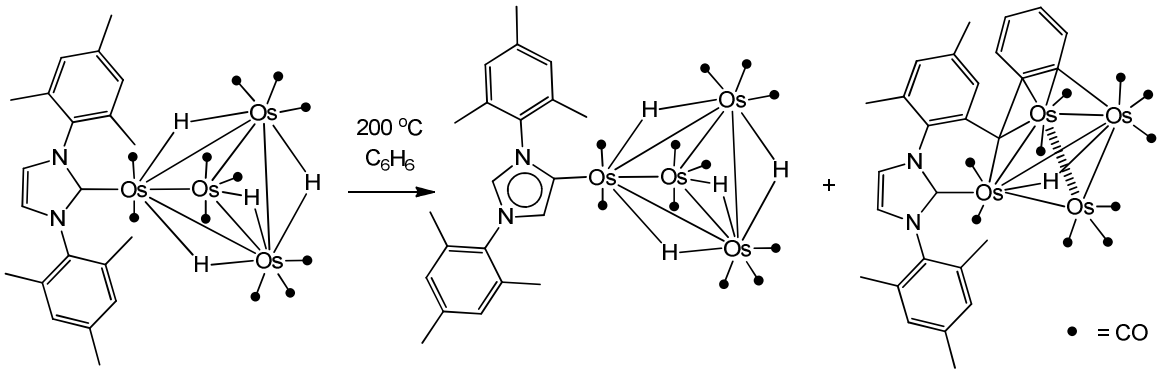

Scheme 2.1.6: C-H bond activation products of $Os_4(\mu\text{-}H)_4(IMes)(CO)_{11}$ upon heating.

2.1.3 Ruthenium clusters in catalysis

For decades, the development of catalytic reactions which involve the cleavage of unreactive C-H bonds has been a subject of considerable interest. The first example of C-H activation was reported in 1962 when naphthalene was found to undergo oxidative addition to $Ru(dmpe)_2$ (dmpe = $Me_2PCH_2CH_2PMe_2$) to give a C-H activated product (**Scheme 2.1.7**).[12]

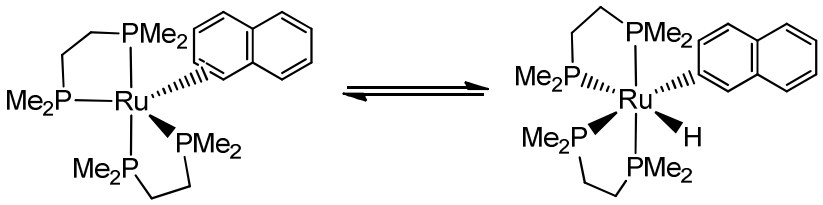

Scheme 2.1.7: The C-H activation of naphthalene.

This observation stimulated research into the catalytic manipulation of C-H bonds. One example has been described by Murai and co-workers who reported the ruthenium catalysed addition of aromatic ketones to a range of alkenes using $RuH_2(PPh_3)_3(CO)$[13] in addition to a number of publications showing chelation-assisted regioselective activation of sp^2 and sp^3 hybridised C-H bonds.[14] Transition metal catalysed carbonylation of C-H bonds provides an efficient method for the incorporation of a carbonyl moiety into an organic molecule. $Ru_3(CO)_{12}$ is especially well suited to carbonylation chemistry, as illustrated in **Scheme 2.1.8**.[15]

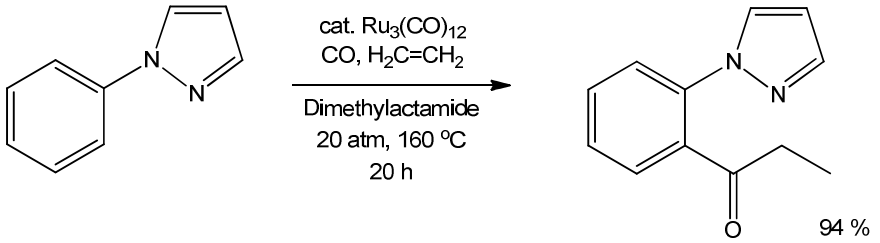

Scheme 2.1.8: Regioselective carbonylation utilising $Ru_3(CO)_{12}$ as a catalyst.

The ruthenium cluster is also an active catalyst for the intermolecular [2+2+1] cyclocoupling of alkenes (or alkynes), ketones and CO shown in **Scheme 2.1.9**. The addition of various phosphine ligands to the solution has been shown to increase the catalytic activity considerably.[16] This effect has also been seen in the $Ru_3(CO)_{12}$ catalysed amination of primary and secondary alcohols,[17] suggesting that there may be an important role for donor ligands within such catalytic reactions. As such, NHCs may find a role within these types of reactions, although to the best of our knowledge, no such investigations have been reported to date.

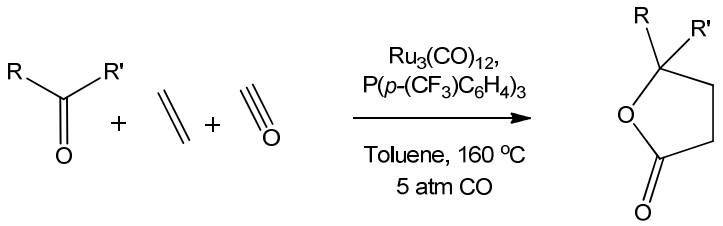

Scheme 2.1.9: [2+2+1] Cyclocoupling reaction catalysed by $Ru_3(CO)_{12}$ and PR_3.

2.2 N-Heterocyclic carbene chemistry with ruthenium carbonyl clusters

2.2.1 Preface

Our interest into this area was initially sparked by the publication detailing the C-H activation of the NHC ligand in $Ru_3(IMe_2)(CO)_{11}$ by Cabeza and co-workers in 2005.[3] Results from our group detailing the reaction of $Ru_3(CO)_{12}$ with a number of 'small' and 'large' NHCs have been summarised in **Scheme 2.1.3** and **2.1.4** respectively.[3,6-7]

We wanted to bridge the gap between large and small NHCs to see how the types of products formed changed with intermediate steric bulk, as well as investigating the reaction of $Os_3(CO)_{12}$ with bulky NHCs to allow a comparison to the ruthenium chemistry. Additionally, we were interested in investigating the catalytic potential of the abnormal complexes **2.1-2.4** which we had prepared (see **Scheme 2.1.4**). It was hoped the increased donor properties of abnormal carbenes would lead to greater catalytic activity in the types of transformations noted earlier for $Ru_3(CO)_{12}$. In all cases the number of equivalents of NHC used in these reactions relates to NHC per M_3 cluster.

2.2.2 Formation of $Ru(IMes)(CO)_4$ (2.5) and $Ru(IMes)_2(CO)_3$ (2.6)

Previous reactions of $Ru_3(CO)_{12}$ with IEt_2Me_2, I^iPr_2 and $I^iPr_2Me_2$ have required 6 equivalents of NHC to achieve full conversion,[6] whereas the formation of an abnormally bound complex with the bulky carbene I^tBu took place with only one.[7a] It was thought that IMes would provide an intermediate example of steric bulk, and thus the ruthenium cluster was reacted with different equivalents of this carbene.

Treatment of $Ru_3(CO)_{12}$ with 1, 2, 3 and 6 equivalents of IMes at room temperature in resealable NMR tubes in THF-d_8 led in all cases to the spontaneous evolution of gas which continued for *ca.* 30 minutes. All of the solutions darkened from light orange to dark red. In the

case of the 1:1, 1:2 and 1:3 reactions, the presence of unreacted $Ru_3(CO)_{12}$ was apparent by IR spectroscopy, whereas no remaining cluster was noted when 6 equivalents of IMes was used. ^1H NMR spectroscopy of the different reaction mixtures revealed that the reactions proceeded in the same manner regardless of the number of equivalents of NHC. It was evident that two IMes containing products in a 1:1 ratio were formed, with two distinct set of resonances seen for the aromatic and backbone C-H protons. Recrystallisation from a saturated THF solution layered with hexane resulted in orange crystals shown by X-ray crystallography shown to be a co-crystallised mixture of $Ru(IMes)(CO)_4$ (**2.5**) and $Ru(IMes)_2(CO)_3$ (**2.6**) (**Figure 2.2.1**). These compounds have been reported previously by the groups Bruce (**2.5**) and Whittlesey (**2.6**).[5, 18]

The $^{13}C\{^1H\}$ NMR spectrum of the co-crystallised **2.5** and **2.6** revealed two distinct resonances for the carbenic carbon (C2) atoms at 179.2 ppm for **2.5** and 186.9 ppm for **2.6** which were assigned by ^1H-$^{13}C\{^1H\}$ HMBC correlation of the C2 carbon and C4/5 protons. The signal for the carbenic carbon of **2.5** had not been previously reported. Whittlesey and co-workers reported the resonance for **2.6** at 186.8 ppm (C_6D_6) similar to the value found in THF-d_8.[18]

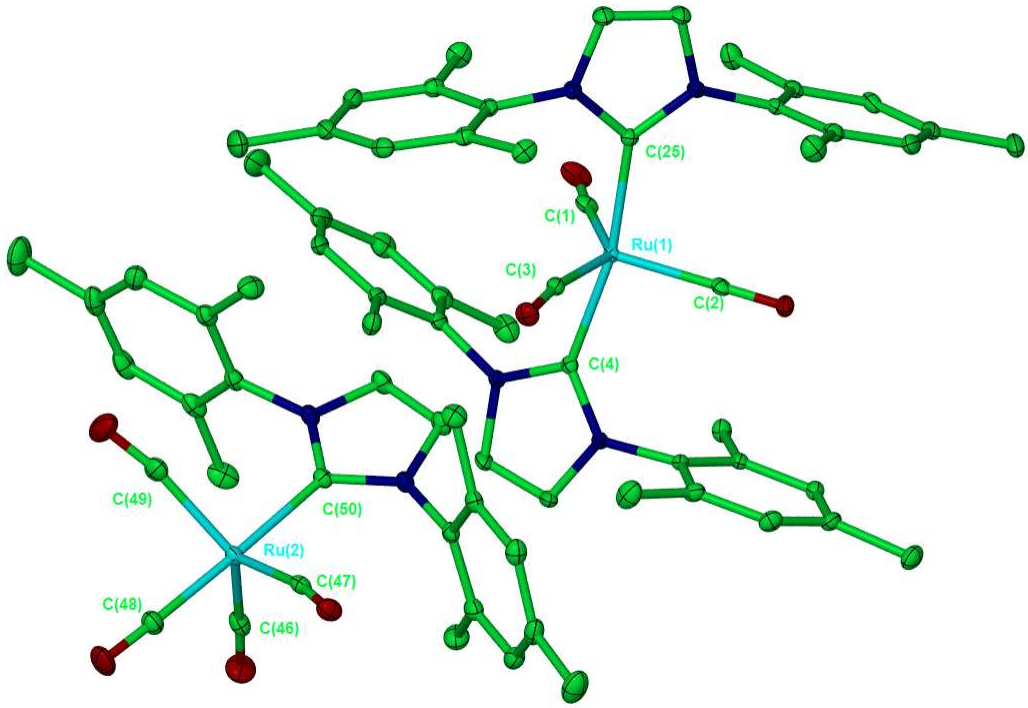

Figure 2.2.1: X-ray crystal structure of co-crystallised **2.5** and **2.6**. Thermal ellipsoids are set at 30% probability. Hydrogen atoms have been omitted for clarity.

Examination of the IR spectrum of a solution containing the mixture of **2.5** and **2.6** in C_6D_6 revealed 7 carbonyl bands (**Table 2.2.1)**. There was a slight deviation between the frequencies of

the carbonyl bands and those for the separate components. It is likely that this discrepancy arose from the different media used to record the IR spectra.

Compound	ν_{CO} / cm^{-1}
2.5 and **2.6**	2047, 2020, 2011, 1986, 1964, 1935, 1919 (C_6D_6)
$Ru(IMes)(CO)_4$	2044, 2007, 1955, 1921 (nujol) [5]
$Ru(IMes)_2(CO)_3$	1950, 1879, 1830 (KBr) [18]

Table 2.2.1: IR data for co-crystallised **2.5** and **2.6** and their individual literature values.

Structural data for co-crystallised **2.5** and **2.6** compares well with that for the individual complexes as shown in **Table 2.2.2**. The data for **2.5** shows that the accommodation of the NHC ligand causes the equatorial OC-Ru-CO angles to become asymmetric, with one large and two smaller angles (123.82(10)° *c.f.* 117.49(9)° and 118.10(10)°). This helps to reduce the interaction between the IMes wingtips and the carbonyl ligands. This effect has also been noted by Bruce and co-workers for $Ru(IPr)(CO)_4$ but to a larger extent, due to the bulkier nature of the IPr ligand.[5]

Complex **2.6** also exhibits considerable asymmetry around the equatorial $Ru(CO)_3$ plane as revealed by the significantly different OC-Ru-CO angles of 105.29(8)°, 117.09(9)° and 137.57(9)°. The asymmetry is amplified by the two IMes ligands in **2.6** compared to **2.5**. This is a feature which has also been observed previously in $Ru(IEt_2Me_2)_2(CO)_3$[6] and $Ru(IMes)(PPh_3)(CO)_3$.[19]

Bond lengths (Å) and angles (°)	Co-crystallised (2.5)	$Ru(IMes)(CO)_4$[5] (2.5)	Co-crystallised (2.6)	$Ru(IMes)_2(CO)_3$[18] (2.6)
$Ru-C_{NHC}$	2.139(2)	2.123(3)	2.1118(19)	2.1093(19)
			2.1177(19)	2.1125(19)
$Ru-C_{CO}$	1.907(2)	1.920(6)	1.903(2)	1.900(3)
	1.925(2)	1.928(6)	1.919(2)	1.927(2)
	1.934(2)	1.954(4)	1.922(2)	1.944(3)
	1.949(3)	1.954(4)		
$C_{CO}-Ru-C_{CO}$	123.82(10)	121.0(2)	137.57(9)	139.56(14)
	117.49(9)	119.33(12)	105.29(8)	109.12(13)
	118.10(10)	119.33(12)	117.09(9)	111.32(12)
$C_{CO/NHC}-Ru-C_{NHC}$	177.97(9)	176.5(2)	168.76(7)	169.16(7)

Table 2.2.2: Selected bond lengths (Å) and bond angles (°) for $Ru(IMes)(CO)_4$ (**2.5**) and $Ru(IMes)_2(CO)_3$ (**2.6**).

2.2.3 Synthesis of Ru_3(ab-IPr)$(CO)_{11}$ (2.7)

Reaction of $Ru_3(CO)_{12}$ with 6 equivalents of IPr in THF-d_8 resulted in an immediate darkening of the orange coloured solution to deep red, although in contrast to the reaction of IMes, no gas was evolved. After 24 h, the solution was examined by ^{1}H NMR spectroscopy, which showed a large quantity of the free NHC and a small amount of an imidazolium side product. The reaction was left at room temperature for a further 4 days and examined again. This time there was evidence for coordination with the appearance of two doublets at 9.21 ppm and 6.53 ppm (J_{HH} = 1.6 Hz) in a 1:1 ratio. The appearance of two such low field doublets is indicative of the formation of an abnormally coordinated NHC, as they arise from the individual proton environments at the C2 and C4/5 positions, as shown in **Table 2.2.3**.

Compound	^{1}H δ of C2/C5 imidazol protons (ppm)
Ru_3(ab-IPr)$(CO)_{11}$ (**2.7**)	6.87 (d, J_{HH} = 1.61 Hz)
	6.50 (d, J_{HH} = 1.61 Hz)[a]
Ru_3(ab-I^{t}Bu)$(CO)_{11}$ (**2.1**)	8.42 (d, J_{HH} = 1.50 Hz)[7a]
	6.43 (d, J_{HH} = 1.50 Hz)[b]
Ru_3(ab-IAd)$(CO)_{11}$ (**2.2**)	8.38 (d, J_{HH} = 2.0 Hz)[7b]
	6.47 (d, J_{HH} = 2.0 Hz)[b]
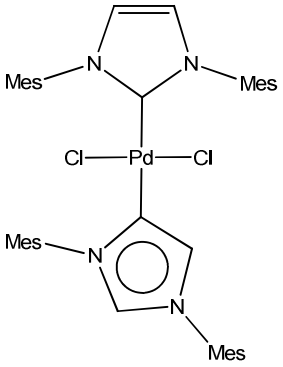	7.47 (d, J_{HH} = 1.70 Hz)[20]
	6.57 (d, J_{HH} = 1.70 Hz)[c]
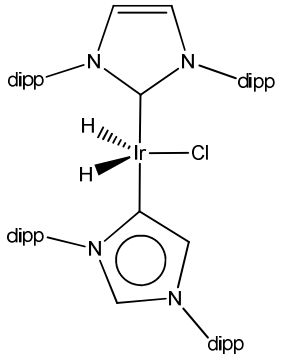	7.13 (s)[21]
	7.10 (s)[a]

Table 2.2.3: The C2/5 ^{1}H NMR resonances of abnormal NHC complexes ([a] C_6D_6, 500/300 MHz. [b] THF-d_8, 500 MHz. [c] $CDCl_3$, 400 MHz).

The product (**2.7**) was isolated by extraction into benzene. A ^{1}H NMR spectrum in C_6D_6 revealed that the doublet resonances had significantly shifted to 6.87 and 6.50 ppm (**Figure 2.2.2**). The extent of this shift prompted us to look for comparable behaviour elsewhere. Both **2.1** and **2.2** exhibit high frequency resonances at 8.42 and 8.38 ppm respectively in THF-d_8 (**Table 2.2.3**), but their poor solubility precluded spectra from being recorded in C_6D_6. The abnormal complex IrH_2Cl(ab-IPr)(IPr) run in C_6D_6 exhibits comparable resonances at 7.10 and 7.13 ppm for the abnormal protons (**Table 2.2.3**), although no data has been reported in THF-d_8.[21]

The effect of counter-ions on the abnormal NHC Ir complex (**Scheme 1.1.4**) provides some clues as to the factors behind these shifts of the C2 proton NMR resonances. Crabtree and co-workers showed that coordinating counter anions interact to better shield the C2 proton i.e. $[Br]^-$

resulted in a higher chemical shift (9.71 ppm) for the C2 proton compared with the less coordinating $[SbF_6]^-$ which led to a value of 8.50 ppm.[22] It seems reasonable to suggest that changing the solvent from THF to C_6D_6 could likewise decrease the shielding of the C2 proton causing the observed changes in frequency.

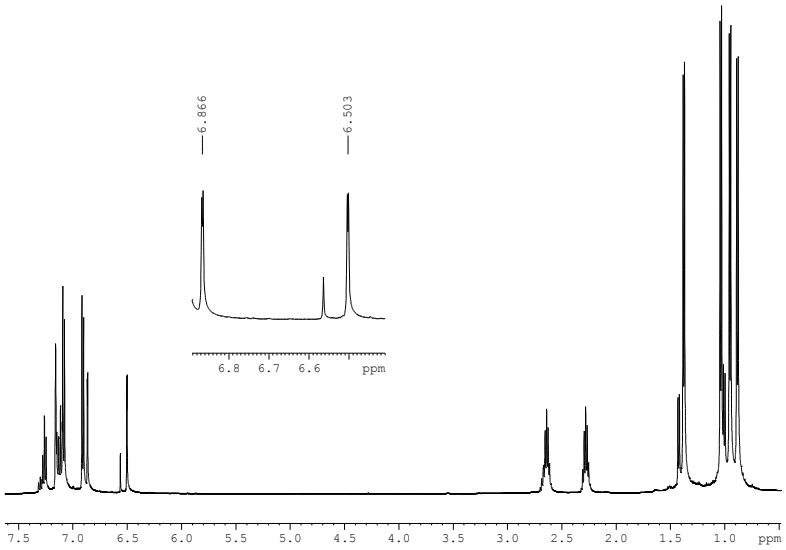

Figure 2.2.2: ^{1}H NMR spectrum of **2.7** (C_6D_6, 298 K, 500 MHz).

Coupling is evident between the C2 and C4/5 protons (J_{HH} = 1.6 Hz) over 4 bonds of the imidazol in **2.7**, an effect aided by aromaticity of the ring, and is illustrated in the ^{1}H-^{1}H COSY spectrum, shown in **Figure 2.2.3**.

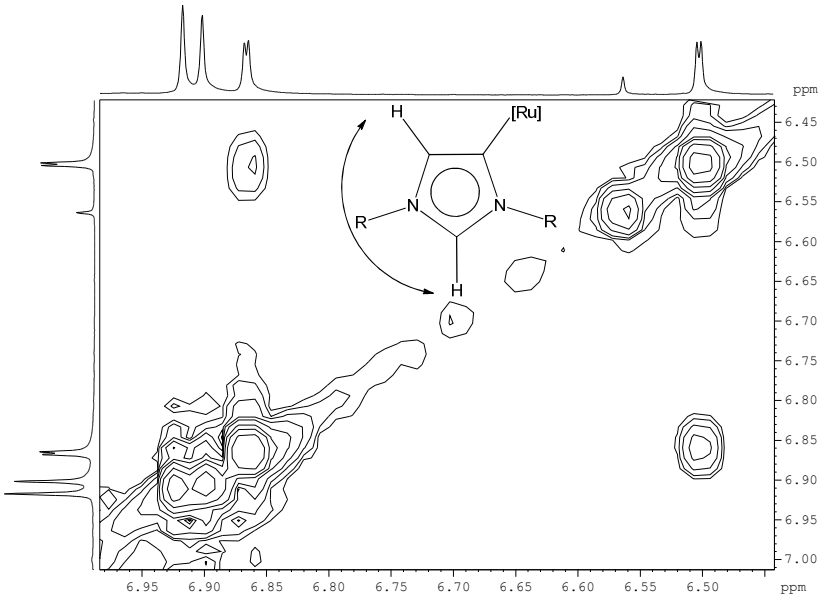

Figure 2.2.3: COSY spectrum of **2.7** (C_6D_6, 298 K, 500 MHz).

Additional evidence for the formation of an abnormally coordinated compound comes from the comparison of $^{13}C\{^1H\}$ NMR resonances and IR carbonyl stretches. The $^{13}C\{^1H\}$ NMR resonances for **2.7** were assigned via PENDANT, ^1H-$^{13}C\{^1H\}$ HMQC and HMBC experiments. The pertinent resonances are at 147.8 ppm for the abnormal carbenic carbon and at 136.6 and 133.3 ppm for imidazol C-H carbons. The resonance for the abnormal carbene is comparable to reported values for abnormal carbenes as stated in a review by Arnold *et. al.*; most abnormal NHCs shifts are located in the region of 140 ppm, with normal NHC shifts typically at higher frequency.[23] Further comparison can be made to the $^{13}C\{^1H\}$ NMR and IR data for **2.1**, **2.2**, $Ru_3(IMe_2)(CO)_{11}$ and $Ru_3(SIEt_2)(CO)_{11}$ as shown in **Table 2.2.4**.[2-3, 7a]

Compound	Ru-C_{NHC} (δ)	ν_{CO} / cm^{-1}
Ru_3(ab-IPr)$(CO)_{11}$ (**2.7**)	147.8[a]	2047-1921[a]
Ru_3(ab-I^{t}Bu)$(CO)_{11}$ (**2.1**)[7a]	134.1[b]	2085-1943[b]
Ru_3(ab-IAd)$(CO)_{11}$ (**2.2**)[7b]	132.2[c]	2085-1947[c]
$Ru_3(IMe_2)(CO)_{11}$ [3]	204.9[d]	2093-1949[d]
$Ru_3(SIEt_2)(CO)_{11}$ [2]	198.6[e]	2096-1950[e]

Table 2.2.4: Ru-C_{NHC} chemical shifts and IR bands of selected Ru_3-NHC compounds [a] C_6D_6, [b] THF-d_8, KBr. [c] THF-d_8, nujol. [d] CDCl, CH_2Cl_2. [e] tol-d_8, hexane.

This table shows that **2.1**, **2.2** and **2.7** have lower C_{NHC} chemical shifts as well as marginally lower frequency carbonyl bands compared with the two 'normal' NHC compounds, consistent with the stronger σ donating ability of abnormal NHCs.[23-24] Unfortunately attempts to grow X-ray quality crystals of **2.7** from a range of solvents failed and therefore no structural characterisation was obtained.

2.2.4 Comparison of the reactivity observed for IMes and IPr to the literature

During the course of this work the reactivity of $Ru_3(CO)_{12}$ towards both IMes and IPr was reported by Cabeza and Bruce. Cabeza isolated $Ru_3(IMes)(CO)_{11}$ and $[IPrH]_2[Ru_6(\mu_3\text{-}CO)_2(\mu\text{-}CO)_2(CO)_{14}]$,whilst Bruce generated **2.5** and $Ru(IPr)(CO)_4$.[4-5]

The mononuclear products seen by Bruce and co-workers can be attributed to the manner in which the reactions were carried out. Due to the low solubility of $Ru_3(CO)_{12}$ in THF, Bruce ensured that the cluster was fully dissolved before the addition of a separate solution of carbene. This was achieved by the use of 20 mL of THF for 135 mg of $Ru_3(CO)_{12}$ to ensure that the reaction was carried out in a true 1:3 Ru_3:NHC ratio, and facilitated the formation of $Ru(NHC)(CO)_4$ as the

major product of both the IMes and IPr reactions. In contrast, our synthesis of complexes **2.5**, **2.6** and **2.7** was achieved in the presence of a large excess of NHC as a typical reaction involved the use of 100 mg of $Ru_3(CO)_{12}$ in approximately 5 mL of THF. As a consequence, the cluster would not be fully dissolved in the solvent, and the reaction would always proceed with an excess of carbene.

The compounds isolated by Cabeza vary as do the reaction conditions. In the case of IMes, this was generated *in situ* from the reaction of [IMesH]Cl and KO^{t}Bu before addition of a single equivalent of $Ru_3(CO)_{12}$. As a result, traces of KO^{t}Bu, KCl and ^{t}BuOH were present in the reaction mixture; this may have had an effect on the product of the reaction. For the reaction with IPr, Cabeza and co-workers used the free isolated NHC, so there would be no influence from side products. They reported a reaction time of only 4 h at room temperature. After this same time, we also observed only the formation of the imidazolium species $[IPrH]_2[Ru_6(\mu_3\text{-}CO)_2(\mu\text{-}CO)_2(CO)_{14}]$ which was proposed to arise from the reaction of $Ru_3(CO)_{12}$ and IPr in the presence of adventitious moisture in the reaction mixture. However, by allowing the reaction to continue at room temperature for several days we were able to isolate **2.7**.

The long reaction time needed for the formation of **2.7** could be rationalised by the steric bulk of the 2,6-diisopropyl substituents which impeded the approach of the carbene to the ruthenium centre. However examination of the steric properties of IPr compared to I^{t}Bu using the $\%V_{Bur}$ model indicate that IPr is less bulky than I^{t}Bu (**Table 2.2.5**), with the latter forming the abnormal compound at room temperature in only 2 h.

Ligand	$\%V_{Bur}$
I^{t}Bu	36.0*, 37.7†
IPr	34.2*, 35.2†

Table 2.2.5: $\%V_{Bur}$ values for M-NHC length at 2.00 Å from (NHC)AuBr$_3$* and (NHC)Pd(η^3-allyl)Cl†.[25]

2.2.5 Formation of Os_3(ab-I^{t}Bu)$(CO)_{11}$ (2.8)

Following the formation of **2.1** we sought to investigate if such reactivity was restricted to ruthenium. Reaction of $Os_3(CO)_{12}$ and I^{t}Bu in a 1:1 Os_3:NHC ratio at room temperature in THF-d_8 was therefore attempted. After 1 hour, a ^{1}H NMR spectrum showed that no reaction had taken place. Subsequent heating of the solution at 70 °C for 5 h (after degassing via the freeze-pump-thaw technique) led to the appearance of characteristic low field doublets at 8.38 and 6.73 ppm (J_{HH} = 1.9 Hz) for the imidazol protons, suggesting the formation of an abnormally coordinated NHC

complex. This was confirmed by X-ray crystallography to be Os_3(ab-I^{t}Bu)$(CO)_{11}$ (**2.8**) shown in **Figure 2.2.4**.

As for **2.7**, the $^{13}C\{^1H\}$ NMR resonances of **2.8** were easily assigned through the use of ^1H-$^{13}C\{^1H\}$ HMQC/HMBC spectroscopy; the significant resonances were found at 136.5, 132.2 ppm for the two C-H carbon atoms of the imidazol ring and 113.5 ppm for the abnormal carbenic carbon. The signal for the carbenic carbon is comparable to that in the analogous complex Os_3(ab-Ad)$(CO)_{11}$ (**2.9**, **Table 2.2.6),** but is at lower frequency than a range of Os ab-NHC complexes as well as the ruthenium complexes **2.7** (147.8 ppm) or **2.1** (134.1 ppm).[7b, 11, 26] **Table 2.2.6** summarises the M-C_{NHC} resonances and IR carbonyl stretches for all the ruthenium and osmium cluster abnormal complexes.

Compound	M-C_{NHC} (δ)	ν_{CO} / cm^{-1}
Ru_3(ab-I^{t}Bu)$(CO)_{11}$ (**2.1**)	134.1[a]	2085-1943[c]
Ru_3(ab-IPr)$(CO)_{11}$ **(2.7)**	147.8[b]	2047-1921[b]
Os_3(ab-I^{t}Bu)$(CO)_{11}$ **(2.8)**	113.5[a]	2093-1923[d]
Os_3(ab-IAd)$(CO)_{11}$[7b] (**2.9**)	111.6[a]	2094-1927[d]

Table 2.2.6: M-C_{NHC} $^{13}C\{^1H\}$ NMR and IR bands for M_3(ab-NHC)$(CO)_{11}$ (M = Ru/Os). [a] THF-d_8,. [b] C_6D_6. [c] KBr. [d] nujol.

Table 2.2.7 displays the important metrics for **2.8** as well as Os_3(ab-IAd)$(CO)_{11}$ (**2.9**).[7b] Examination of the Os-Os bond lengths in **2.8** show that the Os(2)-Os(3) bond (see **Figure 2.2.4**) is longer than the remaining two (2.9054(3) Å compared with 2.8658(3) and 2.8773(3) Å). This is likely to be due to the steric interaction between the NHC ligand and the carbonyl group situated on Os(3). This bond elongation impacts on the Os-Os angles so that the Os(2)-Os(1)-Os(3) angle is the largest. This effect is also seen in **2.9** although it is less obvious with smaller differences observed between the Os-Os distances *e.g.* Os(2)-Os(3): 2.9051(8) Å vs. Os(1)-Os(2): 2.8831(8) Å.

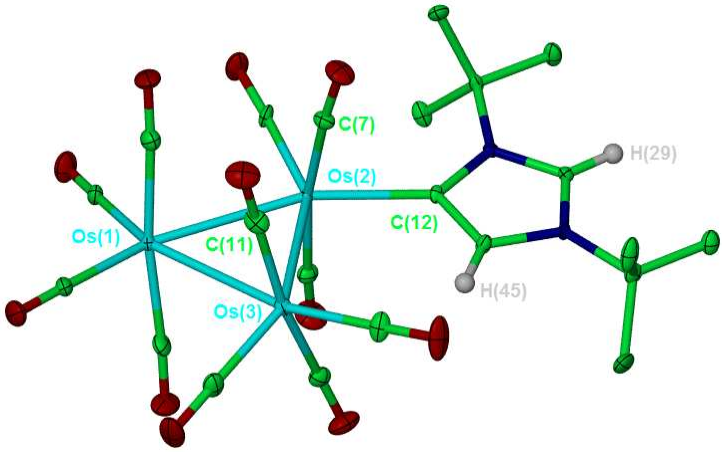

Figure 2.2.4: X-ray structure of **2.8**. Thermal ellipsoids are set at 30% probability. All hydrogen atoms except for those on the imidazol ring have been omitted for clarity.

Bond length (Å) / angle (°)	Os_3(ab-I^{t}Bu)(CO)$_{11}$ (2.8)	Os_3(ab-IAd)(CO)$_{11}$ (2.9)[7b]
Os(2)-C(12)	2.161(6)	2.128(12)
Os(1)-Os(2)	2.8658(3)	2.8831(8)
Os(1)-Os(3)	2.8773(3)	2.8911(5)
Os(2)-Os(3)	2.9054(3)	2.9051(8)
Os(1)-Os(3)-Os(2)	59.413(8)	59.66(2)
Os(1)-Os(2)-Os(3)	59.806(8)	59.930(13)
Os(2)-Os(1)-Os(3)	60.781(8)	60.41(2)

Table 2.2.7: The bond lengths (Å) and angles (°) for **2.8** and **2.9**.

The crystal structures of **2.1**, **2.8** and **2.9** show that in each case the 'abnormal' NHC ligand occupies a site in the equatorial plane of the M_3 rings which is the expected geometry for M_3(NHC)(CO)$_{11}$ complexes as this arrangement minimises steric interactions.[27] The M-C_{NHC} bond lengths for **2.1**, **2.8** and **2.9**[7b] are all the same within experimental error. In addition these bond lengths are comparable to those in Os_4(μ-H)$_4$(ab-IMes)(CO)$_{11}$[11] and [OsH_5(ab-IMes)(P^{i}Pr$_3$)$_2$]BPh_4[26] as shown in **Table 2.2.8**.

Compound	M-C_{NHC} bond length (Å)
Os_3(ab-I^{t}Bu)$(CO)_{11}$ **(2.8)**	2.161(6)[7b]
Ru_3(ab-I^{t}Bu)$(CO)_{11}$ **(2.1)**	2.151(2)[7a]
Os_3(ab-IAd)$(CO)_{11}$ **(2.9)**	2.128(12)[7b]
$Os_4(\mu\text{-H})_4$(ab-IMes)$(CO)_{11}$	2.123(6)[11]
$[OsH_5$(ab-IMes)$(P^iPr_3)_2]BPh_4$	2.120(4)[26]

Table 2.2.8: Comparison of M-C_{NHC} bond lengths in 'abnormal' Ru and Os NHC complexes.

A major difference between **2.8** and **2.9** is in the angle between the plane of the M_3 core and the imidazol ring (**Figure 2.2.5**). For **2.8** the angle is acute (9.1°), whereas it is much larger in **2.9** (36.7°). The twisting between these planes is believed to reduce the steric interactions between the carbonyl ligands and the abnormal carbene, and as such the bulkiest ligand IAd exhibits the largest angle. In all cases, the steric bulk of the 'abnormal' NHC pushes the geminal equatorial CO of the M_{NHC} group away from the ligand to a similar extent: **2.8**; 108.0(3)° and **2.9**; 107.7(5)° (C_{NHC}-Ru-CO angle).

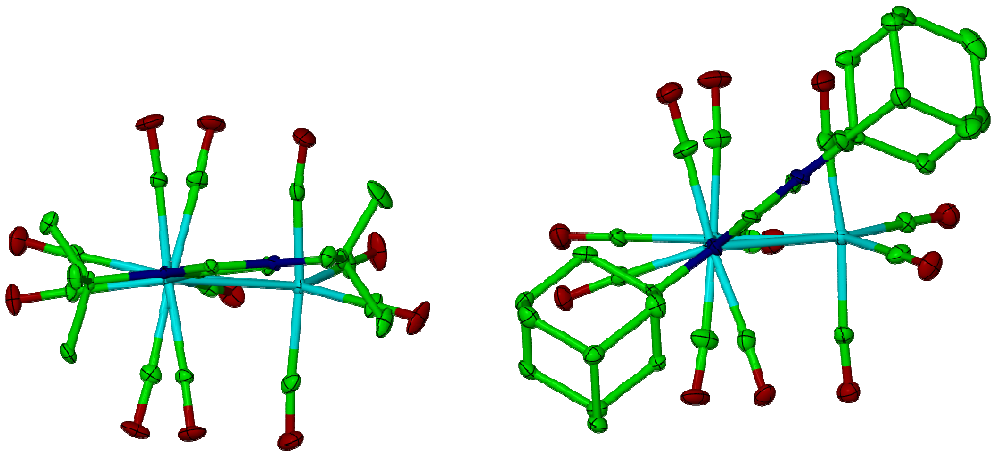

Os_3(ab-I^{t}Bu)$(CO)_{11}$ (**2.8**) Os_3(ab-IAd)$(CO)_{11}$ (**2.9**)

Figure 2.2.5: The variation of the M_3-imidazole twist viewed along the C_{NHC}-M bond.

2.2.6 C-H activation of Ru_3(ab-IPr)$(CO)_{11}$ (2.7) and Os_3(ab-I^{t}Bu)$(CO)_{11}$ (2.8)

The activation of abnormal complexes as shown in **Scheme 2.2.1** can be conveniently followed by ^{1}H NMR spectroscopy by monitoring the loss of the C2 and C5 ($\mathbf{H_a}$ and $\mathbf{H_b}$) protons. These appear in ^{1}H NMR spectra as doublets at approximately 9 and 6 ppm. As the activation

progresses, new signals corresponding to the C2 proton (**Hc**) and the bridging hydride (**H$_d$**) become apparent at approximately 9 and -19 ppm respectively.

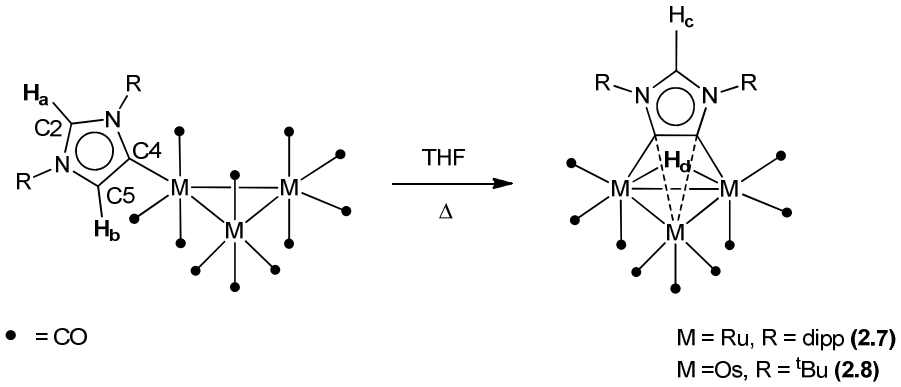

Scheme 2.2.1: Double activation of abnormal carbenes.

The activation of **2.7** took place upon heating in THF-d_8 at 70 °C. A decrease in intensity of doublets in the ^{1}H NMR spectrum at 9.21 and 6.53 ppm (**H$_a$** and **H$_b$**) was accompanied by the appearance of singlets at 9.44 and -19.55 ppm (**H$_c$** and **H$_d$**). The new C4/C5 quaternary carbon resonances were identified by ^{1}H-^{13}C{^{1}H} HMQC and HMBC experiments from the correlation between **H$_c$**, the C2 carbon at 152.2 ppm and the C4/5 carbons at 146 ppm. These signals are somewhat higher in frequency than the resonances seen for Ru_3(ab-I^{t}Bu)(CO)$_{11}$ (144 and 139 ppm for C2 and C4/5 respectively). Heating at 70 °C was required for 72 h to achieve near full conversion, whereas the activation of **2.1** occurred after only 12 h at 50 °C. Despite extended attempts to afford X-ray quality crystals of the activated product to confirm the molecular structure were unsuccessful.

Heating **2.8** at 70 °C in THF-d_8 for extended periods of time did not afford any activation products. Therefore **2.8** was heated in pyridine-d_5 (because of poor solubility in toluene) at 120 °C for several hours. This led to the appearance of signals at 8.93 ppm (**H$_c$**) and -18.10 ppm (**H$_d$**) in a 1:1 ratio, as well as the disappearance of **Ha** and **H$_b$** at 8.53 and 6.93 ppm as shown in **Figure 2.2.6**. It was clear that the reaction also gave a number of imidazolium side products and that C-H activation was only occurring in low yield. This thwarted efforts to record either good quality ^{13}C{^{1}H} NMR data or to isolate clean product for elemental analysis. Similar observations were made by Crittall *et. al*. upon the attempted activation of **2.9**.[7b]

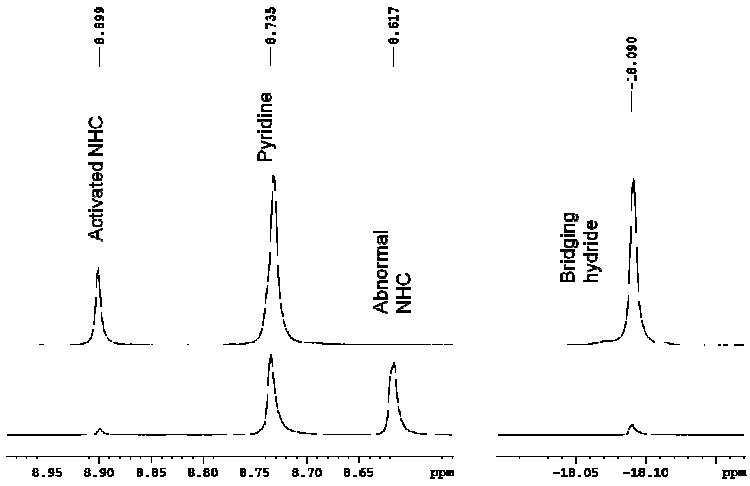

Figure 2.2.6: ^{1}H NMR spectra showing C-H activation of **2.8**; spectrum below before heating, spectrum above after heating at 120 °C, 5 hours (298 K, 500 MHz, pyridine-d_5).

2.2.7 Reaction of Ru_3(ab-I^{t}Bu)$(CO)_{11}$ (2.1) with H_2

The reactivity of **2.1** was investigated with H_2 in THF-d_8 and shown to proceed cleanly at room temperature to give complete conversion to an imidazolium product. ^{1}H NMR spectroscopy showed the formation of signals at 8.88 and 7.91 ppm for the imidazolium protons and a bridging hydride at -12.56 ppm. Upon crystallisation from THF/hexane, the compound was structurally characterised as [I^{t}BuH][Ru_3(μ-H)(μ-CO)$(CO)_{10}$] shown in **Figure 2.2.7**. This anion has been previously characterised as a range of salts.[28]

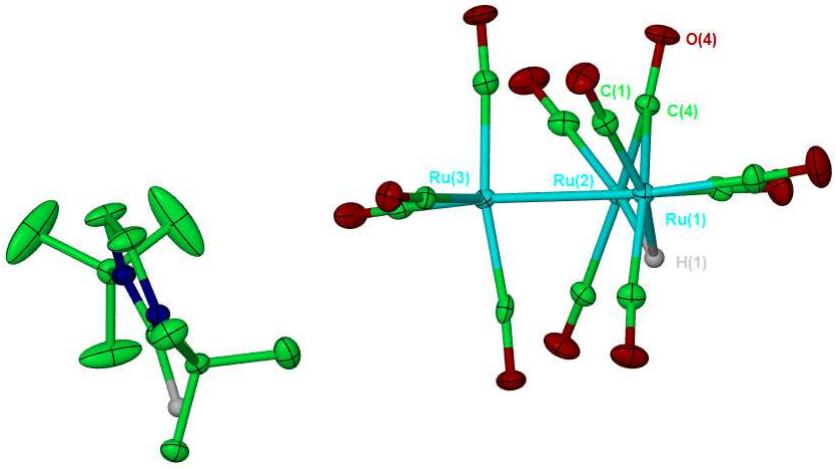

Figure 2.2.7: Crystal structure of [I^{t}BuH][Ru_3(μ-H)(μ-CO)$(CO)_{10}$] with thermal ellipsoids set at 30% probability and hydrogen atoms (except imidazol and hydride protons) omitted for clarity.

Reaction of **2.1** with D_2 was used to confirm the positions of hydrogen addition; **Figure 2.2.8** shows the ^{1}H NMR spectra recorded upon addition of both H_2 and D_2. On reaction with H_2, imidazolium (**H_a**, **H_b**) and hydride (**H_c**) resonances were shown to integrate in a 1:2:1 ratio, whereas on reaction with D_2, a 1:1:0 ratio of signals was revealed. The decrease in signal intensity for **H_b** and **H_c** confirmed deuterium incorporation at these positions.

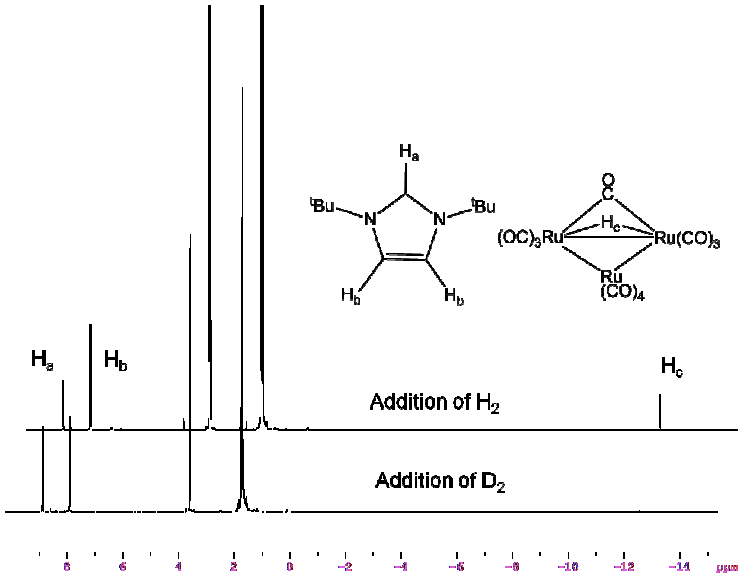

Figure 2.2.8: ^{1}H NMR spectra recorded upon the addition of H_2 and D_2 to **2.1** (298 K, 500 MHz, THF-d_8).

A similar reaction has previously been reported between H_2 and **2.3**.[7a] However unlike the previous example with **2.1**, the reaction required prolonged heating at 50 °C for 40 h to generate the tetra-nuclear imidazolium complex [I^{t}BuH][Ru_4(μ-H)$_3$(CO)$_{12}$] (**Scheme 2.2.2**).[7a]

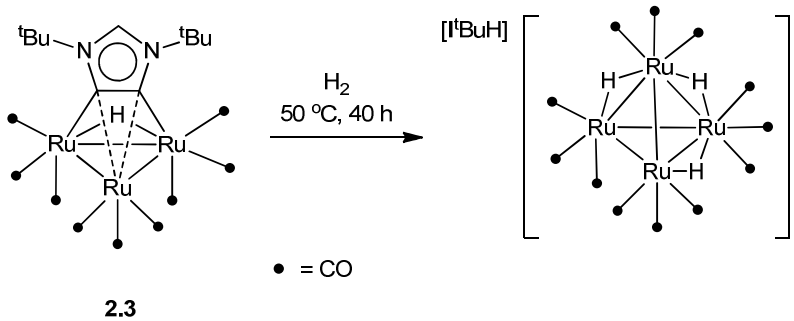

2.3

Scheme 2.2.2: The thermolysis of **2.3** with H_2 to afford [I^{t}BuH][Ru_4(μ-H)$_3$(CO)$_{12}$].

2.3 Saturated 5/6 membered carbenes

2.3.1 Introduction

The reactivity of NHCs and ruthenium clusters to date has been restricted to unsaturated carbenes, with the sole exception of $SIEt_2$ described by Lappert and discussed in the Introduction.[2] Most saturated 5-membered NHCs are restricted to N-aryl systems apart from the sterically bulky SI^{t}Bu as less sterically encumbered saturated N-alkyl carbenes readily dimerise.[29] We decided to investigate the reactivity of the bulky NHC SIPr along with the saturated 6-membered carbenes 6^{i}Pr$_2$ and 6*o*-Tol. We postulated that these should lead to the formation of compounds with different coordination chemistry compared with their unsaturated analogues, given that abnormal binding should not be possible.

2.3.2 Reaction of $Ru_3(CO)_{12}$ and SIPr

A J. Young's NMR tube containing $Ru_3(CO)_{12}$, three equivalents of SIPr·C_6F_5H and THF-d_8 was heated at 60 °C for 4 h affording a dark green solution. ^{1}H NMR spectroscopy confirmed the formation of free SIPr by the appearance of a multiplet at 5.8 ppm corresponding to the released C_6F_5H. From IR spectroscopy it was observed that three equivalents of SIPr·C_6F_5H were required to react all of the cluster starting material, suggesting that the reaction proceeded with cleavage of the ruthenium cluster, possibly generating $Ru(SIPr)(CO)_4$. This was supported by the IR spectrum of the reaction mixture which exhibited carbonyl bands at 2000, 1983, and 1958 cm^{-1}. For comparison, Bruce and co-workers reported bands at 2044 and 1936 cm^{-1} for $Ru(IPr)(CO)_4$ and at 2044, 2007, 1955 and 1921 cm^{-1} for $Ru(IMes)(CO)_4$.[5] A ^{1}H-^{13}C{^{1}H} HMBC correlation experiment provided evidence for a carbenic carbon resonance at 213.5 ppm, the high frequency signal being expected for a saturated NHC ligand.[2,18b] Attempts to isolate the product by extraction into benzene and recrystallisation from hexane at -30 °C resulted in a colour change of the solution from green to a pale yellow, even though no change was apparent by proton spectroscopy. Crystals slowly appeared from the hexane solution over 7 days, but surprisingly, X-ray crystallography revealed that the compound was not a ruthenium containing species, rather the N-formyl-N,N'-*bis*(diisopropylphenyl)ethylenediamine shown in **Figure 2.3.1**.

This structure was confirmed by ^{1}H NMR which revealed a high frequency signal at 8.23 ppm and a broad peak at 3.62 ppm corresponding to the aldehydic and NH protons. ^{13}C{^{1}H} NMR revealed a signal at 163.8 ppm, and no quaternary carbenic carbon resonance at 213.5 ppm. The product can also be observed by IR spectroscopy by signals at 2965 and 1680 cm^{-1} assigned to NH and aldehydic CO stretching frequencies.

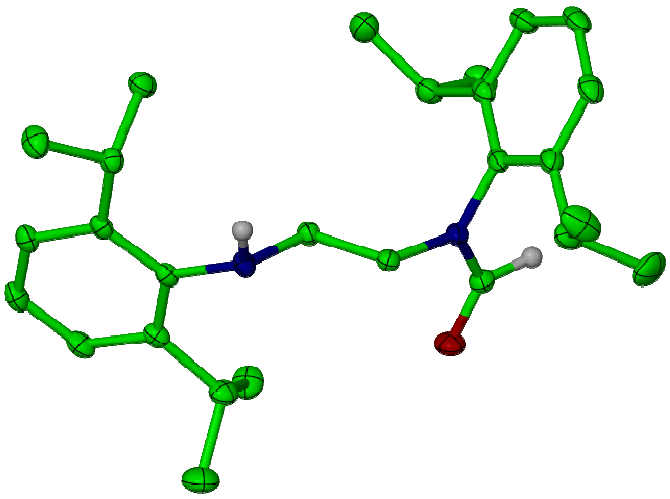

Figure 2.3.1: Crystal structure of the ring opened decomposition product of SIPr. Thermal ellipsoids are set to 30% probability and hydrogen atoms (except amino and aldehydic protons) omitted for clarity.

Comparable ring opening of free SI^{t}Bu by water was first reported by Denk in 2001.[29] During the course of writing this thesis, the SIPr decomposition product was described by Hechaev and co-workers upon reaction of Cu(SIPr)$(OAc)_2$ with wet chloroform over the course of 2 h at room temperature.[30] This feature of free NHCs has been recently investigated by Hollóczki *et. al.*[31] They showed that the reaction of I^{t}Bu, IMe_2 and IPr with excess H_2O led to the formation of an imidazolium-hydroxide product; in contrast, the reaction with traces of H_2O gave the ring opened product shown in **Scheme 2.3.1**. It was noted that the hydrolysis of saturated NHCs by trace amounts of water is significantly faster than for their unsaturated analogues *i.e.* the complete hydrolysis of a saturated carbene can occur instantaneously whereas a full 3 months was needed for an unsaturated NHC.

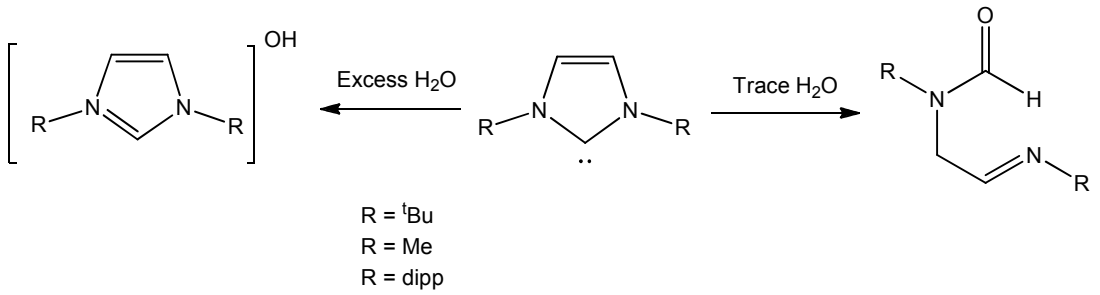

Scheme 2.3.1: The hydrolysis products of an unsaturated NHC.

This would suggest that the decomposition of the SIPr complex is caused by the reaction with adventitious water, although extended efforts to ensure that the solvent contained absolutely no water failed to stop the ring opening from occurring.

2.3.3 Synthesis of $Ru_3(6^iPr_2)(\mu\text{-}CO)_2(CO)_8$ (2.10)

Reaction of two equivalents of *in-situ* generated 6^iPr_2 with $Ru_3(CO)_{12}$ in THF led to the formation of a deep red solution.[32] The reaction mixture was reduced to dryness and the product was extracted with hexane.[33] The proton spectrum of the filtrate showed the presence of a 6^iPr_2 containing product by the presence of isopropyl resonances at 3.58, 1.35 and 1.21 ppm, and no hydride resonances were detected at frequencies as low as -40 ppm. The $^{13}C\{^1H\}$ NMR spectrum revealed the presence of a carbenic carbon signal at 198.7 ppm consistent with other saturated and ring expanded NHC complexes (*c.f.* $Ru_3(SIEt_2)(CO)_{11}$: 198.6 and $Ru(6Mes)(PPh_3)(CO)HF$: 211.8 ppm).[2, 34] The IR spectrum was very informative, revealing 6 carbonyl bands between 2084 and 1968 cm^{-1} and, most indicatively, a bridging carbonyl stretch at 1792 cm^{-1}. X-ray quality crystals were grown from a saturated solution of hexane at -30 °C and were shown to be the coordinatively unsaturated 46-electron cluster complex $Ru_3(6^iPr_2)(\mu\text{-}CO)_2(CO)_8$ (**2.10**) shown in **Figure 2.3.2**. A search for any possible hydride ligands was conducted using HYDEX, which is a quantitative method for indirectly locating hydride ligands bound to metal clusters.[35] This programme failed to locate any hydride ligands confirming the compound as the first example of a 46-electron ruthenium cluster.

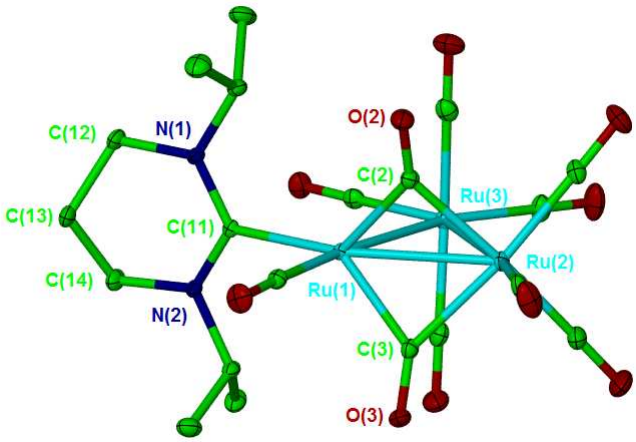

Figure 2.3.2: Crystal structure of $Ru_3(6^iPr_2)(\mu\text{-}CO)_2(CO)_8$ (**2.10**). Thermal ellipsoids are set at 30% probability, hydrogen atoms have been omitted for clarity.

The structure of **2.10** is evidently a balance between alleviation of the steric bulk with bridging carbonyls and the need to stabilise the coordinatively unsaturated 16-electron metal centre, as suggested by the asymmetry in the molecule. For example, the bridging carbonyl groups are evidently pulled closer to Ru(1) possessing the shorter Ru(1)-C(2/3) bond lengths of 1.9791(19) and 2.0128(19) Å compared with those of Ru(2)-C(2/3) (2.1252(2) and 2.118(2) Å) (**Table 2.3.1**). The unsaturated nature of the metal centre also results in significant shortening of the Ru(1) terminal CO group, which exhibits a bond length of 1.873(2) Å compared with the other equatorial carbonyl ligands: 1.929(2), 1.909(2) and 1.951(2) Å. The asymmetry of the Ru_3 core is demonstrated by the difference in Ru-Ru bond lengths across the Ru_3 core. For instance, the Ru(1)-Ru(2/3) bond distances (2.7287(2) and 2.8020(2) Å respectively) are significantly shorter than the Ru(2)-Ru(3) interaction (2.8815(2) Å). Despite these effects, the Ru-NHC bond length of 2.1178(17) Å is comparable to those in $Ru_3(IMes)(CO)_{11}$ (2.144(3) Å) and $Ru_3(IMe_2)(CO)_{11}$ (2.115(4) Å).[3, 8]

Bond length (Å) / Angle (°)	**$Ru_3(6^iPr_2)(\mu\text{-}CO)_2(CO)_8$ (2.10)**
Ru(1)-C(11)	2.1178(17)
Ru(1)-Ru(2)	2.7287(2)
Ru(1)-Ru(3)	2.8020(2)
Ru(2)-Ru(3)	2.8815(2)
Ru(1)-C(2)	1.9791(19)
Ru(1)-C(3)	2.0128(19)
Ru(2)-C(2)	2.1252(2)
Ru(2)-C(3)	2.118(2)
Ru(1)-C(2)-Ru(2)	82.64(7)
Ru(1)-C(3)-Ru(2)	83.25(7)
Ru(1)-Ru(3)-Ru(2)	57.290(5)
Ru(1)-Ru(2)-Ru(3)	60.019(5)
Ru(2)-Ru(1)-Ru(3)	62.692(6)

Table 2.3.1: Selected bond lengths (Å) and angles (°) for **2.10**.

As seen previously, the carbene ligand in **2.10** also lies in the equatorial plane of the M_3 core, however the twist between the M_3 core and the heterocyclic ring of the carbene is much greater (87.34°) than in the other $Ru_3(NHC)(CO)_{11}$ species shown in **Table 2.3.2**. As a consequence, the N-substituents of the NHC lie in the same plane as the axial carbonyl ligands. The inherent steric strain of this conformation may be somewhat alleviated by the formation of bridging carbonyl ligands.

Complex	Ru_3 plane versus imidazole plane (°)
Ru_3(ab-I^{t}Bu)$(CO)_{11}$ (**2.1**)	9.8[7a]
Ru_3(IMes)$(CO)_{11}$	37.69[4]
Ru_3(6^{i}Pr$_2$)(μ-CO)$_2(CO)_8$ (**2.10**)	87.34

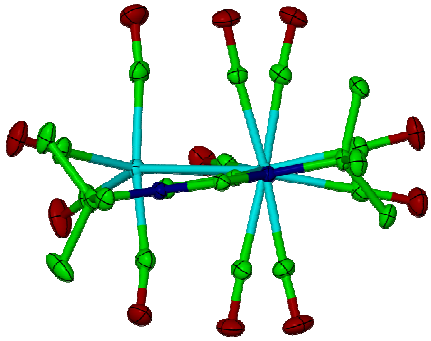

Ru_3(ab-I^{t}Bu)$(CO)_{11}$ (**2.1**)

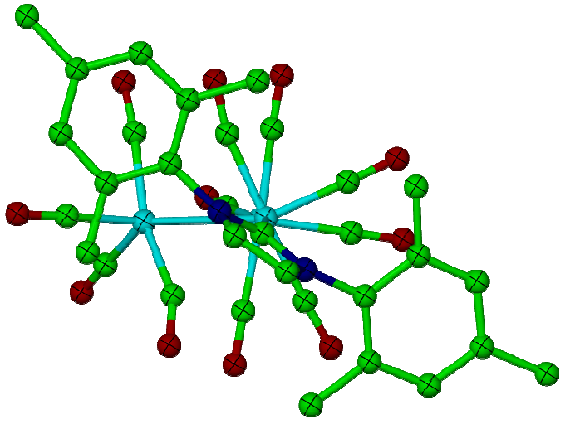

Ru_3(IMes)$(CO)_{11}$

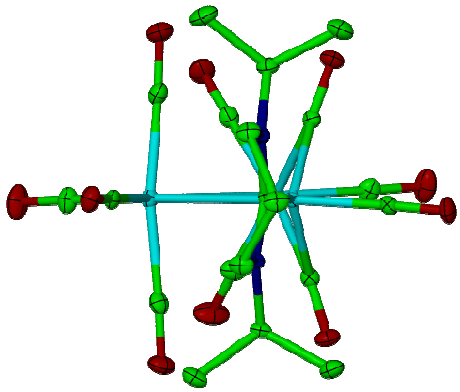

Ru_3(6^{i}Pr$_2$)(μ-CO)$_2(CO)_8$ (**2.10**)

Table 2.3.2: The twist of the NHC relative the Ru_3 plane in the series of Ru_3(NHC) based complexes.

Complex **2.10** was found to be stable in air for short periods of time in both solid and solution states. To our surprise, treatment of **2.10** with carbon monoxide at either 70 °C or 120 °C for up to 48 h, had no effect on the IR spectra indicating that no new products were formed. The use of ^{13}CO revealed that the substitution of carbonyl ligands is prevalent at room temperature evidenced by the appearance of three high frequency signals at 200.5, 203.2 and 203.5 ppm (**Figure 2.3.3**), only observed on ^{13}C labelling. In attempt to afford an addition product, **2.10** was reacted with H_2 at either high temperatures (70 °C) or with photolysis at low temperatures (-78 °C).

However, both methods resulted in the reductive elimination of the NHC generating a range of imidazolium products shown by a number of high frequency resonances in the proton spectra.

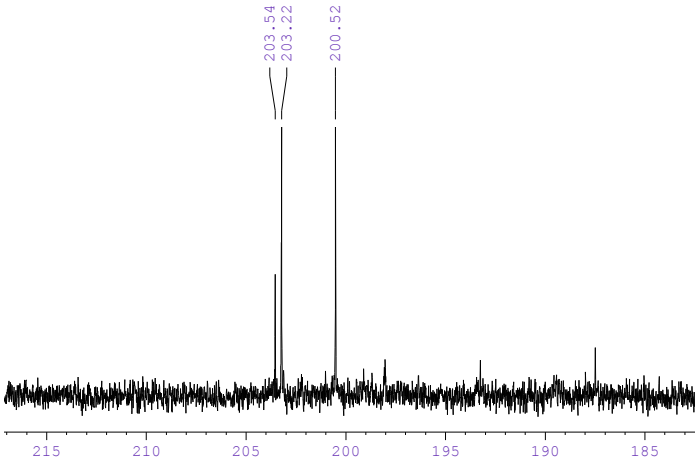

Figure 2.3.3: $^{13}C\{^{1}H\}$ NMR spectrum displaying the ^{13}CO enhanced carbonyl resonances for **2.10** (THF-d_8, 298K, 125 MHz).

2.3.4 Reaction of $Ru_3(CO)_{12}$ and 6*o*-Tol

The reaction of $Ru_3(CO)_{12}$ and 6*o*-Tol was carried out in the same manner as $6^{i}Pr_2$, although there was a noticeable difference in reactivity since the yield of imidazolium salt was much higher (~90%). The remaining product, however, was extracted with hexane and analysed by IR spectroscopy, which revealed no bridging carbonyl ligands were present. The IR did show a set of low intensity carbonyl bands at 2038, 1994, 1948 cm^{-1}, along with more intense features at 2960 and 1677 cm^{-1}. The latter bands are consistent with a ring opened compound analogous to that seen for SIPr. During recrystallisation, a single crystal was obtained and was shown to be the activated 6*o*-Tol dimer, $[Ru(6o\text{-}Tol^{*})(CO)_3]_2$ by X-ray crystallography (**Figure 2.3.4**).

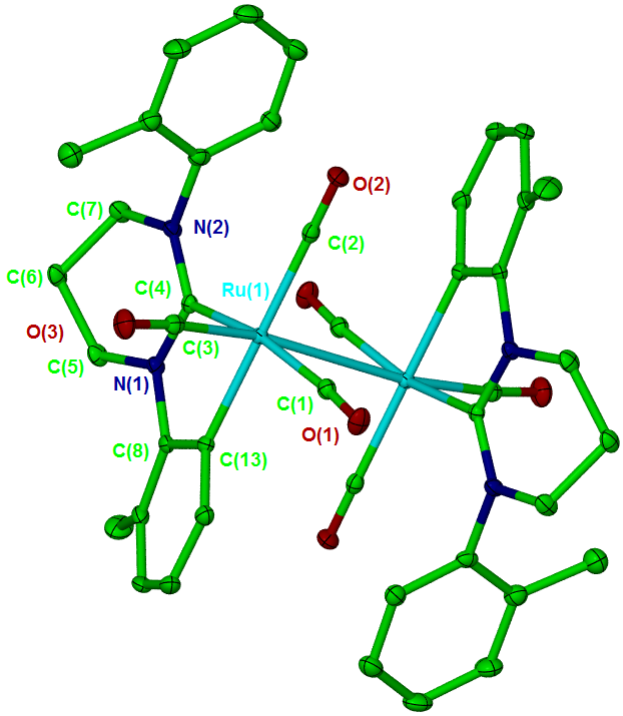

Figure 2.3.4: Crystal structure of [Ru(6*o*-Tol*)$(CO)_3]_2$. Thermal ellipsoids set 30% probability and hydrogen atoms have been omitted for clarity.

We assume that the carbonyl bands at 2038, 1994, 1948 cm^{-1} arise from [Ru(6*o*-Tol*)$(CO)_3]_2$. However the yield was so low that no further characterisation was possible, and so further experiments would be required to prove this conclusively. Pertinent bond lengths and angles are displayed in **Table 2.3.3**.

Bond length (Å) / Angle (°)	**[Ru(6*o*-Tol*)$(CO)_3]_2$**
Ru-C_{NHC}	2.092(2)
Ru-C_{Tol}	2.186(2)
Ru-Ru	3.0848(4)
C_{NHC}-Ru-C_{Tol}	77.25(9)
Tolyl ring planes	73.75

Table 2.3.3: Bond lengths (Å) and angles (°) of [Ru(6*o*-Tol*)$(CO)_3]_2$.

2.4 Applications of Ru_3(NHC) complexes in the catalytic acylation of pyridine

The functionalisation of C-H bonds is one of the most important and useful synthetic strategies in organic synthesis. In 1992, Moore and co-workers reported the efficient ruthenium catalysed acylation of pyridine by carbon monoxide with a range of alkenes. Acylation took place selectively at the *ortho* position of pyridine with 1-hexene and CO in the presence of catalytic amounts of $Ru_3(CO)_{12}$.[36]

The mechanism for the catalytic reaction is believed to occur initially by the coordination of the pyridine nitrogen to the ruthenium complex, which places the *ortho*-CH group in close proximity to the metal centres where the bond can be cleaved by oxidative addition, as observed in stoichiometric reactions of a range of N-heterocycles.[36-37] This generates a hydride-ruthenium complex (**Figure 2.4.1**), which undergoes alkene insertion to give an alkyl complex that is followed by CO insertion, then reductive elimination to generate the final product. However, it is not known whether the catalytically active species is an intact cluster or a di- or mononuclear ruthenium species.[38]

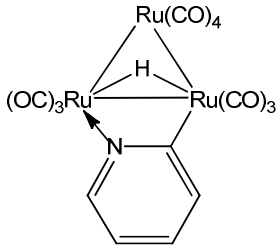

Figure 2.4.1: Possible trinuclear ruthenium intermediate in the acylation of pyridine.

Moore reported that the acylation of 1-hexene and pyridine under CO in the presence of catalytic amounts of $Ru_3(CO)_{12}$ (1.3 mol%) produced pyridyl ketones with moderate turnover frequencies of ca. 160/h. The typical reaction conditions involved 150 °C and 10 atm of CO to afford a conversion of 65% after 16 h (**Scheme 2.4.1**), with the formation of linear:branched isomers in a ratio of 13:1.[39]

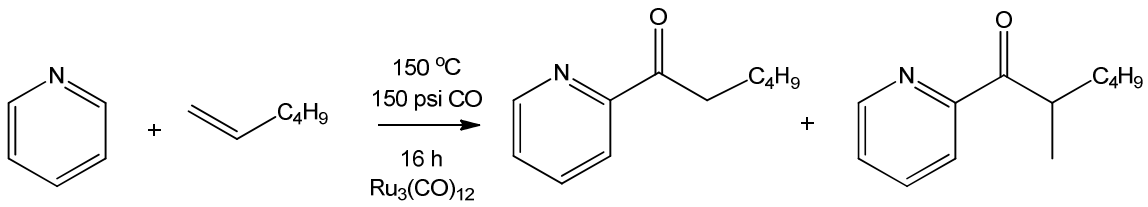

Scheme 2.4.1: The acylation of pyridine to form linear and branched pyridyl ketone products.

We set out to investigate if the abnormal NHC ruthenium clusters **2.1-2.4** and the coordinatively unsaturated complex **2.10** were active in this catalytic process. Abnormal NHC complexes have been shown previously to be very active in a range of catalytic reactions including palladium catalysed hydrogenation, Suzuki-Miyaura and Heck C-C coupling reactions due to their strong electron donor properties.[20, 40] This is particularly beneficial for the acylation of alkenes, as electron rich metal centres have been shown to favour oxidative addition which possibly increases the efficiency of the first step of the catalytic cycle.[41]

The same conditions used by Moore and co-workers were employed. After the reaction, an aliquot of solution was removed from the reactor and the products identified by comparison of ^{1}H NMR spectra to literature values. The linear product displays a characteristic triplet at 3.22 ppm while the branched isomer exhibits a distinctive multiplet at 4.1 ppm. The results are shown in **Table 2.4.1**.[39]

Catalyst	Conversion (%)		Selectivity for
	Linear	Branched	linear product (%)
$Ru_3(CO)_{12}$	60	5	92
Ru_3(ab-I^{t}Bu)$(CO)_{11}$ (**2.1**)	88	7	93
$Ru_3(\mu$-H)(dab-I^{t}Bu)$(CO)_9$ (**2.3**)	87	0	100
Ru_3(ab-IAd)$(CO)_{11}$ (**2.2**)	91	9	91
$Ru_3(\mu$-H)(dab-IAd)$(CO)_9$ (**2.4**)	86	0	100
$Ru_3(6^iPr_2)(\mu$-CO$)_2(CO)_8$ (**2.10**)	77	6	93

Table 2.4.1: Conversion (%) of 1-hexene to linear and branched pryidyl ketone products with 1.3 mol% catalyst.

The abnormal NHC containing clusters are significantly more active than either $Ru_3(CO)_{12}$ or **2.10** with total conversions ranging from 86% for **2.4** to 100% for **2.2**. The activated abnormal complexes **2.1**/**2.2** show the highest selectivity for the linear product. Interestingly complex **2.10**

shows the lowest conversion to the linear product of the cluster compounds despite being coordinatively unsaturated.

We also investigated whether the reaction could be run with stoichiometric quantities of pyridine and 1-hexene, using toluene rather than pyridine as the solvent (**Table 2.4.2**).

Catalyst	Conversion		Selectivity (%)
	Linear	Branched	for linear product
Ru_3(ab-I^{t}Bu)$(CO)_{11}$ (**2.1**)	72	18	80
Ru_3(μ-H)(dab-I^{t}Bu)$(CO)_9$ (**2.3**)	70	0	100
Ru_3(ab-IAd)$(CO)_{11}$ (**2.2**)	71	0	100
Ru_3(μ-H)(dab-IAd)$(CO)_9$ (**2.4**)	75	0	100

Table 2.4.2: Conversion (%) for the catalysed stoichiometric reaction between 1-hexene and pyridine with 1.3 mol% catalyst.

Catalytic activity was retained when a stoichiometric amount of pyridine was used, although in all cases the conversions were lower in comparison with reactions using pyridine as the solvent. However, all the catalysts perform more favourably than $Ru_3(CO)_{12}$. The catalysts all display similar activity in toluene in terms to conversion of the linear product. With **2.1** exhibiting the highest total conversion although with poorer selectivity overall.

2.5 Summary

The reaction of IMes and IPr with $Ru_3(CO)_{12}$ has been shown to afford the products **2.5**, **2.6** and **2.7**. These compounds are different from those isolated by other groups with the same NHCs, although this has been rationalised by the variation of reaction conditions employed.

The reaction of the sterically bulky NHC I^{t}Bu with $Os_3(CO)_{12}$ led to the synthesis of the abnormal osmium cluster **2.8**, which is analogous and structurally similar to the reported ruthenium compound **2.1**. Evidence for the activation of the remaining C4/5 position of the abnormal compounds **2.7** and **2.8** has been observed by the appearance of a low field resonance and a bridging hydride signal.

Synthesis of the first example of a coordinatively unsaturated ruthenium cluster **2.10** has been achieved by the reaction of $Ru_3(CO)_{12}$ with the ring expanded NHC 6^{i}Pr$_2$. The product has been shown to be remarkably stable to reactions with air, moisture and carbon monoxide. Reaction of **2.10** with hydrogen led to the reductive elimination of the NHC to give a mixture of imidazolium products. In contrast the reactions of SIPr and 6*o*-Tol were shown to result in a ring

opening decomposition reaction of the carbenes to form the corresponding formamides, possibly due to the presence of adventitious water.

The catalytic activity of the previously reported abnormal NHC clusters and **2.10** were tested in the acylation of pyridine and were shown to be highly active for this transformation, outperforming $Ru_3(CO)_{12}$ both in terms of overall conversion as well as selectivity.

2.6 References

1. Bruce, M. I., *Comprehensive Organometallic Chemistry III*. Elsevier: Oxford, UK, 2007; Vol. 6.
2. Lappert, M. F.; Pye, P. L., *J. Chem. Soc., Dalton. Trans.* **1977**, 2172-2180.
3. Cabeza, J. A.; del Rió, I.; Miguel, D.; Sánchez-Vega, M. G., *Chem. Commun.* **2005**, 3956-3958.
4. Cabeza, J. A.; del Rió, I.; Miguel, D.; Pérez-Carreño, E.; Sánchez-Vega, M. G., *Organometallics* **2008**, *27,* 211-217.
5. Bruce, M. I.; Cole, M. L.; Fung, R. S. C.; Forsyth, C. M.; Hilder, M.; Junk, P. C.; Konstas, K., *Dalton Trans.* **2008**, 4118-4128.
6. Ellul, C. E.; Saker, O.; Mahon, M. F.; Apperley, D. C.; Whittlesey, M. K., *Organometallics* **2008**, *27,* 100-108.
7. (a) Ellul, C. E.; Mahon, M. F.; Saker, O.; Whittlesey, M. K., *Angew. Chem. Int. Ed.* **2007**, *46,* 6343-6345; (b) Crittall, M. R.; Ellul, C. E.; Mahon, M. F.; Saker, O.; Whittlesey, M. K., *Dalton Trans.* **2008**, 4209-4211.
8. Cabeza, J. A.; Pérez-Carreño, E., *Organometallics* **2008**, *27,* 4697-4702.
9. Cabeza, J. A.; del Rió, I.; Miguel, D.; Pérez-Carreño, E.; Sánchez-Vega, M. G., *Dalton Trans.* **2008**, 1937-1942.
10. Cabeza, J. A.; del Rió, I.; Fernandez-Colinas, J. M.; Pérez-Carreño, E.; Sánchez-Vega, M. G.; Vazquez-Garcia, D., *Organometallics* **2010**, *29,* 3828-3836.
11. Cooke, C. E.; Jennings, M. C.; Pomeroy, R. K.; Clyburne, J. A. C., *Organometallics* **2007**, *26,* 6059-6062.
12. (a) Chatt, J.; Watson, H. R., *J. Chem. Soc.* **1962**, 2545-2549; (b) Chatt, J.; Davidson, J. M., *J. Chem. Soc.* **1965**, 843-855.
13. Murai, S.; Kakiuchi, F.; Sekine, S.; Tanaka, Y.; Kamatani, A.; Sonoda, M.; Chatani, N., *Nature* **1993**, *366,* 529-531.
14. (a) Kakiuchi, F.; Matsumoto, M.; Tsuchiya, K.; Igi, K.; Hayamizu, T.; Chatani, N.; Murai, S., *J. Organomet. Chem.* **2003**, *686,* 134-144; (b) Kakiuchi, F.; Usui, M.; Ueno, S.; Chatani, N.; Murai, S., *J. Am. Chem. Soc.* **2004**, *126,* 2706-2707.
15. (a) Chatani, N.; Asaumi, T.; Yorimitsu, S.; Ikeda, T.; Kakiuchi, F.; Murai, S., *J. Am. Chem. Soc.* **2001**, *123,* 10935-10941; (b) Asaumi, T.; Chatani, N.; Matsuo, T.; Kakiuchi, F.; Murai, S., *J. Org. Chem.* **2003**, *68,* 7538-7540; (c) Chatani, N.; Fukuyama, T.; Tatamidani, H.; Kakiuchi, F.; Murai, S., *J. Org. Chem.* **2000**, *65,* 4039-4047; (d) Ie, Y.; Chatani, N.; Ogo, T.; Marshall, D. R.; Fukuyama, T.; Kakiuchi, F.; Murai, S., *J. Org. Chem.* **2000**, *65,* 1475-1488.

16. (a) Chatani, N.; Tobisu, M.; Asaumi, T.; Murai, S., *Synthesis* **2000**, 925-928; (b) Tobisu, M.; Chatani, N.; Asaumi, T.; Amako, K.; Ie, Y.; Fukumoto, Y.; Murai, S., *J. Am. Chem. Soc.* **2000**, *122,* 12663-12674.
17. Hollmann, D.; Tillack, A.; Michalik, D.; Jackstell, R.; Beller, M., *Chem-Asian J* **2007**, *2,* 403-410.
18. (a) Jazzar, R. F. R.; Bhatia, P. H.; Mahon, M. F.; Whittlesey, M. K., *Organometallics* **2003**, *22,* 670-683; (b) Chantler, V. L.; Chatwin, S. L.; Jazzar, R. F. R.; Mahon, M. F.; Saker, O.; Whittlesey, M. K., *Dalton Trans.* **2008**, 2603-2614.
19. Dharmasena, U. L.; Foucault, H. M.; dos Santos, E. N.; Fogg, D. E.; Nolan, S. P., *Organometallics* **2005**, *24,* 1056-1058.
20. Lebel, H.; Janes, M. K.; Charette, A. B.; Nolan, S. P., *J. Am. Chem. Soc.* **2004**, *126,* 5046-5047.
21. Tang, C. Y.; Smith, W.; Vidovic, D.; Thompson, A. L.; Chaplin, A. B.; Aldridge, S., *Organometallics* **2009**, *28,* 3059-3066.
22. Appelhans, L. N.; Zuccaccia, D.; Kovacevic, A.; Chianese, A. R.; Miecznikowski, J. R.; Macchioni, A.; Clot, E.; Eisenstein, O.; Crabtree, R. H., *J. Am. Chem. Soc.* **2005**, *127,* 16299-16311.
23. Arnold, P. L.; Pearson, S., *Coord. Chem. Rev.* **2007**, *251,* 596-609.
24. Albrecht, M., *Chem. Commun.* **2008**, 3601-3610.
25. Clavier, H.; Nolan, S. P., *Chem. Commun.* **2010**, *46,* 841-861.
26. Eguillor, B.; Esteruelas, M. A.; Olivan, M.; Puerta, M., *Organometallics* **2008**, *27,* 445-450.
27. Johnson, B. F. G.; Lewis, J.; Pippard, D. A., *J. Chem. Soc., Dalton. Trans.* **1981**, 407-412.
28. (a) Knight, J.; Mays, M. J., *J. Chem. Soc., Dalton. Trans.* **1972**, 1022-1029; (b) Johnson, B. F. G.; Lewis, J.; Orpen, A. G.; Raithby, P. R.; Süss, G., *J. Organomet. Chem.* **1979**, *173,* 187-197; (c) Liu, Y. C.; Yeh, W. Y.; Lee, G. H.; Peng, S. M., *Organometallics* **2003**, *22,* 4163-4166.
29. Denk, M. K.; Rodezno, J. M.; Gupta, S.; Lough, A. J., *J. Organomet. Chem.* **2001**, *617,* 242-253.
30. Kolychev, E. L.; Shuntikov, V. V.; Khrustalev, V. N.; Bush, A. A.; Nechaev, M. S., *Dalton Trans.* **2011**, 3074-3076.
31. Hollóczki, O.; Terleczky, P.; Szieberth, D.; Mourgas, G.; Gudat, D.; Nyulászi, L., *J. Am. Chem. Soc.* **2010**, *133,* 780-789.
32. Two equivalents of $6^{i}Pr_2$ were needed to react all $Ru_3(CO)_{12}$.
33. The remaining solid was shown to be an imidazolium product by a resonance at 8.19 ppm in the ^{1}H NMR spectrum.

34. Armstrong, R.; Ecott, C.; Mas-Marzá, E.; Page, M. J.; Mahon, M. F.; Whittlesey, M. K., *Organometallics* **2010**, *29,* 991-997.
35. Orpen, A. G., *J. Chem. Soc., Dalton Trans.* **1980**, 2509-2516.
36. Fish, R. H.; Kim, T. J.; Stewart, J. L.; Bushweller, J. H.; Rosen, R. K.; Dupon, J. W., *Organometallics* **1986**, *5,* 2193-2198.
37. (a) Bruce, M. I.; Humphrey, M. G.; Snow, M. R.; Tiekink, E. R. T.; Wallis, R. C., *J. Organomet. Chem.* **1986**, *314,* 311-322; (b) Eisenstadt, A.; Giandomenico, C. M.; Frederick, M. F.; Laine, R. M., *Organometallics* **1985**, *4,* 2033-2039; (c) Deeming, A. J.; Peters, R.; Hursthouse, M. B.; Backerdirks, J. D. J., *J. Chem. Soc., Dalton. Trans.* **1982**, 787-791.
38. Ritleng, V.; Sirlin, C.; Pfeffer, M., *Chem. Rev.* **2002**, *102,* 1731-1769.
39. Moore, E. J.; Pretzer, W. R.; O'Connell, T. J.; Harris, J.; Labounty, L.; Chou, L.; Grimmer, S. S., *J. Am. Chem. Soc.* **1992**, *114,* 5888-5890.
40. (a) Heckenroth, M.; Neels, A.; Garnier, M. G.; Aebi, P.; Ehlers, A. W.; Albrecht, M., *Chem.-Eur. J.* **2009**, *15,* 9375-9386; (b) John, A.; Shaikh, M. M.; Ghosh, P., *Dalton Trans.* **2009**, 10581-10591.
41. (a) Graham, D. C.; Cavell, K. J.; Yates, B. F., *Dalton Trans.* **2006**, 1768-1775; (b) Cavell, K. J.; McGuinness, D. S., *Coord. Chem. Rev.* **2004**, *248,* 671-681; (c) Crudden, C. M.; Allen, D. P., *Coord. Chem. Rev.* **2004**, *248,* 2247-2273.

3.1 Introduction

3.1.1 Preface

Palladium clusters bearing phosphine and carbonyl ligands of the general type $Pd_n(PR_3)_y(CO)_x$ form the basis of a wide range of Pd_n complexes ranging from high nuclearity species such as $Pd_{54}(PEt_3)_{14}(CO)_{40}$,[1] $Pd_{66}(PEt_3)_{16}(CO)_{45}$,[2] and $Pd_{145}(PEt_3)_{30}(CO)_x$ ($x \approx 60$)[3] to smaller clusters of the form $Pd_3(PR_3)_x(\mu\text{-}CO)_3$ ($x = 3$ or 4), for example, $Pd_3(P^tBu_3)_3(\mu\text{-}CO)_3$[4] and $Pd_3(P(p\text{-}Tol)_3)_4(\mu\text{-}CO)_3$.[5] These smaller clusters have been known for almost 40 years and since then a wide range of clusters bearing a number of ligands including phosphines, isocyanides, carbon monoxide, sulfur dioxide and halides have been reported and reviewed.[6]

This introduction describes the literature with the view of developing the first examples of analogous NHC palladium clusters of the form $Pd_3(NHC)_3(\mu\text{-}CO)_3$ and investigating the reactivity of such complexes.

3.1.2 Synthesis of palladium clusters

There are two main strategies used for the synthesis of palladium cluster compounds, the first of which involves the aggregation of unsaturated monomers. Many of these are often reactive intermediates which can either be formed *in situ* by the loss of a labile ligand from a palladium(0) complex or by reduction of a higher oxidation state to Pd(0) as shown in **Scheme 3.1.1**.

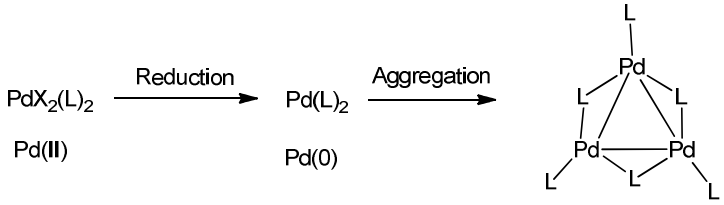

Scheme 3.1.1: A generalised method for the synthesis of palladium clusters.

The second method involves the conversion of existing cluster compounds to afford new previously unknown clusters.[6] As there were no prior examples of NHC palladium cluster compounds, we concentrated on searching for a method whereby palladium clusters could be synthesised from either a palladium(0) or a palladium(II) starting material.

3.1.3 Synthesis from palladium(0)

One example of palladium carbonyl cluster formation from a palladium(0) precursor was reported by Otsuka and co-workers in 1977. They showed that the reaction of the *bis*-phosphine palladium(0) complex $Pd(PR_3)_2$ (R = P^tBu_3 or PPh^tBu_2) with carbon monoxide at room temperature gave the *tris*-palladium cluster $Pd_3(PR_3)_3(\mu\text{-}CO)_3$ (**Scheme 3.1.2**).[4]

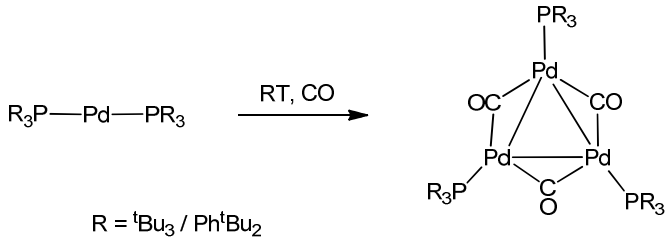

Scheme 3.1.2: The formation of a *tris*-palladium cluster from $Pd(PR_3)_2$ (R = $^tBu_3$ / Ph^tBu_2).

An alternative palladium(0) complex, $Pd(PMe_3)(COD)$, was also reported by Goddard *et. al*. to react with carbon monoxide at low temperature. After working up the reaction, they were able to structurally characterise the high nuclearity palladium species $Pd_7(PMe_3)_7(\mu_3\text{-}CO)_4(\mu\text{-}CO)_3$.[7] In the case of $[Pd_2(dba)_3]\cdot CHCl_3$, reaction with carbon monoxide and PMe_3 at room temperature gave the slightly larger species $Pd_8(PMe_3)_7(\mu_3\text{-}CO)_2(\mu\text{-}CO)_6$.[8]

Apart from carbon monoxide, other two electron donors can be used to bridge palladium centres. One such class of ligands are isocyanides; for example, the isocyanide CNXyl (CNXyl = 2,6-dimethylphenyl isocyanide) reacts with $Pd_2(dba)_3$ (dba = dibenzylideneacetone) at room temperature under an inert atmosphere to form the *tris*-palladium cluster $Pd_3(\mu\text{-}CNXyl)_3(CNXyl)_3$, which exhibits both bridging and terminal isocyanide ligands.[9] Conversely, altering the conditions from an Ar atmosphere to an atmosphere of SO_2 gave $Pd_5(\mu\text{-}SO_2)_3(\mu\text{-}CNXyl)_2(CNXyl)_5$ containing bridging SO_2 groups as well as terminal and bridging isocyanide ligands (**Scheme 3.1.3**).[10] The complex $Pd(CN^tBu)_2$ has been shown to react directly with SO_2 to form the *tris*-palladium cluster $Pd_3(\mu\text{-}SO_2)_2(CN^tBu)_5$.[11]

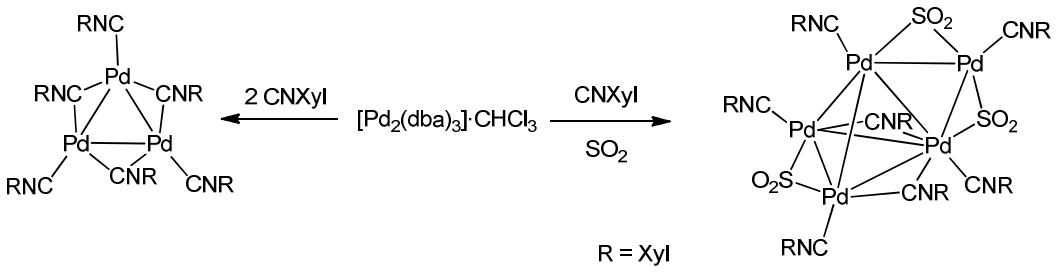

Scheme 3.1.3: Formation of palladium clusters from $Pd_2(dba)_3$.

3.1.4 Synthesis from palladium(II)

The synthesis of palladium clusters from a higher oxidation state was first reported in the 1960s by Uchida and co-workers. They showed that the reduction of $Pd(acac)_2$ by $AlEt_3$ in the presence of PPh_3 and carbon monoxide afforded the *tris*-Pd(0) cluster $Pd_3(PPh_3)_4(\mu\text{-}CO)_3$ bearing four PPh_3 groups; this is in contrast to the cluster which contains only three of the more bulky P^tBu_3 and PPh^tBu_2 ligands shown in **Scheme 3.1.2**. It was proposed that the reaction went via the palladium(0) intermediate $Pd(PPh_3)_3(CO)$ followed by the loss of PPh_3 to afford $Pd_3(PPh_3)_4(\mu\text{-}CO)_3$.[12] Later they reported the synthesis of the same product from the reduction of $PdCl_2(PPh_3)_2$ under an atmosphere of carbon monoxide using either $NaBH_4$,[13] or a range of amines in methanol (**Scheme 3.1.4**).[14]

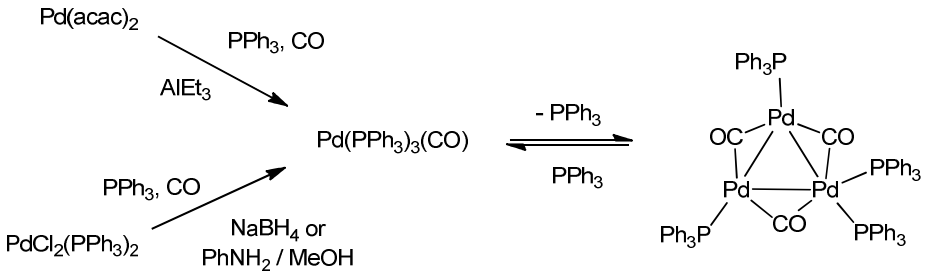

Scheme 3.1.4: The synthesis of $Pd_3(PPh_3)_4(\mu\text{-}CO)_3$ via reduction of Pd(II) precursors.

Under certain conditions, carbon monoxide can act both as a ligand and as a reducing agent for transforming palladium(II) complexes into neutral Pd(0) clusters. For example, Mednikov and co-workers reported that the direct reaction between $Pd(acac)_2$, PPh_3 and carbon monoxide afforded the tetra-nuclear cluster $Pd_4(PPh_3)_4(\mu\text{-}CO)_5$.[15] In another case, the reaction of dinitro(*bis*-phosphine) palladium(II) complexes of the form $Pd(NO_2)_2(PR_3)$ (PR_3 = PPh_3, $PMePh_2$, PEt_3) with CO at room temperature gave the tetra palladium clusters $Pd_4(PR_3)_4(\mu\text{-}CO)_5$ (**Scheme 3.1.5**).[16]

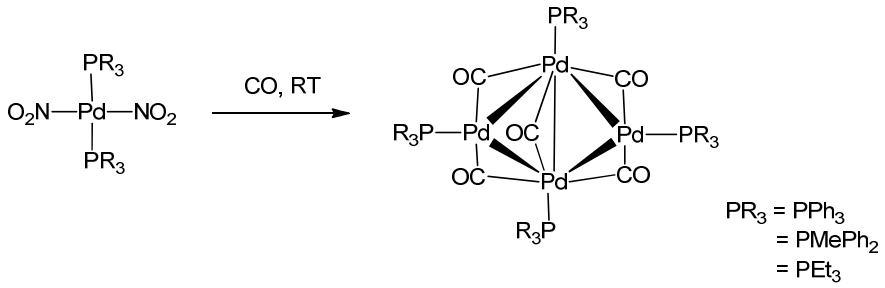

Scheme 3.1.5: The synthesis of $Pd_4(PR_3)_4(\mu\text{-}CO)_5$ via reduction with CO.

3.1.5 Interconversion between clusters

The interconversion of a cluster into a new previously unknown one can often be achieved simply by the substitution of one ligand for another. Other processes may also occur, including aggregation of more than one cluster to form a higher nuclearity cluster or, conversely, the fragmentation of a cluster, leading to a reduction in the number of palladium atoms within the compound. For instance, the reaction of $Pd_8(PMe_3)_7(\mu_3\text{-}CO)_2(\mu\text{-}CO)_6$ with SO_2 leads not only to the full substitution of the carbonyl ligands for SO_2, but also to a reduction in the number of metal atoms within the cluster from Pd_8 to Pd_5 with formation of $Pd_5(PMe_3)_5(\mu_3\text{-}SO_2)_2(\mu\text{-}SO_2)_2$.[17]

In addition to ligand substitution reactions, it is possible to increase the nuclearity of a palladium cluster by the addition of a suitable monomer. For example, palladium acetate reacts with $Pd_{10}(PEt_3)_6(\mu_3\text{-}CO)_4(\mu\text{-}CO)_8$ to form $Pd_{23}(PEt_3)_{10}(\mu_3\text{-}CO)_8(\mu\text{-}CO)_{14}$.[18] It is also possible to react palladium clusters with other metal monomers to generate mixed metal clusters, one example being the addition of the gold fragment '$Au(PPh_3)$' to the anionic palladium cluster $Y[Pd_3(\mu\text{-}Cl)(PPh_3)_3(\mu\text{-}SO_2)_2]$ ($Y = [PPPh_3(CH_2Ph)]^+$).[19] The gold unit caps the palladium triangle to give a neutral 56-electron complex, $Pd_3Au(\mu\text{-}Cl)(PPh_3)_4(\mu\text{-}SO_2)_2$, as shown in **Scheme 3.1.6**.

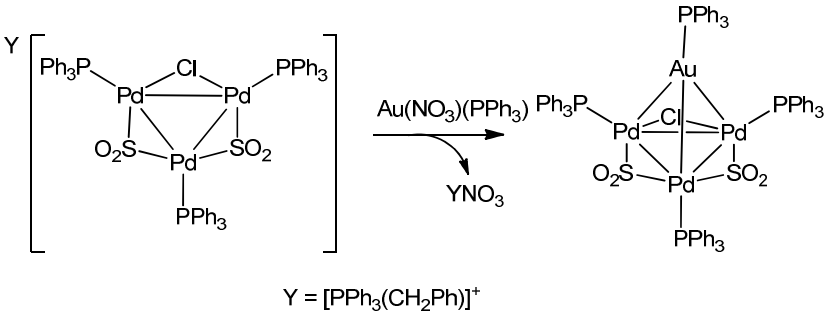

Scheme 3.1.6: The formation of the gold capped palladium cluster $Pd_3Au(\mu\text{-}Cl)(PPh_3)_4(\mu\text{-}SO_2)_2$.

3.2 Palladium N-heterocyclic carbene clusters

It is evident from the above examples that there are a vast array of monomeric palladium complexes that can be used as precursors to form palladium clusters including both palladium(0) and palladium(II) compounds. Furthermore, there are a number of routes available to synthesise such clusters including the use of a variety of bridging and terminal ligands as well as the use of a number of reducing agents in the case of palladium(II). In many systems, the cluster ligands are present in the monomeric starting material, and so afford palladium clusters bearing N-heterocyclic carbene ligands, a suitable monomeric Pd-NHC moiety was desired.

The area of palladium NHC chemistry is vast due to the use of palladium NHC complexes in catalytic C-C and C-N bond forming reactions.[20] Although a large quantity of this work concentrates on the use of *in situ* prepared complexes which are synthesised in the course of the catalytic reaction, there are still a number of isolated complexes suitable for the synthesis of palladium clusters which are analogous to the phosphine compounds discussed above. These provide a number of promising starting points for the formation of palladium clusters bearing NHC ligands.

A number of routes and starting materials were investigated in an attempt to synthesise new palladium clusters bearing NHC ligands (**Scheme 3.2.1**). The most straightforward method we hypothesised involved the addition of an atmosphere of carbon monoxide to a palladium(0) NHC complex in the hope of forming a palladium complex of the form $Pd_3(NHC)_3(\mu\text{-}CO)_3$. The two compounds which we believed would have promise were the mixed phosphine/NHC and *bis*-NHC Pd(0) complexes $Pd(NHC)(PR_3)$ and $Pd(NHC)_2$.

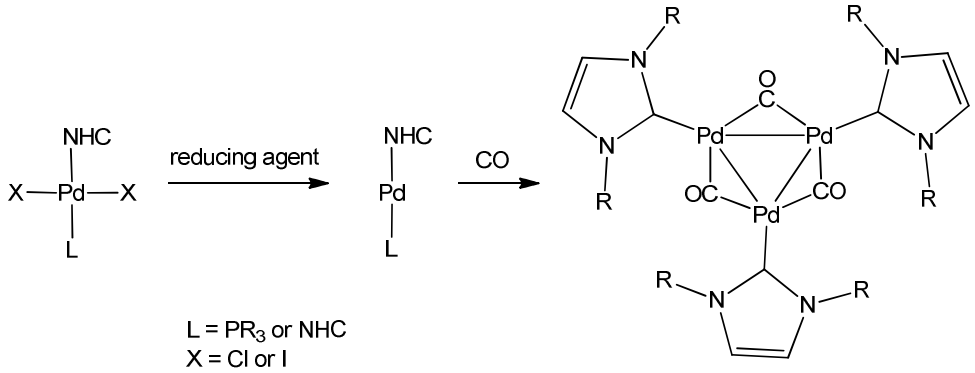

Scheme 3.2.1: Possible route for the formation of a palladium NHC cluster from a palladium(0)/(II) source.

3.2.1 Synthesis from palladium(0) N-heterocyclic carbene complexes

The mixed phosphine/NHC palladium(0) compound, Pd(NHC)(PR_3) could be seen as a more promising starting material over the *bis*-NHC compound, as it would be assumed that during the formation of a cluster the loss of phosphine would be favoured over the loss of the more strongly bound NHC ligand. The formation of mixed phosphine/NHC palladium(0) complexes can be achieved by two methods. The first method was developed by Herrmann and co-workers and involves the substitution of a phosphine ligand for an NHC in Pd($P(o\text{-Tol})_3)_2$ via careful control of the reaction stoichiometry.[21] In the case of IAd, the very large steric bulk of the adamantyl side groups restricts the substitution to only one of the phosphines even with an excess of NHC, leading to the formation of Pd(IAd)($P(o\text{-Tol})_3$) in 78% yield.[22] An alternative route for the formation of Pd(NHC)(PR_3) compounds was developed later by Nolan and co-workers, who utilised the initial formation of the palladium(II) compound PdCl(η^3-allyl)(NHC).[23] Reduction with KO^tBu allowed the resulting palladium(0) compound to be trapped by the addition of a tertiary phosphine (or another NHC ligand). This versatile two step procedure can lead to the formation of a number of different mixed NHC/phosphine species as well as the formation of mixed *bis*-NHC palladium(0) complexes as shown in **Scheme 3.2.2**.

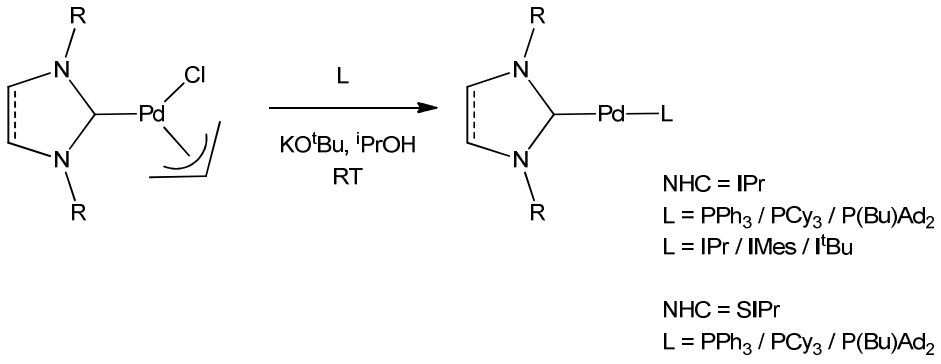

Scheme 3.2.2: The formation of mixed NHC/phosphine and *bis*-NHC palladium(0) complexes.

The compound Pd(IMes)($P(o\text{-Tol})_3$) was synthesised using the route developed by Fantasia and Nolan.[23] Subsequent treatment with one atmosphere of CO in THF for 24 h gave a colour change from yellow to an orange solution. The outcome of the reaction was probed by IR spectroscopy, which showed that no characteristic bridging carbonyl signals were present. The reaction mixture was also examined by ^1H and $^{31}P\{^1H\}$ NMR spectroscopy. The proton spectrum showed the presence of a number of IMes containing products, whereas the phosphorus spectrum showed the formation of just a single new unidentified phosphine containing complex. This reaction was not followed up as it was evident that a number of products were formed, none of

which appeared to be the desired cluster complex. This led us to move to a *bis*-NHC palladium(0) precursor.

The first *bis*-NHC palladium(0) complex was synthesised by Cloke and co-workers in 1999 by the co-condensation of palladium metal vapour with I^{t}Bu to form the stable, linear, two coordinate complex Pd(I^{t}Bu)$_2$ in 32% yield.[24] A more general and efficient method was later developed by Herrmann and co-workers.[25] They reported the synthesis of the compounds Pd(NHC)$_2$ (NHC = I^{t}Bu, IMes, I^{i}Pr$_2$ and ICy) in yields ranging from 61-91% upon substitution of both the tri-*ortho*-tolylphosphine ligands in Pd(P(*o*-Tol)$_3$)$_2$ by the corresponding free NHCs at room temperature (**Scheme 3.2.3**). Alternatively, Pd(I^{t}Bu)$_2$ can also be synthesised by the reduction of [Pd(η^3-allyl)(μ-Cl)]$_2$ with sodium dimethylmalonate in the presence of free I^{t}Bu.[26] This method was also used to synthesise the saturated NHC compounds Pd(SI^{t}Bu)$_2$ and Pd(SIPr)$_2$.[21, 27]

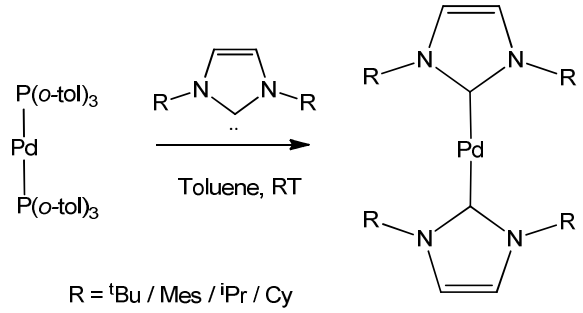

Scheme 3.2.3: The preparation of palladium(0) *bis*-NHC complexes.

The *bis*-NHC Pd complex Pd(IMes)$_2$ was synthesised by a method adapted from Herrmann and co-workers and reacted with CO as above to give a colour change from yellow to red. Again, no evidence for the formation of a palladium cluster complex was observed by either IR or NMR spectroscopy; these showed only the formation of a number of carbene containing products. Attempts to force both the mixed phosphine/NHC and *bis*-NHC reactions by increasing the reaction temperature to 70 °C and duration (max 48 h) failed to give cluster compounds.

3.2.2 Synthesis from palladium(II) NHC complexes

It has been shown that treatment of PdCl$_2$(PPh$_3$)$_2$ with a variety of reducing agents in the presence of carbon monoxide forms Pd$_3$(PPh$_3$)$_4$(μ-CO)$_3$.[14, 28] Mixed NHC/phosphine Pd(II) precursors were synthesised by Herrmann and co-workers in 1999.[29] The reaction of palladium acetate with a large excess of sodium iodide and only one equivalent of imidazolium salt gave the iodide bridged Pd dimer [Pd(μ-I)I(NHC)]$_2$, which can be easily broken up upon addition of a phosphine ligand to form a mixed NHC/phosphine palladium(II) compound. Herrmann later

showed that the method was applicable to a range of NHC and phosphine ligands,[30] as illustrated in **Scheme 3.2.4**.

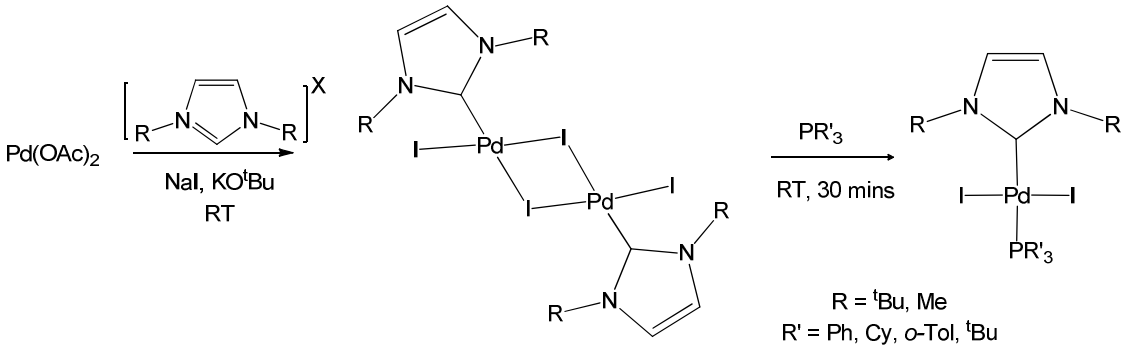

Scheme 3.2.4: Preparation of mixed NHC/phosphine palladium(II) complexes.

Attempts to reduce $PdI_2(IMes)(PPh_3)$ under an atmosphere of carbon monoxide failed to give any cluster products. In the case of $NaBH_4$, no reaction was observed to take place by $^{31}P\{^1H\}$ NMR spectroscopy. With the more aggressive reducing agent KC_8, only decomposition of the starting material and the formation of palladium black was observed.

Palladium(II) *bis*-NHC complexes can be easily synthesised from the reaction of the corresponding imidazolium salt and palladium acetate. This was first shown by Herrmann and co-workers who reacted $[IMe_2H]I$ with $Pd(OAc)_2$ to form *cis*-$PdI_2(IMe_2)_2$.[31] This methodology was later used by Lebel *et. al.* with [IMesH]Cl to generate the complex $PdCl_2(IMes)_2$, but instead of both NHCs binding in the normal fashion via the C2 carbon, X-ray crystallography revealed that one IMes ligand was abnormally bound via the C4 carbon.[32] If the reaction was repeated with $PdCl_2$, Cs_2CO_3 and [IMesH]Cl, the expected 'normal' complex $PdCl_2(IMes)_2$ was formed, as shown in **Scheme 3.2.5**.

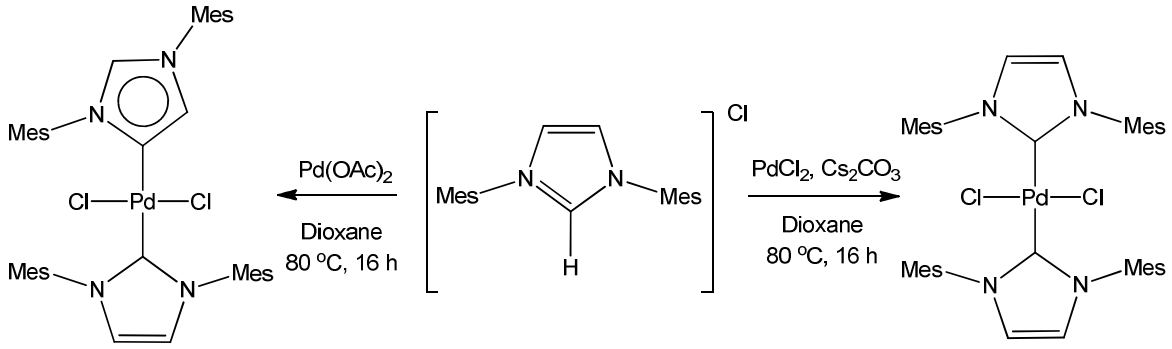

Scheme 3.2.5: The formation of palladium(II) complexes bearing normal and abnormal IMes ligands.

Reduction of $PdCl_2(IMes)_2$ with $NaBH_4$ in THF under CO resulted in a colourless solution and deposition to palladium black over a period of 30 mins. In contrast, reaction of $PdCl_2(IMes)_2$ with KC_8 at 70 °C for 16 h under 1atm of CO led to the formation of a dark red solution which, after work up, afforded $Pd_3(IMes)_3(\mu\text{-}CO)_3$ (**3.1**) as an air sensitive deep red solid in 38% yield (**Scheme 3.2.6**).[33]

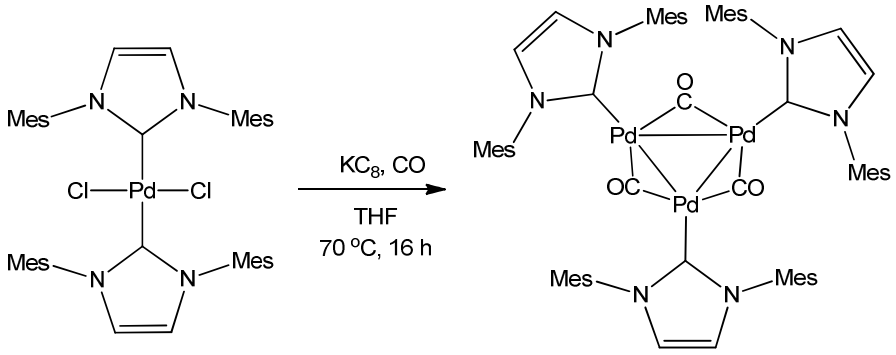

Scheme 3.2.6: The formation of the palladium cluster $Pd_3(IMes)_3(\mu\text{-}CO)_3$ (**3.1**) from $PdCl_2(IMes)_2$.

The formation of **3.1** was evident by the observation of a characteristic band in the bridging carbonyl region of the IR spectrum at 1796 cm^{-1}. This frequency is significantly lower than the value of 1850 cm^{-1} reported for $Pd_3(PPh_3)_3(\mu\text{-}CO)_3$ consistent with the stronger σ-donor ability of NHCs.[14, 16a, 28] The ^1H NMR spectrum showed only one set of IMes resonances at δ 6.81 and 6.14 for the backbone and mesityl C-H protons respectively, and at 2.34 and 2.04 ppm for the mesityl CH_3 groups on the NHC ligand, consistent with the product possessing high symmetry in solution. The $^{13}C\{^1H\}$ NMR spectrum showed two characteristic high frequency resonances at 249.2 and 198.8 ppm which were assigned to Pd-CO and Pd-C_{NHC} respectively on the basis of $^{13}C\{^1H\}$-^1H HMBC experiments. Structural characterisation of **3.1** is considered below.

The success in using $PdCl_2(IMes)_2$ as a Pd cluster precursor prompted us to prepare the new compounds $PdCl_2(I^iPr_2)_2$ and $PdCl_2(I^nBu_2)_2$, which were synthesised using the same method reported by Lebel *et. al.*.[32] Both complexes were isolated as white solids in yields of 70% and 33% respectively. The crystal structure of $PdCl_2(I^iPr_2)_2$ is shown in **Figure 3.2.1**. Comparison of the structural data for $PdCl_2(IMes)_2$ and $PdCl_2(I^iPr_2)_2$ revealed very similar Pd-C_{NHC} (IMes: 2.045 Å,[34] I^iPr_2: 2.0369(18) Å) and Pd-Cl bond lengths (IMes: 2.316 Å,[34] I^iPr_2: 2.3121(5) Å), with both adopting structures with a rigid square planar geometry as shown by the C_{NHC}-Pd-Cl bond angles of 89.38° and 89.94(5)° respectively.

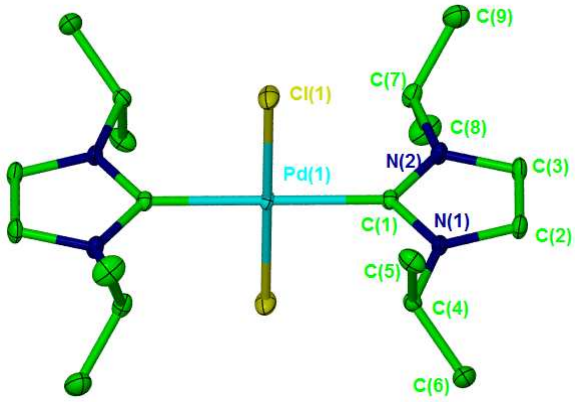

Figure 3.2.1: The crystal structure of $PdCl_2(I^iPr_2)_2$. Thermal ellipsoids set at 30% probability, hydrogen atoms omitted for clarity.

The reduction of both $PdCl_2(I^iPr_2)_2$ and $PdCl_2(I^nBu_2)_2$ with KC_8 under an atmosphere of carbon monoxide gave over a period of 16 h at 70 °C in THF the deep red palladium clusters $Pd_3(I^iPr_2)_3(\mu\text{-}CO)_3$ (**3.2**) and $Pd_3(I^nBu_2)_3(\mu\text{-}CO)_3$ (**3.3**). Compound **3.2** was only isolated in very low yield (5%) and was observed to decompose to palladium black in solution even under an inert atmosphere. However, the compound could be stored under CO in solution preventing degradation. A solution of the I^nBu_2 product **3.3** was unstable even under an atmosphere of carbon monoxide, preventing isolation of analytically pure material. The instability of the N-alkyl NHC clusters **3.2** and **3.3** relative to the IMes analogue **3.1** is most likely due to the decreased steric shielding of the palladium core by the N-substituents of the carbenes.

Both **3.2** and **3.3** exhibited a characteristic bridging carbonyl IR band at 1793 cm^{-1}. As for **3.1**, only one set of NHCs resonances was observed in the corresponding ^1H NMR spectra, again suggesting a high degree of symmetry within the molecules. For **3.2** it was possible to see the high frequency $^{13}C\{^1H\}$ NMR resonance for the Pd-C_{NHC} at 196.1 ppm, comparable to that for **3.1**. Due to the instability of **3.3**, $^{13}C\{^1H\}$ NMR data could not be determined with good enough signal to noise to identify the quaternary signals.

3.2.3 Structural comparison of 3.1, 3.2 and 3.3

X-ray quality crystals of **3.1-3.3** were grown from THF/hexane solutions. The molecular structures are shown in **Figure 3.2.2-3.2.4** for **3.1**, **3.2** and **3.3**.

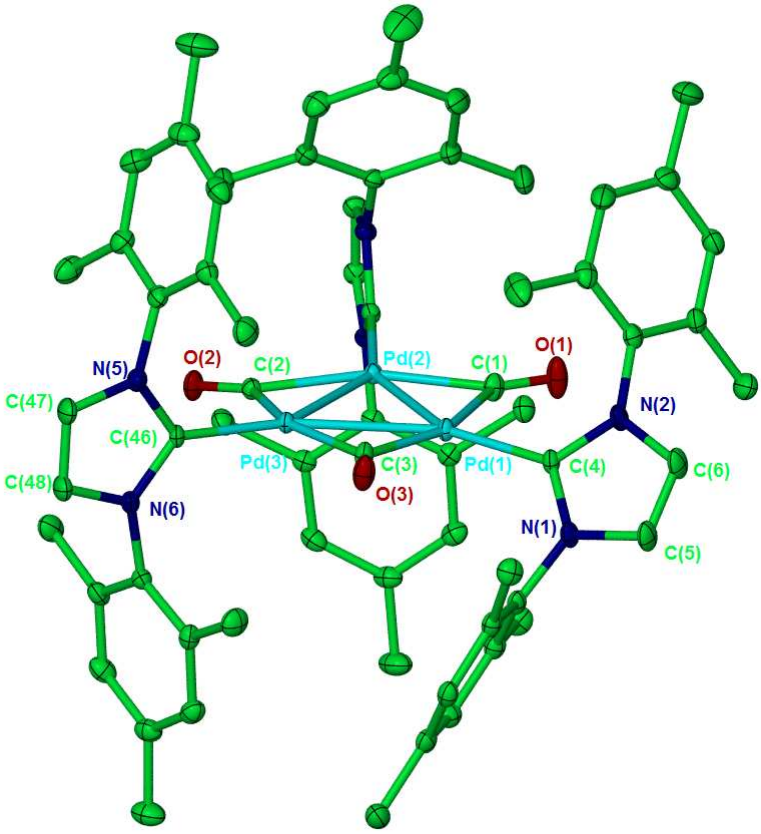

Figure 3.2.2: Crystal structure of $Pd_3(IMes)_3(\mu\text{-}CO)_3$ (**3.1**). Thermal ellipsoids set at 30% probability, hydrogen atoms omitted for clarity.

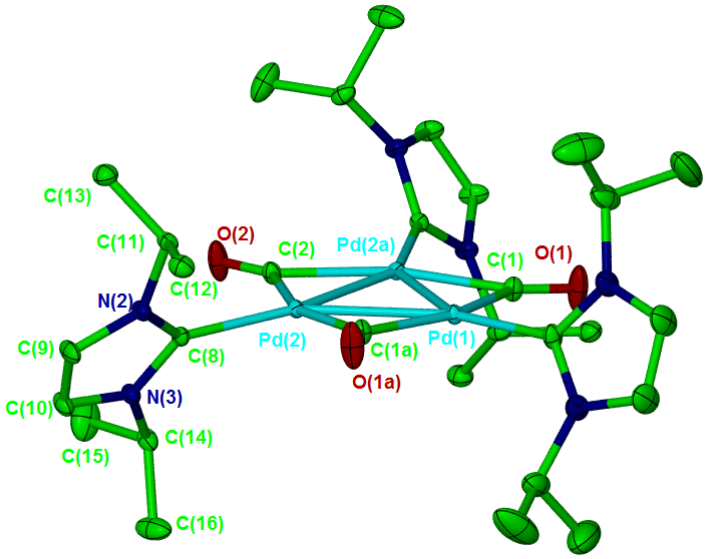

Figure 3.2.3: Crystal structure of $Pd_3(I^iPr_2)_3(\mu\text{-}CO)_3$ (**3.2**). Thermal ellipsoids set at 30% probability, hydrogen atoms omitted for clarity.

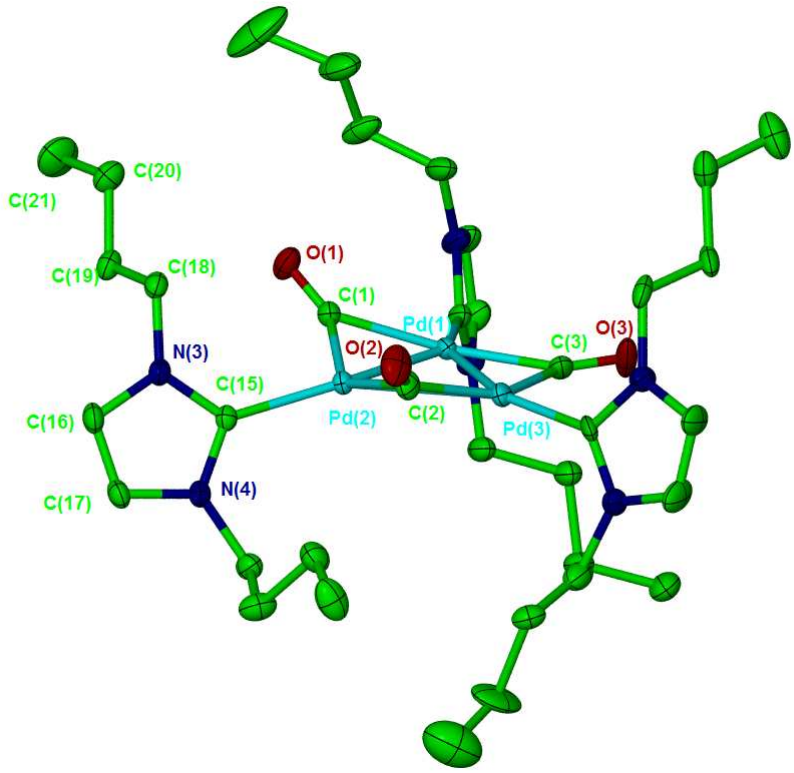

Figure 3.2.4: Crystal structure of $Pd_3(I^nBu_2)_3(\mu\text{-}CO)_3$ (**3.3**). Thermal ellipsoids set at 30% probability, hydrogen atoms omitted for clarity.

Pertinent bond lengths and angles for **3.1-3.3** are shown in **Table 3.2.1**. The Pd-C_{NHC} bond lengths in **3.1**, **3.2** and **3.3** are comparable to each other and range from 2.072(3) Å to 2.095(4) Å. In general, **3.1** displays the shortest bond lengths on average compared to **3.2** and **3.3** (**3.1**: 2.072(3)-2.083(3) Å, **3.2**: 2.088(4)-2.095(2) Å and **3.3**: 2.083(5)-2.095(4) Å). A degree of asymmetry is apparent in both the Pd-C_{CO} and Pd-Pd distances, as illustrated by variation of the Pd-C_{CO} distances from 2.039(4)-2.076(3) Å in **3.1**, 2.043(3)-2.077(3) Å in **3.2** and 2.034(5)-2.059(4) Å in **3.3**. One of the Pd-Pd distances in **3.1** and **3.3** exhibits a small but significant lengthening compared with the remaining two bonds (**3.1**: 2.6904(3) *c.f.* 2.6580(3) and 2.6520(3) Å ; **3.3**: 2.6945(5) *c.f.* 2.6703(5) and 2.6769(4) Å). This asymmetry is less noticeable in **3.2**, although the two independent Pd-Pd distances are also marginally asymmetric (2.6624(3), 2.6773(3) Å).

Bond lengths (Å) / Angles (°)	$Pd_3(IMes)_3(\mu\text{-}CO)_3$ (3.1)	$Pd_3(I^iPr_2)_3(\mu\text{-}CO)_3$ (3.2)	$Pd_3(I^nBu_2)_3(\mu\text{-}CO)_3$ (3.3)
Pd-C_{NHC}	2.072(3)	2.088(4)	2.083(5)
	2.076(3)	2.095(2)	2.093(10)
	2.083(3)		2.095(4)
Pd-Pd	2.6520(3)	2.6624(3)	2.6703(5)
	2.6580(3)	2.6773(3)	2.6769(4)
	2.6904(3)		2.6945(5)
Pd-C_{CO}	2.039(4)	2.043(3)	2.034(5)
	2.054(4)	2.058(3)	2.037(5)
	2.061(3)	2.077(3)	2.049(5)
	2.066(3)		2.051(5)
	2.072(3)		2.057(5)
	2.076(3)		2.059(4)
OC-Pd-CO	160.86(14)	159.78(14)	153.69(19)
	156.98(14)	158.61(9)	152.0(2)
	157.93(13)		140.02(18)
Pd-CO-Pd	80.48(13)	80.96(9)	81.56(18)
	81.88(12)	80.27(13)	81.7(2)
	80.12(13)		81.97(16)
Pd-Pd-Pd plane vs.	7.75	4.49	22.23
Pd-C_{CO}-Pd plane	4.47	4.49	19.11
	0.86	0	2.16

Table 3.2.1: Bond lengths (Å) and angles (°) for **3.1**, **3.2** and **3.3**.

Further scrutiny of the metrics of **3.1**, **3.2** and **3.3** revealed some additional interesting comparisons. The distortion of the bridging CO ligands from the Pd_3 plane (**Figure 3.2.5**) varies considerably in **3.1**-**3.3**. The smallest distortions are observed in compound **3.2** where the respective Pd-C_{CO}-Pd mean planes deviate by 0°, 4.49° and 4.49° (the molecule exhibits two-fold rotation symmetry). In **3.1**, the IMes ligand imparts a higher degree of deformation shown by angles of 0.86°, 4.47° and 7.75°. It would appear that this reflects the steric demand of these bridging fragments, or the bulk of the carbene substituents. However in **3.3**, with the least bulky NHC (I^nBu_2), there is still a significant deviation from the Pd_3 plane with angles of 22.23°, 19.11° and 2.16°. Clearly this does not agree with the argument that greater steric bulk is the only factor that increases the distortions between the palladium bound atoms and the bridging fragments. In **3.3**, the ability of the *n*-butyl substituents of the carbene to align themselves away from the

palladium core, alleviates the steric bulk giving the carbonyl groups more space to move above the plane of the three palladium atoms. This is supported by the C_{NHC}-N-C_N angle which is largest for **3.3** (124.2(4)°) in comparison with **3.1** (123.8(4)°) and **3.2** (123.9(8)°). This effect is emphasised by the $Pd_{centroid}$-Pd-C_{NHC} angles (average) which shows that the ligands in **3.3** (7.77°) lie further below the Pd_3 plane compared with **3.1** and **3.2** which have values of 4.32° and 3.02° respectively (**Figure 3.2.7**).

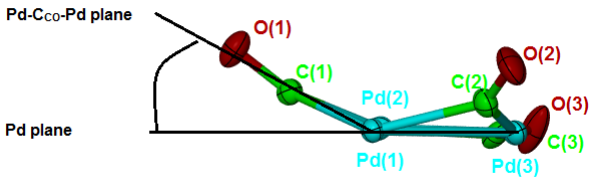

Figure 3.2.5: Pictorial representation of the angle between the Pd_3 and Pd-C_{CO}-Pd planes.

Unfortunately, there is no structural data available for an analogous $Pd_3(PR_3)_3(\mu\text{-}CO)_3$ for comparison.[6] However, $Pd_3(PBz_3)_3(\mu\text{-}CO)_2(\mu\text{-}SO_2)$ has been structurally characterised and, like the NHC clusters it is a 42-electron *triangulo*-cluster complex, thus allowing some comparison.[35] The crystal structure and structural data for this species are given in **Table 3.2.2**.

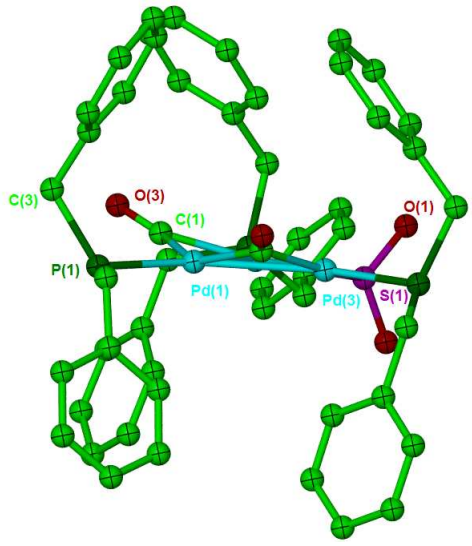

Bond lengths (Å) / Angles (°)	**$Pd_3(PBz_3)_3(\mu\text{-}CO)_2(\mu\text{-}SO_2)$**
Pd-P	2.322(1)
	2.332(1)
	2.312(1)
Pd-Pd	2.6850(6)
	2.694(6)
	2.7192(6)
Pd-C_{CO}	2.068(6)
	2.068(6)
Pd-Pd-Pd plane vs.	14.49
Pd-C_{CO}-Pd plane	16.55

Table 3.2.2: Bond lengths (Å) and angles (°) for $Pd_3(PBz_3)_3(\mu\text{-}CO)_2(\mu\text{-}SO_2)$. The crystal structure has the thermal ellipsoids set at 30% probability. Hydrogen atoms and two equatorial Bz groups have been removed for clarity.

The Pd-Pd bond lengths in $Pd_3(PBz_3)_3(\mu\text{-}CO)_2(\mu\text{-}SO_2)$ show a small level of asymmetry (2.6850(6) Å, 2.694(6) Å, 2.7192(6) Å) but, in contrast to the NHC clusters, the Pd-C_{CO} bond distances are the same (2.068(6) Å). The angles between the plane of the palladium core and the plane of the Pd-CO-Pd fragments are 14.49° and 16.55°, which are within the range of angles observed for **3.1**, **3.2** and **3.3**. This agrees with the idea that the steric bulk of the ligands are not the only factor affecting the distortion between planes. The less bulky Bz substituents on the phosphorus ligands are also able to direct themselves away from the palladium centres to some extent because of the presence of the CH_2 linker between the phosphorus and the phenyl group. The CH_2 linker forms a pocket of space allowing the CO groups freedom to move away from the plane (**Table 3.2.2**).

3.2.4 Reactivity of $Pd_3(IMes)_3(\mu\text{-}CO)_3$ (3.1)

Reactivity studies of **3.1** were carried out as this cluster was isolable in the highest yield and was the easiest to handle. Addition of 3 equivalents of CN^iPr to a THF or toluene solution of **3.1** failed to bring about substitution of the CO ligand even after 24 h at 120 °C. The addition of a different metal centre was attempted, similar to the reaction seen in **Scheme 3.1.6**, but instead of $Au(NO_3)(PPh_3)$, $AgCl(I^iPr_2)$ was used. It was hoped that like the gold complex, the silver species would cap the palladium cluster. One equivalent of $AgCl(I^iPr_2)$ was added to a THF solution of **3.1** and the reaction mixture stirred at room temperature. After a period of 2 h, the colour of the solution had lightened to a pale yellow colour, although this was accompanied by the formation of a black precipitate (either Pd or Ag), resulting from decomposition of either ligand or cluster.

When a slow stream of SO_2 was bubbled through a THF solution of **3.1** an exothermic reaction took place along with a rapid darkening of the solution to a blood red colour. The stream of SO_2 was continued until the solution had cooled. IR spectroscopy showed the loss of the parent carbonyl stretch at 1796 cm^{-1} and the appearance of three new lower frequency bands at 1261, 1099 and 1017 cm^{-1}. These are comparable to those reported for $Pd_3(PPh_3)(\mu\text{-}SO_2)_2(CNXyl)_2$ at 1203, 1055 and 1044 cm^{-1}, which were attributed to the SO_2 ligands.[36] The ^1H NMR spectrum showed a single set of IMes resonances at 7.12 and 6.79 ppm for the backbone and aryl C-H groups, and at 2.33 and 1.95 ppm for the mesityl CH_3 arms (*c.f.* **3.1**: 6.81, 6.14, 2.34 and 2.04 ppm). X-ray quality crystals, grown from THF/hexane, confirmed the structure of the product as the SO_2 substituted cluster $Pd_3(IMes)_3(\mu\text{-}SO_2)_3$ (**3.4**) shown in **Figure 3.2.6**.

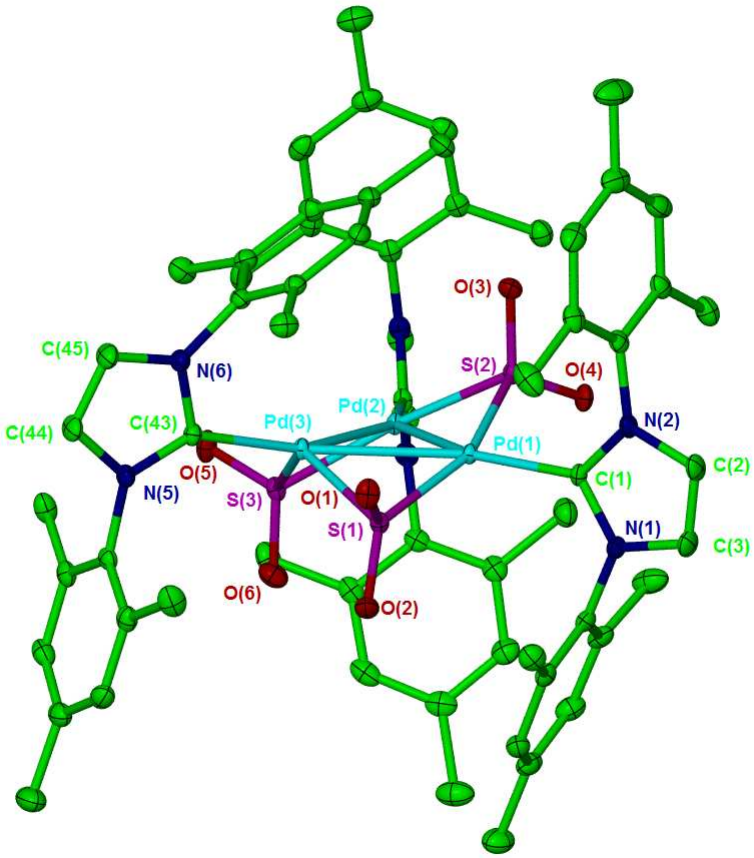

Figure 3.2.6: Crystal structure of $Pd_3(IMes)_3(\mu\text{-}SO_2)_3$ (**3.4**). Thermal ellipsoids set at 30% probability, hydrogen atoms omitted for clarity.

The bond lengths and angles in **3.4** are compared with those of the parent carbonyl cluster **3.1** in **Table 3.2.3**. Substitution of the carbonyl ligands for SO_2 results in a slight lengthening of the Pd-C_{NHC} distances from 2.072(3), 2.076(3) and 2.083(3) Å in **3.1** to 2.080(2), 2.080(2) and 2.095(2) Å in **3.4**. This may be due to the increased steric bulk of the SO_2 ligands compared to CO. The asymmetry seen in **3.1** is retained in **3.4** as shown by the range of Pd-SO_2 bond lengths (2.2522(6)-2.2878(6) Å) and Pd-Pd distances (2.8007(2), 2.7738(2) and 2.7888(2) Å).

Bond Length (Å) / Angle (°)	$Pd_3(IMes)_3(\mu\text{-}SO_2)_3$ (3.4)	$Pd_3(IMes)_3(\mu\text{-}CO)_3$ (3.1)
Pd-C_{NHC}	2.080(2)	2.072(3)
	2.080(2)	2.076(3)
	2.095(2)	2.083(3)
Pd-Pd	2.7738(2)	2.6520(3)
	2.7888(2)	2.6580(3)
	2.8007(2)	2.6904(3)
Pd-R	2.2522(6)	2.039(4)
	2.2530(6)	2.054(4)
	2.2638(6)	2.061(3)
	2.2738(6)	2.066(3)
	2.2870(6)	2.072(3)
	2.2878(6)	2.076(3)
R-Pd-R	156.78(2)	160.86(14)
	156.27(2)	156.98(14)
	122.17(2)	157.93(13)
Pd-R-Pd	75.869(18)	80.48(13)
	76.004(18)	81.88(12)
	75.571(19)	80.12(13)
Pd-Pd-Pd plane vs.	36.74	7.75
Pd-R-Pd plane	30.43	4.47
	-34.69	0.86

Table 3.2.3: Bond lengths (Å) and angles (°) of **3.1** and **3.4 (**R = μ-SO_2 or μ-CO).

The angles between the Pd core and the plane of the Pd-S-Pd fragments in **3.4** (30.43°, -34.69° and 36.74°) are much greater than those seen for the carbonyl ligands in **3.1** (0.86°, 4.47° and 7.75°), again presumably due to the greater steric bulk of SO_2. It is notable that two SO_2 ligands lie to one side of the Pd_3 plane while the third one is orientated on the opposite side. In addition to this, the carbene ligands also tilt relative to the average plane through the Pd centres in a fashion that minimises the steric interaction between neighbouring SO_2 groups. This is shown by small deviations of the carbene carbons from the mean plane of the palladium atoms (0.17°, 5.34° and 11.03°), but more markedly by the asymmetry induced in the Pd-C_{NHC}-N_{NHC} angles within each carbene fragment. These angle differences range from 1.3°-9.5° in **3.1** and 0°-25.5° in **3.4**. It is also worth noting that the positioning of two SO_2 groups on one side of the Pd_3 plane in **3.4** dramatically

reduces one of the S-Pd-S angles (122.17(2)° *c.f.* 156.78(2)°, 156.27(2)°) such that the structure cannot really be considered as a combination of three T-shaped ML_3 fragments in the solid state.

By way of comparison to **3.4**, $Pd_3(PBz_3)_3(\mu\text{-}SO_2)_3$[35] and $Pt_3(PR_3)_3(\mu\text{-}SO_2)$ (R = Ph,[37] Cy[38]) exhibit planar $M_3(\mu\text{-}SO_2)_3$ arrangements, although in the case of the platinum cluster, non-planarity can be induced by increasing the cluster count from 42- to 44-electron upon addition of another ligand, as in the case of $Pt_3(PCy_3)_3(dppp)(\mu\text{-}SO_2)_3$ (dppp = 1,3-*bis*(diphenylphosphino)propane).[39] A comparison of the metrics for **3.4** and $Pd_3(PBz_3)_3(\mu\text{-}SO_2)_3$ is shown in **Table 3.2.4**.

Bond length (Å) / Angle (°)	**$Pd_3(IMes)_3(\mu\text{-}SO_2)_3$ (3.4)**	**$Pd_3(PBz_3)_3(\mu\text{-}SO_2)_3$**
Pd-Pd	2.7738(2)	2.7225(9)
	2.7888(2)	
	2.8007(2)	
Pd-SO_2	2.2522(6)-2.2878(6)	2.264(2)
		2.2841(2)
S-Pd-S	156.78(2)	166.01(6)
	156.27(2)	
	122.17(2)	
Pd-S-Pd	75.869(18)	73.53(6)
	76.004(18)	
	75.571(19)	
Pd-Pd-Pd plane	36.74	2.12
vs. Pd-S-Pd plane	30.43	
	34.69	

Table 3.2.4: Comparison of bond lengths (Å) and angles (°) for **3.4** and $Pd_3(PBz_3)_3(\mu\text{-}SO_2)_3$.

Unlike **3.4**, $Pd_3(PBz_3)_3(\mu\text{-}SO_2)_3$ is highly symmetrical, evident from the arrangement of the palladium atoms in an equilateral triangle with a crystallographically imposed three fold axis. The Pd-Pd distances for this complex are slightly shorter than those in **3.4** (2.7225(9) *c.f.* 2.7738(2), 2.7888(2), 2.8007(2) Å). Again this may be due to the decreased steric bulk of the PBz_3 ligand compared with the IMes ligand in **3.4**. There is a degree of asymmetry associated with $Pd_3(PBz_3)_3(\mu\text{-}SO_2)_3$ which is comparable with **3.4** *i.e.* there is a small but significant difference between Pd-SO_2 bond distances (2.264(2) and 2.2841(2) Å, **3.4**: 2.2522(6)-2.2878(6) Å). Upon comparing the angles between the Pd core and the Pd-S-Pd plane, $Pd_3(PBz_3)_3(\mu\text{-}SO_2)_3$ was found to be more planar than **3.4**, with an angle of 2.12° compared to 36.74°, 30.43° and 34.69°. In addition, the planarity of the phosphine ligands (*i.e.* the angle between the Pd core versus Pd-P/Pd-C_{NHC}, **Figure 3.2.7**) is much greater than for the IMes ligands in **3.3**. In $Pd_3(PBz_3)_3(\mu\text{-}SO_2)_3$ the

phosphorus atom deviates from the Pd core by 3.46° in comparison with angles of 0.17°, 5.39° and 11.03° in **3.4**.

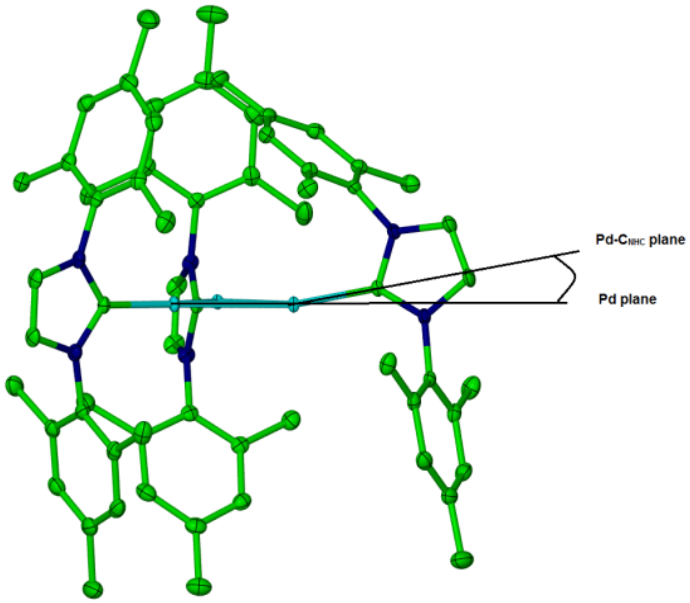

Figure 3.2.7: Pictorial representation of the angle between the Pd core and the Pd-L plane.

3.3 Summary

The synthesis of the first examples of palladium NHC carbonyl clusters $Pd_3(IMes)_3(\mu\text{-}CO)_3$ (**3.1**), $Pd_3(I^iPr_2)_3(\mu\text{-}CO)_3$ (**3.2**) and $Pd_3(I^nBu_2)_3(\mu\text{-}CO)_3$ (**3.3**) has been achieved upon reduction of $PdCl_2(NHC)_2$ with potassium graphite under a carbon monoxide atmosphere. Treatment of **3.1** with SO_2 yields $Pd_3(IMes)_3(\mu\text{-}SO_2)_3$ (**3.4**).[40] Complexes **3.1-3.4** show different levels of sensitivity; **3.1** and **3.4** are stable under an inert atmosphere, whereas complex **3.2** is only stable under CO and **3.3** degrades even when stored under CO in solution over a short period of time.

The carbonyl clusters are structurally similar with asymmetry observed around the palladium core, this being most apparent in **3.3**. The closest non-NHC cluster for comparison is $Pd_3(PBz_3)_3(\mu\text{-}CO)_2(\mu\text{-}SO_2)$, which also shows asymmetry, but exhibits symmetrical Pd-CO bond lengths. The increased bulk of the SO_2 ligands has the effect of increasing the Pd-Pd distances in **3.4** in comparison with those in **3.1**, **3.2** and **3.3**. Similarly, in **3.4** the angles between the Pd_3 core and the Pd-SO_2-Pd planes also increase. The presence of the bulky N-mesityl substituents on the carbene helps to stabilise $Pd_3(\mu\text{-}CO)_3$ against the degradation seen with smaller, more flexible I^iPr_2 and I^nBu_2 ligands.

3.4 References

1. Mednikov, E. G.; Ivanov, S. A.; Dahl, L. F., *Angew. Chem. Int. Ed.* **2003**, *42,* 323-327.
2. Mednikov, E. G.; Ivanov, S. A.; Slovokhotova, I. V.; Dahl, L. F., *Angew. Chem. Int. Ed.* **2005**, *44,* 6848-6854.
3. Tran, N. T.; Powell, D. R.; Dahl, L. F., *Angew. Chem. Int. Ed.* **2000**, *39,* 4121-4125.
4. Yoshida, T.; Otsuka, S., *J. Am. Chem. Soc.* **1977**, *99,* 2134-2140.
5. Mednikov, E. G.; Eremenko, N. K.; Gubin, S. P., *Koord. Khim.* **1984**, *10,* 711-714.
6. Burrows, A. D.; Mingos, D. M. P., *Trans. Met. Chem.* **1993**, *18,* 129-148.
7. Goddard, R.; Jolly, P. W.; Kruger, C.; Schick, K. P.; Wilke, G., *Organometallics* **1982**, *1,* 1709-1712.
8. Bochmann, M.; Hawkins, I.; Hursthouse, M. B.; Short, R. L., *Polyhedron* **1987**, *6,* 1987-1991.
9. Christofides, A., *J. Organomet. Chem.* **1983**, *259,* 355-365.
10. Burrows, A. D.; Fleischer, H.; Mingos, D. M. P., *J. Organomet. Chem.* **1992**, *433,* 311-321.
11. Otsuka, S.; Tatsuno, Y.; Miki, M.; Aoki, T.; Yoshioka, H.; Nakatsu, K., *J. Chem. Soc., Chem. Commun.* **1973**, 445-446.
12. Misono, A.; Uchida, Y.; Hidai, M.; Kudo, K., *J. Organomet. Chem.* **1969**, *20,* P7-P8.
13. Kudo, K.; Hidai, M.; Uchida, Y., *J. Organomet. Chem.* **1971**, *33,* 393-398.
14. Hidai, M.; Kokura, M.; Uchida, Y., *J. Organomet. Chem.* **1973**, *52,* 431-435.
15. Mednikov, E. G.; Ermenko, N. K.; Slovokhotov, Y. L.; Struchkov, Y. T.; Gubin, S. P., *Koord. Khim.* **1987**, 979-982.
16. (a) Dubrawski, J.; Kriegesimondsen, J. C.; Feltham, R. D., *J. Am. Chem. Soc.* **1980**, *102,* 2089-2091; (b) Feltham, R. D.; Elbaze, G.; Ortega, R.; Eck, C.; Dubrawski, J., *Inorg. Chem.* **1985**, *24,* 1503-1510.
17. Bott, S. G.; Ezomo, O. J.; Mingos, D. M. P., *J. Chem. Soc., Chem. Commun.* **1988**, 1048-1049.
18. Mednikov, E. G.; Eremenko, N. K.; Slovokhotov, Y. L.; Struchkov, Y. T., *J. Organomet. Chem.* **1986**, *301,* C35-C37.
19. Burrows, A. D.; Machell, J. C.; Mingos, D. M. P., *J. Chem. Soc. Dalton. Trans.* **1992**, 1939-1947.
20. Kantchev, E. A. B.; O'Brien, C. J.; Organ, M. G., *Angew. Chem. Int. Ed.* **2007**, *46,* 2768-2813.
21. Titcomb, L. R.; Caddick, S.; Cloke, F. G. N.; Wilson, D. J.; McKerrecher, D., *Chem. Commun.* **2001**, 1388-1389.

22. Gstöttmayr, C. W. K.; Böhm, V. P. W.; Herdtweck, E.; Grosche, M.; Herrmann, W. A., *Angew. Chem. Int. Ed.* **2002**, *41,* 1363-1365.
23. Fantasia, S.; Nolan, S. P., *Chem.-Eur. J.* **2008**, *14,* 6987-6993.
24. Arnold, P. L.; Cloke, F. G. N.; Geldbach, T.; Hitchcock, P. B., *Organometallics* **1999**, *18,* 3228-3233.
25. Böhm, V. P. W.; Gstöttmayr, C. W. K.; Weskamp, T.; Herrmann, W. A., *J. Organomet. Chem.* **2000**, *595,* 186-190.
26. Caddick, S.; Cloke, F. G. N.; Clentsmith, G. K. B.; Hitchcock, P. B.; McKerrecher, D.; Titcomb, L. R.; Williams, M. R. V., *J. Organomet. Chem.* **2001**, *617,* 635-639.
27. Arentsen, K.; Caddick, S.; Cloke, F. G. N., *Tetrahedron* **2005**, *61,* 9710-9715.
28. Kudo, K.; Hidai, M.; Uchida, Y., *J. Organomet. Chem.* **1971**, *33,* 393.
29. Weskamp, T.; Böhm, V. P. W.; Herrmann, W. A., *J. Organomet. Chem.* **1999**, *585,* 348-352.
30. Herrmann, W. A.; Böhm, V. P. W.; Gstöttmayr, C. W. K.; Grosche, M.; Reisinger, C. P.; Weskamp, T., *J. Organomet. Chem.* **2001**, *617,* 616-628.
31. Herrmann, W. A.; Elison, M.; Fischer, J.; Kocher, C.; Artus, G. R. J., *Angew. Chem. Int. Ed.* **1995**, *34,* 2371-2374.
32. Lebel, H.; Janes, M. K.; Charette, A. B.; Nolan, S. P., *J. Am. Chem. Soc.* **2004**, *126,* 5046-5047.
33. $Pd_3(IMes)_3(\mu\text{-}CO)_3$ can be synthesised from both the normal and abnormal $PdCl_2(IMes)_2$ complexes.
34. Bond lengths and angles measured from CIF file.
35. Arifhodzic-Radojevic, S.; Burrows, A. D.; Choi, N.; McPartlin, M.; Mingos, D. M. P.; Tarlton, S. V.; Vilar, R., *J. Chem. Soc., Dalton. Trans.* **1999**, 3981-3988.
36. Burrows, A. D.; Machell, J. C.; Mingos, D. M. P.; Powell, H. R., *J. Chem. Soc., Dalton. Trans.* **1992**, 1521-1530.
37. Moody, D. C.; Ryan, R. R., *Inorg. Chem.* **1977**, *16,* 1052-1055.
38. Bott, S. G.; Hallam, M. F.; Ezomo, O. J.; Mingos, D. M. P.; Williams, I. D., *J. Chem. Soc., Dalton. Trans.* **1988**, 1461-1466.
39. Hallam, M. F.; Howells, N. D.; Mingos, D. M. P.; Wardle, R. W. M., *J. Chem. Soc., Dalton. Trans.* **1985**, 845-850.
40. Attempts to form the analogous I^iPr_2 complex by the reaction of $Pd_3(I^iPr_2)_3(\mu\text{-}CO)_3$ with SO_2 led to the rapid decomposition of the product.

4.1 Introduction

4.1.1 Preface

Polydentate N-heterocyclic carbene (NHC) ligands represent a small subset of the vast array of NHCs now present in the literature.[1] Of the tripodal NHCs reported, the examples isolated by Fehlhammer and Smith, and Meyer have received most attention.[2,3,4] These tripodal carbenes contain small central atoms or groups which allow the ligand to bind a selection of single metal atoms such as Mn, Fe, Co, Ni and Cu. In contrast, tripodal NHCs with large central arene groups have been largely overlooked because the large central group restricts what can be accommodated between the three carbene arms.

4.1.2 Tripodal N-heterocyclic carbenes

Tripodal carbene ligands commonly consist of a central atom or group which acts as an anchor for the three pendant arms bearing the NHC groups. A number of central anchors have been used in tripodal NHCs, including carbon,[5] boron,[2a] nitrogen[4c] and arene groups.[6] The arms of the tripodal carbene can separated from the central moiety by linker chains which generally are small alkyl groups. By alternating these groups, the topological properties of the ligand, such as steric hindrance, bite angle, chirality and fluxional behaviour can be fine tuned. Variation of the central group and the linkers can have a dramatic impact on the coordination chemistry of the ligand.

A gradual increase in the number of tripodal NHC complexes has been seen over the past decade, since the first example was reported in 1996 by Fehlhammer and co-workers. This work showed that the *tris*-imidazolium salt, similar to Trofimenko's *tris*-pyrazolyl borate ligand, could be deprotonated with ^{n}BuLi and reacted with $FeCl_2$ to afford a *bis*-tripodal NHC Fe(III) complex (**Scheme 4.1.1**).[2a] Furthermore this ligand can coordinate to Co(III),[2b] Ag(I),[2g] Au(I)[2g] and Cu(I),[3] affording hexacarbene complexes similar to the iron compound. Interestingly, the imidazolium precursor was also shown to coordinate lithium upon reaction with ^{n}BuLi affording a bimetallic complex containing two tripodal ligands.[2c] In each of these cases, the ligand binds in a *fac* geometry as there is only marginal space for coordination due to the small central group and the absence of linker groups. This type of ligand can also bind to heavy earth metals such as Mg, Ca, Sr and Ba with one tripodal carbene coordinated to a single metal centre generating complexes of the form $[(HB(Im^{tBu})M\{N(SiMe_3)_2\}_2]$ (**Scheme 4.1.1**).[2h] In addition, the central boron atom can be functionalised to incorporate a phenyl group, which has led to the synthesis of Co(II) and air stable Mn(IV) complexes bearing only one tripodal NHC.[2e,2f]

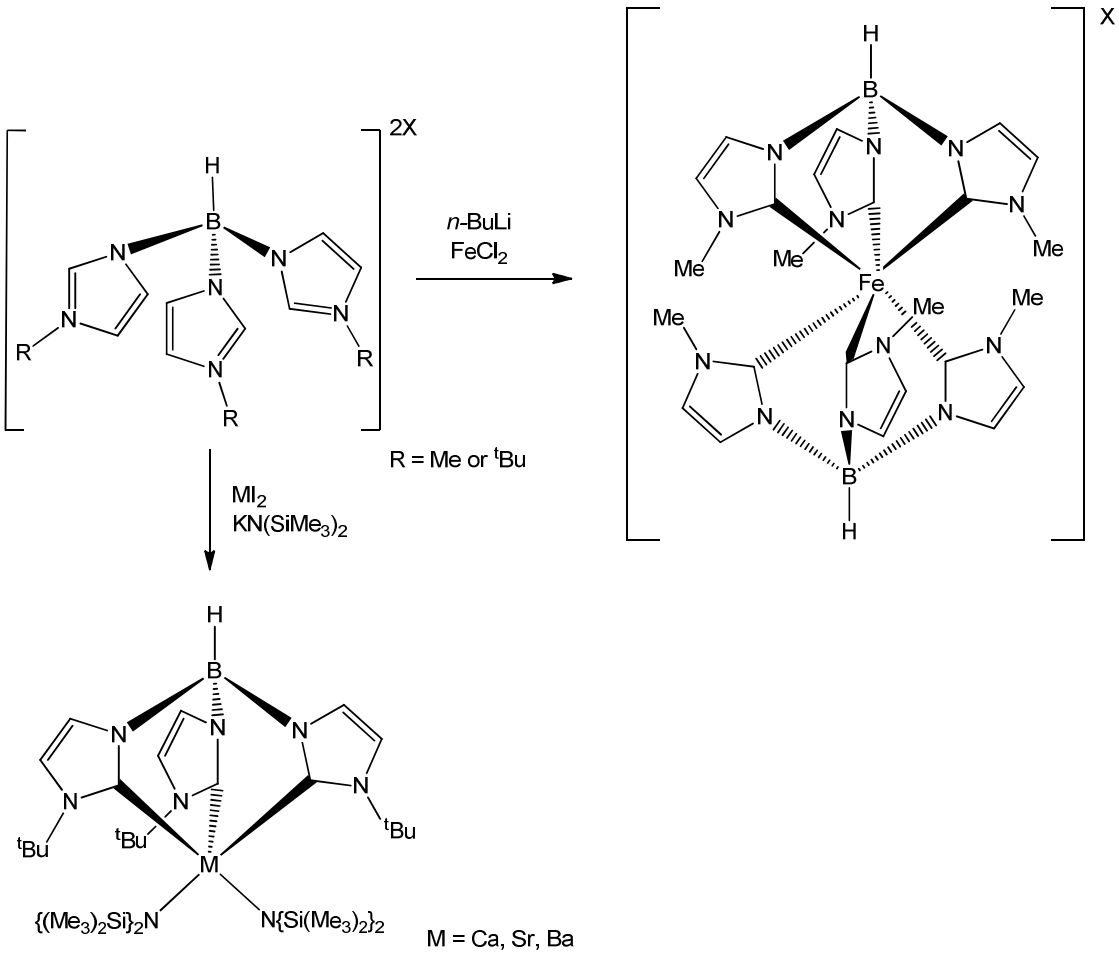

Scheme 4.1.1: The synthesis of *bis*- and mono- tripodal NHC complexes.

In 2003, Meyer and co-workers reported the synthesis of a new *tris*-carbene ligand 1,1,1-{*tris*(3-alkylimidazole-2-ylidene)methyl}ethane ($TIME^R$), and its coordination to the group 11 metals Cu and Ag. Although the tripodal carbene possesses the topological requirements to bind in a *fac* arrangement, only di- and trimetallic species were formed.[7] For example, the complex $[(TIME^{tBu})_2Cu_2](PF_6)_2$ shown in **Scheme 4.1.2**, has two tripodal ligands coordinated in both normal and abnormal binding modes to two copper centres. This is due to the larger cavity afforded by the presence of methylene linker groups allowing coordination of the ligand to multiple metal centres.

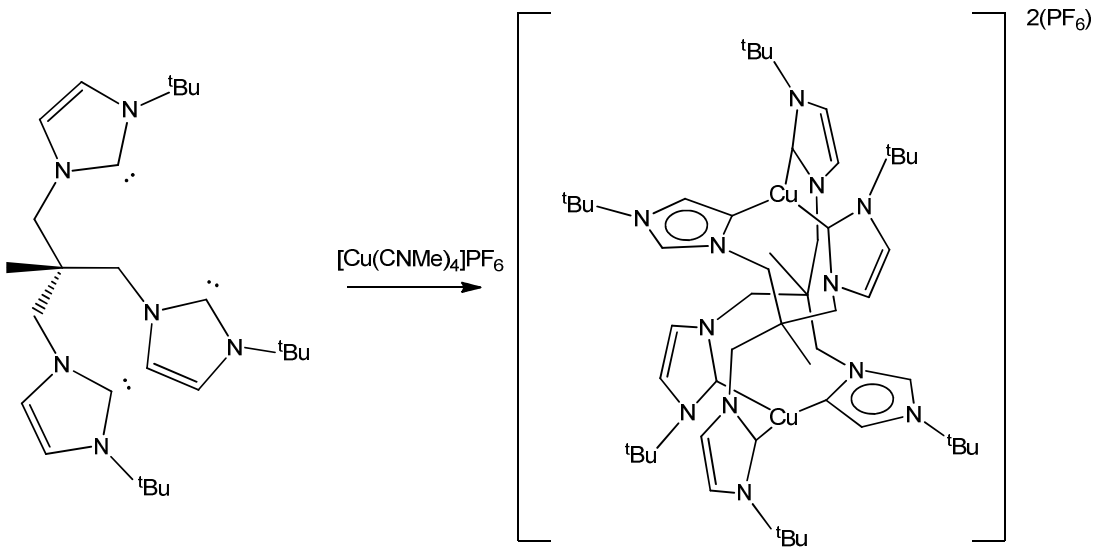

Scheme 4.1.2: The coordination of TIME^{tBu} to copper(I).

The coordination chemistry of this variety of tripodal ligand has been extended to Rh and Ir upon reaction with $[MCl(COD)]_2$ where, depending on the reaction conditions, two separate compounds can be formed. In the presence of a weak base such as NEt_3, mononuclear Rh(I) and Ir(I) species can be isolated, in which two of the NHC arms are coordinated to the same metal centre and the third arm remains out of the coordination sphere as an imidazolium cation. In contrast, when the NHC was first coordinated to silver by reaction with Ag_2O and then transmetallated to Rh or Ir, complexes containing the ligand bridged between two metal fragments were generated (**Scheme 4.1.3**).[5]

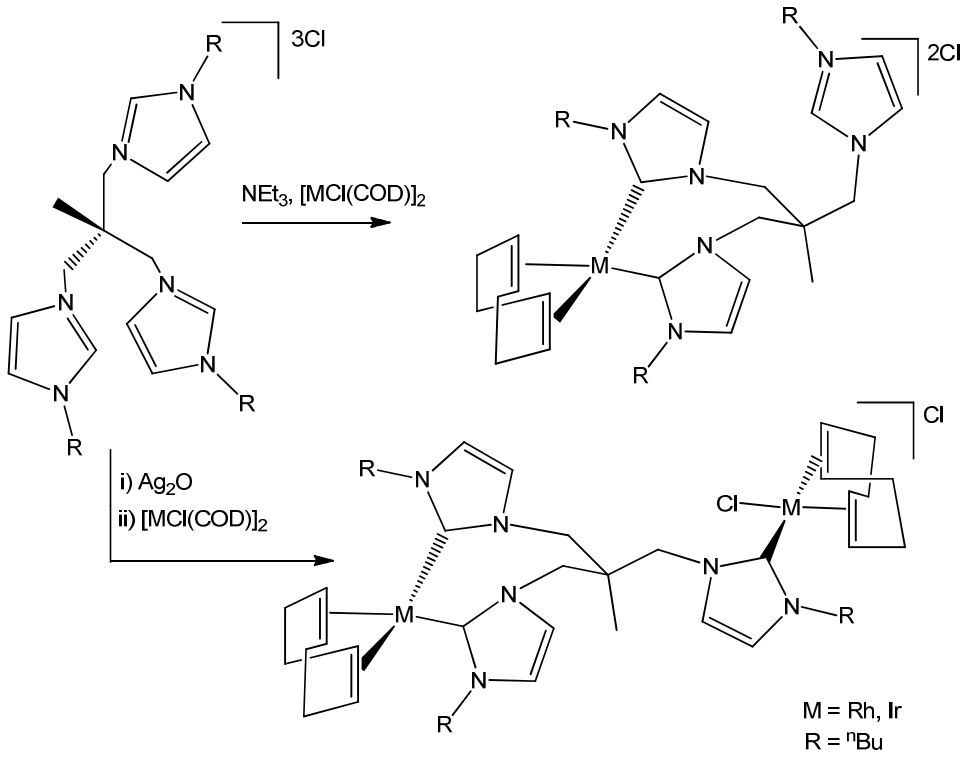

Scheme 4.1.3: The different coordination modes of $TIME^{nBu}$ in Rh(I) and Ir(I) complexes.

Tripodal NHCs with larger central cavities can still bind in a *fac*-arrangment. For example, a tripodal NHC containing a central nitrogen anchor with ethylene linkers ($TIMEN^{R}$) has been shown to coordinate to a number of metals, including, Co[4b, c] Ni,[4d] Cu[4a, 4e] and, more recently, Fe.[4f, 8] The inclusion of a nitrogen atom enables the carbene to coordinate in a *fac* tri- or tetradentate form. One interesting example is shown in **Scheme 4.1.4** where the ligand coordinates in a tridentate arrangement to a Ni(0) centre which upon one electron oxidation affords the corresponding Ni(I) complex with the ligand now coordinated in a tetradentate form through ligation of the apical nitrogen. Complexes of this nature have been shown to provide interesting reactivity, for example [($TIMEN^{Xyl}$)Co]Cl has been shown to activate small molecules including CO and O_2.[4c]

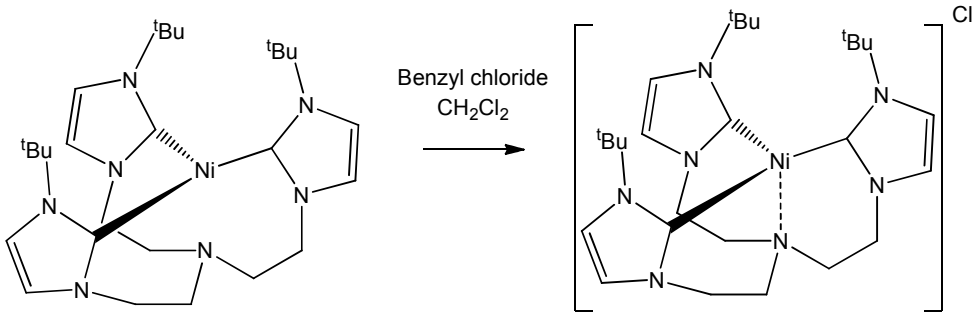

Scheme 4.1.4: The synthesis of Ni(0)/(I) TIMEN^{tBu} complexes.

The tripodal NHC containing a central mesityl group 1,3,5-[*tris*(3-*tert*-butylimidazole-2-ylidene)methyl]-2,4,6-trimethylbenzene (timtmb^{tBu}) was first reported in 1994 by Dias and co-workers.[6] The arene central group leads to the presence of a very large cavity which has restricted the coordination chemistry of this type of ligand. One example of its complexation has been shown by the reaction of the free carbene with Tl(OTf) (**Scheme 4.1.5**).[9] The compound is highly temperature sensitive and readily decomposes at room temperature, in contrast to other Tl(III) NHC complexes which display high thermal stabilities.[10]

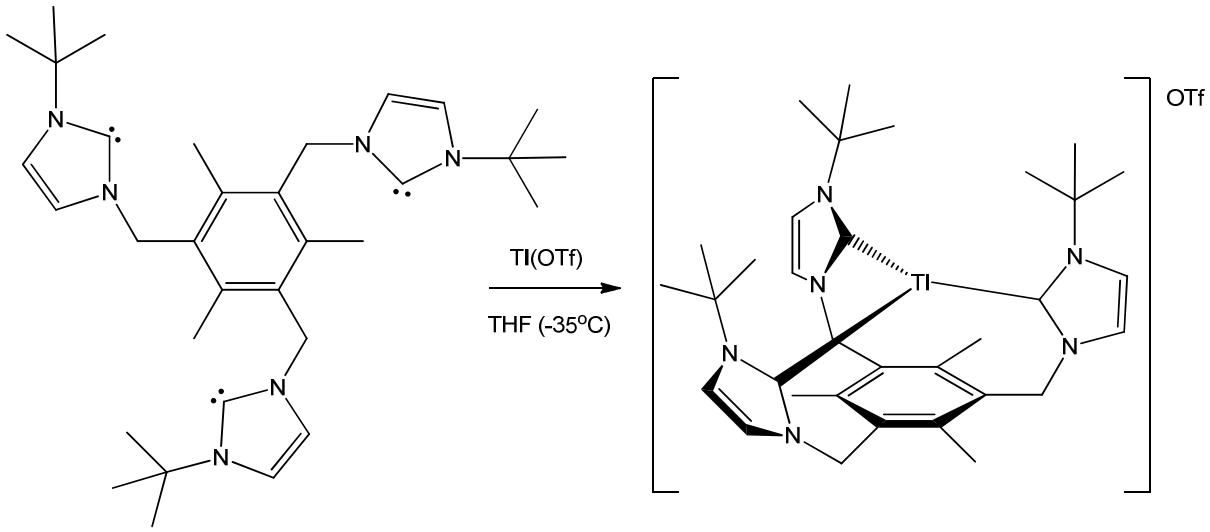

Scheme 4.1.5: The coordination of the NHC timtmb^{tBu} to Tl(I).

Another example of the coordination chemistry of this type of tripodal ligand was reported by Hahn and co-workers in 2010 in which a tripodal NHC bearing a central phenyl group with no linker groups was coordinated to both Ag and Au.[11] The Ag product was prepared by the reaction of two equivalents of the tripodal imidazolium salt with three equivalents Ag_2O to afford $[Ag_3(NHC)_2]X_3$. This was subsequently reacted with three equivalents of $AuCl(SMe_3)$ to generate

the analogous gold complex. In these examples, the carbene bridges three metal fragments in a monodentate manner, so that each carbene is coordinated to a separate metal centre, leading to a *bis*-tripodal NHC complex of the form $[M_3(NHC)_2](PF_6)_3$, as shown for M = Ag in **Scheme 4.1.6**.

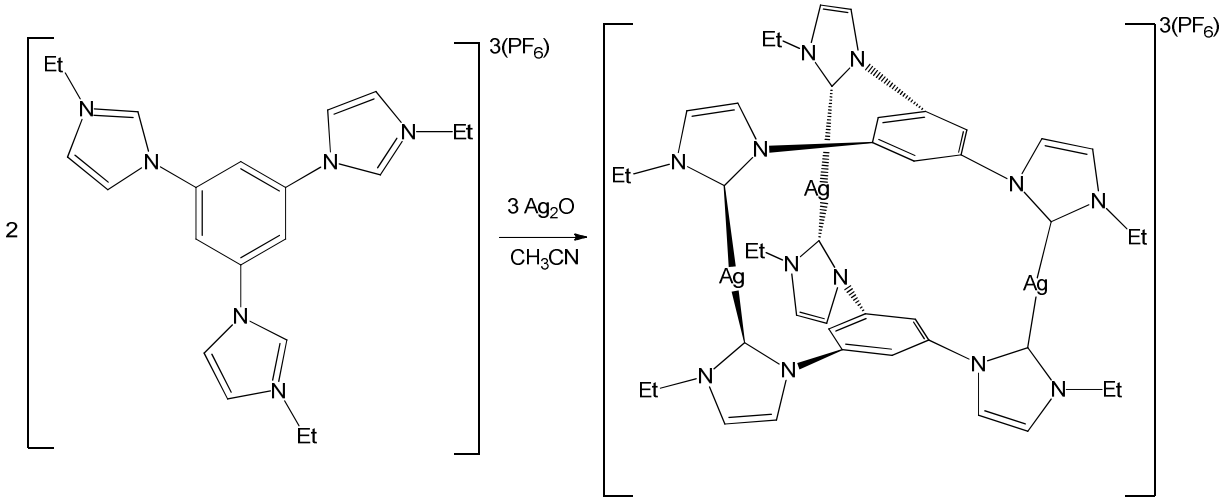

Scheme 4.1.6: Synthesis of the *bis*-tripodal carbene complex $[Ag_3(NHC)_2](PF_6)_3$.

A further binding mode of tripodal NHCs with large central arene anchors has been illustrated by Steed and co-workers. In this case a *tris*-carbene cage made up of two central arene groups bridged by the three imidazole rings has been shown to react with silver oxide affording a complex where the silver ion is essentially trapped within the cage. As an previous examples, two of the carbene arms have coordinated to a silver atom, whereas the third remains free as an imidazolium cation (**Figure 4.1.1**).[12]

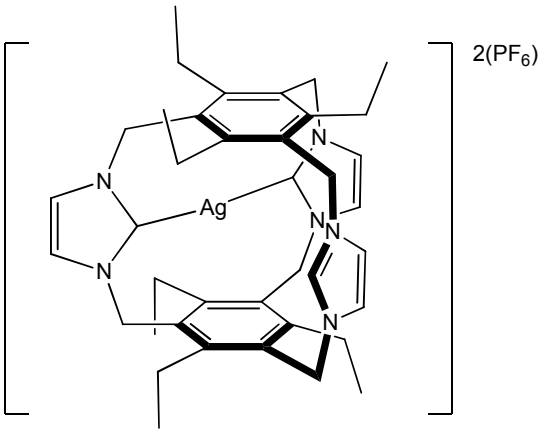

Figure 4.1.1: The tripodal NHC cage coordinated with Ag(I).

4.1.3 Tripodal carbene complexes in catalysis

NHCs have been proven to be excellent ligands for catalysts, providing complexes with enhanced performance and higher stabilities.[13] Similarly, the use of polydentate NHC ligands has allowed the synthesis of new compounds whose stability is entropically enhanced by the chelate effect.[1a, 1e] Most of the examples reported so far are bidentate and pincer (tridentate-*mer*) *bis*-carbene ligands coordinated to Pd, Rh, Ru and Ir.[1a, 1c] In contrast, complexes containing tripodal NHCs have rarely been utilised in catalytic reactions. The examples discussed below are, to our knowledge, the only examples of the use of tripodal *tris*-NHC ligands in catalysis.

The catalytic activity of Rh and Ir complexes (both mono- and bimetallic) of TIMEN^{iPr} has been utilised in the catalytic cyclisation of acetylenic carboxylic acids.[14] The analogous complexes bearing TIME^{nBu} (**Scheme 4.1.3)** have been reported by Peris and co-workers for the hydrosilylation of terminal alkynes (**Scheme 4.1.7**).[5]

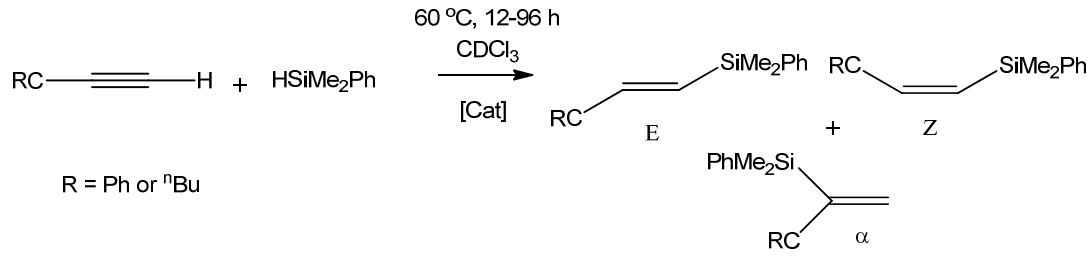

Scheme 4.1.7: Rh/Ir tripodal NHC catalysed hydrosilylation of alkynes.

They showed that the Rh complexes were far more active than the analogous Ir examples, with the bimetallic Rh complex being the most active. The catalytic activity was compared with the similar *bis*-NHC complex $[RhI(COD)]_2(NHC)$ (**Figure 4.1.2**)[15] but, unfortunately, the *tris*-carbene complexes were shown to exhibit lower catalytic activity. It was believed that the inactivity of the tripodal complexes towards oxidation to M(III) inhibited the catalytic rates, as oxidative addition of the silane to the metal complex is proposed to be the rate-dependent step in the hydrosilylation reaction.

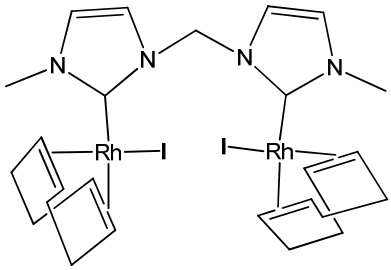

Figure 4.1.2: $[RhI(COD)]_2(NHC)$ complex used to compare catalytic rates of tripodal NHC complexes.

The use of the tripodal NHC complexes $[Cu_3(HB(MeIm)_3)_2]BF_4$ (**C1**) and $[Cu_3(HB(^nBuIm)_3)_2]Br$ (**Figure 4.1.3**) in C-O, C-N and C-C coupling reactions has been reported by Biffis and co-workers.[3] They investigated the catalytic activity of both complexes in comparison with the monomeric copper carbene complex CuCl(IPr) (**C2**).[16] They argued that this was the most active copper carbene catalyst and therefore a good complex against which to evaluate the activity of the tripodal complexes. It was shown that both trinuclear copper(I) carbene complexes displayed enhanced catalytic activity in the Ullmann-type arylation reactions of azoles and phenols (C-N and C-O coupling), converting aryl iodides, bromides and even activated aryl chlorides at comparatively low reaction temperatures in comparison with **C2**. This suggests the tripodal NHC makes a positive contribution to the catalytic efficiency. The activity of these compounds will be discussed in greater detail later on.

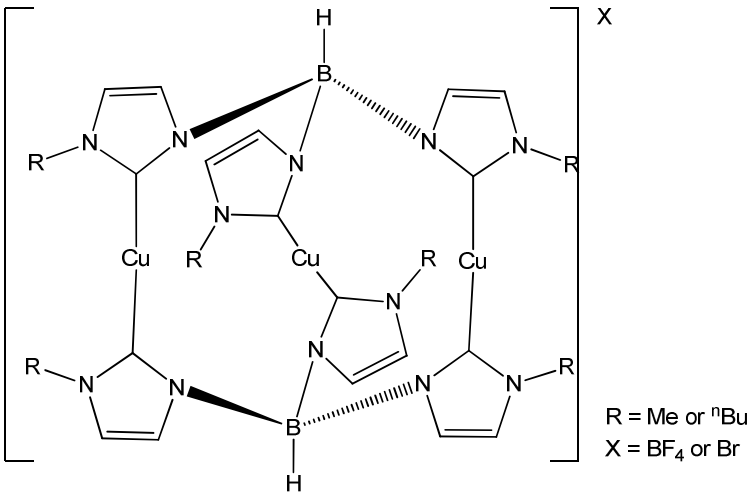

Figure 4.1.3: The copper(I) complexes utilised in C-C, C-N and C-O coupling reactions.

4.2 Palladium complexes bearing tripodal NHCs

4.2.1 Preface

As discussed above, the coordination of tripodal NHCs bearing arene anchors has been overlooked with few examples reported in the literature.[9, 11-12] A result of this, there was scope for the development of their coordination chemistry. We were interested in testing the catalytic activity of any complex synthesised with these tripodal ligands and hoped to see an improvement in catalytic activity compared with their mono and bidentate analogues.

In this chapter we will discuss the synthesis and coordination of the tripodal NHCs 1,3,5-{*tris*(R-imidazol-2-ylidene)methyl}-2,4,6-triethylbenzene, abbreviated to timteb^{R}, where R = *tert*-butyl or 2,6-diisopropylphenyl (dipp), shown in **Figure 4.2.1**.

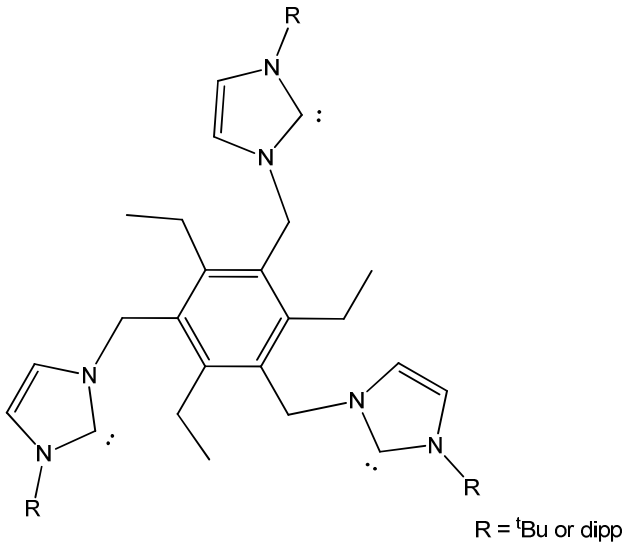

Figure 4.2.1: Pictorial representation of timteb^{R}.

4.2.2 Synthesis of timteb^{R}

The attempted synthesis of the timteb^{tBu} imidazolium salt was based initially on the method developed by Dias and co-workers for the trimethylbenzene analogue, involving reaction between 1,3,5-*tris*(chloromethyl)-2,4,6-trimethylbenzene and *tert*-butyl imidazole at 100 °C for 24 h.[6] However, we were unable to afford the desired product cleanly, evidenced by a number of high frequency imidazolium peaks in the ^{1}H NMR spectrum of the reaction mixture. This resulted in the use of the bromo-arene analogue as the weaker C-Br bonds were expected to react more cleanly under less forcing conditions. 1,3,5-*tris*(bromomethyl)-2,4,6-triethylbenzene was synthesised

according to the route described by Wallace *et. al.*,[17] and reacted with either *tert*-butyl or 2,6-diisopropylphenyl (dipp) substituted imidazoles at room temperature.[18] In both cases, subsequent warming to 50 °C for a short period cleanly afforded the tripodal imidazolium salts as white solids in good yields (**Scheme 4.2.1**). Analysis of the products by NMR spectroscopy revealed the presence of a single high frequency resonance at 10.88 and 10.69 ppm for $[timteb^{tBu}H_3]Br_3$ and $[timteb^{dipp}H_3]Br_3$ respectively corresponding to the imidazolium protons. The signals integrated to the central arene ethyl peaks in 3:6 (CH_2) and 3:9 (CH_3) ratios confirming that all three arms of the ligand were attached. The imidazolium NCHN group was also evident in the $^{13}C\{^1H\}$ PENDANT NMR spectra at 135.9 and 137.9 ppm for the ^{t}Bu and dipp derivatives respectively.

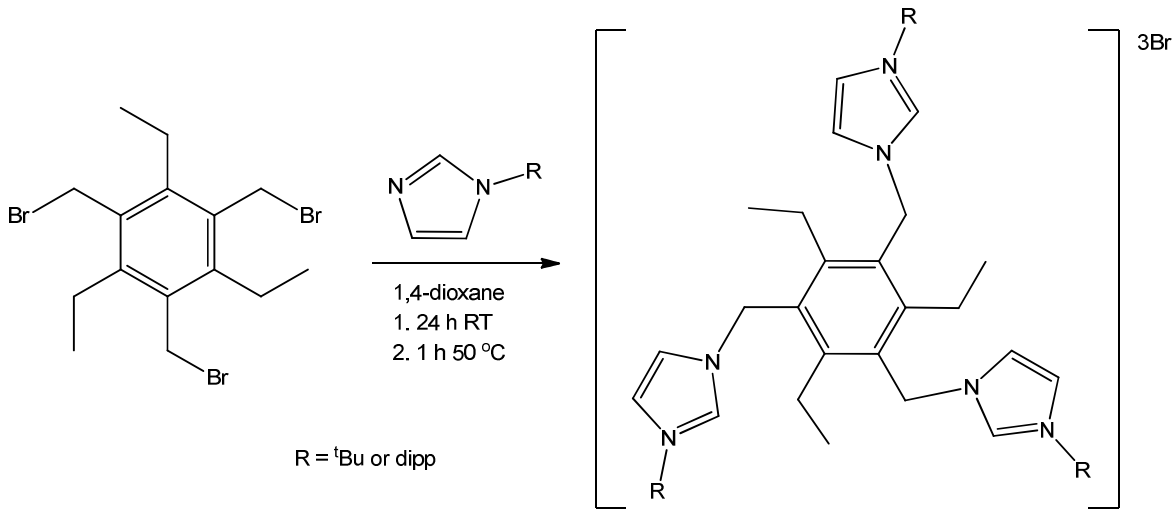

Scheme 4.2.1: Synthesis of the tripodal carbene precursor $[timteb^RH_3]Br_3$ (R = ^{t}Bu, dipp).

Like most imidazolium salts, $[timteb^RH_3]Br_3$ can be readily deprotonated with $KN(SiMe_3)_2$ in THF to form the free carbenes. These were isolated as stable white solids which were stored under an inert atmosphere and spectroscopically characterised by the appearance of high frequency quaternary carbenic carbon resonances in the $^{13}C\{^1H\}$ NMR spectra at 214.5 ppm for $timteb^{tBu}$ and 218.9 ppm for $timteb^{dipp}$.

4.2.3 Synthesis of $(timteb^{tBu})\{PdI_2(ICy)\}_3$ (4.1)

We believed that the synthesis of new palladium tripodal NHC complexes would enable us to achieve the goals set out in the preface of this section. The reaction of $timteb^R$ with palladium would allow us to test the coordination of the NHCs and determine whether they would lead to similar complexes as those as described by Hahn and co-workers (**Scheme 4.1.6**). In addition to

this the use of palladium would allow for the investigation of the catalytic activities, to see if the trimetallic complexes would exhibit enhanced catalytic activity over their monomeric analogues.

Our initial thoughts were to synthesise a palladium(II) complex bearing one monodentate NHC as well as the tripodal ligand, forming a *bis*-NHC Pd(II) complex. With this in mind, we prepared the dimer $[Pd(\mu\text{-}I)I(ICy)]_2$ using the route reported by Herrmann and co-workers (**Scheme 4.2.2**), as a convenient precursor to afford the desired compound (timteb^{tBu})$\{PdI_2(ICy)\}_3$.[19] The addition of timteb^{tBu} to a THF solution containing 3 equivalents of $[Pd(\mu\text{-}I)I(ICy)]_2$ resulted in an immediate colour change from red to pale yellow at room temperature. A ^{1}H NMR spectrum of the reaction mixture revealed only extremely broad proton resonances even upon cooling to a temperature as low as -50 °C, although it was clear that the solution contained a mixture of products. This led us to employ the phosphine complex *trans*-$PdI_2(ICy)(PPh_3)$ (**Scheme 4.2.2**), which had the major advantage of possessing a phosphorus ligand that would allow the progress of the reaction to be followed by $^{31}P\{^1H\}$ NMR spectroscopy.

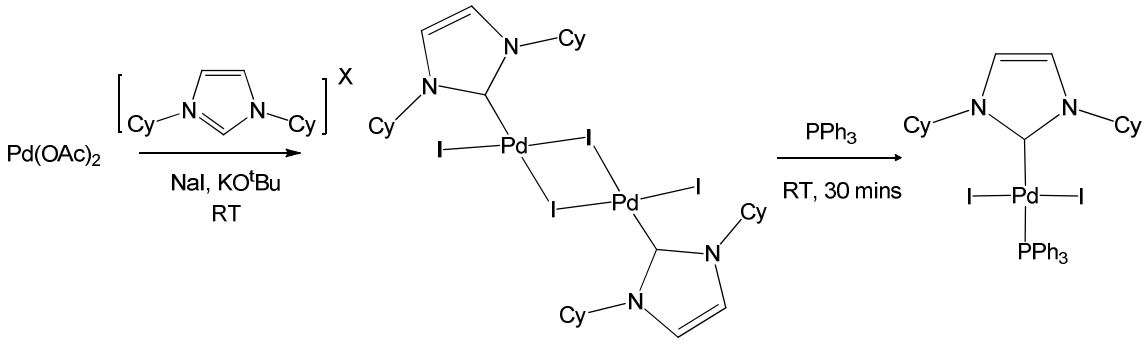

Scheme 4.2.2: Synthesis of $PdI_2(ICy)(PPh_3)$.

A J Young's ampoule was charged with three equivalents of *trans*-$PdI_2(ICy)(PPh_3)$ and timteb^{tBu} in THF. The solution was heated at 70 °C for 4 h, resulting in a colour change from orange to a pale yellow. The proton spectrum of the solution was again very broad, but suggested that the reaction mixture was somewhat cleaner than the reaction with timteb^{tBu} and $[Pd(\mu\text{-}I)I(ICy)]_2$. Three broad singlets were apparent at 7.00, 6.93 and 6.14 ppm corresponding to backbone C-H groups of the NHC, as well as a single broad quartet at 2.65 ppm for the methylene group of the central arene anchor. The $^{31}P\{^1H\}$ NMR spectrum was significantly easier to interpret as the resonance for $PdI_2(ICy)(PPh_3)$ at 17.9 ppm was replaced by a signal at ~ -5 ppm corresponding to free PPh_3. The $^{13}C\{^1H\}$ NMR spectrum contained two quaternary carbenic carbon signals at 167.6 and 164.9 ppm revealing that only a single palladium complex containing two different NHCs have been formed, suggesting that formation of the desired product (timteb^{tBu})$\{PdI_2(ICy)\}_3$ had occurred (**Scheme 4.2.3**).

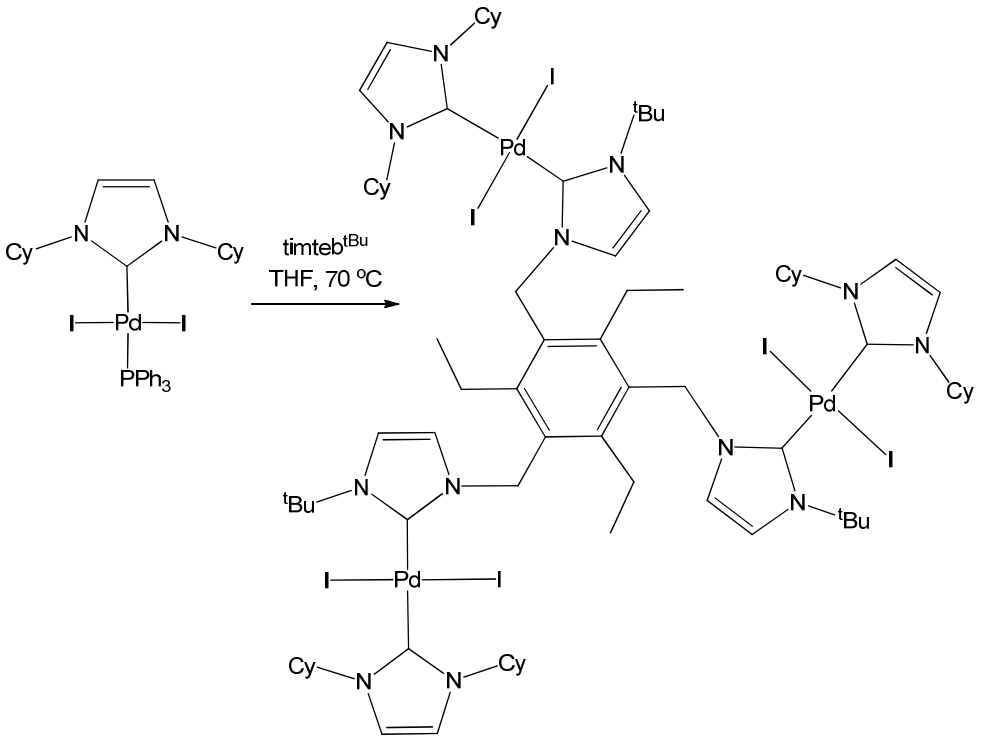

Scheme 4.2.3: Synthesis of (timteb^{tBu}){PdI_2(ICy)}$_3$ (**4.1**).

This species was isolated by removal of the solvent to afford a yellow, air stable, solid in 68% yield which was subsequently confirmed as (timteb^{tBu}){PdI_2(ICy)}$_3$ (**4.1**) by X-ray crystallography (**Figure 4.2.2**) with bond lengths and angles summarised in **Table 4.2.1**.

Bond length (Å) / Angle (°)	**(timteb^{tBu}){PdI_2(ICy)}$_3$ (4.1)**
Pd-C_{NHC}-ICy	2.013(9)
	2.031(8)
	2.033(8)
Pd-C_{NHC}-timteb^{tBu}	2.024(8)
	2.030(8)
	2.049(8)
C_{NHC}-Pd-C_{NHC}	175.5(3)
	177.5(3)
	178.0(3)
I-Pd-I	171.84(3)
	172.65(3)
	176.22(3)

Table 4.2.1: Bond lengths (Å) and angles (°) of (timteb^{tBu}){PdI_2(ICy)}$_3$ (**4.1**).

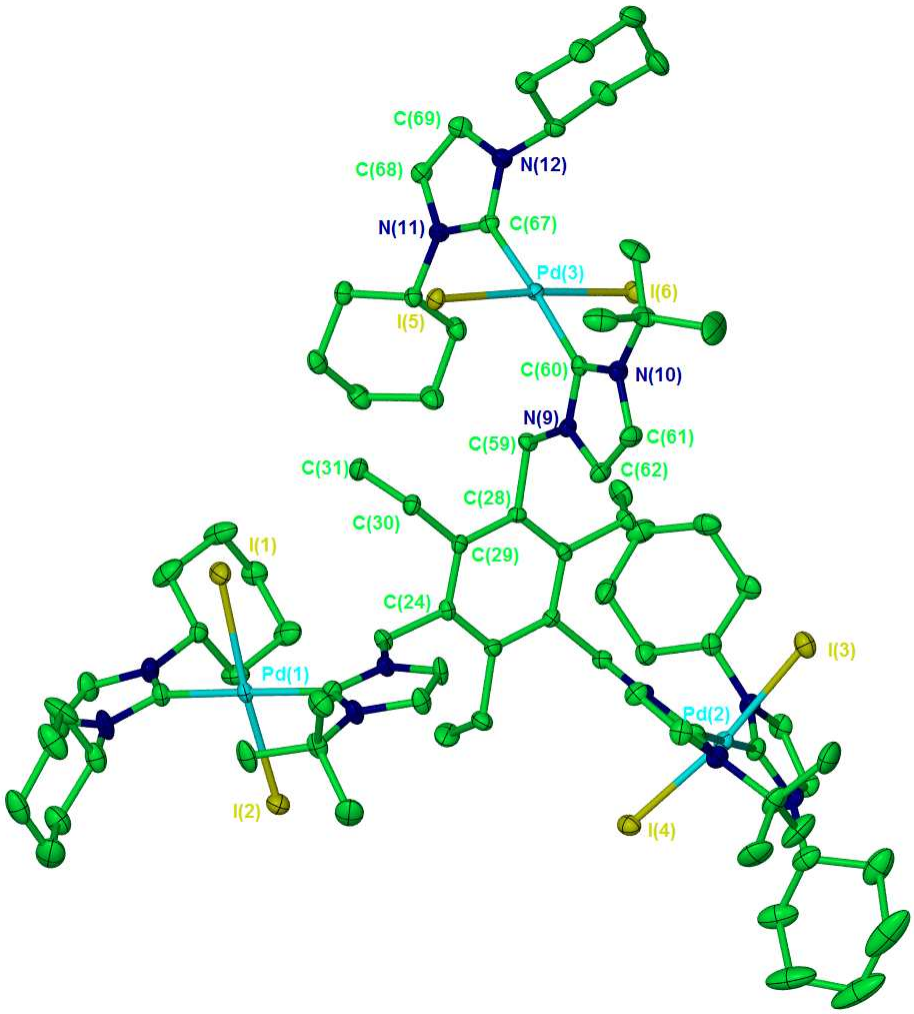

Figure 4.2.2: Crystal structure of (timteb^{tBu}){PdI_2(ICy)}$_3$ (**4.1**). Thermal ellipsoids set at 30% probability, hydrogen atoms omitted for clarity.

The compound adopts an idealised C_3-symmetrical arrangement with the three PdI_2-(ICy) fragments directed out on opposite sides of the central ring to the three ethyl substituents. Each palladium centre has a square planar configuration with a *trans*-timteb^{tBu}-Pd-ICy geometry which is shown by the C_{NHC}-Pd-C_{NHC} angles of 177.5(3)°, 178.0(3)° and 175.5(3)°. All six Pd-C_{NHC} bond lengths range between 2.013(9) and 2.049(8) Å *i.e.* for Pd-ICy: 2.013(9), 2.033(8), 2.031(8) Å and Pd-timteb^{tBu}: 2.024(8), 2.030(8), and 2.049(8) Å. These Pd-C_{NHC} bond lengths are all the same within experimental error and are typical of Pd(II)-NHC complexes.[20]

4.2.4 Syntheses of (timteb^{tBu}){PdI$_2$(PPh$_3$)}$_3$ (4.2) and (timteb^{dipp}){PdI$_2$(PPh$_3$)}$_3$ (4.3)

A number of reports have detailed the higher catalytic activity of NHC-Pd-phosphine complexes relative to their *bis*-NHC analogues.[19, 21] We therefore synthesised the corresponding palladium(II) phosphine species of the form (timteb^R){PdI$_2$(PPh$_3$)}$_3$ (R = ^{t}Bu, dipp). Complexes containing both substituents were prepared using a similar method to the two step procedure reported by Herrmann (**Scheme 4.2.2**).[19] The first step led to the generation of red/orange solids which were believed to be the *bis*-timteb^R dimers (timteb^R)$_2${Pd$_6$(μ-I)$_6$I$_6$} (**Figure 4.2.3**), although the lack of both definitive NMR data and X-ray quality crystals prevented unambiguous characterisation of these species. Similar cage like complexes have been discussed previously (**Scheme 4.1.6** and **Figure 4.1.1**).[11-12]

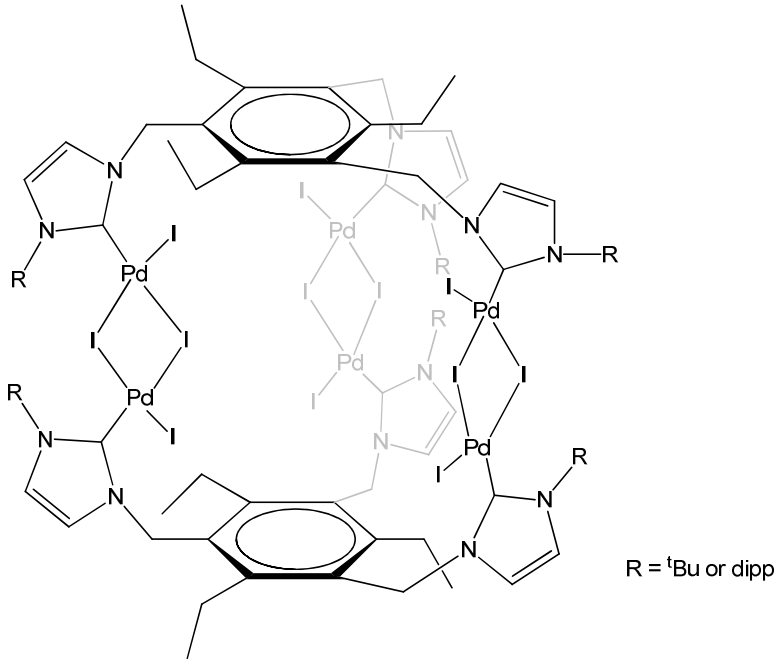

Figure 4.2.3: Pictorial representation of the hypothesised tripodal NHC dimer.

Nevertheless, reaction of both complexes with PPh$_3$ in THF led to immediate colour changes from red to pale orange. After 30 minutes at room temperature, the complexes (timteb^R){PdI$_2$(PPh$_3$)}$_3$ (R = ^{t}Bu **4.2**, dipp **4.3**) were isolated. These were analysed by ^{31}P{^{1}H}, ^{13}C{^{1}H} and ^{1}H NMR spectroscopy. The phosphorus spectra showed a single resonance at 18.0 and 16.2 ppm for **4.2** and **4.3** respectively for the coordinated PPh$_3$ ligands. The high frequency region of the ^{13}C{^{1}H} NMR spectrum was the most diagnostic in terms of spectroscopic characterisation; doublet carbene resonances at 155.0 (**4.2**) and 163.2 ppm (**4.3**) with large splittings of 192 and 196

Hz respectively were observed, consistent with *trans* arrangements of the carbenic carbons and phosphine ligands. As for **4.1**, the ^{1}H NMR spectrum was broad and uninformative. However it was evident that no starting imidazolium salt remained since no high frequency proton resonances were observed.

The molecular structure of **4.2** was confirmed by X-ray crystallography as shown in **Figure 4.2.4** although the moderate quality of the crystals prevented the collection of excellent data.[22] The important bond lengths and angles are summarised in **Table 4.2.2**.

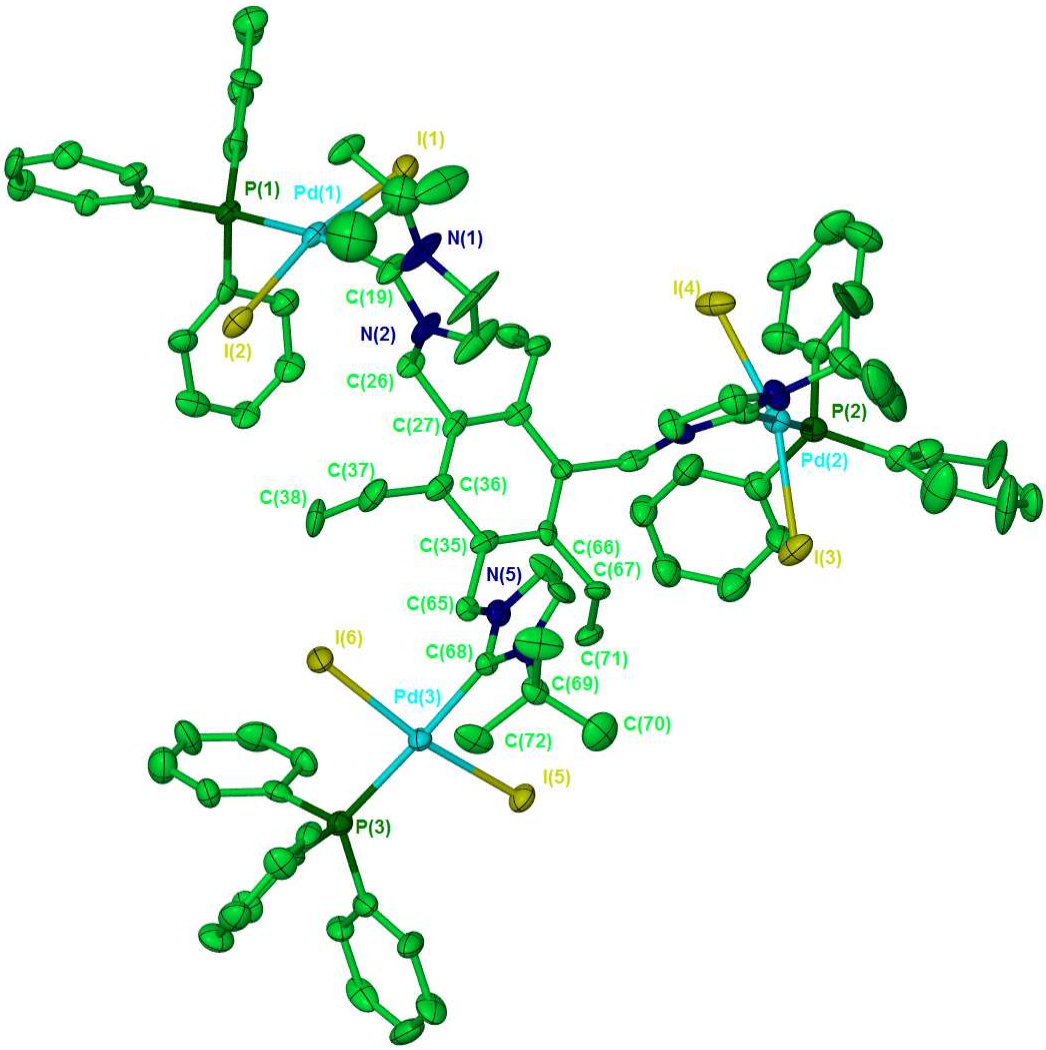

Figure 4.2.4: Crystal structure of (timteb^{tBu}){$PdI_2(PPh_3)$}$_3$ (**4.2**). Thermal ellipsoids set at 30% probability, hydrogen atoms omitted for clarity.

As for **4.1**, **4.2** adopts an idealised C_3-symmetrical arrangement with the three PdI_2-(PPh_3) fragments directed out on the opposite sides of the central ring to the three ethyl substituents. Each palladium centre displays an distorted square planar *trans*-timteb^{tBu}-Pd-PPh_3 geometry, as shown

by the C_{NHC}-Pd-P angles of 169.4(5)°, 177.3(5)° and 179.2(5)°. The Pd-C_{NHC} bond lengths were 1.994(18), 2.037(16) and 2.050(18) Å, comparable with the distances in **4.1**. The Pd-P bond lengths range between 2.309(5) and 2.324(5) Å and are similar to those in many previously reported *trans*-Pd(II) NHC phosphine complexes (*e.g.* $PdI_2(I^tBu)(PPh_3)$ 2.374(1) Å).[19]

Comparison of the metrics for **4.1** and **4.2** show that the two complexes are structurally very similar with the greatest difference seen in the distortion of the square planar arrangement of the Pd core.

Bond lengths (Å) / Angles (°)	**(timteb^{tBu}){$PdI_2(PPh_3)$}$_3$ (4.2)**
Pd-C_{NHC}	1.994(18)
	2.037(16)
	2.050(18)
Pd-P	2.309(5)
	2.319(5)
	2.324(5)
C_{NHC}-Pd-P	169.4(5)
	177.3(5)
	179.2(5)
I-Pd-I	160.70(8)
	166.94(8)
	168.87(6)

Table 4.2.2: Bond lengths (Å) and angles (°) for (timteb^{tBu}){$PdI_2(PPh_3)$}$_3$ (**4.2**).

4.3 Palladium catalysed C-C cross coupling

The use of Pd-NHC based catalyst systems in C-C cross coupling reactions is well documented in the literature.[13c] These display greatly improved performances and stabilities over catalysts bearing only tertiary phosphine ligands. Quite often, palladium NHC catalysts employed in C-C cross coupling reactions are generated *in situ*, which removes the need to handle air and moisture sensitive compounds.

One focus of this study was to demonstrate the potential of timteb^R as a supporting ligand for palladium catalysis, and we therefore decided to investigate **4.1**-**4.3** in Suzuki-Miyaura and Sonogashira C-C coupling reactions. To our knowledge there are no other tripodal NHC palladium complexes reported in the literature which have been applied in C-C bond forming reactions.[13d, 23]

4.3.1 Suzuki-Miyaura coupling

The Suzuki-Miyaura reaction involves the coupling of an aryl halide with an organoboron reagent such as an aryl-boronic acid. This is one of the more popular methods for the formation of biphenyls, and is widely used in organic chemistry. Catalytic reactions were investigated using a combination of $PhB(OH)_2$ (0.75 mmol), aryl halide (0.5 mmol), Cs_2CO_3 (1.0 mmol) and palladium complex (1 mol%) in 1,4-dioxane (1.5 mL) (**Scheme 4.3.1**).

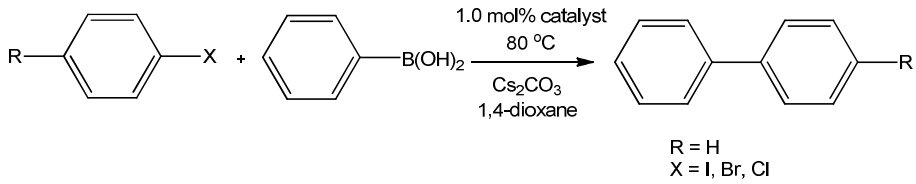

Scheme 4.3.1: Pd catalysed cross coupling of aryl halides and phenyl boronic acid.

The reactants were charged to J Young's ampoule and heated at either 80 °C or 120 °C for 2 h. Upon cooling to room temperature, the mixture was analysed by GC with anisole as an internal standard. The results for the C-C cross coupling between phenylboronic acid and iodobenzene or bromobenzene at 80 °C in 2 hours are shown in **Table 4.3.1**.

Aryl halide	**R**	**Conversion (%)**		
		4.1	**4.2**	**4.3**
PhI	H	73	75	86
PhBr	H	3	58	70

Table 4.3.1: Conversions (%) for the catalytic C-C coupling of PhX (X = I, Br) and phenyl boronic acid at 80 °C in 2 hours with 1 mol% $(NHC)Pd_3$ catalysts

The results show that complex **4.3** is the most active catalyst precursor with the highest conversion rates of 86 and 70% for the coupling of PhI and PhBr respectively. The *bis*-NHC complex **4.1** exhibits the lowest catalytic rates, highlighted by PhBr, which affords a conversion of only 3% compared with 58 and 70% for **4.2** and **4.3**.

All three compounds were also tested at 120 °C for 2 hours, and investigated for the coupling of chlorobenzene. The results are summarised in **Table 4.3.2**.

Aryl halide	R	Conversion (%)		
		4.1	**4.2**	**4.3**
PhI	H	80	100	100
PhBr	H	48	100	100
PhCl	H	0	21	16

Table 4.3.2: Conversions (%) for the catalytic C-C coupling of phenyl halides and phenyl boronic acid at 120 °C for 2 hours with 1 mol% (NHC)Pd_3 catalysts.

The results in **Table 4.3.2** reinforce the observations that the mixed NHC/phosphine systems are more active than the *bis*-NHC complex. Complexes **4.2** and **4.3** showed small but significant activity with the most inert aryl halide PhCl with conversions of 21 and 16%. Comparison of complexes **4.1-4.3** with the literature examples shown in **Figure 4.3.1** are displayed in **Table 4.3.3**.

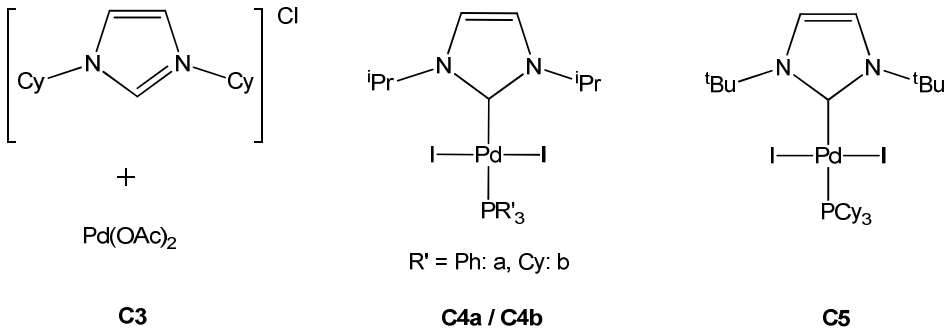

Figure 4.3.1: Catalysts **C3**,[24] **C4a/b**[25] and **C5**[19] for comparison to complexes **4.1-4.3**.

Catalyst	Aryl Halide	R	Catalyst loading (mol%)	Solvent	Base	Temperature (°C)	Time (h)	Conversion (%)
C3	PhCl	Me	2.5	dioxane	Cs_2CO_3	80	2	14
C4a	PhCl	H	1.0	xylene	Cs_2CO_3	130	13	7
C4b	PhCl	H	1.0	xylene	K_2CO_3	130	13	42
C4a	PhBr	H	1.0	xylene	K_2CO_3	130	13	99
C5	PhBr	OMe	1.0	xylene	K_2CO_3	130	12	55

Table 4.3.3: Conversion (%) values of literature examples for Suzuki-Miyaura coupling.

For the *in situ* generated catalyst **C3** the active species can be assumed to be similar to **4.1** as reactions between $Pd(OAc)_2$ and [NHC]X have been shown to generate complexes of the form $PdX_2(NHC)_2$.[19, 26] **Table 4.3.3** shows that **C3** exhibits low activity towards the activated aryl halide 4-chlorotoluene (14%), whereas **4.1** displays no activity. The difference in catalytic activity may be due to the *in situ* preparation of **C3**, as this method of generating catalysts has been shown previously to lead to higher activities compared with preformed analogues.[13c] Other factors might include the use of an activated aryl halide that possesses a weaker C-Cl bond compared with PhCl and the higher catalytic loading.

The activity exhibited by mixed phosphine/NHC complexes **4.2** and **4.3** for the coupling of PhCl is comparable with the literature examples **C4a** and **C4b**. The conversions with **4.2** and **4.3** (21% and 16% after 2 h at 120 °C) indicate that the catalysts are more active than both **C4a** and **C4b** (7% and 42%) which needed reaction times of 13 h at 130 °C. In addition to this, complexes **4.2** and **4.3** also show promising activities in the coupling of PhBr compared with **C4a** and **C5**. Conversions of 100% for **4.2**/**4.3** are achieved in comparison with either **C4a** (99%) or **C5** (55%) which again employ significantly more forcing conditions and longer reaction times.

The data shows that the tripodal carbene Pd complexes exhibit good catalytic activity against the mononuclear species reported in the literature, with the mixed species **4.2** and **4.3** being the most active. This enhanced activity could be attributed to the trimetallic arrangement allowing co-operative catalysis between the metal centres.

4.3.2 Sonogashira coupling

Sonogashira coupling was also probed in light of the relatively low impact that Pd-NHC complexes have made on this class of coupling reaction.[23b, 27] Sonogashira reactions involve the coupling of aryl halides with terminal alkynes as shown in **Scheme 4.3.2**. In addition to the palladium catalyst, a copper(I) halide is often employed as co-catalyst to inhibit the formation of any undesired oxidative dimerisation product.[19]

The reactions were carried out using a range of aryl halides (0.5 mmol), phenyl acetylene (0.7 mmol), caesium carbonate (1.0 mmol), copper iodide (2.0 mol%) and palladium complex (1 mol%) in 1,4-dioxane (1.5 mL) at either 80 °C or 120 °C for 2 hours. The reaction outcome was analysed by GC (with anisole as an internal standard) and the results given in **Table 4.3.4** with the yields for the dimerisation product, 1,4-diphenylbutadiyne in parentheses.

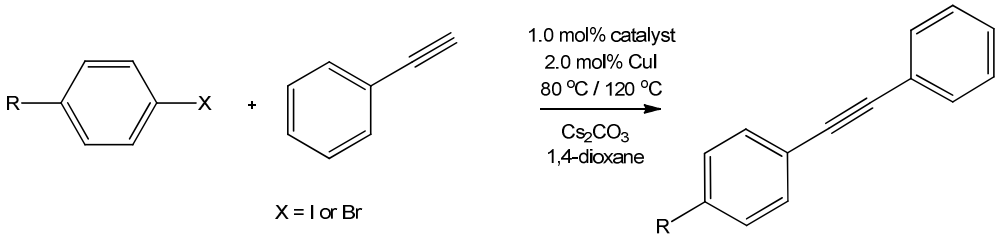

Scheme 4.3.2: The Sonogashira coupling of phenyl acetylene with aryl halides.

Aryl halide	R	Temperature (°C)	Conversion (%)		
			4.1	**4.2**	**4.3**
PhI	H	80	20 (3)	24 (0)	7 (3)
PhI	H	120	28 (3)	54 (3)	13 (2)
PhBr	H	120	0 (0)	4 (3)	0 (0)

Table 4.3.4: Conversions (%) for the Sonogashira C-C coupling reaction of aryl halides and phenyl acetylene with 1 mol% (NHC)Pd_3 catalysts.

Table 4.3.4 illustrates that the complexes **4.1-4.3** exhibit only moderate conversions, even with PhI at 80 °C, and that increasing the temperature to 120 °C has only a marginal effect on the conversions. The most catalytically active precursor is complex **4.2**, which was also the only compound to show any activity for the coupling of PhBr (4%). Interestingly, **4.3** showed the lowest activity, in contrast to the results of the Suzuki-Miyaura coupling reactions.

Most examples of palladium catalysed Sonogashira coupling involve the use of *in situ* prepared compounds.[13c] A number of catalysts are available for comparison (**Figure 4.3.2**), which highlight the different activities exhibited by *in situ* prepared species as well as compounds with bi- and tridentate ligands. The catalysis results are summarised in **Table 4.3.5**.

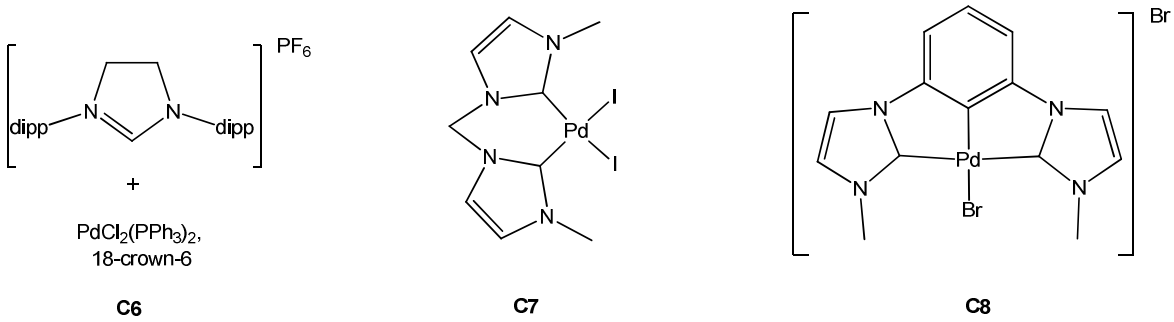

Figure 4.3.2: Catalysts **C6**[27e] **C7**[28] and **C8**[27b] as a comparison to **4.1**, **4.2** and **4.3**.

Catalyst	R	X	Catalyst loading (mol%)	Solvent	Base	Temperature (°C)	Time (h)	Conversion (%)
C6	H	Br	3	THF	KO^tBu	65	12	47
C7	COMe	Br	1	Et_3N	Et_3N	90	48	76
C7	F	Br	1	Et_3N	Et_3N	90	48	71
C8	H	I	1	C_4H_9N	C_4H_9N	90	1	10

Table 4.3.5: Conversion (%) for the Sonogashira reactions of aryl halides with phenyl acetylene utilising catalysts **C6**, **C7** and **C8**.

Table 4.3.5 demonstrates that catalysts **C6** and **C7** are more active for the Sonogashira coupling of PhBr with phenyl acetylene compared with complexes **4.1**-**4.3**. Although the reaction times (and catalytic loading for **C6**) needed to afford the conversions are significantly higher, the reaction temperature that the reaction is run at is much lower (65 and 90 °C *c.f.* 120 °C). The tridentate NHC catalyst **C8** displays the lowest conversion rates of all the catalysts, including **4.1**-**4.3**.

For the Sonogashira coupling reactions it appears that there are no benefits to be gained from the tripalladium arrangement generated with the tripodal NHCs, as the most active catalyst for these transformations has been the *in situ* prepared mononuclear compound **C6**.

4.4 Summary

The syntheses of three tripodal NHC palladium complexes have been reported. The *bis*-NHC species $(timteb^{tBu})\{PdI_2(ICy)\}_3$ (**4.1**) is formed upon reaction of $PdI_2(ICy)(PPh_3)$ with $timteb^{tBu}$. Two mixed phosphine/NHC complexes $(timteb^{R})\{PdI_2(PPh_3)\}_3$ (R = ^{t}Bu (**4.2**), dipp (**4.3**)) have been prepared by reaction of the corresponding imidazolium salts with $Pd(OAc)_2$ followed by the addition of PPh_3. All three complexes have been characterised by a range of spectroscopic techniques, as well as by X-ray crystallography for **4.1** and **4.2**. Complexes **4.1** and **4.2** have been shown to be structurally similar with both compounds displaying idealised C_3-symmetrical arrangements with the $PdI_2(L)$ (L = ICy and PPh_3) fragments accommodated on the same face of the arene anchor opposite to the three ethyl substituents.

The catalytic activity of **4.1-4.3** has been probed in both Suzuki-Miyaura and Sonogashira C-C coupling reactions and compared with literature examples. For Suzuki-Miyaura coupling, the tripodal NHC Pd complexes exhibit good catalytic activity compared with a number of

monometallic palladium NHC catalysts. Disappointingly, only moderate activity was found in Sonogashira coupling reactions.

4.5 Copper(I) tripodal NHC complexes

4.5.1 Preface

The coordination of the tripodal timteb^{R} based NHCs to copper(I) would further develop our understanding of the coordination chemistry of these ligands. Previous examples of the reactivity of copper with tripodal NHC based ligands by Biffis' group have been described earlier with the resulting complexes used in a range of C-C, C-N and C-O coupling reactions. These findings suggest timteb^{R} copper complexes could be synthetically and structurally interesting, as well as catalytically promising.[3, 29]

4.5.2 Synthesis of Synthesis of [(timteb^{tBu})Cu$_3$(μ$_3$-O)]PF$_6$ (4.4)

Treatment of [Cu(NCMe)$_4$]PF$_6$ with [timteb^{tBu}H$_3$]Br$_3$ and NaO^{t}Bu in THF at room temperature for 2 hours led to a colour change in the resulting suspension from colourless to pale yellow and, after work up, the isolation of a white solid in moderate yield. The subsequent proton spectrum showed a set of resonances corresponding to the tripodal carbene at 7.33 and 7.28 ppm for the NHC backbone C-H groups and one quartet at 2.53 ppm (J_{HH} = 7.57 Hz) for the CH$_2$ of the ethyl arms. Interestingly, in contrast to **4.1-4.3**, the resonances were sharp, suggesting that the fluxionality of the ligand had been disabled. In the $^{13}C\{^{1}H\}$ NMR spectrum only one quaternary carbenic carbon peak was observed at 169.2 ppm, indicating that the three arms of the tripodal carbene were in equivalent environments. The structure was elucidated by X-ray crystallography and shown to be [(timteb^{tBu})Cu$_3$(μ$_3$-O)]PF$_6$ (**4.4**) (**Figure 4.5.1**), where the three Cu centres are capped by an unusual μ$_3$-bonded oxygen atom. The oxygen appears to originate from both the base (NaO^{t}Bu) and the solvent (THF). Thus, **4.4** was still formed when the reaction was carried out with KN(SiMe$_3$)$_2$ in THF. Even replacement of both NaO^{t}Bu and THF by KN(SiMe$_3$)$_2$ and MeCN gave low yields of **4.4** alongside a number of other unidentified products, possibly due to the presence of adventitious water.

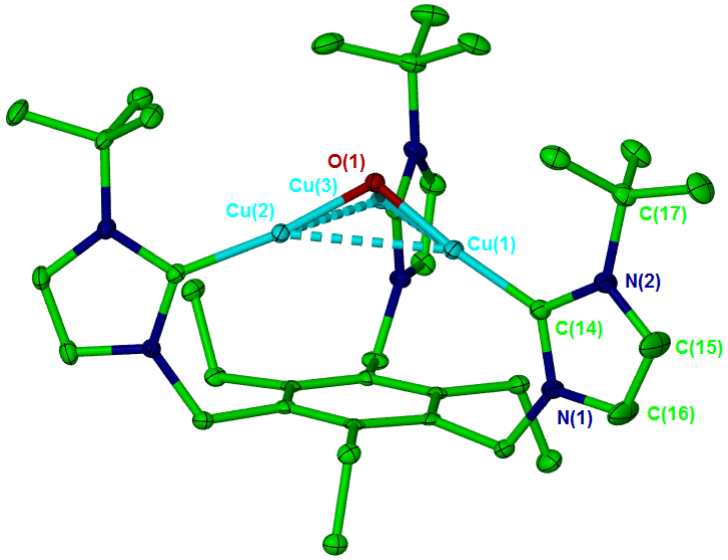

Figure 4.5.1: Crystal structure of the cation in [(timteb^{tBu})Cu_3(μ_3-O)]PF_6 (**4.4**). Thermal ellipsoids set at 30% probability, hydrogen atoms omitted for clarity.

Complex **4.4** displays pseudo-C_3 symmetry with an axis running through the μ_3-O cap, the centre of the Cu plane, and the centroid of the anchoring arene ring. The capping oxygen is located 0.811 Å above the plane of the three Cu atoms, which themselves lie 3 Å above the arene ring of the carbenes. **Table 4.5.1** summarises the important bond lengths and angles in **4.4**.

The Cu-O bond lengths of 1.807(2), 1.812(2) and 1.821(2) Å are comparable with the values reported by Hakansson and Meyer for a Cu^{I}_4(μ_4-O) fragment which exhibits an average value of 1.851(5) Å.[30] Both the Cu-Cu bond distances (2.7557(6), 2.7564(6) and 2.9078(5) Å) and the Cu-Cu-Cu bond angles (63.678(14)°, 58.149(14)° and 58.173(14)°) indicate asymmetry in the Cu_3 core. The Cu-Cu lengths are outside the generally accepted range for d^{10}-d^{10} interactions and therefore cannot be considered as formally bonded.[31]

Two of the ethyl groups point in the direction of the central aryl moiety in **4.4**, whereas the third is directed at the Cu core (*c.f.* **4.1** and **4.2**). This reflects, in part, an opening of the pocket created by the presence of the Cu_3(μ_3-O) scaffold, which can accommodate a twist of the third ethyl group. This is evidenced by the averages of the angles between the arene group and the five membered rings of the three carbene ligands (C_{aryl}-CH_2-$N_{imidazole}$) which are 112° (**4.1**), 111° (**4.2**) and 116° (**4.4**) as shown in **Figure 4.5.2**.

Bond length (Å) / angle (°)	[(timteb^{tBu})Cu$_3$(μ$_3$-O)]PF$_6$ (**4.4**)	[(timteb^{dipp})Cu$_3$(μ$_3$-O)]BF$_4$ (**4.5**)
Cu-Cu	2.7557(6)	2.7901(18)
	2.7564(6)	2.8192(17)
	2.9078(5)	2.8940(18)
C_{NHC}-Cu	1.860(3)	1.856(11)
	1.868(3)	1.871(10)
	1.869(3)	1.878(11)
Cu-O	1.807(2)	1.813(6)
	1.812(2)	1.822(6)
	1.821(2)	1.826(6)
Cu-Cu-Cu	58.149(14)	58.45(4)
	58.173(14)	59.44(4)
	63.678(14)	62.12(5)
C_{NHC}-Cu-Cu$_{centroid}$	154.72	153.73
	157.87	154.14
	158.04	156.01

Table 4.5.1: Selected bond lengths (Å) and angles (°) for [(timteb^{tBu})Cu$_3$(μ$_3$-O)]PF$_6$ (**4.4**) and [(timteb^{dipp})Cu$_3$(μ$_3$-O)]BF$_4$ (**4.5**).

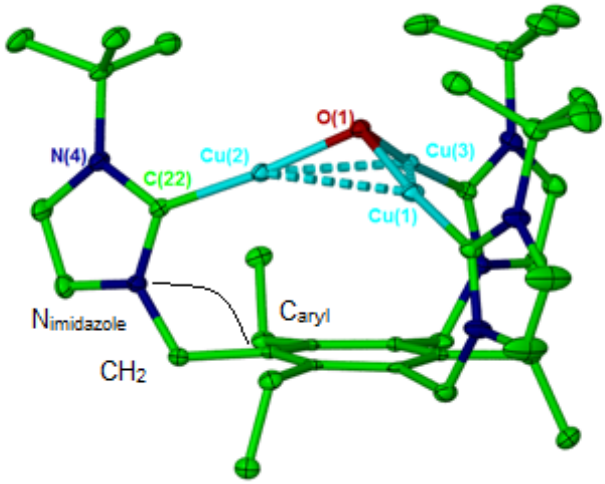

Figure 4.5.2: Pictorial representation of the C_{aryl}-CH_2-$N_{imidaozole}$ angle.

4.5.3 Synthesis of [(timteb^{dipp})Cu$_3$(μ$_3$-O)]BF$_4$ (4.5)

The analogous reaction of [timteb^{dipp}H$_3$]Br$_3$ and [Cu(NCMe$_4$)]BF$_4$ proceeded as for **4.4** generating a white solid in ca. 90% yield after work up which was analysed by ^{1}H and ^{13}C{^{1}H} NMR spectroscopy. The proton spectrum showed characteristic peaks at 7.31 and 6.94 ppm for the backbone protons and resonances at 2.79 ppm (t, J_{HH} = 6.8 Hz) and 2.36 ppm (sept, J_{HH} = 7.6 Hz) for the CH$_2$ group of the ethyl arm and the CH isopropyl proton. The ^{13}C{^{1}H} spectrum showed a single carbenic carbon resonance at 177.6 ppm (*c.f.* 169.2 ppm for **4.4**). X-ray quality crystals were grown from CH$_2$Cl$_2$/hexane and the structure established as [(timteb^{dipp})Cu$_3$(μ$_3$-O)]BF$_4$ (**4.5**) (**Figure 4.5.3**).

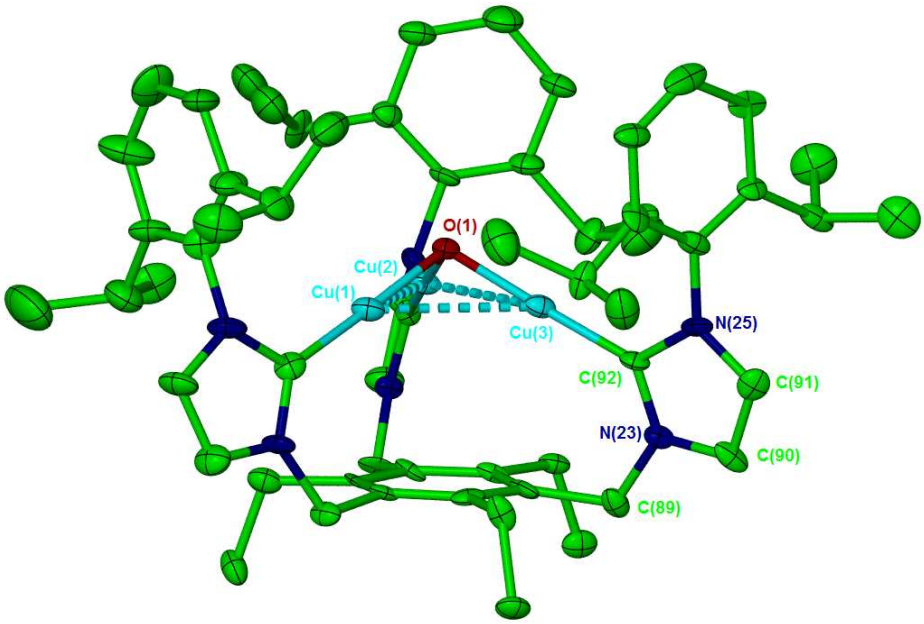

Figure 4.5.3: Crystal structure of the cation in [(timteb^{dipp})Cu$_3$(μ$_3$-O)]BF$_4$ (**4.5**). Thermal ellipsoids set at 30% probability. Hydrogen atoms have been removed for clarity.

A comparison of the metrics for **4.4** and **4.5** shows that the two compounds are very similar (**Table 4.5.1**). The Cu-Cu and Cu-O bond lengths are comparable (within experimental error). The Cu-Cu interactions and Cu-Cu-Cu bond angles indicate asymmetry around the Cu core.

One difference between **4.4** and **4.5** is that in **4.5** the ethyl groups of the central moiety are all on the same side of the arene, pointing away from the Cu core. In contrast **4.5** does not have an opening of the pocket created by the presence of the Cu$_3$O scaffold, in which to accommodate the third ethyl arm. Again this can be illustrated by the average of the C$_{aryl}$-CH$_2$-N$_{imidazole}$ angles (**Figure 4.5.2**), which are 113° for **4.5** compared with 116° for **4.4**.

4.5.4 Structural comparison of [(timteb^{tBu})Cu_3(μ$_3$-O)]PF_6 (4.4) to literature

A structural comparison of **4.4** and the copper tripodal complex $[Cu_3\{HB(MeIm)_3\}_2]PF_6$ reported by Biffis and co-workers and discussed in the introduction (**Figure 4.1.3**), is shown in **Table 4.5.2**.[32]

Bond length (Å) / angle (°)	[(timteb^{tBu})Cu_3(μ$_3$-O)]PF_6 (4.4)	$[Cu_3\{HB(MeIm)_3\}_2]PF_6$
Cu-Cu	2.7557(6)	2.7049(10)
	2.7564(6)	2.6965(9)
	2.9078(5)	2.6199(9)
Average C_{NHC}-Cu	1.866(3)	1.908(5)
Cu-Cu-Cu	58.149(14)	58.03(2)
	58.173(14)	60.82(2)
	63.678(14)	61.15(3)

Table 4.5.2: Bond lengths (Å) and angles (°) for **4.4** and $[Cu_3\{HB(MeIm)_3\}_2]PF_6$.

The average Cu-Cu interactions for $[Cu_3\{HB(MeIm)_3\}_2]PF_6$ are much shorter compared with **4.4**, *i.e.* 2.6738(9) versus 2.8067(6) Å. This can be attributed to the small cavity of the borate derived NHC ligand forcing the copper centres into closer contact. In contrast, our tripodal NHC has a large cavity allowing more space for the copper centres, even with the oxygen cap pulling the copper centres together. Comparison of the Cu-NHC bond lengths reveal that they are shorter in **4.4** than in $[Cu_3\{HB(MeIm)_3\}_2]PF_6$, with average distances of 1.866(3) and 1.908(5) Å respectively, reflecting the different geometries of the compounds.

4.6 Copper catalysed coupling reactions

4.6.1 Preface

Biffis and co-workers have employed the complexes shown in **Figure 4.1.3** in a range of C-C, C-O and C-N coupling reactions. We therefore tested **4.4** and **4.5** using the same reaction conditions as Biffis and used the results reported for $[Cu_3\{HB(MeIm)_3\}_2]BF_4$ (**C1**) and CuCl(IPr) (**C2**) as a direct comparison.[3]

4.6.2 Sonogashira C-C coupling

Sonogashira coupling reactions were carried out using 0.5 mmol aryl halide, 1 equivalent of phenyl acetylene, caesium carbonate (1.0 mmol) and Cu catalyst (1 mol%) in DMSO (**Scheme 4.6.1**). The mixtures were heated and stirred at 120 °C for 24 hours and analysed by ^{1}H NMR spectroscopy after work up to determine conversion. The products were identified by comparison with their spectral data in the literature.[33] The results are shown in **Table 4.6.1** along with the results found with the Cu NHC-borate complex.[3b]

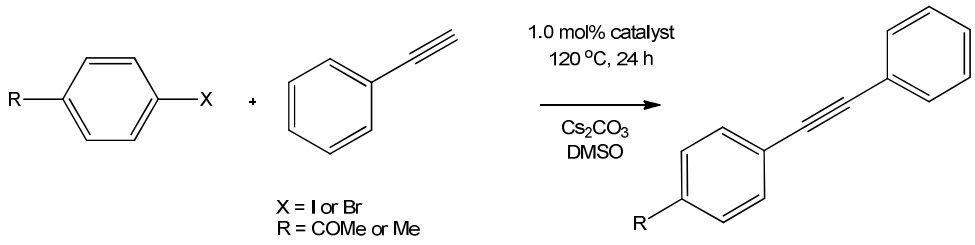

Scheme 4.6.1: The Sonogashira coupling of phenyl acetylene with activated aryl halides.

Aryl halide	Conversion (%)		
	4.4	**4.5**	**$[Cu_3\{HB(MeIm)_3\}_2]BF_4$ (C1)**
4-iodoacetophenone	96	86	90
4-iodotoluene	86	91	>99[34]
4-bromoacetophenone	83	72	10

Table 4.6.1: Conversion rates (%) for the copper catalysed Sonogashira reaction of aryl halides and phenyl acetylene with 1 mol% catalyst.

The conversions with both **4.4** and **4.5** are comparable with those of **C1**. Interestingly the tripodal timteb^{R} copper complexes show much higher activity than **C1** towards the more challenging substrate 4-bromoacetophenone. The mononuclear copper(I) complex **C2** has been reported to be inactive for all of these substrates under identical conditions.[3b]

4.6.3 Ullmann-type C-N coupling

Ullmann-type C-N coupling of azoles with aryl halides using copper catalysts is a well established area of research and has been known for over 100 years.[35] The C-N coupling between

azoles and activated aryl halides was carried out in the same way to the Sonogashira coupling reactions above (**Scheme 4.6.2**).

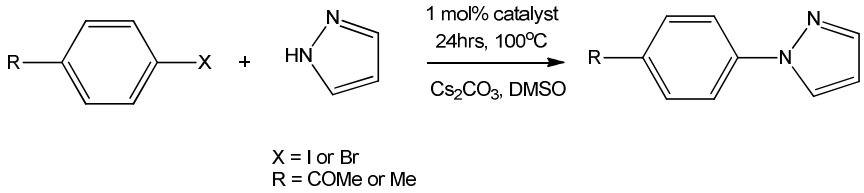

Scheme 4.6.2: The Ullmann type coupling of aryl halides and pyrazole.

Aryl halide (1.0 mmol), pyrazole (1.5 mmol), caesium carbonate (2.0 mmol) and Cu catalyst (1 mol%) in DMSO was utilised. The reaction mixture was heated at 100 °C for 24 h and the products analysed after work up by ^{1}H NMR spectroscopy to determine the conversion. The products were identified by comparison of the NMR data to the literature.[36]

Aryl halide	**Conversion (%)**			
	4.4	**4.5**	**$[Cu_3\{HB(MeIm)_3\}_2]BF_4$ (C1)**	**CuCl(IPr) (C2)**
4-iodoacetophenone	90	91	93	90
4-iodotoluene	21	39	54	23
4-bromoacetopheneone	65	68	73	60

Table 4.6.2: Conversion rates for copper catalysed C-N coupling reactions of aryl halides and pyrazole with 1 mol% catalyst.

The results in **Table 4.6.2** show that the conversion rates for **4.4** and **4.5** are very similar. Disappointingly, the conversions exhibited for 4-iodotoluene were somewhat lower. No activity for the most inert aryl halide 4-chlorotoluene was observed with either of the copper compounds even with longer reaction times of up to 48 hours. But, promisingly the coupling exhibited by **4.4** and **4.5** with the acetophenone substrates took place with good conversions, and are comparable with the literature examples.

4.6.4 Ullmann-type C-O coupling

C-O coupling reactions were also investigated with *p*-cresol (**Scheme 4.6.3**) using the same method and conditions as above; the results displayed in **Table 4.6.3**.

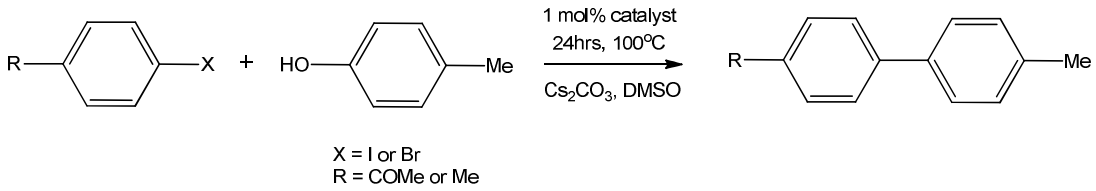

Scheme 4.6.3: The coupling of activated aryl halides and *p*-cresol.

Aryl halide	Conversion (%)			
	4.4	**4.5**	**C1**	**C2**
4-iodoacetophenone	76	90	99	85
4-bromoacetophenone	52	52	70	86
4-iodotoluene	52	-	-	-

Table 4.6.3: Conversions of the Ullmann type C-O coupling reactions of aryl halides and *p*-cresol with 1 mol% catalyst.

These results show that complexes **4.4** and **4.5** are useful in C-O coupling reactions exhibiting good conversions with iodoacetophenone (**4.4**: 76%, **4.5**: 90%). The conversion of bromoacetophenone is promising, with the conversions slightly less than the results found for the literature examples **C1** and **C2**.

4.7 Summary

The synthesis of two new copper(I) tripodal NHC complexes; $[(timteb^{tBu})Cu_3(\mu_3\text{-}O)]PF_6$, (**4.4**) $[(timteb^{dipp})Cu_3(\mu_3\text{-}O)]BF_4$ (**4.5**) has been achieved by reaction of $[Cu(NCMe)_4]X$ (X = PF_4 or BF_4) with the *in situ* generated $timteb^R$ (R = ^{t}Bu or dipp). The Cu compounds have been shown to possess 'bowl like' arrangements, which are unexpectedly capped by a μ_3-O group that arises from the base and the solvent used in the reaction. Both complexes display pseudo C_3 geometries with an axis directed through the oxygen cap and the centroids of the copper plane and the arene ring.

Complexes **4.4** and **4.5** prove active in a range of C-C, C-N and C-O coupling reactions. For the Sonogashira coupling of alkynes with aryl halides, they exhibit higher conversions with the more inert aryl bromides in comparison with the borate based tripodal carbene complex $[Cu_3\{HB(MeIm)_3\}_2]BF_4$ reported by Biffis and co-workers.[3] Results from Ullmann type C-N and C-O coupling reactions have shown that **4.4** and **4.5** possess comparable activity to a range of copper complexes. Although the catalytic activities of **4.4** and **4.5** maybe slightly lower than for the literature examples, the conditions in which the reactions were carried out were not optimised,

indicating that the timteb^{R} ligand has potential for inducing enhanced catalytic activity in a range of copper catalysed reactions.

4.8 Efforts to coordinate timteb^{tBu} to iron metal centres

Unpublished work by Pascu and co-workers has shown that timteb^{tBu} will react with $Fe_3(CO)_{12}$ to form (timteb^{tBu}){Fe(CO)$_4$}$_3$ (**Figure 4.8.1**), although there is no yield or spectroscopic characterisation to support the X-ray structure. We therefore set out to try to repeat the formation of this compound to clarify the experimental details and provide full characterisation.

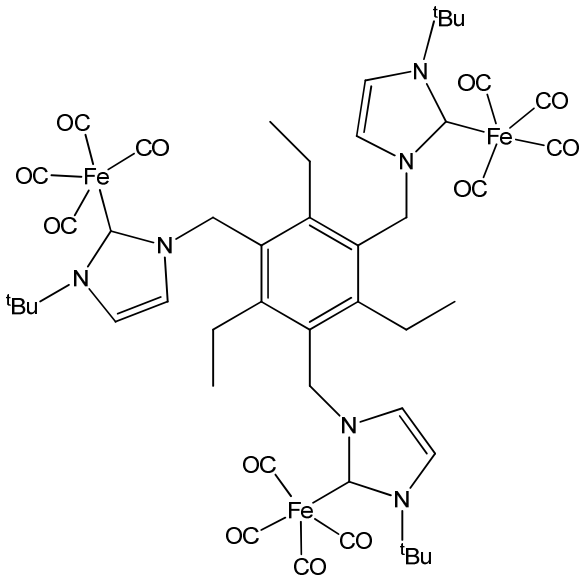

Figure 4.8.1: Pictorial representation of the iron carbonyl timteb^{tBu} complex.

Reaction of timteb^{tBu} and $Fe_3(CO)_{12}$ in a 1:1 ratio in THF resulted in a rapid colour change from dark green to brown, accompanied by the evolution of gas. Analysis of the solution by ^{1}H NMR spectroscopy showed an extremely broad spectrum which failed to sharpen even upon cooling to ~-90 °C. Evidence for substitution of carbonyl ligands came instead from the IR spectrum of the solution which showed carbonyl bands at 2033, 1968, 1939, 1914 and 1864 cm^{-1}; $Fe_3(CO)_{12}$ exhibits bands at 2047, 2026 and 2006 cm^{-1}. The distribution of the bands is similar to that seen for the phosphine cluster complex $Fe_3(PPh_3)(CO)_{11}$ which appear at 2083, 2031, 2009, 1978 and 1825 cm^{-1}.[37] Attempts to isolate a clean compound were hampered by the failure to redissolve the solid residue left after removal of the THF in a range of solvents including CH_2Cl_2, THF, MeCN or DMSO.

Attempts were made to alter the outcome by changing the conditions; varying the solvent from THF to MeCN or benzene, carrying out the reaction at either low temperatures or at reflux

and using a range of equivalents of NHC. The reaction was also carried out in the presence of trimethyl N-oxide (to enhance extraction of CO), as well as under photochemical irradiation at low temperature.[38, 39] In all cases, it was not possible to determine the result of the reaction or isolate a clean product. Therefore no conclusive evidence for the formation of the desired (timteb^{tBu})Fe_3 species was obtained.

As a result we attempted to synthesise the desired product using a new precursor. The addition of $Fe(CO)_5$ to a solution of timteb^{tBu} in THF at room temperature immediately formed a precipitate and a solution devoid of NHC containing products. In addition to this the precipitate could not be redissolved in a range of solvents. When the reaction was carried out in THF at low temperature (-78 °C) and warmed over 16 hours, a dark red solid precipitated out of solution. An IR spectrum showed the presence of two carbonyl bands at 1915 and 1867 cm^{-1}. Upon cooling a hexane solution of the compound to -30 °C, crystals were isolated and the structure shown to be the imidazolium species [(timteb$^{tBu}H_3)_2$][{$Fe_2(CO)_8$}$_3$] (**Figure 4.8.2**). This anion has been previously reported as $[Et_4N]_2[Fe_2(CO)_8]$, displaying carbonyl bands in the IR spectrum at 1920 and 1852 cm^{-1} which are similar to the IR bands observed for [(timteb$^{tBu}H_3)_2$][{$Fe_2(CO)_8$}$_3$].[40]

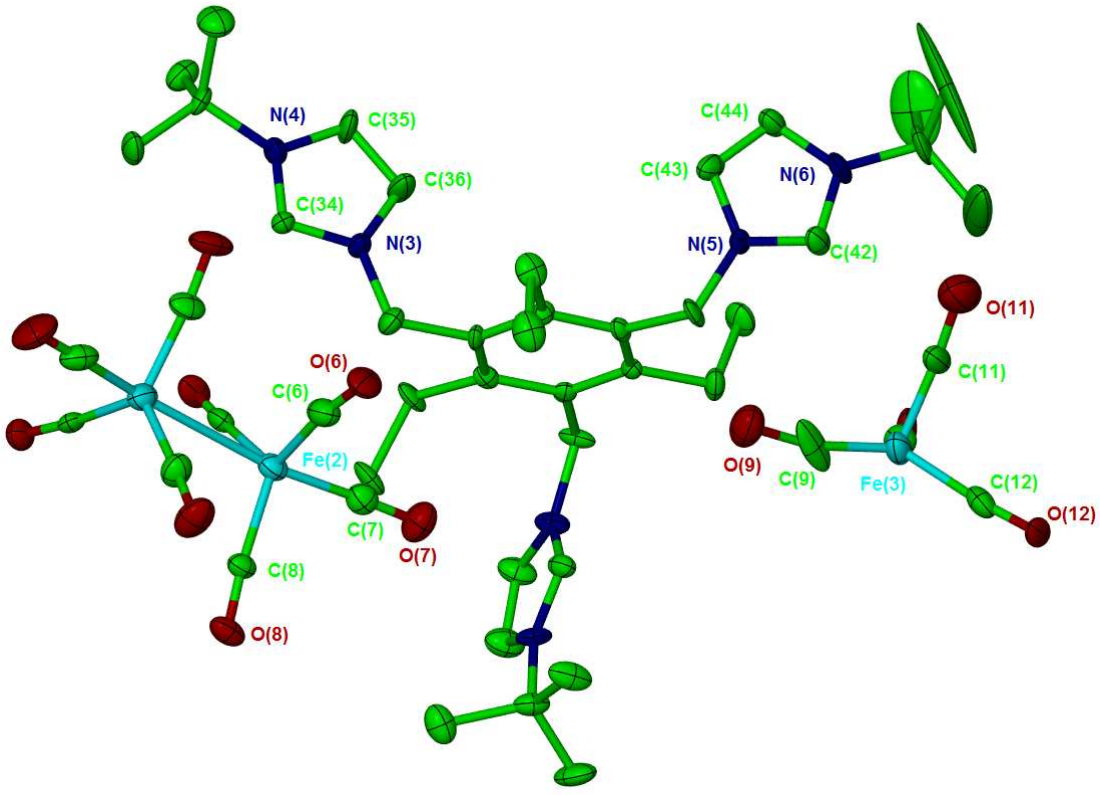

Figure 4.8.2: Crystal structure of half a unit cell containing [(timteb$^{tBu}H_3)_2$][{$Fe_2(CO)_8$}$_3$]. Thermal ellipsoids are set to 30% probability and the hydrogen atoms removed for clarity.

A final attempt to synthesise (timteb^{tBu}){Fe(CO)$_4$}$_3$ from Fe$_2$(μ-CO)$_3$(CO)$_6$ was carried out. A survey of the literature revealed that this complex reacts with pyridine to afford the compound Fe(Pyr)(CO)$_4$[41] and it was hoped that either the *in situ* reaction of the NHC with Fe$_2$(μ-CO)$_3$(CO)$_6$ or direct reaction of Fe(Pyr)(CO)$_4$ with the tripodal carbene at low temperature would afford (timteb^{tBu}){Fe(CO)$_4$}$_3$. However, in both cases, on the basis of IR spectroscopy, the imidazolium product [timteb^{tBu}H$_3$]$_2$[Fe$_2$(CO)$_8$]$_3$ was the only species generated.

4.9 Summary

All efforts to generate the promising (timteb^{tBu}){Fe(CO)$_4$}$_3$ complex, characterised only as an X-ray crystal structure, have so far been unsuccessful. This result along with the unexpected formation of the Cu$_3$(μ$_3$-O) species would appear to indicate that tripodal carbene chemistry does not always lead to the product expected.

4.10 References

1. (a) Peris, E.; Crabtree, R. H., *Coord. Chem. Rev.* **2004**, *248,* 2239-2246; (b) Pugh, D.; Danopoulos, A. A., *Coord. Chem. Rev.* **2007**, *251,* 610-641; (c) Mata, J. A.; Poyatos, M.; Peris, E., *Coord. Chem. Rev.* **2007**, *251,* 841-859; (d) Hahn, F. E.; Radloff, C.; Pape, T.; Hepp, A., *Chem.-Eur. J.* **2008**, *14,* 10900-10904; (e) Corberan, R.; Mas-Marzá, E.; Peris, E., *Eur. J. Inorg. Chem.* **2009**, 1700-1716; (f) Williams, K. A.; Bielawski, C. W., *Chem. Commun.* **2010**, *46,* 5166-5168.
2. (a) Kernbach, U.; Ramm, M.; Luger, P.; Fehlhammer, W. P., *Angew. Chem. Int. Ed.* **1996**, *35,* 310-312; (b) Frankel, R.; Kernbach, U.; Bakola-Christianopoulou, M.; Plaia, U.; Suter, M.; Ponikwar, W.; Noth, H.; Moinet, C.; Fehlhammer, W. P., *J. Organomet. Chem.* **2001**, *617,* 530-545; (c) Frankell, R.; Birg, C.; Kernbach, U.; Habereder, T.; Noth, H.; Fehlhammer, W. P., *Angew. Chem. Int. Ed.* **2001**, *40,* 1907-1910; (d) Nieto, I.; Cervantes-Lee, F.; Smith, J. M., *Chem. Commun.* **2005**, 3811-3813; (e) Cowley, R. E.; Bontchev, R. P.; Duesler, E. N.; Smith, J. M., *Inorg. Chem.* **2006**, *45,* 9771-9779; (f) Forshaw, A. P.; Bontchev, R. P.; Smith, J. M., *Inorg. Chem.* **2007**, *46,* 3792-3794; (g) Biffis, A.; Lobbia, G. G.; Papini, G.; Pellei, M.; Santini, C.; Scattolin, E.; Tubaro, C., *J. Organomet. Chem.* **2008**, *693,* 3760-3766; (h) Arrowsmith, M.; Heath, A.; Hill, M. S.; Hitchcock, P. B.; Kociok-Kohn, G., *Organometallics* **2009**, *28,* 4550-4559.
3. (a) Tubaro, C.; Biffis, A.; Scattolin, E.; Basato, M., *Tetrahedron* **2008**, *64,* 4187-4195; (b) Biffis, A.; Tubaro, C.; Scattolin, E.; Basato, M.; Papini, G.; Santini, C.; Alvarez, E.; Conejero, S., *Dalton Trans.* **2009**, 7223-7229.
4. (a) Hu, X. L.; Castro-Rodriguez, I.; Meyer, K., *J. Am. Chem. Soc.* **2003**, *125,* 12237-12245; (b) Hu, X. L.; Meyer, K., *J. Am. Chem. Soc.* **2004**, *126,* 16322-16323; (c) Hu, X. L.; Castro-Rodriguez, I.; Meyer, K., *J. Am. Chem. Soc.* **2004**, *126,* 13464-13473; (d) Hu, X. L.; Castro-Rodriguez, I.; Meyer, K., *Chem. Commun.* **2004**, 2164-2165; (e) Hu, X. L.; Meyer, K., *J. Organomet. Chem.* **2005**, *690,* 5474-5484; (f) Vogel, C.; Heinemann, F. W.; Sutter, J.; Anthon, C.; Meyer, K., *Angew. Chem. Int. Ed.* **2008**, *47,* 2681-2684; (g) Meyer, K.; Bart, S. C., *Adv. Inorg. Chem.* **2008**, *60,* 1-30.
5. Mas-Marzá, E.; Poyatos, M.; Sanau, M.; Peris, E., *Inorg. Chem.* **2004**, *43,* 2213-2219.
6. Dias, H. V. R.; Jin, W. C., *Tetrahedron Lett.* **1994**, *35,* 1365-1366.
7. (a) Hu, X. L.; Castro-Rodriguez, I.; Meyer, K., *Organometallics* **2003**, *22,* 3016-3018; (b) Hu, X. L.; Castro-Rodriguez, I.; Olsen, K.; Meyer, K., *Organometallics* **2004**, *23,* 755-764; (c) Hu, X. L.; Tang, Y. J.; Gantzel, P.; Meyer, K., *Organometallics* **2003**, *22,* 612-614.
8. Vogel, C. S.; Heinemann, F. W.; Khusniyarov, M. M.; Meyer, K., *Inorg. Chim. Acta* **2010**, *364,* 226-237.

9. Nakai, H.; Tang, Y. J.; Gantzel, P.; Meyer, K., *Chem. Commun.* **2003**, 24-25.
10. Cole, M. L.; Davies, A. J.; Jones, C., *J. Chem. Soc., Dalton. Trans.* **2001**, 2451-2452.
11. Rit, A.; Pape, T.; Hahn, F. E., *J. Am. Chem. Soc.* **2010**, *132,* 4572-4573.
12. Willans, C. E.; Anderson, K. M.; Junk, P. C.; Barbour, L. J.; Steed, J. W., *Chem. Commun.* **2007**, 3634-3636.
13. (a) Herrmann, W. A., *Angew. Chem. Int. Ed.* **2002**, *41,* 1290-1309; (b) Herrmann, W. A.; Elison, M.; Fischer, J.; Kocher, C.; Artus, G. R. J., *Angew. Chem. Int. Ed.* **1995**, *34,* 2371-2374; (c) Kantchev, E. A. B.; O'Brien, C. J.; Organ, M. G., *Angew. Chem. Int. Ed.* **2007**, *46,* 2768-2813; (d) Hillier, A. C.; Grasa, G. A.; Viciu, M. S.; Lee, H. M.; Yang, C. L.; Nolan, S. P., *J. Organomet. Chem.* **2002**, *653,* 69-82.
14. Mas-Marzá, E.; Peris, E.; Castro-Rodriguez, I.; Meyer, K., *Organometallics* **2005**, *24,* 3158-3162.
15. (a) Kocher, C.; Herrmann, W. A., *J. Organomet. Chem.* **1997**, *532,* 261-265; (b) Poyatos, M.; Sanau, M.; Peris, E., *Inorg. Chem.* **2003**, *42,* 2572-2576.
16. (a) Kaur, H.; Zinn, F. K.; Stevens, E. D.; Nolan, S. P., *Organometallics* **2004**, *23,* 1157-1160; (b) Jurkauskas, V.; Sadighi, J. P.; Buchwald, S. L., *Org. Lett.* **2003**, *5,* 2417-2420.
17. Wallace, K. J.; Hanes, R.; Anslyn, E.; Morey, J.; Kilway, K. V.; Siegel, J., *Synthesis* **2005**, 2080-2083.
18. Liu, J. P.; Chen, J. B.; Zhao, J. F.; Zhao, Y. H.; Li, L.; Zhang, H. B., *Synthesis* **2003**, 2661-2666.
19. Herrmann, W. A.; Böhm, V. P. W.; Gstöttmayr, C. W. K.; Grosche, M.; Reisinger, C. P.; Weskamp, T., *J. Organomet. Chem.* **2001**, *617,* 616-628.
20. Viciu, M. S.; Navarro, O.; Germaneau, R. F.; Kelly, R. A.; Sommer, W.; Marion, N.; Stevens, E. D.; Cavallo, L.; Nolan, S. P., *Organometallics* **2004**, *23,* 1629-1635.
21. Liao, C. Y.; Chan, K. T.; Tu, C. Y.; Chang, Y. W.; Hu, C. H.; Lee, H. M., *Chem.-Eur. J.* **2009**, *15,* 405-417.
22. Attempts to grow better quality crystals were unfruitful.
23. (a) Díez-González, S.; Marion, N.; Nolan, S. P., *Chem. Rev.* **2009**, *109,* 3612-3676; (b) Herrmann, W. A.; Öfele, K.; Von Preysing, D.; Schneider, S. K., *J. Organomet. Chem.* **2003**, *687,* 229-248.
24. Grasa, G. A.; Viciu, M. S.; Huang, J. K.; Zhang, C. M.; Trudell, M. L.; Nolan, S. P., *Organometallics* **2002**, *21,* 2866-2873.
25. Weskamp, T.; Böhm, V. P. W.; Herrmann, W. A., *J. Organomet. Chem.* **1999**, *585,* 348-352.
26. (a) Lebel, H.; Janes, M. K.; Charette, A. B.; Nolan, S. P., *J. Am. Chem. Soc.* **2004**, *126,* 5046-5047; (b) Ellul, C. E.; Mahon, M. F.; Whittlesey, M. K., *J. Organomet. Chem.* **2010**, *695,* 6-10.

27. (a) McGuinness, D. S.; Cavell, K. J., *Organometallics* **2000**, *19,* 741-748; (b) Loch, J. A.; Albrecht, M.; Peris, E.; Mata, J.; Faller, J. W.; Crabtree, R. H., *Organometallics* **2002**, *21,* 700-706; (c) Mas-Marzá, E.; Segarra, A. M.; Claver, C.; Peris, E.; Fernandez, E., *Tetrahedron Lett.* **2003**, *44,* 6595-6599; (d) Kim, J. H.; Lee, D. H.; Jun, B. H.; Lee, Y. S., *Tetrahedron Lett.* **2007**, *48,* 7079-7084; (e) Ma, Y. D.; Song, C.; Jiang, W.; Wu, Q. S.; Wang, Y.; Liu, X. Y.; Andrus, M. B., *Org. Lett.* **2003**, *5,* 3317-3319.
28. Herrmann, W. A.; Reisinger, C. P.; Spiegler, M., *J. Organomet. Chem.* **1998**, *557,* 93-96.
29. (a) Diez-Gonzalez, S.; Escudero-Adan, E. C.; Benet-Buchholz, J.; Stevens, E. D.; Slawin, A. M. Z.; Nolan, S. P., *Dalton Trans.* **2010**, *39,* 7595-7606; (b) Diez-Gonzalez, S.; Nolan, S. P., *Synlett* **2007**, 2158-2167; (c) Lin, J. C. Y.; Huang, R. T. W.; Lee, C. S.; Bhattacharyya, A.; Hwang, W. S.; Lin, I. J. B., *Chem. Rev.* **2009**, *109,* 3561-3598.
30. (a) Hakansson, M.; Ortendahl, M.; Jagner, S.; Sigalas, M. P.; Eisenstein, O., *Inorg. Chem.* **1993**, *32,* 2018-2024; (b) Stollenz, M.; Gross, C.; Meyer, F., *Chem. Commun.* **2008**, 1744-1746.
31. Pyykkö, P., *Chem. Rev.* **1997**, *97,* 597-636.
32. Due to poor quality of data for **4.5** comparison was only made for **4.4**.
33. Deng, C. L.; Xie, Y. X.; Yin, D. L.; Li, J. H., *Synthesis* **2006**, 3370-3376.
34. Reaction run in DMF instead of DMSO.
35. (a) Hassan, J.; Sevignon, M.; Gozzi, C.; Schulz, E.; Lemaire, M., *Chem. Rev.* **2002**, *102,* 1359-1469; (b) Lindley, J., *Tetrahedron* **1984**, *40,* 1433-1456; (c) Monnier, F.; Taillefer, M., *Angew. Chem. Int. Ed.* **2008**, *47,* 3096-3099.
36. Cristau, H. J.; Cellier, P. P.; Spindler, J. F.; Taillefer, M., *Eur. J. Org. Chem.* **2004**, 695-709.
37. Bruce, M. I.; Kehoe, D. C.; Matisons, J. G.; Nicholson, B. K.; Rieger, P. H.; Williams, M. L., *J. Chem. Soc., Chem. Commun.* **1982**, 442-444.
38. Luh, T. Y., *Coord. Chem. Rev.* **1984**, *60,* 255-276.
39. (a) Leadbeater, N. E., *J. Organomet. Chem.* **1999**, *573,* 211-216; (b) Edwards, A. J.; Leadbeater, N. E.; Lewis, J.; Raithby, P. R., *J. Organomet. Chem.* **1995**, *503,* 15-20.
40. Farmery, K.; Kilner, M.; Greatrex, R.; Greenwoo.Nn, *J. Am. Chem. Soc., Inorg. Phys. Theor.* **1969**, 2339-2345.
41. Cotton, F. A.; Troup, J. M., *J. Am. Chem. Soc.* **1974**, *96,* 3438-3443.

5.1 Experimental

5.1.1 General procedures

All manipulations were carried out using standard Schlenk, high vacuum and glovebox techniques using dried and degassed solvents, unless otherwise stated. Solvents were purified on an MBraun SPS solvent system (hexane, diethyl ether, dichloromethane, toluene) or Innovative Technologies solvent system (THF, MeOH) or under a nitrogen atmosphere from purple solutions of sodium benzophenone ketyl (benzene, 1,4-dioxane) or Mg/I_2 (ethanol) DMSO (anhydrous, Aldrich, 99.9%) was used as received. Deuterated solvents (Fluorochem) were vacuum transferred from potassium (benzene-d_6, toluene-d_8, THF-d_8) or calcium hydride (chloroform-d_1, dichloromethane-d_2). H_2 (BOC, 99.9%), CO (BOC, 99.9%), SO_2 (Aldrich, 99.9%) and $Pd(OAc)_2$ (Alfa Aesar, 99.8%) were used as received. $Ru_3(CO)_{12}$ and $[Cu(NCMe_4)]X$ were prepared according to the literature.[1] $RuCl_3.3H_2O$ was kindly donated by Johnson-Matthey.

5.1.2 Physical and analytical techniques

Solution NMR spectra were recorded on Bruker Avance 250, 300, 400 and 500 MHz NMR spectrometers at 298 K unless otherwise stated, and referenced as follows (^1H; $^{13}C\{^1H\}$): benzene (δ 7.15; δ 128.0), chloroform (δ 7.26; δ 77.4), dichloromethane (δ 5.32; δ 54.5), THF (δ 3.58; δ 25.4) or toluene (δ 2.04; δ 20.4). $^{31}P\{^1H\}$ NMR chemical shifts were reference externally to 85% H_3PO_4 (δ 0.0). 2D experiments (^1H COSY, ^1H-$^{13}C\{^1H\}$ HMQC, HMBC, HSQC) were performed using standard Bruker pulse sequences. IR spectra were recorded on a Nicolet Nexus FTIR spectrometer. X-ray crystal structures were recorded on a Nonius KappaCCD diffractometer or on a Oxford Diffraction Gemini diffractometer, with structural solutions and refinements performed using SHELXS-97[2] and SHELXL-97[2] respectively. Elemental analyses were performed by Elemental Micro-analysis Ltd., Okehampton, Devon, or the Elemental Analysis Service, London Metropolitan University, London. Mass spectrometry was undertaken using a micrOTOF electrospray time-of-flight (ESI-TOF) mass spectrometer (Bruker Daltonik GmbH) or by the ESPRC National Mass Spectrometry Service (Swansea, UK).

5.2 Preparation of N-heterocyclic carbenes

5.2.1 General preparation of 1,3-R-imidazolium chloride[3,4]

In air, a 500 mL round bottomed flask was charged with amine (0.1 mol), undried toluene (100 mL) and paraformaldehyde (3.0 g, 0.1 mol). The reaction mixture was stirred for 30 min at room temperature. The flask was then cooled to 0 °C, and a second equivalent of amine (0.1 mol) was added. The solution was allowed to stir at 0 °C for a further 10 min followed by the drop wise addition of HCl (25 mL, 4 M in dioxane, 0.1 mol). The solution was then warmed to room temperature and 40% aqueous glyoxal (14.5 mL, 0.1 mol) was added. The resulting suspension was stirred at 37 °C for 48 h. After the mixture had cooled to room temperature, Et_2O (100 mL) and saturated Na_2CO_3 solution (50 mL) were added, and the layers separated. The phase between the organic and aqueous layers was kept with the organic phase and the aqueous phase was washed with Et_2O (3 x 100 mL). The volatiles were removed *in vacuo*, and the residue extracted with dry CH_2Cl_2 (50 mL), dried over $MgSO_4$ and filtered. The product was isolated after removal of the solvent and stored in a dry and inert atmosphere due to its hygroscopic nature.

5.2.2 1,3-*bis*(isopropyl)imidazolium chloride

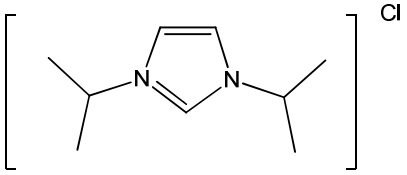

Yield: 10.1 g (54%); ^{1}H NMR ($CDCl_3$, 400 MHz): δ 10.74 (br s, 1H. NC*H*N), 7.55 (s, 1H, NC*H*=C*H*N), 7.54 (s, 1H, NC*H*=C*H*N), 4.83 (sept, J_{HH} = 6.7 Hz, 2H, C*H*(CH_3)$_2$), 1.50 (d, J_{HH} = 6.7 Hz, 12H, CH(C*H*$_3$)$_2$).

5.2.3 1,3-*bis*(*n*-butyl)imidazolium chloride

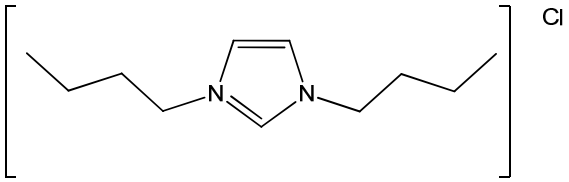

Yield: 14.7 g (68%); ^{1}H NMR ($CDCl_3$, 500 MHz): δ 10.47 (s, 1H, NC*H*N), 7.48 (d, J_{HH} = 1.5 Hz, 2H, NC*H*=C*H*N), 4.22 (t, J_{HH} = 7.5 Hz, 4H, NCH_2), 1.76 (m, 4H, NCH_2CH_2), 1.23 (m, 4H, $NCH_2CH_2CH_2$), 0.80 (t, J_{HH} = 7.5 Hz, 6H, $NCH_2CH_2CH_2CH_3$).

5.2.4 1,3-*bis*(*tert*-butyl)imidazolium chloride

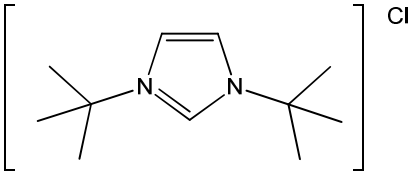

Yield: 11.4 g (60%); ^{1}H NMR ($CDCl_3$, 400 MHz): δ 10.26 (t, J_{HH} = 1.6 Hz, 1H, NC*H*N), 7.58 (d, J_{HH} = 1.6 Hz, 2H, NC*H*=C*H*N), 1.67 (s, 18H, ^{t}Bu). $^{13}C\{^{1}H\}$ ($CDCl_3$, 101 MHz): δ 134.8 (s, NCHN), 120.0 (s, NCH=CHN), 60.9 (s, $C(CH_3)_3$), 30.3 (s, $C(CH_3)_3$).

5.2.5 Preparation of 1,3-*bis*(cyclohexyl)imidazolium tetrafluoroborate[5]

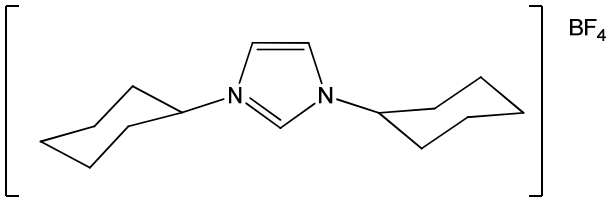

Undried toluene (15 mL) was combined with paraformaldehye (3.0 g, 0.1 mol) in a round bottomed flask and the mixture was chilled in an ice bath. Cyclohexylamine (23 mL, 0.2 mol) was added dropwise over 1 h to the chilled swirling solution. A solution of hydrochloric acid (25 mL, 4 M in dioxane, 0.1 mol) was then added dropwise over 30 min. The cloudy mixture was warmed to room temperature and 40% aqueous glyoxal (14.5 mL, 0.1 mmol) was added. The mixture was stirred at room temperature for 1 h and then toluene (30 mL) was added. Water was removed from the mixture *via* a Dean-Stark trap and the volatiles were removed by rotary evaporation to yield a

dark brown sticky solid. The solid was dissolved in water (75 mL) and tetrafluoroboric acid (13 mL) was added. The mixture was stirred for 30 min to yield a brown precipitate. The residue was filtered through a glass frit, washed with water and dried under vacuum to afford a pale brown solid. Yield = 20.5 g (64%). ^{1}H NMR ($CDCl_3$, 400 MHz) δ 8.91 (d, J_{HH} = 1.7 Hz, 1H, NC*H*N), 7.41 (d, J_{HH} = 1.7 Hz, 2H, NC*H*=C*H*N), 4.29 (tt, J_{HH} = 11.9 Hz, J_{HH} = 3.8 Hz, 2H, NC*H*), 2.15 (m, 4H, CH_2), 1.89 (m, 4H, CH_2), 1.67 (m, 4H, CH_2), 1.45 (m, 4H, CH_2), 1.24 (m, 4H, CH_2). ^{13}C{^{1}H} NMR ($CDCl_3$, 125 MHz) δ 133.2 (s, N*C*HN), 120.2 (s, N*C*H=*C*HN), 60.0 (s, N*C*H), 33.2 (s, *C*H_2), 24.9 (s, *C*H_2), 24.5(s, *C*H_2).

5.2.6 Preparation of 1,3-*bis*(*tert*-butyl)imidazol-2-ylidene (I^{t}Bu)

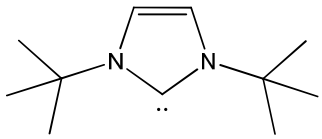

A Schlenk tube was charged with 1,3-*bis*(*tert*-butyl)imidazolium chloride (2.97g, 13.7 mmol) and $KN(SiMe_3)_2$ (3.28 g, 16.4 mmol). The Schlenk was cooled to -78 °C before addition of THF (20 mL). The suspension was stirred at -78 °C for 1 h before warming to room temperature and then stirred for a further 30 min. The solvent was removed under vacuum and the product extracted with toluene (2 x 20 mL) and filtered through celite. The solvent was removed *in vacuo* to afford the product was a white solid. Yield: 1.43 g (58%). ^{1}H NMR (C_6D_6, 300 MHz): δ 6.75 (s, 2H, NC*H*=C*H*N), 1.50 (s, 18H, ^{t}Bu). ^{13}C{^{1}H} NMR (C_6D_6, 101 MHz): δ 213.2 (s, N*C*N), 115.8 (s, N*C*H=*C*HN), 56.5 (s, *C*$(CH_3)_3$), 32.1 (s, C(*C*$H_3)_3$).

5.3 Preparation of N-aryl NHCs

5.3.1 Preparation of 1,3-*bis*(2,4,6-trimethylphenyl)imidazol-2-ylidene[3,6] (IMes)

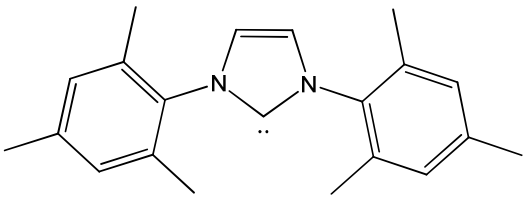

5.3.2 Preparation of 1,3-*bis*(2,4,6-trimethylphenyl)diazabutadiene

In air, a 1 L round bottomed flask was charged 2,4,6-trimethylphenylamine (135.2 g, 1.0 mol), 40% aqueous glyoxal (72.6 g, 0.5 mol) and EtOH (500 mL). The mixture was stirred for 12 h at room temperature, during which time a thick yellow precipitate was formed. The precipitate was isolated by filtration and washed with cold EtOH (3 x 50 mL). The product was dried under vacuum for 6 h. Yield: 212.0 g (73%). ^{1}H NMR ($CDCl_3$, 300 MHz): δ 8.13 (s, 2H, NC*H*=C*H*N), 6.93 (s, 4H, *m*-C*H*), 2.32 (s, 6H, *p*-CH_3), 2.19 (s, 12H, *o*-CH_3).

5.3.3 Preparation of 1,3-*bis*(2,4,6-trimethylphenyl)imidazolium chloride

In air, 250 mL round bottomed flask was charged with *bis*-(2,4,6-trimethylphenyl)-diazabutadiene (20.0 g , 68.5 mmol), paraformaldehyde (2.0 g, 66.6 mmol) and undried toluene (100 mL). The reaction mixture was heated to 100 °C and then cooled to 40 °C at which point HCl (16.5 mL, 4 M in dioxane) was introduced. The reaction was then heated to 70 °C for 5 h, then allowed to cool to room temperature and stirred for a futher 36 h. The product was isolated by filtration and washed with THF (3 x 50 mL). Yield: 15.6 g (69%). ^{1}H NMR ($CDCl_3$, 300 MHz): δ 10.31 (s, 1H, NC*H*N), 7.65 (s, 2H, NC*H*=C*H*N), 6.88 (s, 4H, *m*-C*H*), 2.22 (s, 6H, *p*-CH_3), 2.04 (s, 12H, *o*-CH_3).

5.3.4 Preparation of 1,3-*bis*(2,4,6-trimethylphenyl)imidazol-2-ylidene (IMes)

A 250 mL round bottomed flask was charged with 1,3-*bis*(2,4,6-trimethylphenyl)imidazolium chloride (4.00 g, 11.8 mmol), THF (100 mL) and potassium metal chunks (0.80 g, 20.0 mmol). The resulting slurry was heated at reflux for 3 h under argon to produce a red solution and a brown precipitate. The mixture was filtered through

Celite, and the solvent evaporated under vacuum. The solid residue was washed with cold hexane to afford the product as a white solid. Yield: 2.82 g (79%). ^{1}H NMR (C_6D_6, 300 MHz): δ 6.80 (s, 4H, *m*-C*H*), 6.51 (s, 2H, NC*H*=C*H*N), 2.16 (s, 6H, *p*-CH_3), 2.14 (s, 12H, *o*-CH_3).

5.3.5 Preparation of 1,3-*bis*(2,6-diisopropylphenyl)imidazol-2-ylidene[7] (IPr)

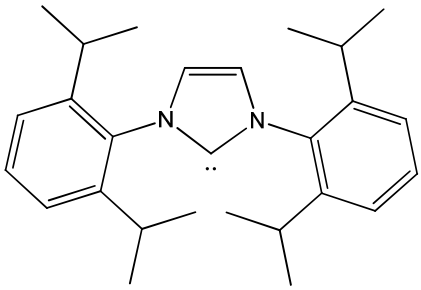

5.3.6 Preparation of *bis*(2,6-diisopropylphenyl)diazabutadiene

In air, 1 L round bottomed flask was charged with 2,6-diisopropylamine (53 mL, 0.28 mol), 40% aqueous glyoxal (16 mL, 0.14 mol) and undried EtOH (250 mL). A few drops of formic acid were added and the mixture was stirred at room temperature for 48 h to yield a yellow solid. The solid was filtered and washed with cold methanol before drying under vacuum for 6 h. Yield: 39.4 g (75%). ^{1}H NMR ($CDCl_3$, 300 MHz): δ 8.28 (s, 2H, NC*H*=C*H*N), 7.34-7.15 (m, 6H, $C_6{}^{i}Pr_2H_3$), 3.22 (sept, J_{HH} = 6.9 Hz, 4H, C*H*(CH_3)$_2$), 1.27 (d, J_{HH} = 6.9 Hz, 24H, NCH(CH_3)$_2$). ^{13}C{^{1}H} NMR ($CDCl_3$, 75.5 MHz): δ 163.2 (s, N*C*H=*C*HN), 148.0 (s, *C*CH(CH_3)$_2$), 136.8 (s, NC_{ipso}), 125.3 (s, *p*-*C*H), 123.3 (s, *m*-*C*H), 28.1 (s, *C*H(CH_3)$_2$), 22.5 (s, CH(*C*H_3)$_2$).

5.3.7 Preparation of 1,3-*bis*(2,6-diisopropylphenyl)imidazolium chloride

In air, 1 L round bottomed flask was charged with paraformaldehyde (2.0 g, 66 mmol), *bis*(2,6-diisopropylphenyl)diazabutadiene (25.8 g, 68.5 mmol) and toluene (500 mL). The reaction mixture was heated to 100 °C till most of the paraformaldehyde has dissolved, then cooled to 40 °C before the addition of HCl (16.5 mL, 4M in dioxane, 66 mmol), and heated at 70 °C for 5 h. The reaction mixture was cooled to room temperature and stirred for a further 5 days, before filtration and washing with THF (3 x 50 mL) to afford a purple solid. Yield: 12.7 g (45%). ^{1}H NMR ($CDCl_3$, 300 MHz): δ 10.07 (s, 1H, NC*H*N), 8.11 (s, 2H, NC*H*=C*H*N), 7.57 (m, 4H, *m*-C*H*), 7.23 (m, 2H, *p*-C*H*), 2.44 (sept, J_{HH} = 6.8 Hz, 4H, C*H*(CH_3)$_2$), 1.27 (d, J_{HH} = 6.8 Hz, 12H, CH(CH_3)$_2$), 1.23 (d, J_{HH} = 6.8 Hz, 12H, CH(CH_3)$_2$). ^{13}C{^{1}H} NMR (DMSO-d_6, 75 MHz): δ 144.8 (s, *C*CH(CH_3)$_2$), 139.4 (s,

NCHN), 131.8 (s, *p*-*C*H), 130.1 (s, C_{ipso}), 126.2 (s, NCH=CHN), 124.6 (s, *m*-*C*H), 28.6 (s, $CH(CH_3)_2$), 24.2 (s, $CH(CH_3)_2$), 23.1 (s, $CH(CH_3)_2$)

5.3.8 Preparation of 1,3-*bis*(2,6-diisopropylphenyl)imidazol-2-ylidene (IPr)

A Schlenk tube was charged with 1,3-*bis*(2,6-diisopropylphenyl)imidazolium chloride (6.50 g, 15 mmol), KO^{t}Bu (1.78 g, 18 mmol) and THF (40 mL). The resulting suspension was stirred at room temperature for 4 h, after which the volatiles were removed under vacuum to leave a brown residue this was extracted in toluene (100 mL), filtered through Celite and reduced to dryness to yield the product as an off-white solid. Yield: 5.4 g (92%). ^{1}H NMR (C_6D_6, 400 MHz): δ 7.24 (t, J_{HH} = 7.6 Hz, 2H, *p*-C*H*), 7.12 (d, J_{HH} = 7.6 Hz, 4H, *m*-C*H*), 6.57 (s, 2H, NC*H*=C*H*N), 2.92 (sept, J_{HH} = 6.8 Hz, 4H, C*H*$(CH_3)_2$), 1.24 (d, J_{HH} = 6.8 Hz, 12H, CH(CH_3)$_2$), 1.14 (d, J_{HH} = 6.8 Hz, 12H, CH(CH_3)$_2$). ^{13}C{^{1}H} NMR (C_6D_6, 101 MHz): δ 220.6 (s, N*C*N), 146.3 (s, *C*CH$(CH_3)_2$), 139.0 (s, NC_{ipso}), 129.0 (s, *p*-*C*H), 123.7 (s, *m*-*C*H), 121.6 (s, NCH=*C*HN), 28.8 (s, *C*H$(CH_3)_2$), 24.8 (s, CH(CH$_3$)$_2$), 23.6 (s, CH(CH$_3$)$_2$).

5.3.9 Preparation of 1,3-*bis*(2,6-diisopropylphenyl)-2(pentafluoro-phenyl)imidazolidene (SIPr·C_6F_5H)[8]

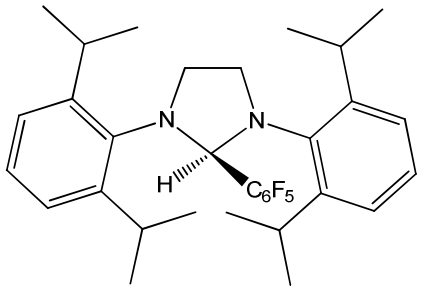

5.3.10 Preparation of N,N'-*bis*(2,6-diisopropylphenyl)aminoethane

A Schlenk tube was charged with *bis*(2,6-diisopropylphenyl)diazabutadiene (5.00 g, 13 mmol) and $NaBH_4$ (5.02 g, 13 mmol) in the glove box, and stirred at room temperature for 1.5 h in a 40:60 mixture of dry methanol (40 mL) and THF (60 mL). Over this time the yellow solution had turned clear. Slow addition of a saturated aqueous solution of NH_4Cl (20 mL) by pipette to quench excess $NaBH_4$ was followed by extraction with diethyl ether (3 x 50 mL) into a separating funnel. After washing the extract with water (3 x 100 mL) and drying with $MgSO_4$ the solvent was removed *in vacuo*. Yield: 4.2 g (85%). ^{1}H NMR ($CDCl_3$, 300 MHz): δ 7.17-7.07 (m, 6H, Aryl-C*H*), 3.39 (sept, J_{HH} = 6.90 Hz, 4H, C*H*$(CH_3)_2$), 3.19 (s, 4H, NCH_2), 1.28 (d, J_{HH} = 6.90 Hz, 24H,

$CH(CH_3)_2$). $^{13}C\{^1H\}$ NMR ($CDCl_3$, 75 MHz): δ 143.4 (s, C_{ipso}), 142.5 (s, $CCH(CH_3)_2$), 123.9 (s, *p*-*C*H), 123.7 (s, *m*-*C*H), 52.4 (s, NCH_2), 27.9 (s, $CH(CH_3)_2$), 24.4 (s, $CH(CH_3)_2$).

5.3.11 Preparation of 1,3-*bis*(2,6-diisopropylphenyl)-2(pentafluoro-phenyl)imidazolidene (SIPr·C_6F_5H)

In air, a Schlenk tube was charged with solid pentafluorobenzaldehyde (4.33 g, 22 mmol). A minimum amount of glacial acetic acid (*ca.* 5 mL) and N,N'-*bis*(2,6-diisopropylphenyl)aminoethane (4.20 g, 11 mmol) were then added. After stirring at room temperature for 1 h was followed by concentration *in vacuo*, filtration, the solid was washed with cold methanol (3 x 50 mL) and drying to give a white product, which was stored under argon. Yield 3.7 g (60%). ^1H MR ($CDCl_3$, 300 MHz): δ 7.22-7.13 (m, 4H, *m*-C*H*), 7.04-7.01 (m, 2H, *p*-C*H*), 6.31 (s, 1H, C*H*C_6F_5), 3.81-3.87 (m, 2H, NCH_2), 3.69-3.60 (m, 4H, CH_2 + C*H*$(CH_3)_2$), 3.53 (sept, J_{HH} = 9.00 Hz, 2H, C*H*$(CH_3)_2$), 1.41 (d, J_{HH} = 9.00 Hz, 6H, $CH(CH_3)_2$), 1.29 (d, J_{HH} = 9.00 Hz, 6H, $CH(CH_3)_2$), 1.17 (d, J_{HH} = 9.00 Hz, 6H, $CH(CH_3)_2$), 0.79 (d, J_{HH} = 9.0 Hz, 6H, $CH(CH_3)_2$).

5.4 Preparation of ring-expanded N-heterocyclic carbenes

5.4.1 Preparation of 1,3-*bis*(2-propyl)-3,4,5,6-tetrahyrdropyrimidin-1-ium tetrafluoroborate[9] [6^{i}Pr$_2$H]BF_4

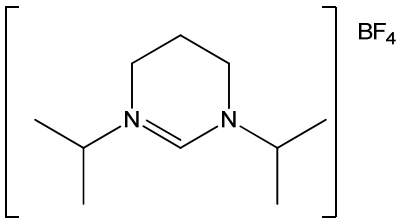

In air, a 250 mL round bottomed flask was charged with N,N-diisopropylpropane-1,3-diamine (1.5 g, 9.48 mmol), ammonium chloride (519 mg, 9.7 mmol) and triethyl orthoformate (12 mL). The reaction mixture was heated to 150 °C for 3 h affording a pale yellow oil. The solvent was removed by distillation to leave a waxy yellow solid. Washing with Et_2O (3 x 5 mL) gave 1,3-*bis*(2-propyl)-3,4,5,6-tetrahyrdopyrimidin-1-ium chloride as white solid. The white solid was dissolved in acetonitrile (20 mL) and treated with a solution of $NaBF_4$ (1.04 g, 9.48 mmol) in water (5 mL). The reaction mixture was stirred for 30 min at room temperature, after which the solvent was removed *in vacuo*. The residual solid was dissolved in CH_2Cl_2 (30 mL) and washed with water (3 x 10 mL), the layers were separated and the organic phase was collected. The solvent was

reduced to approximately 10 mL and Et_2O was added until the product precipitated out as a white solid. Yield: 2.0 g (82%). ^{1}H NMR ($CDCl_3$, 250 MHz): δ 8.03 (s, 1H, NC*H*N), 3.96 (sept, J_{HH} = 6.48 Hz, 2H, C*H*$(CH_3)_2$), 3.32 (t, J_{HH} = 5.78 Hz, 4H, NCH_2), 2.06 (quint, J_{HH} = 5.78 Hz, 2H, NCH_2CH_2), 1.29 (d, J_{HH} = 6.48 Hz, 12H, $CH(CH_3)_2$).^{13}C{^{1}H} NMR ($CDCl_3$, 75.5 MHz): δ 150.5 (s, N*C*HN), 56.8 (s, N*C*$H(CH_3)_2$) 38.7 (s, N*C*H_2), 20.0 (s, $NCH(CH_3)_2$), 19.0 (s, N*C*H_2CH_2).

5.4.2 Preparation of 1,3-*bis*(2-methylphenyl)-3,4,5,6-tetrahydro-3H-[1,3]pyrimidinium tetrafluoroborate[10] [6*o*-TolH]BF_4

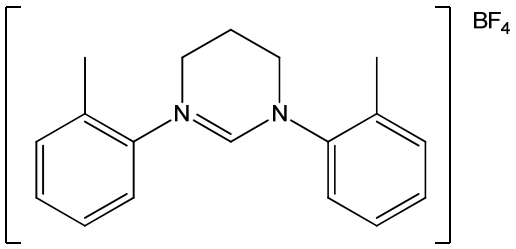

5.4.3 Preparation of N,N'-*bis*(2-methylphenyl)formamidine

An ampoule was charged with toluidine (6.5 g, 60.6 mmol), triethyl orthoformate (4.38 g, 29.6 mmol) glacial acetic acid (3 mL). The resulting mixture was then heated at 110 °C for 24 h. The product was isolated by filtration and washed with toluene (10 mL). Yield 4.28 g (65%). ^{1}H NMR ($CDCl_3$, 300 MHz): δ 8.06 (s, 1H, NC*H*N), 7.18-7.02 (m, 9H, Aryl-C*H*, N*H*), 2.32 (s, 6H, CH_3).

5.4.4 Preparation of 1,3-*bis*(2-methylphenyl)-3,4,5,6-tetrahydro-3H-[1,3]pyrimidinium tetrafluoroborate [6*o*-TolH]BF_4

In air, a 250 mL round bottomed flask was charged with N,N'-*bis*(2-methylphenyl)formamidine (2.0 g, 8.9 mmol), K_2CO_3 (621 mg, 4.5 mmol) and 1,4-diiodobutane (2.79 g, 9.0 mmol) and acetonitrile (30 mL). The reaction mixture was heated to reflux for 24 h, after which the reaction was cooled to room temperature and the solvent removed under vacuum. The product was then extracted into CH_2Cl_2 (20 mL) and then treated with $NaBF_4$ (988 mg, 9.0 mmol) in water (20 mL). The reaction mixture was allowed to stir for 30 min at room temperature and the solvent then removed *in vacuo*. The residual solid was dissolved in CH_2Cl_2 (30 mL), washed with water (3 x 10 mL), the layers separated and the organic phase collected. The solvent was reduced to ca. 10 mL and Et_2O was added until the product precipitated out as a white solid. Yield: 2.44 g (78%). ^{1}H NMR ($CDCl_3$, 300 MHz): δ 7.75 (d, J_{HH} = 7.66 Hz, 2H, *o*-C*H*), 7.62 (s,

1H, NC*H*N), 7.31-7.17 (m, 6H, *m,p*-C*H*), 4.02 (t, J_{HH} = 5.37 Hz, 4H, NCH_2), 2.54 (qunit, J_{HH} = 5.37 Hz, 2H, NCH_2CH_2), 2.34 (s, 6H, CH_3). $^{13}C\{^1H\}$ NMR ($CDCl_3$, 75.5 MHz): δ 153.1 (s, N*C*HN), 139.9 (s, C_{ipso}), 133.5 (s, *C*CH_3), 131.5 (s, Aryl-*C*H), 130.1 (s, Aryl-*C*H), 127.8 (s, Aryl-*C*H), 47.3 (s, N*C*H_2), 19.4 (s, NCH_2CH_2), 17.6 (s, C*C*H_3)

5.5 Preparation of tripodal N-heterocyclic carbenes

5.5.1 Preparation of 1,3,5-*tris*(bromomethyl)-2,4,6-triethylbenzene[11]

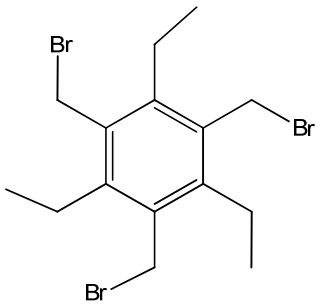

A condenser was connected to a 250 mL round bottomed flask which was charged with zinc powder (5 g, 76 mmol) and acetic acid (glacial, 50 mL) in air. At room temperature to the stirred reaction mixture hydrogen bromide in acetic acid (33 %wt, 50 mL) was added slowly through the condenser over 0.5 h period. The reaction mixture was stirred until all of the zinc powder had dissolved leaving a tan orange coloured solution. To this 2,4,6-triethylbenzene (10 g, 62 mmol), paraformaldehyde (15 g) and hydrogen bromide in acetic acid (33 %wt, 148 mL) were added together. The resulting slurry was then heated to 90 °C (keeping between 85 – 95 °C) for 48 h resulting in a dark brown solution. The solution was cooled to room temperature with continuous stirring, upon a white precipitate formed. The solid was filtered and washed with water (3 x 20 mL). The remaining solution was collected and reheated at 90 °C for a further 24 h allowing the formation of a second crop of product. Yield 15.8 g (59%). ^1H NMR ($CDCl_3$, 300 MHz): δ 4.58 (s, 6H, CH_2Br), 2.94 (q, J_{HH} = 7.6 Hz, 6H, CH_2CH_3), 1.34 (t, J_{HH} = 7.6 Hz, 9H, CH_2CH_3). $^{13}C\{^1H\}$ NMR ($CDCl_3$, 75.5 MHz): δ 145.0 (s, *C*CH_2Br), 132.6 (s, *C*CH_2CH_3), 28.5 (s, C*C*H_2Br), 22.7 (s, C*C*H_2CH_3), 15.6 (s, CCH_2CH_3).

5.5.2 Preparation of 1-*tert*-butylimidazole

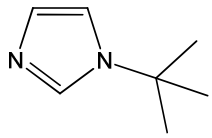

In air, an aqueous solution of glyoxal (40 %wt, 147 mL, 1.28 mol), formaldehyde (37%, 97 mL, 1.28 mol) and ^{i}PrOH (10 mL) were added to an addition funnel. A second addition funnel was carefully charged with ammonia solution (35%, 70 mL, 1.28 mol) and *tert*-butylamine (132 mL, 1.28 mol). The addition funnels were attached to a three necked round bottomed flask containing ^{i}PrOH (20 mL). The contents of both addition funnels were added dropwise over 1 h ensuring the temperature of the solution remained below 70 °C, to give a yellow suspension. The reaction mixture was refluxed for 2 h to yield a red solution. The volatiles were then removed in vacuum and the product isolated by vacuum distillation collecting the fraction between 50-57 °C. The product was isolated as a yellow oil. Yield 59.7 g (39%). ^{1}H NMR ($CDCl_3$, 300 MHz): δ 7.52 (s, 1H, NC*H*N), 6.95 (br s, 2H, NC*H*=C*H*N), 1.46 (s, 9H, ^{t}Bu). $^{13}C\{^{1}H\}$ NMR ($CDCl_3$, 75.5 MHz): δ 133.6 (s, N*C*HN), 128.1 (s, N*C*H=*C*HN), 115.8 (s, N*C*H=*C*HN), 62.4 (s, *C*$(CH_3)_3$), 29.9 (s, C(*C*$H_3)_3$).

5.5.3 Preparation of 1-(2,6-diisopropylphenyl)imidazole[12]

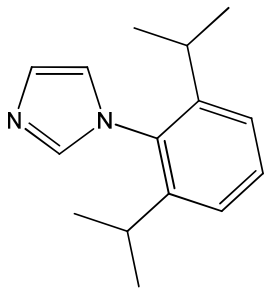

In air, a 1 L round bottomed flask was charged with 2,4-diisopropylphenylaniline (18.9 mL, 0.1 mmol), glyoxal (40 %wt, 12.15 mL, 0.1 mmol) and MeOH (50 mL). The reaction mixture was allowed to stir for 16 h at room temperature afford a yellow solid. To this ammonium chloride (10.7 g, 0.2 mmol), and formaldehyde (37% aq, 16 mL, 0.2 mmol) were added. The mixture was then diluted with MeOH (400 mL) and refluxed for 1 h. After cooling to room temperature, *ortho*-phosphoric acid (85%, 14 mL) was added over a period of 10 min. The resulting mixture was then refluxed for a further 8 h. After removal of the solvent, ice (300 g) was added to the dark residue. Aqueous solution of potassium hydroxide was added to bring the solution to pH 9. The product was

extracted by addition of Et_2O (3 x 150 mL). The organic phases were combined and washed with water (100 mL), saturated NaCl aqueous solution (100 mL) and then dried over $MgSO_4$. The solvent was then removed to afford the product as a brown solid. Yield 10.0 g (44%). ^{1}H NMR ($CDCl_3$, 300 MHz): δ 7.45 (br s, 1H, NC*H*N), 7.24 (m, 1H, *p*-C*H*), 7.29 (br s, 1H, NC*H*=C*H*N), 7.22 (m, 2H, *m*-C*H*), 6.92 (br s, 1H, NC*H*=C*H*N), 2.37 (sept, J_{HH} = 6.88 Hz, 2H, C*H*$(CH_3)_2$), 1.02 (d, J_{HH} = 6.88 Hz, 12H, CH(CH_3)$_2$). ^{13}C{^{1}H} NMR ($CDCl_3$, 75.5 MHz): δ 146.9 (s, N*C*HN), 138.8 (s, *C*CH$(CH_3)_2$), 133.1 (s, C_{ipso}), 130.3 (s, *p*-*C*H), 129.5 (s, *m*-*C*H), 124.2 (NCH=*C*HN), 122.0 (s, N*C*H=*C*HN), 28.5 (s, *C*H$(CH_3)_2$). 24.8 (s, CH(*C*H_3)$_2$), 24.7 (s, CH(*C*H_3)$_2$).

5.5.4 Preparation of 1,3,5-{*tris*(tert-butylimidazol-2-ylidene)methyl}-2,4,6-triethylbenzene (timteb^{tBu})

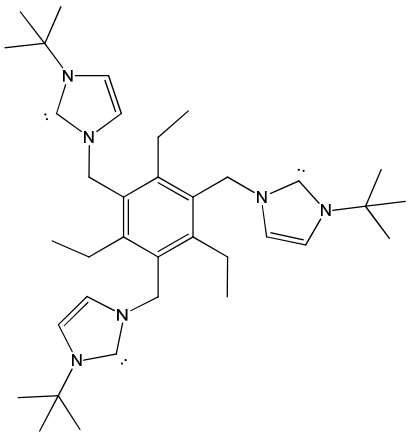

5.5.5 Preparation of 1,3,5-{*tris*{3-tert-butylimidazolium)methyl}-2,4,6-triethylbenzene tribromide [timteb^{tBu}H$_3$]Br$_3$

In air, 1,3,5-*tris*(bromomethyl)-2,4,6-triethylbenzene (2.0 g, 4.58 mmol) was dissolved in 1,4-dioxane (100 mL) in a 250 mL round bottomed flask. 1-*tert*-butylimidazole (1.66 g, 14 mmol) was added to the vigorously stirring solution, resulting in the immediate formation of a cloudy suspension. This suspension was then stirred for a further 1 h followed by heating at 50 °C for 30 min. After cooling, the solid collected by filtration and washed with Et_2O (3 x 30 mL) and dried under vacuum to give the product as a white solid. Yield: 2.80 g (76%). ^{1}H NMR ($CDCl_3$, 500 MHz): δ 10.88 (s, 3H, NC*H*N), 7.53 (s, 3H, NC*H*=C*H*N), 7.13 (s, 3H, NC*H*=C*H*N), 5.79 (s, 6H, CH_2N), 2.66 (q, J_{HH} = 7.4 Hz, 6H, CH_2CH$_3$), 1.72 (s, 27H, C(CH_3)$_3$), 1.09 (t, J_{HH} = 7.4 Hz, 9H, CH$_2$CH_3). ^{13}C{^{1}H} NMR ($CDCl_3$, 125 MHz): δ 147.0 (s, *C*CH$_2$N or *C*CH$_2$CH$_3$), 135.9 (s, N*C*HN), 126.9 (s, *C*CH$_2$CH$_3$ or *C*CH$_2$N), 135.9 (s, NC*H*=*C*HN), 120.1 (s, NC*H*=*C*HN), 60.9 (s, N*C*$(CH_3)_3$), 47.4 (s, *C*H$_2$N), 30.4 (s, NC(*C*H_3)$_3$), 26.7 (s, *C*H$_2$CH$_3$), 15.4 (s, CH$_2$*C*H$_3$).

5.5.6 Preparation of 1,3,5-{*tris*(3-tert-butylimidazol-2-ylidene)methyl}-2,4,6-triethylbenzene (timteb^{tBu})

A Schlenk tube was charged with [timteb^{tBu}H$_3$]Br$_3$ (1 g, 1.23 mmol) and KN(SiMe$_3$)$_2$ (735 mg, 3.69 mmol) in THF (20 mL). The resulting suspension was allowed to stir at room temperature for 1.5 h. The solution was then filtered through Celite and reduced to dryness. The resulting oily solid was washed with hexane (10 mL) to afford timteb^{tBu} as a white solid. Yield: 625 mg (89%). ^{1}H NMR (THF-d_8, 400 MHz): δ 6.98 (br s, 3H, NC*H*=C*H*N), 6.49 (br s, 3H, NC*H*=C*H*N), 5.74 (s, 6H, NCH$_2$), 2.93 (br q, 6H, C*H*$_2$CH$_3$), 1.53 (s, 27H, C(C*H*$_3$)$_3$), 0.86 (br t, 9H, CH$_2$C*H*$_3$). ^{13}C{^{1}H} NMR (THF-d_8, 101 MHz): δ 214.5 (s, N*C*N), 145.5 (s, *C*CH$_2$N or *C*CH$_2$CH$_3$), 132.5 (s, *C*CH$_2$N or *C*CH$_2$CH$_3$), 117.1 (s, NC*H*=C*H*N), 115.5 (s, NC*H*=C*H*N), 55.8 (s, NC*H*(CH$_3$)$_3$), 49.0 (s, *C*H$_2$N), 31.4 (s, NC(*C*H$_3$)$_3$), 23.7 (s, *C*H$_2$CH$_3$), 15.5 (s, CH$_2$*C*H$_3$).

5.5.7 Preparation of 1,3,5-{*tris*(3-(2,6-diisopropylphenyl)imidazolium)methyl}-2,4,6-triethylbenzene tribromide [timteb^{dipp}H$_3$]Br$_3$

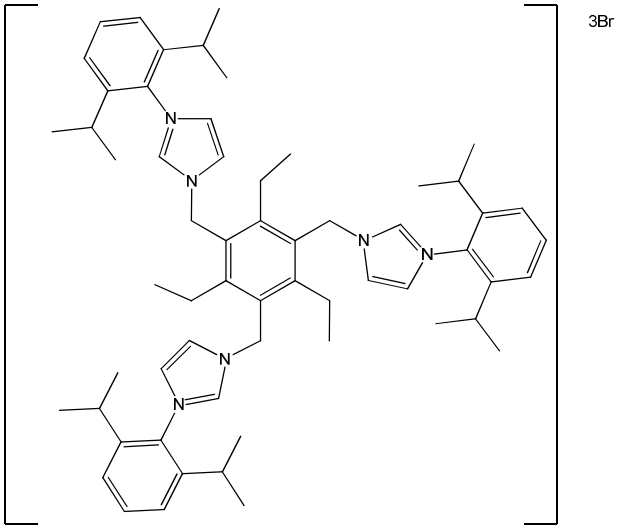

The reaction was performed in a similar way to the ^{t}Bu derivative but using 1,3,5-*tris*(bromomethyl)-2,4,6-triethylbenzene (3.0 g, 6.8 mmol) and 2,6-diisopropylphenylimidazole (4.65 g, 20.4 mmol). The initially formed suspension was stirred for 24 h at room temperature then heated at 50 °C for 1 h. The 1,4-dioxane was removed under vacuum, and the resulting solid filtered and washed with Et$_2$O (3 x 30 mL). Yield: 4.98 g (65%). ^{1}H NMR (CDCl$_3$, 300 MHz): δ 10.69 (s, 3H, NC*H*N), 8.92 (s, 3H, NC*H*=C*H*N), 7.45 (t, J_{HH} = 7.65 Hz, 3H, *p*-C*H*), 7.22 (d, J_{HH} = 7.65 Hz, 6H, *m*-C*H*), 7.07 (s, 3H, NC*H*=C*H*N), 6.10 (s, 6H, NC*H*$_2$), 2.78 (sept, J_{HH} = 7.65 Hz, 6H,

C*H*(CH_3)$_2$), 2.20 (q, J_{HH} = 6.90 Hz, 6H, CH_2CH$_3$), 1.13 (d, J_{HH} = 7.65 Hz, 18H, CH(CH_3)$_2$), 1.07 (d, J_{HH} = 7.65 Hz, 18H, CH(CH_3)$_2$), 0.84 (t, J_{HH} = 7.53 Hz, 9H, CH$_2$CH_3). ^{13}C{^{1}H} NMR ($CDCl_3$, 75.5 MHz): δ 148.9 (s, *C*CH$_2$N), 145.1 (s, C_6^{i}Pr$_2$H$_3$), 137.9 (s, N*C*HN), 131.9 (s, C_6^{i}Pr$_2$H$_3$), 130.4 (s, *C*CH$_2$CH$_3$), 128.6 (s, C_6^{i}Pr$_2$H$_3$), 125.3 (s, N*C*H=*C*HN), 124.7 (s, C_6^{i}Pr$_2$H$_3$), 124.4 (s, N*C*H=*C*HN), 48.7 (s, *C*H$_2$N), 31.1 (s, *C*H(CH_3)$_2$), 24.6 (s, *C*H(CH_3)$_2$), 24.3 (s, *C*H$_2$CH$_3$), 24.2 (s, CH(*C*H$_3$)$_2$), 15.9 (s, CH$_2$*C*H$_3$).

5.6 Syntheses of N-heterocyclic carbene cluster complexes

5.6.1 Synthesis of Ru(IMes)$_2$(CO)$_3$ (2.5) and Ru(IMes)(CO)$_4$ (2.6) co-crystal

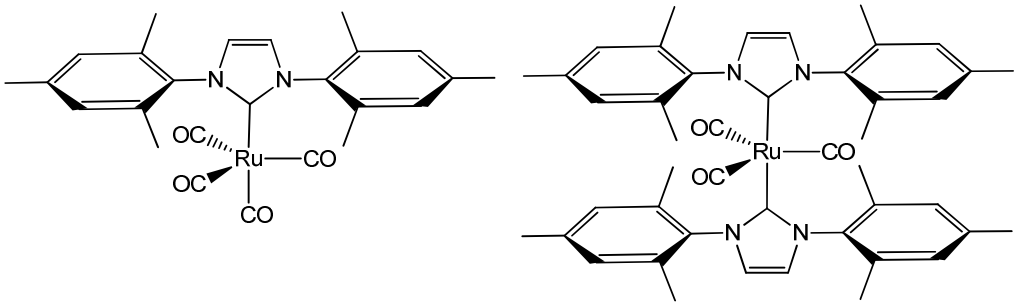

An ampoule fitted with a J. Young's PTFE tap and a magnetic stirrer was charged with $Ru_3(CO)_{12}$ (50 mg, 0.078 mmol) and IMes (107 mg, 0.35 mmol) and THF (2 mL). The solution was stirred for 1 h during which the solution turned from a light orange to a red colour. The solvent was then removed *in vacuo* and the product was washed with hexane (3 x 5 mL) and dried under vacuum. Yield: 103 mg (90%). Ru(IMes)(CO)$_4$ (**2.5**): ^{1}H NMR (THF-d_8, 500 MHz): δ 7.38 (s, 2H, NC*H*=C*H*N), 7.02 (s, 4H, *m*-C*H*), 2.34 (s, 6H, *p*-CH_3), 2.07 (s, 12H, *o*-CH_3). ^{13}C{^{1}H}NMR (THF-d_8, 125 MHz): δ 207.1 (s, *C*O), 179.2 (s, N*C*N), 140.0 (s, *p*-*C*(CH_3)), 138.3 (s, C_{ipso}), 136.4 (s, *o*-*C*(CH_3)), 129.9 (s, *m*-*C*H), 125.2 (s, N*C*H=*C*HN), 21.0 (s, *p*-*C*H_3), 18.2 (s, *o*-*C*H_3). Ru(IMes)$_2$(CO)$_3$ (**2.6**): ^{1}H NMR (THF-d_8, 500 MHz): δ 6.92 (s, 4H, NC*H*=C*H*N), 6.78 (s, 8H, *m*-C*H*), 2.31 (s, 12H, *p*-CH_3), 1.91 (s, 24H, *o*-CH_3). ^{13}C{^{1}H} NMR (THF-d_8, 125 MHz): δ 216.8 (s, *C*O), 186.9 (s, N*C*N), 138.9 (s, C_{ipso}), 137.7 (s, *p*-*C*(CH_3)), 137.0 (s, *o*-*C*(CH_3)), 129.1 (s, *m*-*C*H), 123.8 (s, N*C*H=*C*HN), 21.1 (s, *p*-*C*H_3), 18.7 (s, *o*-*C*H_3). IR (C_6D_6, ν_{CO}, cm^{-1}): 2047, 2020, 2011, 1986, 1964, 1935, 1919. Anal. Found (calcd) for $Ru_2C_{70}N_6O_7H_{72}$: C, 64.11 (64.11); H, 5.53 (5.53); N, 6.40 (6.41).

5.6.2 Synthesis of Ru_3(ab-IPr)$(CO)_{11}$ (2.7)

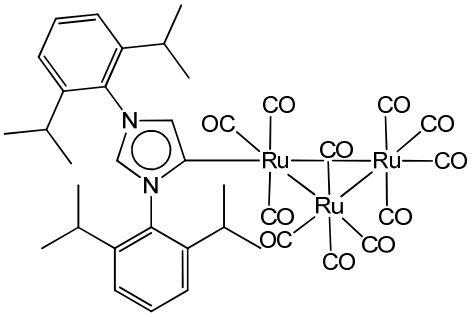

An ampoule fitted with a J. Young's PTFE tap and a magnetic stirrer was charged with $Ru_3(CO)_{12}$ (300 mg, 0.47 mmol) and IPr (182 mg, 0.47 mmol) and THF (4 mL). The dark red solution was stirred for 5 days at room temperature. The solution was filtered then the solvent removed *in vacuo*. The product was extracted into benzene (2 mL). The solvent was removed in vacuum affording the product as a light red solid. Yield: 53 mg (11%). ^{1}H NMR (C_6D_6, 500 MHz): δ 7.26 (t, J_{HH} = 7.91 Hz, 1H, *p*-C*H*), 7.11 (t, J_{HH} = 8.08 Hz, 1H, *p*-C*H*), 7.09 (d, J_{HH} = 7.67 Hz, 2H, *m*-C*H*), 6.91 (d, J_{HH} = 7.81 Hz, 2H, *m*-C*H*), 6.87 (d, J_{HH} = 1.61 Hz, 1H, NC=C*H*N), 6.50 (d, J_{HH} = 1.61 Hz, 1H, NC*H*N), 2.65 (sept, J_{HH} = 6.86 Hz, 2H, C*H*$(CH_3)_2$), 2.28 (sept, J_{HH} = 6.86 Hz, 2H, C*H*$(CH_3)_2$), 1.38 (d, J_{HH} = 6.79 Hz, 6H, CH(C*H*$_3)_2$), 1.04 (d, J_{HH} = 6.79 Hz, 6H, CH(C*H*$_3)_2$), 0.95 (d, J_{HH} = 6.79 Hz, 6H, CH(C*H*$_3)_2$), 0.88 (d, J_{HH} = 6.79 Hz, 6H, CH(C*H*$_3)_2$). ^{13}C{^{1}H} NMR (C_6D_6, 125 MHz): δ 207.4 (s, *C*O), 206.6 (s, *C*O), 147.8 (s, NCH*C*N), 146.9 (s, NC_{ipso}), 146.5 (s, *C*CH$(CH_3)_2$), 145.9 (s, *C*CH$(CH_3)_2$), 136.6 (s, N*C*HCN), 133.3 (s, N*C*HN), 131.9 (s, *p*-*C*H), 131.8 (s, *p*-*C*H), 125.1 (s, *m*-*C*H), 124.7 (s, *m*-*C*H), 29.2 (s, *C*H$(CH_3)_2$), 29.1 (s, *C*H$(CH_3)_2$), 26.8 (s, CH(*C*H$_3)_2$), 25.0 (s, CH(*C*H$_3)_2$), 24.1 (s, CH(*C*H$_3)_2$), 23.1 (s, CH(*C*H$_3)_2$). IR (C_6D_6, ν_{CO}, cm^{-1}): 2047, 2029, 2016, 1997, 1969, 1954, 1935, 1921. Anal. Found (cacld) for $C_{38}H_{36}N_2O_{11}Ru_3$: C; 45.77 (45.64); H, 3.57 (3.63); N, 2.80 (2.73).

5.6.3 Synthesis of [I^{t}BuH][Ru_3(μ-H)(μ-CO)$(CO)_{10}$]

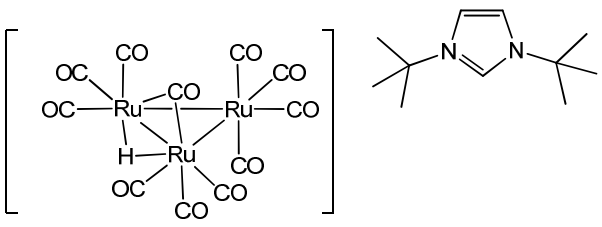

A J. Young's NMR tube fitted with a re-sealable PTFE valve was charged with Ru_3(ab-I^{t}Bu)$(CO)_{11}$ (15 mg, 0.019 mmol) and THF-d_8 (1 mL). The solution was degassed via the

freeze pump thaw method and an atmosphere of hydrogen added to the tube, this resulted in an immediate darkening of the red solution. The volatiles removed under vacuum after 30 min to afford the product as a dark red solid. Yield: 15 mg (99%). ^{1}H NMR (THF-d_8, 500 MHz): δ 8.88 (s, 1H, NC*H*N), 7.91 (s, 2H, NC*H*=C*H*N), 1.71 (s, 9H, C(CH_3)$_3$), -12.56 (s, 1H, μ-*H*). ^{13}C{^{1}H} NMR (DMSO-d_6, 75.5 MHz): δ 132.7 (s, N*C*HN), 120.6 (s, N*C*H=*C*HN), 60.2 (s, *C*(CH$_3$)$_3$), 20.1 (s, C(*C*H$_3$)$_3$). Anal. Found (calcd) for $C_{22}H_{22}N_2O_{11}Ru_3$: C, 33.20 (33.29); H, 2.83 (2.79); N, 3.50 (3.53).

5.6.4 Synthesis of Os_3(ab-I^{t}Bu)(CO)$_{11}$ (2.8)

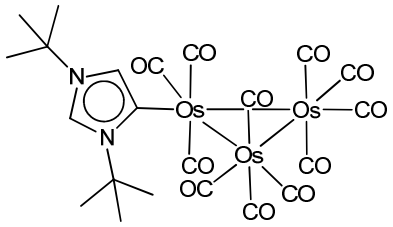

An ampoule fitted with a J. Young's PTFE tap was charged with $Os_3(CO)_{12}$ (50 mg, 0.055 mmol), I^{t}Bu (10 mg, 0.055 mmol) and THF (5 mL). The resulting suspension was degassed and heated at 70 °C for 5 h. The volatiles were then removed *in vacuo* to leave a red solid. The product was extracted with hot fluorobenzene (1 mL) and filtered. After cooling the filtrate was layered with hexane to yield Os_3(ab-I^{t}Bu)(CO)$_{11}$ as red crystals. Yield: 14.6 mg (25%). ^{1}H NMR (THF-d_8, 500 MHz): δ 8.38 (d, J_{HH} = 1.9 Hz, 1H, NC*H*N), 6.73 (d, J_{HH} = 1.9 Hz, 1H, NC=C*H*N), 1.89 (s, 9H, C(CH_3)$_3$), 1.56 (s, 9H, C(CH_3)$_3$). ^{13}C{^{1}H} NMR (THF-d_8, 125 MHz): δ 136.5 (s, NC=*C*HN), 132.2 (s, N*C*HN), 113.5 (s, N*C*=CHN), 61.0 (s, *C*(CH$_3$)$_3$), 30.9 (s, C(*C*H$_3$)$_3$), 30.5 (s, C(*C*H$_3$)$_3$). IR (nujol, ν_{CO}, cm^{-1}): 2093, 2038, 2015, 2002, 1991, 1956, 1932, 1923. Anal. Found (calcd) for $C_{22}H_{20}N_2O_{11}Os_3$: C, 25.21 (24.95); H, 1.88 (1.90); N, 2.65 (2.65).

5.6.5 Synthesis of Ru_3(6^{i}Pr$_2$)(μ-CO)$_2$(CO)$_8$ (2.10)

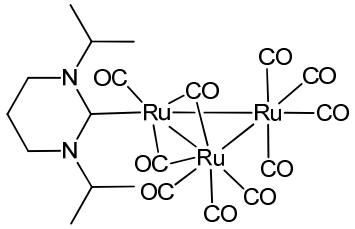

[6^{i}Pr$_2$H]BF$_4$ (40 mg, 0.156 mmol) and KN(SiMe$_3$)$_2$ (31mg, 0.156 mmol) were suspended in THF (15 mL) and stirred at room temperature for 30 minutes. The solution was then filtered into a

Schlenk tube containing $Ru_3(CO)_{12}$ (50 mg, 0.078 mmol) dissolved in THF (15 mL). The solution immediately turned from orange to a blood red colour. After stirring at room temperature for 16 h, the solvent was removed and the product extracted with hexane (40 mL). It was concentrated to ca. 10 mL and cooled to -30 °C to afford $Ru_3(6^iPr_2)(\mu_2\text{-}CO)_2(CO)_8$ as red crystals. Yield: 7.9 mg (13.5%). ^{1}H NMR (THF-d_8, 500 MHz): δ 3.58 (sept, J_{HH} = 6.87 Hz, 2H, C*H*$(CH_3)_2$), 3.41 (m, 2H, NC*H*$_2$), 3.17 (m, 2H, NC*H*$_2$), 2.11 (m, 1H, NCH_2CH_2), 1.88 (m, 1H, NCH_2CH_2), 1.35 (d, J_{HH} = 6.87 Hz, 6H, $CH(CH_3)_2$), 1.21 (d, J_{HH} = 6.87 Hz, 6H, $CH(CH_3)_2$). ^{13}C{^{1}H} NMR (THF-d_8, 125 MHz): δ 198.7 (s, N*C*N) , 57.5 (s, N*C*$H(CH_3)_2$), 40.6 (s, N*C*H_2), 21.6 (s, NCH_2CH_2), 20.5 (s, $NCH(CH_3)_2$), 19.9 (s, $NCH(CH_3)_2$). IR (ν_{CO}, cm^{-1}, C_6D_6): 2084, 2040, 2018, 2004, 1982, 1968, 1792. Anal. Found (calcd) for $C_{20}H_{20}N_2O_{10}Ru_3$: C, 31.96 (31.92); H, 2.68 (2.77); N, 3.73 (3.60).

5.6.6 Formation of N-Formyl-N,N'-*bis*(diisopropylphenyl)ethylenediamine

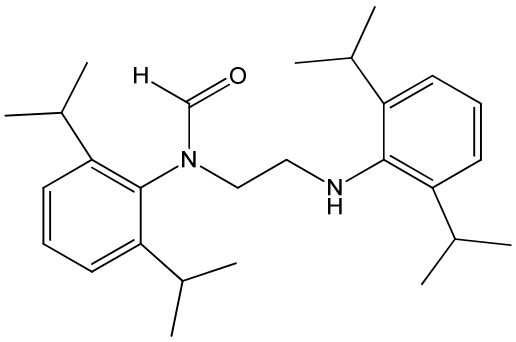

An ampoule fitted with a J. Young's PTFE tap was charged with $Ru_3(CO)_{12}$ (50 mg, 0.055 mmol) and SIPr·C_6F_5H (92 mg, 0.165 mmol) in THF (5 mL). The reaction mixture was heated at 70 °C for 4 h, after which the product was extracted with toluene. The solution was then placed in a freezer at -30 °C for 1 week, during which time the colour changed from green to yellow. The solution was reduced to dryness and the product extracted in hexane, affording a pale yellow solid. Yield: 42.6 mg (63%) ^{1}H NMR (C_6D_6, 500 MHz): δ 8.23 (s, 1H, *H*CO), 7.08 (m, 4H, *m*-C*H*), 6.96 (m, 2H, *p*-C*H*), 3.85 (t, J_{HH} = 6.88 Hz, 2H, NC*H*$_2$), 3.62 (brt, J_{HH} = 6.88 Hz, 1H, N*H*), 3.38 (pent, J_{HH} = 6.83 Hs, 2H C*H*$(CH_3)_2$), 3.17 (q, J_{HH} = 7.06 Hz, 2H, C*H*$_2$NH), 3.04 (p, J_{HH} = 6.83 Hz, 2H, C*H*$(CH_3)_2$), 1.23 (d, J_{HH} = 6.83 Hz, 12H, C*H*$_3$), 1.07 (d, J_{HH} = 6.83 Hz, 6H, C*H*$_3$), 0.95 (d, J_{HH} = 6.83 Hz, 6H, C*H*$_3$). ^{13}C{^{1}H} NMR (C_6D_6, 125 MHz): δ 163.8 (s, H*C*O), 148.4 (s, Aryl-*C*), 142.9 (s, Aryl-*C*), 125.0 (s, *p*-*C*H), 124.3 (s, *m*-*C*H), 50.3 (s, *C*H$_2$NH), 49.7 (s, *C*H$_2$N), 28.9 (s, *C*H$(CH_3)_2$), 28.5 (s, *C*H$(CH_3)_2$), 25.7 (s, *C*H$_3$), 24.85 (s, *C*H$_3$), 23.9 (s, *C*H$_3$). IR (cm^{-1}, C_6D_6): 2965 (ν_{NH}), 1680 (ν_{CO}).

5.6.7 Formation of N-Formyl-N,N'-*bis*(*o*-tolyl)propyldiamine

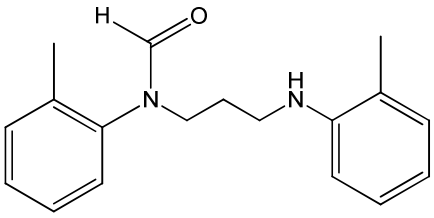

A Schlenk tube was charged with [6*o*-TolH][BF_4] (55 mg, 0.156 mmol) and $KN(SiMe_3)_2$ (30 mg, 0.156 mmol) and THF (10 mL) and stirred at room temperature for 30 min. The solution was then filtered into a Schlenk tube containing $Ru_3(CO)_{12}$ (50 mg, 0.078 mmol) dissolved in THF (10 mL). The reaction was stirred for 16 h during which time the colour changed from a light orange to a dark red. The volatiles were removed *in vacuo* and the product extracted into hexane (20 mL). Removal of solvent in vacuum left a light brown solid. Yield: 9.2 mg (21%) ^{1}H NMR ($CDCl_3$, 300 MHz): 8.00 (s, 1H, *H*CO), 7.28 (m, 1H, Aryl-C*H*), 7.17 (m, 1H, Aryl-C*H*), 7.00 (m, 1H, Aryl-C*H*), 6.94 (m, 2H, Aryl-C*H*), 6.86 (m, 1H, Aryl-C*H*), 6.67 (m, 2H, Aryl-C*H*), 4.37 (br m, 1H, N*H*), 3.51 (br t, 2H, NCH_2), 3.10 (br q, 2H, CH_2NH), 2.27 (s, 3H, CH_3), 1.81 (s, 3H, CH_3), 1.52 (m, 2H, CH_2CH$_2$NH). IR (cm^{-1}, C_6D_6): 2960 (ν_{NH}), 1677 (ν_{CO}).

5.7 Syntheses of palladium N-heterocyclic carbene clusters

5.7.1 Preparation of $PdCl_2(NHC)_2$[13]

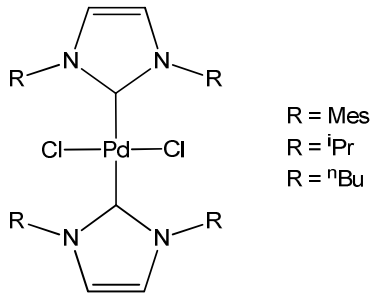

Palladium dichloride (300 mg, 1.69 mmol), imidazolium chloride (3.38 mmol) and caesium carbonate (4.9 g, 15.21 mmol) were suspended in dioxane (10 mL) and heated at 80 °C for 16 h. After cooling to room temperature and removal of the solvent under vacuum, the residue was subjected to flash column chromatography (CH_2Cl_2, silica) to give $PdCl_2(NHC)_2$ as a white microcrystalline solid.

5.7.2 Preparation of $PdCl_2(IMes)_2$

Yield: 919 mg (69%). ^{1}H NMR ($CDCl_3$, 300 MHz): δ 7.50 (s, 8H, *m*-C*H*), 6.39 (s, 4H, NC*H*=C*H*N), 2.71 (s, 12H, *p*-CH_3), 2.51 (s, 24H, *o*-CH_3)

5.7.3 Preparation of $PdCl_2(I^iPr_2)_2$

Yield: 570 mg (70%). ^{1}H NMR (CD_2Cl_2, 300 MHz): δ 6.96 (s, 2H, NC*H*=C*H*N), 5.65 (sept, J_{HH} = 6.79 Hz, 2H, C*H*(CH_3)$_2$), 1.59 (d, J_{HH} = 6.79 Hz, 12H, CH(CH_3)$_2$). ^{13}C{^{1}H} NMR (CD_2Cl_2, 100 MHz): δ 169.8 (s, N*C*N), 116.9 (s, N*C*H=*C*HN), 52.7 (s, N*C*H(CH_3)$_2$), 23.6 (s, NCH(*C*H_3)$_2$).Anal. Found (calcd) for $PdCl_2C_{18}N_4H_{32}$: C, 44.52 (44.87); H, 6.54 (6.69); N, 11.58 (11.63).

5.7.4 Preparation of $PdCl_2(I^nBu_2)_2$

Yield: 301 mg (33%). ^{1}H NMR ($CDCl_3$, 250 MHz): δ 6.79 (s, 2H, NC*H*=C*H*N), 4.50 (t, J_{HH} = 7.65 Hz, 4H, NCH_2), 2.03 (m, 4H, NCH_2CH_2), 1.47 (m, 4H, $NCH_2CH_2CH_2$), 0.99 (t, J_{HH} = 7.40 Hz, 6H, $NCH_2CH_2CH_2CH_3$).

5.7.5 Synthesis of $Pd_3(IMes)_3(\mu\text{-}CO)_3$ (3.1)

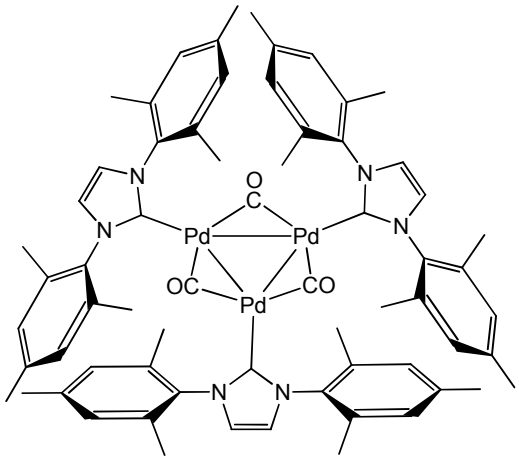

$PdCl_2(IMes)_2$ (200 mg, 0.25 mmol) and KC_8 (69 mg, 0.5 mmol) were loaded into an ampoule fitted with a J. Young's resealable PTFE valve. The vessel was purged with carbon monoxide before CO-saturated THF (10 mL) was added. The suspension was heated at 70 °C for 16 h to afford a dark red solution. This was filtered and the volatiles removed in vacuum. The product was extracted in MeOH (2 mL), filtered and reduced to dryness. The resulting red solid

was washed with hexane (10 mL) dried under vacuum. Yield: 43 mg (38%). ^{1}H NMR (C_6D_6, 400 MHz): δ 6.81 (s, 2H, NC*H*=C*H*N), 6.14 (s, 4H, *m*-C*H*), 2.34 (s, 6H, *p*-CH_3), 2.04 (s, 12H, *o*-CH_3). ^{13}C{^{1}H} NMR (C_6D_6, 101 MHz): δ 249.2 (s, *C*O), 198.8 (s, N*C*N), 137.6 (s, C_{ipso}), 137.0 (s, *p*-*C*CH_3), 136.3 (s, *o*-*C*CH_3), 130.0 (s, N*C*H=*C*HN), 119.1 (s, *m*-*C*H), 21.7 (s, *p*-*C*H_3), 19.1 (s, *o*-*C*H_3). IR (C_6D_6, ν_{CO}, cm^{-1}): 1796. Anal. Found (calcd) for $Pd_3C_{66}N_6O_3H_{72}$: C, 57.63 (60.21); H, 5.61 (5.51); N, 6.45 (6.38). Repeated attempts to determine the CHN content gave a consistently low% carbon.

5.7.6 Synthesis of $Pd_3(I^iPr_2)_3(\mu\text{-}CO)_3$ (3.2)

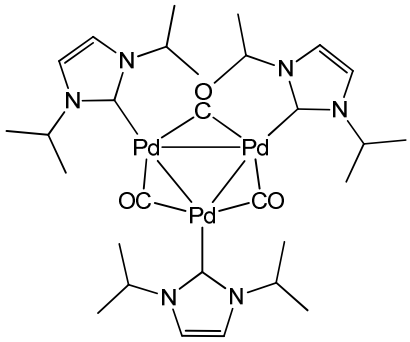

$PdCl_2(I^iPr_2)_2$ (200 mg, 0.4115 mmol) and KC_8 (112 mg, 0.831 mmol) were loaded into an ampoule fitted with a J. Young's resealable PTFE valve. The vessel was purged with CO before CO-saturated THF (10 mL) was added. The suspension was heated at 70 °C for 16 h to afford a red solution. The solution was filtered and reduced in volume by evaporation with a slow stream of CO. The product was isolated upon layering with CO saturated hexane. Yield: 6 mg (5%). NMR and IR spectra were recorded under 1 atm CO to slow the rate of decomposition. ^{1}H NMR (tol-d_8, 400 MHz): δ 6.53 (s, 2H, NC*H*=C*H*N), 5.21 (sept, J_{HH} = 6.79 Hz, 2H, NC*H*(CH_3)$_2$), 1.18 (d, J_{HH} = 6.79 Hz, 12H, CH(CH_3)$_2$). ^{13}C{^{1}H} NMR (tol-d_8, 101 MHz): δ 196.1 (s, N*C*N), 115.4 (s, N*C*H=*C*HN), 52.4 (s, N*C*H(CH_3)$_2$), 23.4 (s, NCH(*C*H_3)$_2$). Note: due to the small quantity of product the ^{13}C signal for Pd-CO could not be detected due to poor signal to noise. IR (C_6D_6, ν_{CO}, cm^{-1}): 1793. Elemental analysis was precluded by the low stability of the complex in the absence of CO.

5.7.7 Synthesis of $Pd_3(I^nBu_2)_3(\mu\text{-}CO)_3$ (3.3)

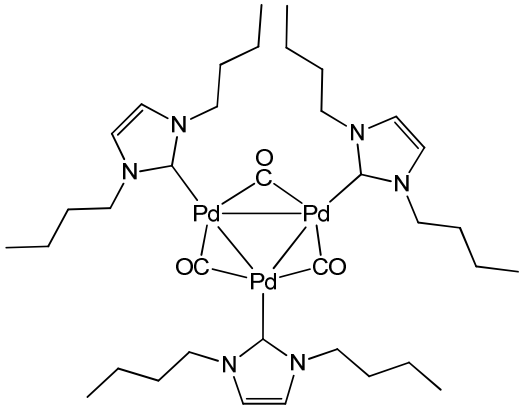

$Pd_3(I^nBu_2)_3(\mu\text{-}CO)_3$ was prepared using the same method as for $Pd_3(I^iPr_2)_3(\mu\text{-}CO)_3$ but due to its instability even under an atmosphere of CO it was not possible to determine the yield. ^{1}H NMR (C_6D_6, 250 MHz): δ 6.38 (s, 2H, NC*H*=C*H*N), 4.13 (t, J_{HH} = 7.22 Hz, 4H, NCH_2), 1.68 (m, 4H, NCH_2CH_2), 1.22 (m, 4H, $NCH_2CH_2CH_2$), 0.81 (t, J_{HH} = 7.41 Hz, 6H, $NCH_2CH_2CH_2CH_3$). IR (C_6D_6, ν_{CO}, cm^{-1}): 1793.

5.7.8 Synthesis of $Pd_3(IMes)_3(\mu\text{-}SO_2)_3$ (3.4)

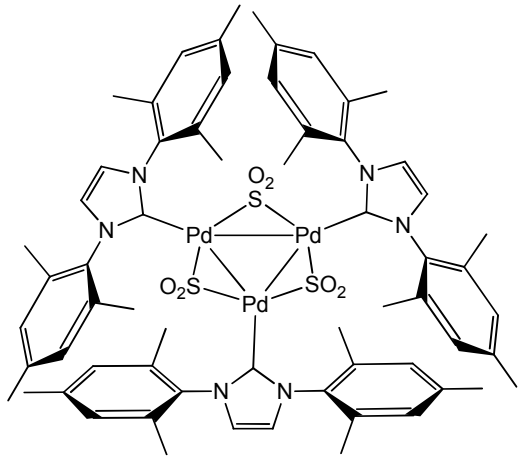

An ampoule fitted with a resealable J Young's PTFE valve was charged with $Pd_3(IMes)_3(\mu\text{-}CO)_3$ (50 mg, 0.037 mmol) and THF (5 mL). A steady stream of SO_2 was bubbled through the solution for ca. 10 min, which resulted in the warming of the solution and an immediate colour change from red to blood red. The solution was left to cool after which the stream of SO_2 was stopped and the solvent removed *in vacuo* to yield the product as a dark red solid. Yield: 53 mg (98%). ^{1}H NMR (THF-d_8, 500 MHz): δ 7.12 (s, 2H, NC*H*=C*H*N), 6.79 (s, 4H, *m*-C*H*), 2.33 (s, 6H, *p*-CH_3), 1.95 (s, 12H, *o*-CH_3). ^{13}C{^{1}H} NMR (THF-d_8, 125 MHz): δ 188.7 (s,

NCN), 138.4 (s, *p*-*C*CH_3), 136.9 (s, *o*-*C*CH_3), 136.8 (s, C_{ipso}), 129.6 (s, NC*H*=*C*HN), 124.6 (s, *m*-*C*H), 21.7 (s, *p*-*C*H_3), 19.0 (s, *o*-*C*H_3). IR (C_6D_6, ν_{SO}, cm^{-1}): 1261, 1099, 1017. Repeated attempts to measure CHN analysis gave consistently erroneous values for% carbon.

5.8 Syntheses of tripodal N-heterocyclic carbene complexes of palladium

5.8.1 Synthesis of (timteb^{tBu}){PdI$_2$(ICy)}$_3$ (4.1)

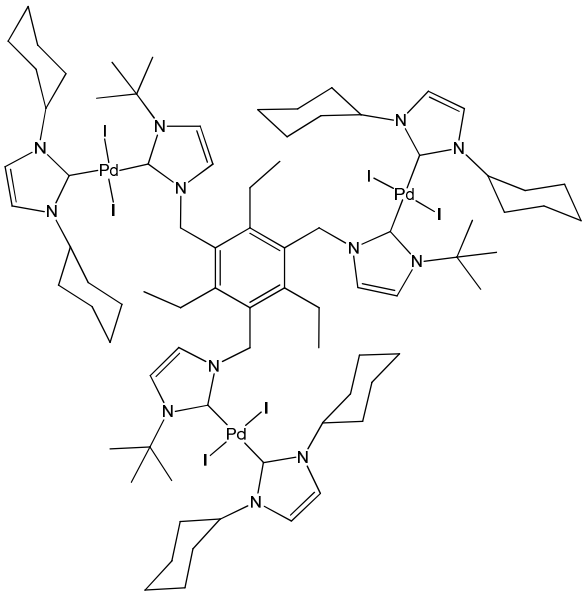

5.8.2 Synthesis of (PdI$_2$(ICy))$_2$[14]

A Schlenk flask was charged with palladium acetate (336 mg, 1.5 mmol), sodium iodide (900 mg, 6.0 mmol), KO^{t}Bu (198 mg, 1.80 mmol), [ICyH][BF_4] (459 mg, 1.5 mmol) and THF (40 mL). The suspension was stirred at room temperature for 16 h, concentrated *in vacuo* and the product separated by column chromatography (silica, Et_2O) collecting the red eluent. The product was isolated as a red solid by removal of volatiles under vacuum. Yield: 628 mg (72%). ^{1}H NMR ($CDCl_3$, 500 MHz): δ 6.99 (s, 2H, NC*H*=C*H*N), 5.23 (m, 2H, NC*H*), 2.30 (m, 4H, CH_2), 1.93 (m, 4H, CH_2), 1.82 (m, 2H, CH_2), 1.63 (m, 4H, CH_2), 1.43 (m, 4H, CH_2), 1.24 (m, 2H, CH_2). ^{13}C{^{1}H} NMR ($CDCl_3$, 125 MHz): δ 148.9 (s, N*C*N), 119.4 (s, N*C*H=*C*HN), 60.7 (s, N*C*H), 33.4 (s, *C*H_2), 25.7 (s, *C*H_2), 25.6 (s, *C*H_2). Anal. Found (calcd) for $Pd_2I_4C_{30}N_4H_{48}$: C, 30.52 (30.40); H, 4.04 (4.08); N, 4.68 (4.73).

5.8.3 Synthesis of *trans*-$PdI_2(ICy)(PPh_3)$

In air, PPh_3 (273 mg, 1.04 mmol) was added to a THF (30 mL) solution of $[PdI_2(ICy)]_2$ (628 mg, 0.52 mmol), which was stirred at room temperature for 30 min. Removal of solvent under vacuum gave an orange residue which was washed with hexane (3 x 10 mL) and then redissolved in dichloromethane (10 mL). Slow addition of hexane precipitated out *cis*-$PdI_2(ICy)(PPh_3)$ leaving *trans*-$PdI_2(ICy)(PPh_3)$ as an orange solid which was recrystallised from chloroform/hexane. Yield: 482 mg (54%). ^{1}H NMR ($CDCl_3$, 500 MHz): δ 7.72 (m, 6H, PPh_3), 7.39 (m, 9H, PPh_3), 6.96 (d, J_{HP} = 1.52 Hz, 2H, NC*H*=C*H*N), 4.78 (m, 2H, NC*H*), 2.38 (m, 4H, CH_2), 1.88 (m, 4H, CH_2), 1.77 (m, 4H, CH_2), 1.42 (m, 4H, CH_2), 1.23 (m, 2H, CH_2), 1.06 (m, 2H, CH_2). ^{31}P{^{1}H} NMR: δ 17.9 (s). ^{13}C{^{1}H} NMR ($CDCl_3$, 125 MHz): δ 152.9 (d, J_{CP} = 191 Hz, N*C*N), 135.6 (d, J_{CP} = 11 Hz, PPh_3), 133.0 (d, J_{CP} = 44 Hz, PPh_3), 131.0 (d, J_{CP} = 3 Hz, PPh_3), 128.0 (d, J_{CP} = 11 Hz, PPh_3), 118.6 (d, J_{CP} = 6 Hz, N*C*H=*C*HN), 60.6 (s, N*C*H), 33.0 (s, *C*H_2), 26.0 (s, *C*H_2), 25.6 (s, *C*H_2). Anal. Found (calcd) for $C_{33}H_{39}N_2PPdI_2{\cdot}CHCl_3$: C, 41.68 (41.92); H, 4.07 (4.13); N, 2.96 (2.87).

5.8.4 Synthesis of (timteb^{tBu}){$PdI_2(ICy)$}$_3$ (4.1)

An ampoule fitted with a J. Young's resealable PTFE valve was charged with *trans*-$PdI_2(ICy)(PPh_3)$ (482 mg, 0.56 mmol) and timteb^{tBu} (161 mg, 0.28 mmol) and THF (30 mL). The mixture was then stirred at 70 °C for 4 h. After cooling to room temperature, the solvent was removed under vacuum and the residue washed with EtOH (1 x 10 mL) and hexane (3 x 10 mL) to afford the product as a pale yellow solid. Yield: 296 mg (68%). ^{1}H NMR ($CDCl_3$, 500 MHz): δ 7.00 (br s, 3H, NC*H*=C*H*N), 6.93 (s, 6H, NC*H*=C*H*N), 6.14 (br s, 3H, NC*H*=C*H*N), 5.94 (br m, 6H, CH_2N), 5.08 (m, 6H, NC*H*), 2.65 (br m, 6H, CH_2CH$_3$), 2.40 (m, 24H, CH_2), 1.98 (s, 27 H, C(CH_3)$_3$), 1.90 (m, 6H, CH_2), 1.74 (m, 6H, CH_2), 1.70 (m, 12H, CH_2), 1.44 (m, 21H, CH_2 + CH$_2$CH_3). ^{13}C{^{1}H}NMR ($CDCl_3$, 125 MHz): δ 167.6 (s, N*C*N), 164.9 (s, N*C*N), 148.9 (s, *C*-CH$_2$N or *C*-CH$_2$CH$_3$), 130.3 (s, *C*-CH$_2$N or *C*-CH$_2$CH$_3$), 118.8 (s, N*C*H=*C*HN), 117.8 (s, N*C*H=*C*HN), 60.3 (s, N*C*H$_2$), 60.1 (s, N*C*H) 58.4 (s, N*C*(CH$_3$)$_3$), 33.4 (s, NC(*C*H$_3$)$_3$), 33.3 (s, *C*H$_2$), 26.3 (s, *C*H$_2$), 25.7 (s, *C*H$_2$), 25.6 (s, *C*H$_2$CH$_3$), 17.8 (s, CH$_2$*C*H$_3$). Anal. Found (calcd) for $C_{81}H_{126}N_{12}Pd_3I_6{\cdot}3C_4H_8O$: C, 43.28 (43.54); H, 5.67 (5.66); N, 6.66 (6.55).

5.8.5 Synthesis of (timteb^{tBu}){$PdI_2(PPh_3)$}$_3$ (4.2)

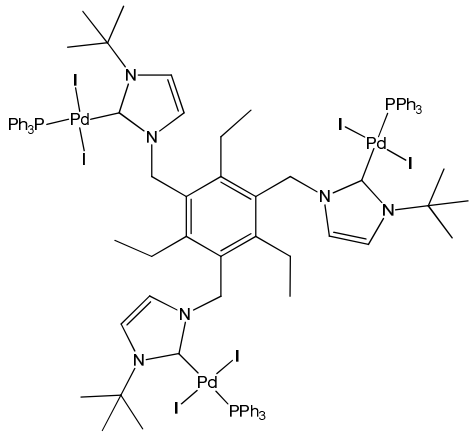

An ampoule fitted with a J. Young's resealable PTFE valve was charged with [timteb^{tBu}H$_3$]Br$_3$ (250 mg, 0.307 mmol), palladium acetate (206 mg, 0.924 mmol), sodium iodide (555 mg, 3.696 mmol), KO^{t}Bu (104 mg, 0.924 mmol) and THF (50 mL). The suspension was stirred at room temperature for 48 h, after which time it was concentrated under vacuum and passed through a silica column using THF. The orange/yellow fraction was collected and reduced to dryness to afford 120 mg of an orange solid. This was redissolved in THF (15 mL) and PPh_3 (70 mg, 0.267 mmol) added. The mixture was stirred at room temperature for 30 min, evaporated to dryness and the residue washed with hexane (3 x 10 mL) to afford a pale yellow solid, which was recrystallised from dichloromethane/hexane. Yield: 160 mg (19%). ^{1}H NMR ($CDCl_3$, 500 MHz): δ 7.75 (m, 18H, PPh_3), 7.38 (m, 27H, PPh_3), 7.00 (br s, 3H, NC*H*=C*H*N), 6.21 (br s, 3H, NC*H*=C*H*N), 5.52 (m, 6H, CH_2N), 2.61 (m, 6H, CH_2CH$_3$), 1.93 (s, 27H, C(CH_3)$_3$), 1.16 (m, 9H, CH$_2$CH_3). ^{31}P{^{1}H} NMR: δ 18.0 (s). ^{13}C{^{1}H} NMR ($CDCl_3$, 125 MHz): δ 155.0 (d, J_{CP} = 192 Hz, N*C*N), 147.2 (s, *C*-CH$_2$N or *C*-CH$_2$CH$_3$), 147.0 (s, *C*-CH$_2$N or *C*-CH$_2$CH$_3$), 135.1 (d, J_{CP} = 11 Hz, PPh_3), 132.9 (d, J_{CP} = 44.4 Hz, PPh_3), 130.2 (s, PPh_3), 128.0 (d, J_{CP} = 10 Hz, PPh_3), 119.9 (s, NC*H*=*C*HN), 119.4 (s, NC*H*=*C*HN), 58.8 (s, N*C*(CH$_3$)$_3$), 50.5 (s, N*C*H$_2$), 37.4 (s, C(*C*H$_3$)$_3$), 27.0 (s, *C*H$_2$CH$_3$), 16.0 (s, CH$_2$*C*H$_3$). Anal Found (calcd) for $C_{90}H_{99}N_6P_3Pd_3I_6$: C, 44.63 (44.33); H, 3.88 (4.09); N, 3.80 (3.45).

5.8.6 Synthesis of (timteb^{dipp}){PdI$_2$(PPh$_3$)}$_3$ (4.3)

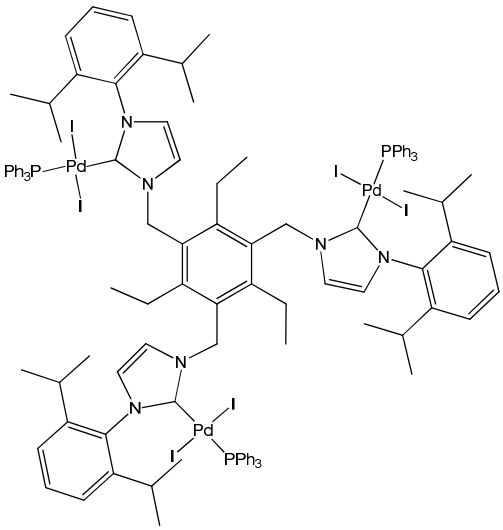

An ampoule fitted with a J. Young's resealable PTFE valve was charged with [timteb^{dipp}H$_3$]Br$_3$ (334.8 mg, 0.298 mmol), palladium acetate (200mg, 0.893 mmol), sodium iodide (535.7 mg, 3.571), KO^{t}Bu (100.3 mg, 0.894 mmol) and THF (50 mL). The suspension was stirred at room temperature for 48 h, the solvent removed *in vacuo* and the product isolated by column chromatography (silica, Et_2O) in air. The red fraction that eluted was collected and the solvent was removed to leave 192 mg of a red solid. This was redissolved in CH_2Cl_2 (15 mL) andPPh_3 (80 mg, 0.305 mmol) added. The reaction mixture was stirred at room temperature for 1 h, the volatiles then removed under vacuum to leave an orange residue which was washed with hexane (3 x 10 mL) and recrystallised from dichloromethane/hexane to afford the product as an orange solid. Yield 153 mg (19%). ^{1}H NMR ($CDCl_3$, 500 MHz): δ 7.56-7.27 (m, 54H, $C_6{}^iPr_2H_3$ + PPh_3), 6.99 (s, 3H, NC*H*=C*H*N), 6.49 (s, 3H, NC*H*=C*H*N), 5.88 (s, 6H, NCH_2), 3.26 (br m, 6H, C*H*$(CH_3)_2$), 2.92 (br s, 6H, CH_2CH$_3$), 1.31 (d, J_{HH} = 5.6 Hz, 18H, CH(CH_3)$_2$), 1.14 (br s, 9H, CH_2CH_3), 1.02 (d, J_{HH} = 5.6 Hz, 18H, CH(CH_3)$_2$). ^{31}P{^{1}H} NMR: δ 16.2 (s). ^{13}C{^{1}H} NMR ($CDCl_3$, 125 MHz): δ 163.2 (d, J_{CP} = 196 Hz, N*C*N), 149.2 (s, *C*-CH_2N or *C*-CH_2CH_3), 147.6 (s, *C*-CH$(CH_3)_2$), 135.4 (d, J_{CP} = 10 Hz, PPh_3), 134.8 (s, *C*-CH_2N or *C*-CH_2CH_3), 133.3 (d, J_{CP} = 45 Hz, PPh_3), 130.5 (d, J_{CP} = 5 Hz, PPh_3), 130.1 (s, $C_6{}^iPr_2H_3$), 127.2 (d, J_{CP} = 10 Hz, PPh_3), 124.8 (s, NCH=*C*HN), 124.3 (s, $C_6{}^iPr_2H_3$), 119.2 (s, N*C*H=*C*HN), 50.7 (s, NCH_2), 29.1 (s, *C*H$(CH_3)_2$), 26.9 (s, CH(*C*H_3)$_2$), 23.6 (s, *C*H_2CH_3), 16.8 (s, CH_2*C*H_3). Anal. Found (calcd) for $C_{114}H_{123}N_6I_6P_3Pd_3$: C, 49.77 (49.65); H, 4.51 (4.43); N, 3.06 (3.15).

5.9 Syntheses of tripodal N-heterocyclic carbene complexes of copper

5.9.1 Synthesis of [(timteb^{tBu})Cu_3(μ$_3$-O)]PF_6 (4.4)

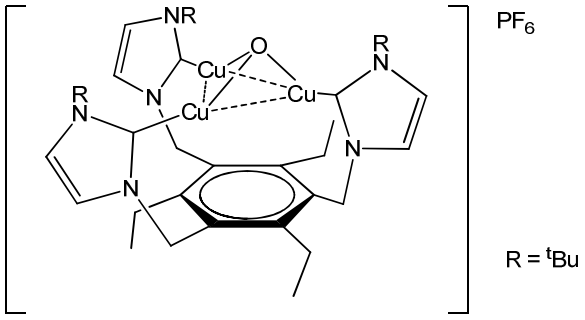

A Schlenk tube was charged with [timteb^{tBu}H$_3$]Br_3 (360 mg, 0.45 mmol), [Cu(NCMe)$_4$]PF_6 (500 mg, 1.34 mmol) and NaO^{t}Bu (129 mg, 1.34 mmol) in THF (20 mL). The suspension was stirred at room temperature for 2 h, passed through Celite and the filtrate reduced to dryness. Extraction with CH_2Cl_2 (20 mL) gave a yellow solution, which upon addition of Et_2O (ca. 10 mL) gave a colourless solution along with a brown oil. The solution was filtered and the solvent removed under vacuum to afford the product as a white solid. Yield 210 mg (51%). ^{1}H NMR (CD_2Cl_2, 500 MHz): δ 7.33 (s, 3H, NC*H*=C*H*N), 7.28 (s, 3H, NC*H*=C*H*N), 5.25 (s, 6H, NCH_2), 2.53 (q, J_{HH} = 7.57 Hz, 6H, CH_2CH$_3$), 1.72 (s, 27H, NC(CH_3)$_3$), 1.17 (br t, 9H, CH$_2$CH_3). ^{13}C{^{1}H} NMR (CD_2Cl_2, 125 MHz): δ 169.2 (s. N*C*N), 148.8 (s, *C*-CH$_2$N or *C*-CH$_2$CH$_3$), 131.4 (s, *C*-CH$_2$N or *C*-CH$_2$CH$_3$), 121.6 (s, N*C*H=*C*HN), 120.1 (s, N*C*H=*C*HN), 58.3 (s, N*C*(CH$_3$)$_3$), 49.1 (s, NCH$_2$), 32.3 (s, NC(*C*H$_3$)$_3$), 24.7 (s, *C*H$_2$CH$_3$), 14.7 (s, CH$_2$*C*H$_3$). Anal. Found (calcd) for $C_{36}H_{54}N_6OCu_3PF_6$: C, 46.28 (46.87); H, 5.82 (5.90); N, 8.73 (9.11). MS (FAB+): *m/z* 777.2, [M]$^+$ calculated 777.0.

5.9.2 Synthesis of [(timteb^{dipp})Cu$_3$(μ$_3$-O)]BF$_4$ (4.5)

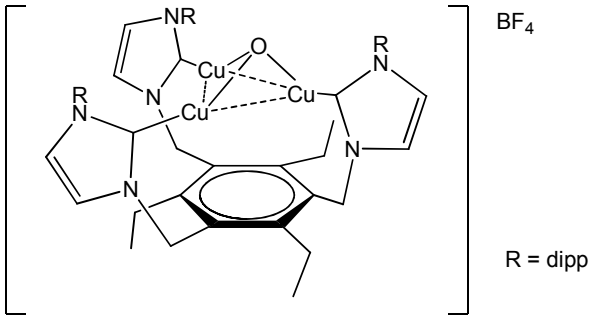

The reaction was performed as for [(timteb^{tBu})Cu$_3$(μ$_3$-O)]PF$_6$ but with [timteb^{dipp}H$_3$]Br$_3$ (563 mg, 0.53 mmol), [Cu(NCMe)$_4$]BF$_4$ (500 mg, 1.59 mmol) and NaO^{t}Bu (153 mg, 1.59 mmol). Yield: 570 mg (91%). ^{1}H NMR (CD_2Cl_2, 400 MHz, 273 K): δ 7.59 (t, J_{HH} = 7.6 Hz, 3H, C$_6$^{i}Pr$_2$*H*$_3$), 7.31 (s, 3H, NC*H*=C*H*N), 7.25 (d, J_{HH} = 7.6 Hz, 6H, C$_6$^{i}Pr$_2$*H*$_3$), 6.94 (s, 3H, NC*H*=C*H*N), 5.49 (s, 6H, C*H*$_2$N), 2.79 (q, J_{HH} = 6.8 Hz, 6H, C*H*$_2$CH$_3$), 2.36 (sept, J_{HH} = 7.6 Hz, 6H, C*H*(CH$_3$)$_2$), 1.17 (d, J_{HH} = 7.6 Hz, 18H, CH(C*H*$_3$)$_2$), 1.09 (d, J_{HH} = 7.6 Hz, 18H, CH(C*H*$_3$)$_2$), 0.92 (t, J_{HH} = 6.8 Hz, 9H, CH$_2$C*H*$_3$). ^{13}C{^{1}H} NMR (CD_2Cl_2, 101 MHz, 273 K): δ 177.6 (s, N*C*N), 148.1 (s, *C*-CH$_2$N or *C*-CH$_2$CH$_3$), 145.7 (s, *C*(CH(CH$_3$)$_2$), 136.0 (s, *C*$_{ipso}$), 130.1 (s, *C*-CH$_2$N or *C*-CH$_2$CH$_3$), 129.8 (s, *p*-*C*H), 124.4 (s, NC*H*=*C*HN), 124.0 (s, *m*-*C*H), 121.9 (s, NC*H*=*C*HN), 48.3 (s, *C*H$_2$N), 31.3 (s, *C*H(CH$_3$)$_2$), 28.4 (s, *C*H$_2$CH$_3$), 24.3 (s, CH(*C*H$_3$)$_2$), 15.5 (s, CH$_2$*C*H$_3$). Anal. Found (calcd) for $C_{60}H_{78}N_6OCu_3BF_4$: C, 60.74 (61.24); H, 6.48 (6.68); N, 6.72 (7.14). MS (FAB+): *m/z* 1089.4, [M]+ calculated 1089.4.

5.10 Catalytic procedures

5.10.1 Pd-catalysed Suzuki-Miyaura coupling

Aryl halide (0.5 mmol), phenylboronic acid (0.75 mmol), caesium carbonate (1.0 mmol), palladium complex (1 mol%) and 1,4-dioxane (1.5 mL) were combined in a J. Young's ampoule modified to fit a Thermo Scientific Omnistation reactor and heated at 80 or 120 °C for 2 or 3 h. After cooling to room temperature, a 30 μL aliquot was withdrawn and diluted with 1 mL of 1,4-dioxane. A 5 μL amount of anisole was added as an internal standard and the mixture analysed by GC.

5.10.2 Pd-catalysed Sonogashira coupling

As for the Suzuki-Miyaura coupling but with aryl halide (0.5 mmol), phenylacetylene (0.7 mmol), caesium carbonate (1.0 mmol), copper iodide (0.01 mmol), palladium complex (1 mol%) and 1,4-dioxane (1.5 mL).

5.10.3 Cu-catalysed Sonogashira coupling

The method used was similar to that for the Suzuki-Miyaura coupling but with aryl halide (0.5 mmol), phenylacetylene (0.6 mmol), caesium carbonate (0.6 mmol), copper catalyst (1 mol%) and DMSO (1.5 mL). The mixture was heated/stirred at 120 °C for 24 h, after which time it was cooled to room temperature, diluted with dichloromethane (10 mL) and filtered. The filtrate was washed with water (3 x 10 mL) and dried over $MgSO_4$. The solvent was removed under vacuum to yield the crude product, which was analysed by NMR to determine the conversion. The products were identified by comparison to the literature.[15]

5.10.4 Cu-catalysed Ullmann-type arylation reactions

The method used was similar to that for the Suzuki-Miyaura coupling but with aryl halide (1.0 mmol), imidazole or phenol (1.5 mmol), caesium carbonate (2.0 mmol), copper catalyst (1 mol%) and DMSO (1.5 mL). The mixture was heated and stirred at 100 °C for 24 h, after which time it was cooled to room temperature, diluted with dichloromethane (10 mL) and filtered. The filtrate was washed with 5% w/w aqueous $KHCO_3$ solution (2 x 10 mL) and water (2 x 10 mL) and dried over $MgSO_4$. The solvent was removed under vacuum to yield the crude product, which was analysed by NMR to determine the conversion. The products were identified by comparison to the literature. [16]

5.10.5 Acylation of pyridine

Pyridine (15 mL), 1-hexene (4.0 mmol) and ruthenium catalyst (0.053 mmol) was added to a Parr Instrument pressure reactor which was pressurised with 10 atm of carbon monoxide and heated at 150 °C for 16 h. After an aliquot was removed from the reaction mixture and the composition of products identified by comparison to the literature.[17]

5.11 References

1. (a) Faure, M.; Saccavini, C.; Lavigne, G., *Chem. Commun.* **2003**, 1578-1579; (b) Kubas, G. J., *Inorg. Synth.* **1990**, *28,* 68-70.
2. Sheldrick, G. M., *Acta Cryst. A* **1990**, *46,* 467-473.
3. Arduengo, A. J.; Krafczyk, R.; Schmutzler, R.; Craig, H. A.; Goerlich, J. R.; Marshall, W. J.; Unverzagt, M., *Tetrahedron* **1999**, *55,* 14523-14534.
4. Herrmann, W. A.; Kocher, C.; Goossen, L. J.; Artus, G. R. J., *Chem.-Eur. J.* **1996**, *2,* 1627-1636.
5. Nolan, S. P.; Singh, R., *Personal Communication*.
6. Gorodetsky, B.; Ramnial, T.; Branda, N. R.; Clyburne, J. A. C., *Chem. Commun.* **2004**, 1972-1973.
7. Jafarpour, L.; Stevens, E. D.; Nolan, S. P., *J. Organomet. Chem.* **2000**, *606,* 49-54.
8. (a) Grasa, G. A.; Viciu, M. S.; Huang, J. K.; Nolan, S. P., *J. Org. Chem.* **2001**, *66,* 7729-7737; (b) Bedford, R. B.; Betham, M.; Blake, M. E.; Frost, R. M.; Horton, P. N.; Hursthouse, M. B.; Lopez-Nicolas, R. M., *Dalton Trans.* **2005**, 2774-2779.
9. Iglesias, M.; Beetstra, D. J.; Knight, J. C.; Ooi, L. L.; Stasch, A.; Coles, S.; Male, L.; Hursthouse, M. B.; Cavell, K. J.; Dervisi, A.; Fallis, I. A., *Organometallics* **2008**, *27,* 3279-3289.
10. (a) Taylor, E. C.; Ehrhart, W. A., *J. Org. Chem.* **1963**, *28,* 1108-1112; (b) Iglesias, M.; Beetstra, D. J.; Kariuki, B.; Cavell, K. J.; Dervisi, A.; Fallis, I. A., *Eur. J. Inorg. Chem.* **2009**, 1913-1919.
11. Wallace, K. J.; Hanes, R.; Anslyn, E.; Morey, J.; Kilway, K. V.; Siegel, J., *Synthesis* **2005**, 2080-2083.
12. Liu, J. P.; Chen, J. B.; Zhao, J. F.; Zhao, Y. H.; Li, L.; Zhang, H. B., *Synthesis* **2003**, 2661-2666.
13. Lebel, H.; Janes, M. K.; Charette, A. B.; Nolan, S. P., *J. Am. Chem. Soc.* **2004**, *126,* 5046-5047.
14. Herrmann, W. A.; Böhm, V. P. W.; Gstöttmayr, C. W. K.; Grosche, M.; Reisinger, C. P.; Weskamp, T., *J. Organomet. Chem.* **2001**, *617,* 616-628.
15. Deng, C. L.; Xie, Y. X.; Yin, D. L.; Li, J. H., *Synthesis* **2006**, 3370-3376.
16. (a) Ghosh, R.; Samuelson, A. G., *New. J. Chem.* **2004**, *28,* 1390-1393; (b) Cristau, H. J.; Cellier, P. P.; Spindler, J. F.; Taillefer, M., *Eur. J. Org. Chem.* **2004**, 695-709; (c) Naidu, A. B.; Jaseer, E. A.; Sekar, G., *J. Org. Chem.* **2009**, *74,* 3675-3679.
17. Moore, E. J.; Pretzer, W. R.; O'Connell, T. J.; Harris, J.; Labounty, L.; Chou, L.; Grimmer, S. S., *J. Am. Chem. Soc.* **1992**, *114,* 5888-5890.

6.1 Appendices

Compound Name	$Ru(IMes)(CO)_4$ **(2.5)** $Ru(IMes)_2(CO)_3$ **(2.6)**	$Os_3(ab\text{-}I^tBu)(CO)_{11}$ **(2.8)**	((*bis*-2,6-diispropyl)amino)ethyl) formamide
Empirical formula	C70 H72 N6 O7 Ru2	C22 H20 N2 O11 Os3	C27 H40 N2 O
Formula weight	1311.48	1059.00	408.61
Temperature	150(2) K	150(2) K	150(2) K
Wavelength	0.71073 Å	0.71073 Å	0.71073 Å
Crystal system	Monoclinic	Monoclinic	Orthorhombic
Space group	P21/c	P21/n	Pcab
Unit cell dimensions	a = 18.83500(10)Å $\alpha = 90^o$	a = 12.9270(1)Å $\alpha = 90^o$	a = 11.8710(1)Å $\alpha = 90^o$
	b = 15.67200(10)Å $\beta = 92.72^o$	b = 13.3980(2)Å $\beta = 107.085\ (1)^o$	b = 19.1400(2)Å $\beta = 90^o$
	c = 21.6260(2)Å $\gamma = 90^o$	c = 16.7890(2)Å $\gamma = 90^o$	c = 22.1900(3)Å $\gamma = 90^o$
Volume	6376.42(8) $Å^3$	2779.47(6) Å3	5041.81(10) $Å^3$
Z	4	4	8
Density (calculated)	1.366 Mg/m^3	2.531 Mg/m3	1.077 Mg/m^3
Absorption coefficient	0.532 mm^{-1}	13.738 mm-1	0.065 mm^{-1}
F(000)	2712	1928	1792
Crystal size	0.20 x 0.20 x 0.15 mm	0.50 x 0.50 x 0.40 mm	0.25 x 0.25 x 0.20 mm
Theta range for data collection	3.82 to 27.48 °.	3.73 to 27.50°	3.71 to 27.49 °.
Index ranges	-24<=h<=24; -20<=k<=20; -28<=l<=28	-16<=h<=16; -17<=k<=17; -21<=l<=21	-15<=h<=15; -24<=k<=24; -28<=l<=28
Reflections collected	113501	43466	101974
Independent reflections	14559 [R(int) = 0.0520]	6343 [R(int) = 0.0758]	5760 [R(int) = 0.0808]
Reflections observed (>2σ)	11981	6000	4412
Data Completeness	0.995	0.994	0.996
Absorption correction	Semi-empirical from equivalents	SHELXA	Semi-empirical from equivalents
Max. and min. transmission	1.00 and 0.94	0.65 and 0.18	0.856 and 0.678
Refinement method	Full-matrix least-squares on F^2	Full-matrix least-squares on F2	Full-matrix least-squares on F^2
Data / restraints / parameters	14559 / 0 / 784	6343 / 0 / 349	5760 / 31 / 308
Goodness-of-fit on F^2	1.058	1.213	1.067
Final R indices [I>2σ(I)]	R1 = 0.0306 wR2 = 0.0686	R1 = 0.0340 wR2 = 0.0859	R1 = 0.0546 wR2 = 0.1227
R indices (all data)	R1 = 0.0445 wR2 = 0.0755	R1 = 0.0364 wR2 = 0.0876	R1 = 0.0759 wR2 = 0.1390
Largest diff. peak and hole	0.604 and -0.522 $eÅ^{-3}$	2.645 and -2.509 eÅ-3	0.280 and -0.296 $eÅ^{-3}$

Compound Name	$Ru_3(6^iPr_2)(\mu\text{-}CO)_3(CO)_8$ **(2.10)**	$[Ru(6o\text{-}Tol)^*(CO)_3]_2$	$PdCl_2(I^iPr_2)_2$
Empirical formula	C20 H20 N2 O10 Ru3	C48 H52 N4 O6 Ru2	C18 H32 Cl2 N4 Pd
Formula weight	751.59	983.08	481.78
Temperature	150(2) K	150(2) K	150(2) K
Wavelength	0.71073 Å	1.54184 Å	0.71073 Å
Crystal system	Orthorhombic	Monoclinic	Monoclinic
Space group	Pcab	P21/c	P21/c
Unit cell dimensions	a = 13.5690(1)Å $\alpha = 90^o$	a = 12.7135(1)Å $\alpha = 90^o$	a = 13.6890(2)Å $\alpha = 90^o$
	b = 13.8300(1)Å $\beta = 90^o$	b = 18.4816(1)Å $\beta = 110.543(1)^o$	b = 10.4150(4)Å $\beta = 103.072(2)^o$
	c = 27.8580(2)Å $\gamma = 90^o$	c = 9.6603(1)Å $\gamma = 90^o$	c = 15.7950(4)Å $\gamma = 90^o$
Volume	5227.81(7) $Å^3$	2125.50(3) $Å^3$	2193.55(11) $Å^3$
Z	8	2	4
Density (calculated)	1.910 Mg/m^3	1.536 Mg/m^3	1.459 Mg/m^3
Absorption coefficient	1.764 mm^{-1}	6.198 mm^{-1}	1.098 mm^{-1}
F(000)	2928	1008	992
Crystal size	0.25 x 0.25 x 0.20 mm	0.26 x 0.15 x 0.09 mm	0.25 x 0.25 x 0.20 mm
Theta range for data collection	3.62 to 27.48°	3.71 to 62.27°	3.87 to 27.37°
Index ranges	-17<=h<=17; -17<=k<=17; -36<=l<=36	-14<=h<=12; -16<=k<=21; -11<=l<=10	-17<=h<=17; -13<=k<=13; -20<=l<=20
Reflections collected	73004	10360	36340
Independent reflections	5972 [R(int) = 0.0534]	3321 [R(int) = 0.0180]	4962 [R(int) = 0.0373]
Reflections observed (>2σ)	5365	3068	3786
Data Completeness	0.997	0.987	0.995
Absorption correction	Semi-empirical from equivalents	Semi-empirical from equivalents	None
Max. and min. transmission	0.708 and 0.547	1.00000 and 0.18181	
Refinement method	Full-matrix least-squares on F^2	Full-matrix least-squares on F^2	Full-matrix least-squares on F^2
Data / restraints / parameters	5972 / 0 / 320	3321 / 0 / 274	4962 / 0 / 237
Goodness-of-fit on F^2	1.057	1.041	1.043
Final R indices [I>2σ(I)]	R1 = 0.0197 wR2 = 0.0434	R1 = 0.0233 wR2 = 0.0582	R1 = 0.0259 wR2 = 0.0604
R indices (all data)	R1 = 0.0246 wR2 = 0.0452	R1 = 0.0261 wR2 = 0.0597	R1 = 0.0404 wR2 = 0.0677
Largest diff. peak and hole	0.499 and -0.549 $eÅ^{-3}$	1.246 and -0.311 $eÅ^{-3}$	0.420 and -0.842 $eÅ^{-3}$

Identification code	$Pd_3(IMes)_3(\mu\text{-}CO)_3$ **(3.1)**	$Pd_3(I^iPr_2)_3(\mu\text{-}CO)_3$ **(3.2)**	$Pd_3(I^nBu_2)_3(\mu\text{-}CO)_3$ **(3.3)**
Empirical formula	C69 H79 N6 O3 Pd3	C30 H48 N6 O3 Pd3	C36 H60 N6 O3 Pd3
Formula weight	1359.58	859.94	944.10
Temperature	150(2) K	150(2) K	150(2) K
Wavelength	0.71073 Å	0.71073 Å	0.71073 Å
Crystal system	Triclinic	Tetragonal	Monoclinic
Space group	P-1	I41/a	P21/a
Unit cell dimensions	a = 12.3910(1)Å α = 96.435(1)^o	a = 12.8790(1)Å α = 90^o	a = 10.3090(2)Å α = 90^o
	b = 12.9570(1)Å β = 98.360(1)^o	b = 12.8790(1)Å β = 90^o	b = 26.4020(5)Å β = 100.138(1)^o
	c = 22.5000(3)Å γ = 115.831(1)^o	c = 43.1800(5)Å γ = 90^o	c = 15.2940(3)Å γ = 90^o
Volume	3153.85(5) Å^3	7162.21(11) Å^3	4097.70(14) Å^3
Z	2	8	4
Density (calculated)	1.432 Mg/m^3	1.595 Mg/m^3	1.530 Mg/m^3
Absorption coefficient	0.897 mm^{-1}	1.527 mm^{-1}	1.342 mm^{-1}
F(000)	1394	3456	1920
Crystal size	1.30 x 1.25 x 0.13 mm	0.20 x 0.20 x 0.15 mm	0.25 x 0.25 x 0.03 mm
Theta range for data collection	3.74 to 27.51 ^{o}.	4.25 to 27.51 ^{o}.	3.56 to 27.54 ^{o}.
Index ranges	-16<=h<=16; -16<=k<=16; -29<=l<=29	-16<=h<=16; -16<=k<=16; -56<=l<=56	-13<=h<=13; -34<=k<=34; -19<=l<=19
Reflections collected	61148	63492	51949
Independent reflections	14371 [R(int) = 0.0617]	4122 [R(int) = 0.0405]	9277 [R(int) = 0.0722]
Reflections observed (>2σ)	12074	3688	7014
Data Completeness	0.991	0.995	0.983
Absorption correction	PSI-Scans	Semi-empirical from equivalents	Semi-empirical from equivalents
Max. and min. transmission	0.90 and 0.83	0.738 and 0.679	0.975 and 0.841
Refinement method	Full-matrix least-squares on F^2	Full-matrix least-squares on F^2	Full-matrix least-squares on F^2
Data / restraints / parameters	14371 / 0 / 731	4122 / 0 / 198	9277 / 14 / 568
Goodness-of-fit on F^2	1.026	1.199	1.080
Final R indices [I>2σ(I)]	R1 = 0.0492 wR2 = 0.0974	R1 = 0.0274 wR2 = 0.0607	R1 = 0.0432 wR2 = 0.0894
R indices (all data)	R1 = 0.0609 wR2 = 0.1048	R1 = 0.0327 wR2 = 0.0629	R1 = 0.0670 wR2 = 0.1035
Largest diff. peak and hole	0.983 and -0.816 eÅ^{-3}	0.612 and -0.821 eÅ^{-3}	0.965 and -1.316 eÅ^{-3}

Identification code	$Pd_3(IMes)_3(\mu\text{-}SO_2)_3$ **(3.4)**	$(timteb^{tBu})\{PdI_2(ICy)\}_3$ **(4.1)**	$(timteb^{tBu})\{PdI_2(PPh_3)\}_3$ **(4.2)**
Empirical formula	C67 H80 N6 O7 Pd3 S3	C86.50 H129 Cl11 I6 N12 Pd3	C93 H102 Cl9 I6 N6 P3 Pd3
Formula weight	1496.75	2807.57	2796.37
Temperature	150(2) K	150(2) K	150(2) K
Wavelength	0.71073 Å	0.71073 Å	0.71073 Å
Crystal system	Monoclinic	Triclinic	Triclinic
Space group	P21/n	P-1	P-1
Unit cell dimensions	a = 22.1200(2)Å $\alpha = 90^o$	a = 15.6880(2)Å $\alpha = 64.251(1)^o$	a = 17.1220(3)Å $\alpha = 113.781(1)^o$
	b = 12.5290(1)Å $\beta = 93.008(1)^o$	b = 19.6950(2)Å $\beta = 87.499(1)^o$	b = 18.2790(3)Å $\beta = 96.783(1)^o$
	c = 24.2110(2)Å $\gamma = 90^o$	c = 20.6950(3)Å $\gamma = 76.260(1)^o$	c = 21.0660(5)Å $\gamma = 108.888(1)^o$
Volume	6700.63(10) $Å^3$	5581.55(12) $Å^3$	5467.95(18) $Å^3$
Z	4	2	2
Density (calculated)	1.484 Mg/m^3	1.671 Mg/m^3	1.698 Mg/m^3
Absorption coefficient	0.946 mm^{-1}	2.445 mm^{-1}	2.489 mm^{-1}
F(000)	3064	2750	2712
Crystal size	0.25 x 0.20 x 0.15 mm	0.30 x 0.30 x 0.25 mm	0.20 x 0.20 x 0.02 mm
Theta range for data collection	3.56 to 27.49^o	3.55 to 27.48^o	3.77 to 22.00^o
Index ranges	-28<=h<=28; -16<=k<=16; -28<=l<=31	-20<=h<=20; -25<=k<=25; -26<=l<=26	-18<=h<=18; -19<=k<=18; -22<=l<=22
Reflections collected	121195	89235	70271
Independent reflections	15343 [R(int) = 0.0515]	25391 [R(int) = 0.0515]	13290 [R(int) = 0.1294]
Reflections observed (>2σ)	12673	18519	8376
Data Completeness	0.997	0.991	0.992
Absorption correction	Semi-empirical from equivalents	Semi-empirical from equivalents	Semi-empirical from equivalents
Refinement method	0.831 and 0.794	0.659 and 0.506	0.962 and 0.886
Data / restraints / parameters	Full-matrix least-squares on F^2	Full-matrix least-squares on F^2	Full-matrix least-squares on F^2
Goodness-of-fit on F^2	15343 / 0 / 793	25391 / 0 / 1082	13290 / 184 / 1224
Final R indices [I>2σ(I)]	1.061	1.085	1.050
R indices (all data)	R1 = 0.0316 wR2 = 0.0724	R1 = 0.0639 wR2 = 0.1633	R1 = 0.0761 wR2 = 0.1632
Largest diff. peak and hole	R1 = 0.0463 wR2 = 0.0801	R1 = 0.0937 wR2 = 0.1822	R1 = 0.1314 wR2 = 0.1986
	1.070 and -1.189 $eÅ^{-3}$	2.281 and -1.861 $eÅ^{-3}$	3.332 and -1.877 $eÅ^{-3}$

Compound Name	[(timteb^{tBu})Cu_3(μ_3-O)]PF_6 **(4.3)**	[(timteb^{dipp})Cu_3(μ_3-O)]BF_4 **(4.4)**
Empirical formula	C75.50 H115 Cl7 Cu6 F12 N12 O2 P2	C174 H286 B2 Cl12 Cu6 F8 N12 O14
Formula weight	2142.13	3750.41
Temperature	150(2) K	150(2) K
Wavelength	0.71073 Å	0.71073 Å
Crystal system	Triclinic	Monoclinic
Space group	P-1	P21/n
Unit cell dimensions	a = 16.8277(5)Å α = 75.988(3)^o	a = 17.8150(3)Å α = 90^o
	b = 16.9316(6)Å β = 89.409(2)^o	b = 20.5850(3)Å β = 90.713(1)^o
	c = 17.3903(5)Å γ = 81.522(3)^o	c = 39.1570(7)Å γ = 90^o
Volume	4753.2(3) Å^3	14358.6(4) Å^3
Z	2	4
Density (calculated)	1.497 Mg/m^3	1.735 Mg/m^3
Absorption coefficient	1.620 mm^{-1}	1.184 mm^{-1}
F(000)	2198	7944
Crystal size	0.43 x 0.21 x 0.04 mm	0.15 x 0.12 x 0.10 mm
Theta range for data collection	3.64 to 26.37^o	3.54 to 22.00^o
Index ranges	-20<=h<=21; -21<=k<=21; -21<=l<=17	-18<=h<=18; -21<=k<=21; -41<=l<=41
Reflections collected	33920	81727
Independent reflections	19379 [R(int) = 0.0295]	16246 [R(int) = 0.1050]
Reflections observed (>2σ)	11896	8560
Data Completeness	0.997	0.922
Absorption correction	Analytical	Semi-empirical from equivalents
Max. and min. transmission	0.748 and 0.177	0.948 and 0.839
Refinement method	Full-matrix least-squares on F^2	Full-matrix least-squares on F^2
Data / restraints / parameters	19379 / 28 / 1062	16246 / 126 / 1433
Goodness-of-fit on F^2	0.904	1.051
Final R indices [I>2σ(I)]	R1 = 0.0405 wR2 = 0.0910	R1 = 0.0896 wR2 = 0.2471
R indices (all data)	R1 = 0.0731 wR2 = 0.0958	R1 = 0.1629 wR2 = 0.2766
Largest diff. peak and hole	0.713 and -0.447 eÅ^{-3}	1.276 and -0.568 eÅ^{-3}